# Regulation of MITF and TFEB

Submitted in partial fulfilment of the
requirements for the degree of
Doctor of Philosophy in Clinical Medicine
University of Oxford
Trinity Term 2016

Supervised by Professor Colin Goding
Ludwig Institute for Cancer Research
Nuffield Department of Clinical Medicine
University of Oxford

Hans Friedrichsen
Keble College, Oxford, OX1 3PG

# Disclaimer

I declare that this submission is my own written work. To the best of my knowledge, it contains no material that has been written by another or previously submitted in the same or a different form as academic work, to this or any other university.

The results presented herein derive from my own experiments, with the exception of Figure 3.2 (work by Alex Schepsky), Figure 3.3a, b and Figure 3.14d (work by Rob Siddaway), Figure 3.5b (structure from Pogenberg et al., 2012) and Figure 3.18 (in collaboration with Zhiqiang Zeng).

Hans Friedrichsen

Trinity Term 2016

# Abstract

Regulation of MITF and TFEB

Hans Friedrichsen, Keble College

D.Phil. Clinical Medicine, Trinity Term 2016

The bHLH-LZ transcription factors MITF and TFEB have been implicated in human disease, with their overexpression increasing the risk of developing cancer. The manner in which their access to E-box target motifs is controlled is an important consideration, as it is via binding to these motifs that bHLH-LZ factors mediate changes in gene expression. In addition to controlling the level of a given transcription factor, mounting evidence suggests that modulating MITF target specificity and TFEB access to the nucleus constitute an important means of regulating their functional output. Post-translational modifications offer one mechanism by which stimuli can rapidly and reversibly alter MITF and TFEB binding to their transcriptional targets.

This thesis aims to expand upon the already substantial literature examining MITF and TFEB post-translational modifications. Specifically, we confirm that MITF can be acetylated and that this occurs within the basic region of the DNA binding domain. Using a naturally occurring acetylation-mimicking mutation, we study the possible functional implications of acetylation on MITF residue K206. Turning to the closely related TFE family member TFEB, we show that TFEB nuclear translocation in response to multiple stimuli is reversible and at least partially mediated by a novel nuclear export signal in the TFEB N-terminus. We show that phosphorylation of nearby S138 by GSK3 requires a priming phosphorylation on S142 and that this latter event may activate an adjacent nuclear export signal.

# Acknowledgements

I am very grateful to my supervisor Professor Colin Goding for providing years of encouragement, feedback and support. The laboratory has been an extremely friendly environment, with help always close at hand. Special thanks go out to Luis Sánchez del Campo Ferrer, Paola Falletta, Kao Chin Ngeow, Rob Siddaway and Pakavarin Louphrasitthiphol. When I joined the lab I had done very little of the type of work that would eventually make up this thesis, and without these folks I would never have been able to pull it together.

Many others outside our laboratory played important roles in my projects. My second supervisor, Panagis Filippakopoulos, was an invaluable source of perspective and can find redeeming bits in even my most flamboyantly failed experiments. Mark Shipman is an absolute wizard with microscopes. Sarah Picaud spent weeks (and weeks) of her valuable time teaching me about the wonderful (and temperamental) world of bacterial protein expression. Elizabeth Patton and Zhiqiang Zeng from the University of Edinburgh and Tatjana Sauka-Spengler and Upeka Senanayake in the WIMM here in Oxford got me interested in zebrafish and helped us do our initial experiments.

I would like to thank the Clarendon Fund, the Nuffield Department of Medicine, Keble College and Cancer Research UK for funding.

Lastly, to my friends, family, Lola, Suzie and Bárbara – it has been a thoroughly enjoyable several years, and I have learned more than I thought you could cram into double that amount of time. Thanks for sticking with me. I'm looking forward to the next step.

# Table of Contents

**DISCLAIMER**.....I
**ABSTRACT**.....II
**ACKNOWLEDGEMENTS**.....III
**TABLE OF CONTENTS**.....IV
**LIST OF ABBREVIATIONS**.....VI
**CHAPTER 1: INTRODUCTION**.....1
1.1 The TFE family of transcription factors.....2
1.1.1 Microphthalmia-associated transcription factor (MITF).....6
1.1.1.1 Transcriptional and post-translational regulation.....10
1.1.1.2 Role in physiology and disease.....14
1.1.2 Transcription factor EB (TFEB).....18
1.1.2.1 Transcriptional and post-translational regulation.....21
1.1.2.2 Role in physiology and disease.....23
1.2 Post-translational modification and transcription factor function.....25
1.2.1 Post-translational regulation of DNA binding.....26
1.2.2 Post-translational regulation of localisation.....29
1.3 Summary and aims.....32
**CHAPTER 2: METHODS**.....34
2.1 Reagents.....35
2.1.1 Chemicals.....35
2.1.2 Antibodies.....35
2.1.3 Purified Proteins.....36
2.1.4 Oligonucleotides.....36
2.1.5 Plasmids.....40
2.2 Nucleic Acid Methods.....43
2.2.1 Plasmid Purification.....43
2.2.2 Agarose gel electrophoresis.....44
2.2.3 Polymerase chain reaction.....44
2.2.4 Site-directed mutagenesis.....45
2.2.5 Restriction enzyme digest.....46
2.2.6 DNA ligation.....46
2.2.7 Purification of mRNA.....46
2.2.8 qPCR.....47
2.3 Protein Methods.....48
2.3.1 Cell extracts.....48
2.3.1.1 Whole cell extracts.....48
2.3.1.2 Subcellular fractionation.....48
2.3.2 Protein purification.....49
2.3.2.1 Immunoprecipitation.....49
2.3.2.2 His-tagged protein purification.....49
2.3.3 SDS-PAGE.....51
2.3.4 Coomassie staining.....51
2.3.5 Western blotting.....52
2.3.6 Electrophoretic mobility shift assay (EMSA).....53
2.3.7 Chromatin immunoprecipitation (ChIP).....54

2.3.8 Peptide SPOT kinase assay....56
2.4 BACTERIAL METHODS....56
2.4.1 Growth Conditions....56
2.4.2 Bacterial Strains....57
2.4.3 Transformation of competent bacteria....57
2.4.4 Expression of recombinant protein....58
2.5 CELL BIOLOGY METHODS....59
2.5.1 Flow cytometry....59
2.5.2 Luciferase reporter assay....59
2.5.3 Fluorescence live cell imaging....59
2.5.4 Immunofluorescence....61
2.6 MAMMALIAN CELL METHODS....61
2.6.1 Cell culture....61
2.6.2 Transient transfection of DNA....62
2.6.3 Stable transfection of DNA....63
2.6.4 Lentiviral transduction....63
2.7 ANIMAL METHODS....64
2.7.1 Zebrafish melanocyte rescue assay....64
**CHAPTER 3: MITF MUTANT K206Q HAS ALTERED FUNCTION....65**
3.1 INTRODUCTION....66
3.2 RESULTS....68
3.2.1 MITF can be acetylated in melanoma cells....68
3.2.2 MITF can be acetylated on multiple sites....74
3.2.3 MITF(K206Q) shows altered DNA binding....82
3.2.4 MITF(K206Q) shows altered function in vitro....104
3.2.4.1 Effect of K206 status on genomic target binding....104
3.2.4.2 Effect of K206 status on *TYR* activation....113
3.2.5 MITF K206Q shows altered function in vivo....119
3.3 DISCUSSION....123
**CHAPTER 4: TFEB IS SUBJECT TO NUCLEAR EXPORT....137**
4.1 INTRODUCTION....138
4.2 RESULTS....139
4.2.1 TFEB expression level and localisation....139
4.2.2 TFEB nuclear translocation is reversible....154
4.2.3 TFEB nuclear export depends upon XPO1....157
4.2.4 The TFEB N-terminus mediates nuclear export....167
4.2.5 TFEB residues 129-152 harbour a functional NES....175
4.2.6 TFEB residues 129-152 mediate signalling-dependent localisation changes....181
4.2.7 S142 phosphorylation primes GSK3 to phosphorylate S138....185
4.3 DISCUSSION....191
**CHAPTER 5: DISCUSSION....205**
6.1 MITF ACETYLATION AND THE K206Q MUTATION....206
6.2 TFEB LOCALISATION AND NUCLEAR EXPORT....208
6.3 CONCLUSION....210
**REFERENCES....211**

# List of Abbreviations

| | |
|---|---|
| acK | pan-acetyl-lysine |
| AKT | RAC-alpha serine/threonine-protein kinase |
| APS | ammonium persulfate |
| ATP | adenosine triphosphate |
| bHLH | basic helix-loop-helix |
| bHLH-LZ | basic helix-loop-helix leucine zipper |
| bp | base pair |
| BSA | bovine serum albumin |
| C-terminal | carboxyl terminal |
| CBP | CREB-binding protein |
| cDNA | complimentary deoxyribonucleic acid |
| ChIP | chromatin immunoprecipitation |
| CMV | cytomegalovirus |
| cpm | counts per minute |
| Da | Dalton |
| DAPI | 4',6-diamidino-2-phenylindole |
| DCT | dopachrome tautomerase |
| DMEM | Dulbecco's Modified Eagle Medium |
| DMSO | dimethyl sulfoxide |
| DNA | deoxyribonucleic acid |
| DPF | days post fertilisation |
| dNTP | deoxynucleotide |
| DTT | dithiothreitol |
| ECL | enhanced chemiluminescence |
| *E. coli* | *Escherichia coli* |
| EDTA | ethylenediaminetetraacetic acid |
| EMSA | electrophoretic mobility shift assay |
| ERK | extracellular signal-related kinase |
| FBS | foetal bovine serum |
| GFP | green fluorescent protein |

| | |
|---|---|
| GSK3 | glycogen synthase kinase 3 |
| GTP | guanosine triphosphate |
| HA | haemagglutinin |
| HDAC | histone acetyltransferase |
| HEPES | 4-(2-hydroxyehtyl)-1-piperazineethanesulfonic acid |
| HRP | horseradish peroxidase |
| IgG | immunoglobulin G |
| IHC | immunohistochemistry |
| IP | immunoprecipitation |
| IPTG | isopropyl-β-D-thiogalactoside |
| kb | kilobase |
| kDa | kilodalton |
| LB | Luria-Bertani |
| LMB | leptomycin B |
| M | molar |
| MAPK | mitogen-activated protein kinase |
| MAPKK/MEK | MAPK kinase |
| MiT | microphthalmia-associated transcription |
| MITF | microphthalmia-associated transcription factor |
| mRNA | messenger ribonucleic acid |
| MTT | 3-(4,5-dimethylthiazol-2-yl)-2,5-diphenyltetrazolium bromide |
| mTOR | mammalian target of rapamycin |
| N-terminal | amino terminal |
| NES | nuclear export signal |
| NLS | nuclear localisation signal |
| NP-40 | Nonylphenylpolyethylene glycol |
| PBS | phosphate-buffered saline |
| PBST | 0.1% Tween in phosphate-buffered saline |
| PCR | polymerase chain reaction |
| PDAC | pancreatic ductal adenocarcinoma |
| PI3K | phosphoinositide 3-kinase |

| | |
|---|---|
| PIC | protease inhibitor cocktail |
| PKI | protein kinase inhibitor |
| PMSF | phenylmethanesulfonylfluoride |
| qPCR | quantitative real-time polymerase chain reaction |
| RCC | renal cell carcinoma |
| RNA | ribonucleic acid |
| RPMI | Roswell Park Memorial Institute |
| SAHA | suberoylanilide hydroxamic acid |
| SCF | stem cell factor |
| SDS | sodium dodecyl sulfate |
| SDS-PAGE | sodium dodecyl sulfate polyacrylamide gel electrophoresis |
| SEM | standard error of the mean |
| SGC | Structural Genomics Consortium |
| shRNA | short hairpin ribonucleic acid |
| SV40 | simian virus 40 |
| TBE | Tris/Borate/EDTA |
| TBS | Tris-buffered saline |
| TBST | 0.1% Tween in Tris-buffered saline |
| TE | Tris/EDTA |
| TEMED | tetramethylethylenediamine |
| TetR | tet repressor |
| TFE3 | transcription factor E3 |
| TFEB | transcription factor EB |
| TFEC | transcription factor EC |
| TPA | tetradecanoyl phorbol acetate |
| Tris | Tris(hydroxymethyl)aminomethane |
| TSS | transcription start site |
| TYR | tyrosinase |
| UV | ultraviolet |
| WT | wild-type |

# Chapter 1: Introduction

## 1.1 The TFE family of transcription factors

The TFE family includes 4 members, MITF, TFEB, TFE3 and TFEC, that belong to the larger family of basic helix-loop-helix leucine zipper (bHLH-LZ) transcription factors (Kuiper et al., 2004). The bHLH domain was identified in 1989 and mediates binding to sequences of the general motif 5'-CANNTG-3', termed the E-box (Murre et al., 1989; Voronova & Baltimore, 1990). The first structure of a bHLH protein bound to DNA indicated that the longer first helix, which includes the basic region, lies in the DNA major groove, while the shorter second helix participates in dimerisation (Ferré-D'Amaré et al., 1994). Some bHLH proteins, including Myc, Max, the TFE family members and others, have an additional sequence termed the leucine zipper, which consists of hydrophobic amino acids placed approximately every 7 residues and participates in dimerisation (Landschulz et al., 1988). Subsequent co-crystal structures of bHLH proteins showed that the positioning of the first helix in relation to the DNA was conserved (Ferré-D'Amaré et al., 1994; Ma et al., 1994; Nair & Burley, 2003; Pogenberg et al., 2012; Wang et al., 2013).

The fact that the composition of bHLH dimers can vary provides an opportunity for regulation. Perhaps the best-studied example involves the bHLH-LZ proteins Myc and Max. A Max/Max homodimer is capable of binding a palindromic E-box sequence with a 5' flanking T and a 3' flanking A (5'-TCACGTGA-3'), whereas a Myc/Max heterodimer can bind motifs of the more generic form 5'-CANNTG-3' but not when they contain a 5' flanking T and a 3' flanking A (Prendergast & Ziff, 1991; Solomon et al., 1993). Another example is found in the inhibitor of DNA-binding (Id) protein family. The four members of this family contain a HLH domain but lack the basic region, rendering them able to dimerise with other bHLH proteins but interfering with DNA binding (Pagliuca et al., 1995). In this way, Id proteins can regulate the function

of bHLH proteins in a dominant-negative fashion (Perk et al., 2005). Interestingly, the Id proteins have been found to be overexpressed in a range of cancers (Fong et al., 2004).

As detailed above, multiple reports examine the implications of formation of transcription factor homo- and heterodimers, but it remains unclear to what extent a homodimer is truly a homodimer. A Max/Max dimer will contain two monomers of the same coding sequence, but asymmetric post-translational modification could result in the formation of what is, effectively, a heterodimer. For example, point mutation of a putative phosphorylation site in Oct4 can impair formation of one of multiple possible types of homodimer while leaving the ability to form the other homodimer and heterodimer configurations intact (Saxe et al., 2009). As the different types of Oct4 homo- and heterodimers have different motif preferences, this may provide a way for post-translational modification to affect target specificity.

Thus, the composition of dimers can have marked effects on the function of bHLH proteins. This is an important consideration for the TFE family, as *in vitro* data indicates that these proteins are capable of homo- or heterodimerising with other TFE family members but not with other proteins from the larger bHLH-LZ group (Fisher et al., 1991; Hemesath et al., 1994; Pogenberg et al., 2012). Recently, it was noted that an MITF/MITF dimer that was bound to a DNA target motif showed a “kink” in the leucine zipper. This appeared to be due to the inclusion of 3 residues uniquely conserved within the TFE family that altered the register of the leucine zipper, restricting dimerisation to the TFE family members while preventing dimerisation with other bHLH proteins (Pogenberg et al., 2012).

Although there is evidence to support a functional role of TFE heterodimers, dimerisation within the TFE family may not function in the same way as has been found for Myc/Max. First, TFE family heterodimers have been observed in cells in culture, and all possible combinations of homo- and heterodimers among the 4 family members were observed *in vitro* (Hemesath et al., 1994; Weilbaecher et al., 1998). Next, multiple members are expressed in certain cell types that have been shown to exhibit defects when one member is mutated, including osteoclasts (Weilbaecher et al., 1998) and melanocytes (Verastegui et al., 2000). However, when the various members of the TFE family were mutated in mice singly and in combination, no phenotypic overlap was seen. For example, *MITF* and *TFE3* null mice only showed defects in osteoclast function when these mutations were present in combination, however some homozygous semi-dominant MITF mutations resulted in a phenotype when no other mutations were introduced (Steingrimsson et al., 2002). This indicates that perhaps the formation of specific heterodimers may not be essential for proper function of members of the TFE family but that rather it is the homodimers that are functional (Steingrímsson et al., 2002). It is interesting though that the TFE family members do not appear to be created equal in this context – combining a *TFEC* null mutation with a null mutation for another TFE family member did not result in a phenotype, whereas the *TFEB* null mutation is embryonic lethal in the absence of any additional mutations of other TFE family members (Steingrimsson et al., 2002; Steingrímsson et al., 1998).

However, there is evidence of significant functional overlap among the family members as well. For example, TFEB and TFE3 have both been shown to play a role in mediating the integrated stress response (Martina et al., 2016) and regulating components of the innate immune system in macrophages (Pastore et al., 2016). Additionally, after the identification of the role of TFEB in regulating the

endolysosomal pathway, MITF was found to regulate expression of the v-ATPase complex and drive endolysosomal biogenesis (Ploper et al., 2015; Zhang et al., 2015). Additionally, gene fusions of both *TFEB* and *TFE3* have been identified in renal cell carcinoma (RCC) chromosomal translocations. Both of these show distinctive and atypical cellular morphologies and share expression of markers not typically found in RCC (Argani, 2015). In fact, the diseases resulting from the Xp11 *TFE3*-overexpressing and t(6:11) *TFEB*-overexpressing translocations were sufficiently similar in terms of their clinical, morphologic and immunohistochemical profiles that they were grouped together in the 2013 ISUP Vancouver classification of renal neoplasias as "MiT family translocation renal cell carcinoma (RCC)" (Argani, 2015).

In addition to showing shared functional aspects, the TFE family shows structural and regulatory similarity (Figure 1.1). Although the N-terminal regions of TFEB and TFE3 are somewhat divergent, large portions of the 4 proteins show a high degree of conservation. This is especially true in regions demonstrated to be of functional importance, such as the DNA-binding bHLH-LZ domain (Figure 1.1; red box). Also of interest is a region in the N-terminus that is targeted by ERK in both MITF and TFEB and by mTOR in TFEB (Figure 1.1; grey box), with phosphorylation mediating changes in localisation and activity (Hemesath et al., 1998; Settembre et al., 2011). The yellow box in Figure 1.1 outlines a conserved region shown to mediate MITF transactivation (Mansky et al., 2002). Importantly, this region also contains a serine residue targeted by mTOR to result in cytoplasmic sequestration of MITF, TFEB and TFE3 (Bronisz et al., 2006; Martina et al., 2014; Settembre et al., 2012) and a lysine residue found to be SUMOylated in these same three family members (Miller et al., 2005; Murakami & Arnheiter, 2005). The last region marked isa serine-rich C-terminal motif showing high conservation throughout the TFE family that has been

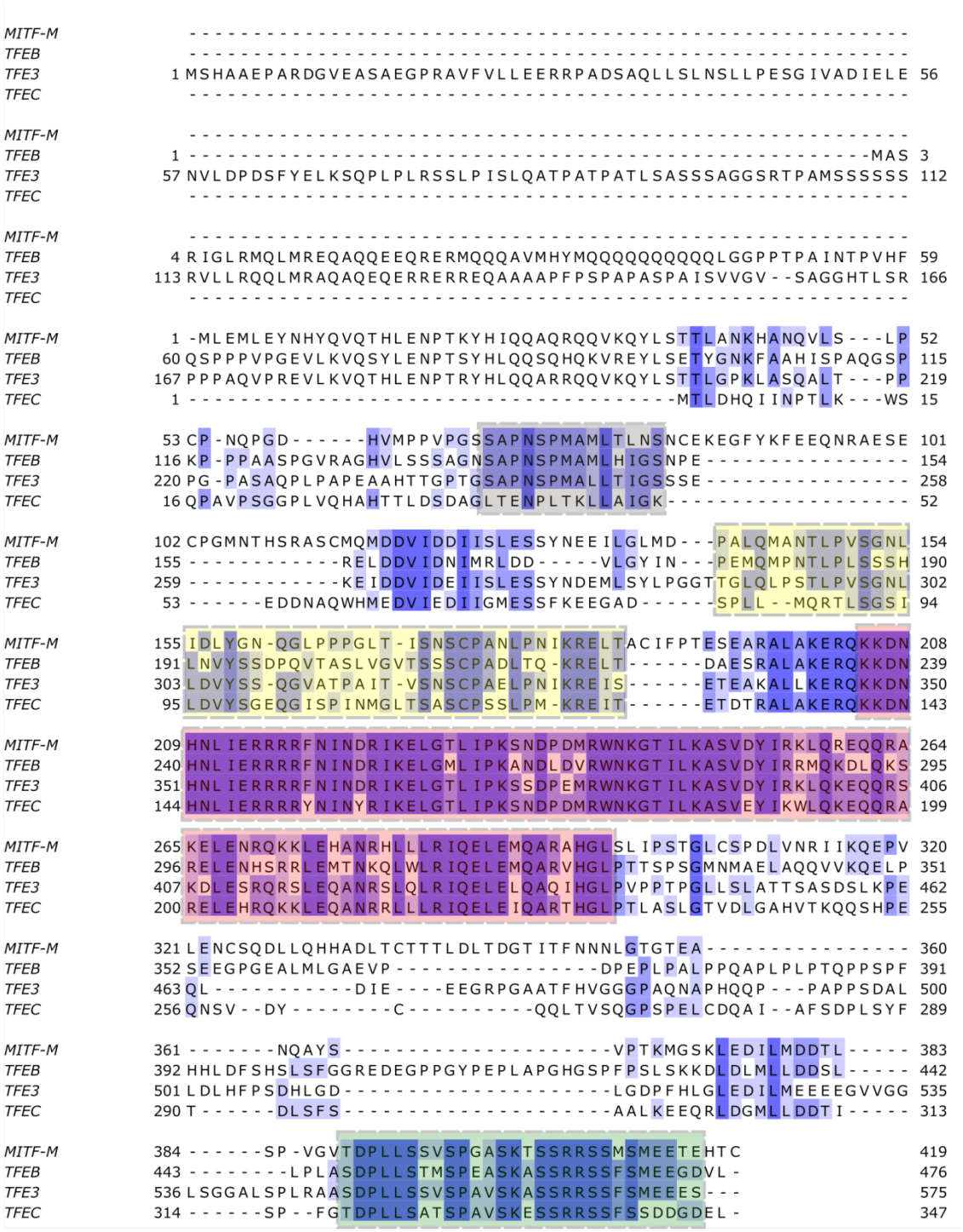



**Figure 1.1. The 4 members of the human TFE family have highly conserved regions that show shared regulation and function.** The protein sequences of the four members of the human TFE family were aligned using an online tool available from the uniprot database (www.uniprot.org). The alignment file was then visualised and annotated in Jalview v.2.10.1 (www.jalview.org). Conservation is indicated in blue, with darker blue corresponding to higher conservation. Several conserved regions known to be of functional and/or regulatory importance have also been highlighted in dashed boxes. These include an N-terminal domain targeted by ERK and/or mTOR (grey), a transactivation domain that also harbours a serine residue targeted by mTOR in multiple members (yellow), a DNA-binding bHLH-LZ domain (red) and a serine-rich C-terminal domain targeted by RSK1, GSK3 and/or PKCβ (green).

shown to be phosphorylated on homologous residues of MITF and TFEB (Figure 1.1, green box). Interestingly, these events appear to be mediated by different kinases, with MITF phosphorylated by RSK1 and GSK3 and TFEB phosphorylated by PKCβ (Ferron et al., 2013; Ploper et al., 2015; Wu et al., 2000). Thus, the 4 members of the TFE family exhibit a high degree of conservation throughout several regions known to mediate key aspects of their function. Importantly, many of these regions are subject to similar regulatory events in the form of post-translational modifications that lead to shared functional outcomes.

### *1.1.1 Microphthalmia-associated transcription factor (MITF)*

The first member of the TFE family to be studied was the microphthalmia-associated transcription factor (MITF), the locus for which, *mi*, was identified in 1942 (Hertwig, 1942). The name derives from the fact that mice in which this gene was mutated had small eyes, in addition to defects in pigmentation and mast cell and osteoclast development. It was not until 50 years later that the gene responsible for this phenotype was cloned and its product identified as a bHLH-LZ transcription factor that was highly conserved between mice and humans (Hodgkinson et al., 1993; Hughes et al., 1994).

Several of the TFE family members exhibit complex gene structure, and MITF is no exception (Kuiper et al., 2004). At least 11 isoforms have been described in humans. These result from the use of alternate promoters, with the majority of the coding sequence (exons 2-9) being shared and only the N-terminus differing (Levy et al., 2006). MITF-M is the primary isoform expressed in melanocytes. It has a unique first exon and is under control of the melanocyte-specific M promoter, resulting in a

different N-terminus compared to both other MITF isoforms and other TFE family members (Fuse et al., 1996). It is also worth noting that MITF-M exhibits alternative splicing of exon 6a, which encodes a stretch of 6 residues. Inclusion of this exon results in MITF(+), while exclusion results in MITF(-), with MAPK signalling shown to bias the ratio of these two proteins toward the (+) form (Hemesath et al., 1994; Primot et al., 2010; Steingrimsson et al., 2002). This thesis will be discussing primarily the (+) form of the MITF-M isoform, and MITF will refer to this protein unless indicated otherwise.

MITF is well conserved from humans to zebrafish, with mutations yielding pigment phenotypes in humans, mice, rats, zebrafish and other species (Hodgkinson et al., 1998; Léger et al., 2012; Lister et al., 1999; Opdecamp et al., 1998; Steingrímsson et al., 2004). The zebrafish is an interesting example, as it harbours two *MITF* genes, *mitfa* and *mitfb*, with the former being expressed in neural crest-derived melanocytes and exhibiting homology to human MITF-M, while the latter shows more homology to a longer isoform in humans, MITF-A (Lister et al., 1999; Lister et al., 2001).

Like other bHLH transcription factors, MITF binds to E-box motifs (5'-CANNTG-3') present in gene regulatory regions to modulate transcription (Levy et al., 2006). However, it has been documented to most frequently bind to two slightly different versions of this motif, 5'-CACGTG-3' and 5'-CATGTG-3' (Cheli et al., 2010; Rob Siddaway, unpublished data). In addition to the nature of the core motif, binding to the 5'-CATGTG-3' motif (but not the 5'-CACGTG-3' motif) was found to depend upon the identity of the residues immediately flanking the hexanucleotide E-box (Aksan & Goding, 1998). The sequence 5'-CATGTG-3' also occurs within the larger 5'-AGTCATGTGCT-3' motif that was observed to be conserved in regulatory regions of several pigmentation genes expressed in melanocytes, leading to it being termed the M-box (Lowings et al., 1992).

It is via binding to these motifs that MITF regulates melanocyte differentiation, with MITF shown to activate transcription of genes involved in the production of pigment via binding to M-box motifs in regulatory regions of *DCT*, *TRP1* and *TYR* (Bentley et al., 1994; Bertolotto et al., 1998b; Yavuzer et al., 1995). In addition to regulating genes directly involved in pigment production, MITF also transcriptionally regulates other genes involved in melanocyte differentiation, including melanoma antigen recognised by T cells (*MLANA*; Du et al., 2003) and premelanosome (*PMEL*; Baxter & Pavan, 2003).

The repertoire of genes regulated by MITF also includes genes involved in proliferation, cell cycle and survival. MITF was found to regulate cell cycle progression by controlling transcription of cyclin-dependent kinase 2 (*CDK2*), permitting progression through G1/S and melanoma cell growth (Du et al., 2004; Widlund et al., 2002). Likewise, silencing of MITF resulted in expression of $p27^{Kip1}$ and a G1/S cell cycle arrest, further supporting a pro-proliferative role of MITF (Carreira et al., 2006). However, MITF expression was also seen to correlate with cell cycle arrest. For example, high levels of MITF were found to mediate a G1/S arrest and increased $p21^{Cip1}$ expression (Carreira et al., 2005). Also, MITF expression in melanocytes resulted in cell cycle arrest via $p16^{INK4A}$ up-regulation, although this was not observed in melanoma cell lines (Loercher et al., 2005). Further support for an anti-proliferative role for MITF comes from studies in which MITF expression inhibited tumour formation *in vivo* and abrogated BRAF(V600E)-mediated proliferation (Selzer et al., 2002; Wellbrock & Marais, 2005).

Changes in MITF expression also impinge on other cellular processes. For example, in addition to mediating cell cycle arrest, silencing of MITF led to DNA damage, mitotic aberrations and senescence (Cheli et al., 2011; Strub et al., 2011).

Further evidence supporting a role for MITF in suppressing senescence was seen in a study where MITF induced *TBX2* expression, a factor that inhibits $p21^{Cip1}$ expression, promoting cell cycle and inhibiting senescence (Carreira et al., 2000; Prince et al., 2004; Vance et al., 2005). MITF may also regulate survival by upregulating the expression of *BCL2*, an anti-apoptotic protein (McGill et al., 2002). Interestingly, despite the fact that MITF down-regulation does not appear to induce apoptosis, a C-terminal fragment of MITF generated by caspase cleavage during apoptosis was found to activate caspase 3 and promote an apoptotic phenotype (Larribere et al., 2005). Evidence concerning the influence of MITF on invasion is conflicting. MITF was found to activate expression of *c-MET*, which is thought to be involved in metastasis and invasion, but low MITF levels were also found to correlate with invasive behaviour (Carreira et al., 2006; McGill et al., 2006). MITF was also shown to influence cellular metabolism by promoting the expression of peroxisome proliferator-activated receptor γ coactivator 1α (*PGC1α*), which in turn promotes mitochondrial biogenesis (Haq et al., 2013; Vazquez et al., 2013).

A rheostat model has been proposed to explain how MITF could mediate such diverse and, at times, seemingly contradictory effects (Carreira et al., 2006; Hoek & Goding, 2010). This model states that MITF activity falls on a spectrum, resulting in a range of phenotypes. High levels of MITF are associated with $p16^{INK4A}$- and $p21^{Cip1}$-dependent cell cycle arrest and expression of genes involved in differentiation (Carreira et al., 2005; Loercher et al., 2005). Low levels of MITF activity are also associated with a cell cycle arrest, however this occurs via $p27^{Kip1}$. In addition to cell cycle arrest, the rheostat poses that low levels of MITF can lead to increased tumorigenic potential and invasiveness, as well as possibly mediating senescence and stemness (Carreira et al., 2006; Cheli et al., 2011; Giuliano et al., 2010). Intermediate levels of MITF are

thought to facilitate proliferation by avoiding cell cycle arrest and senescence on the one hand and differentiation and cell cycle arrest on the other (Hoek & Goding, 2010). Additionally, MITF expression was found to be a determinant of melanoma cell state *in vivo*, mediating shifts between proliferative and invasive phenotypic states (Hoek et al., 2008). Further support for this model comes from data showing that melanoma cell proliferation was inhibited during both forced MITF expression and depletion (Kido et al., 2009). Lastly, the use of a conditional MITF expression system in zebrafish indicated that an intermediate level of MITF facilitated melanoma development, while both increasing and decreasing the amount of MITF prevented tumour development (Lister et al., 2014).

Note that the term MITF activity level in the rheostat model is multifactorial. The actual level of MITF protein is only one of several factors that could influence MITF activity. Other factors that might impinge on the ability of MITF to access target motifs could include the constellation of post-translational modifications present (Miller et al., 2005), dimerisation partners (Hemesath et al., 1994; Steíngrimsson et al., 2002), transcriptional co-activators and co-repressors (Schepsky et al., 2006) and the chromatin state of target motifs and the surrounding regions (Lauss et al., 2015).

#### 1.1.1.1 Transcriptional and post-translational regulation

The transcriptional regulation of *MITF* responds to many different pathways, several of which have established roles in the development of pigment cells. For example, the α-melanocyte stimulating hormone (α-MSH) pathway involves the binding of this peptide hormone to the melanocortin 1 receptor (MC1R). Subsequently, activation of adenylyl cyclase results in an elevation of cyclic AMP, which in term

stimulates phosphorylation of cyclic AMP responsive element binding protein (CREB) by PKA. Phosphorylated CREB then binds to a cAMP responsive element (CRE) present in the *MITF* promoter, resulting in activation of *MITF* transcription (Bertolotto et al., 1998a). Activation of the *MITF* promoter by phosphorylated CREB was later found to require the cooperation of SOX10 (Huber et al., 2003). As *SOX10* expression is restricted to cells derived from the neural crest, this provides a means of limiting MITF expression to the melanocyte lineage.

Other transcriptional activators of *MITF* include ONECUT-2, PGC-1α, PAX3 and LEF1 (Bondurand et al., 2000; Jacquemin et al., 2001; Shoag et al., 2013; Widlund et al., 2002). PAX3 accomplishes transactivation of *MITF* by binding to two motifs in the *MITF* promoter, and it has been shown to cooperate with SOX10 (Bondurand et al., 2000; Lee et al., 2000; Potterf et al., 2000; Verastegui et al., 2000). LEF1 interacts with β-catenin and mediates *MITF* activation by binding to TCF/LEF sites located in the *MITF* promoter (Widlund et al., 2002). Interestingly, MITF can also cooperate with β-catenin to activate its own promoter in a positive feedback loop (Saito et al., 2002).

*MITF* expression can also be repressed. The POU domain transcription factor Brn-2 was shown to bind to the *MITF* promoter and mediate repression at the transcriptional level, although this factor has also been shown to positively regulate *MITF* in the context of oncogenic BRAF expression (Goodall et al., 2008; Wellbrock et al., 2008). Although *Brn-2* and *MITF* are found to be co-expressed in melanoma, there is evidence to indicate that their expression is inversely correlated (Goodall et al., 2008; Thurber et al., 2011; Wellbrock et al., 2008). The microRNA miR-211 may aid in establishing this inverse correlation – its expression is induced by MITF, and it is capable of repressing *Brn-2* expression (Boyle et al., 2011; Levy et al., 2010). *MITF* expression can also be repressed by GLI2 and HIF1, which respond to alterations in

signals from the Hedgehog pathway and hypoxia sensing, respectively (Cheli et al., 2012; Javelaud et al., 2011).

MITF is also regulated post-translationally, with several different types of modifications having been described, including phosphorylation (Ploper et al., 2015; Takeda et al., 2000; Wu et al., 2000), ubiquitination (Xu et al., 2000) and SUMOylation (Bertolotto et al., 2011; Miller et al., 2005; Murakami & Arnheiter, 2005; Yokoyama et al., 2011). Perhaps the best studied of these is the phosphorylation of S73 by ERK (Hemesath et al., 1998). This occurs in response to MAPK signalling resulting from stem cell factor (SCF) binding the Kit receptor, a stimulus that also results in the phosphorylation of S409 by RSK1 (Wu et al., 2000). This latter event was reported to interfere with the binding of the E3 SUMO-protein ligase PIAS3 to the MITF leucine zipper domain, with the end result that S409 phosphorylation facilitates MITF transcriptional activity (Levy et al., 2003). Interestingly, these phosphorylation events are thought to mediate both increased transcriptional activity and proteasomal degradation, the latter possibly being via promotion of MITF ubiquitination (Wu et al., 2000; Xu et al., 2000). However, the influence of S73 and S409 phosphorylation on MITF function is still unclear – although the S73A mutant demonstrated impaired ability to activate the *TYR* promoter, mice harbouring this mutation alone or in concert with the S409A mutation showed no phenotypic abnormalities (Bauer et al., 2009; Bismuth et al., 2008; Hemesath et al., 1998; Wu et al., 2000).

MITF is also targeted for phosphorylation by GSK3 on several residues, with S298 the first to be identified. The impact of this event on MITF function is unclear; mutation of this residue to an alanine impaired transactivation of the *TYR* promoter in one study while having no effect in another (Grill et al., 2013; Takeda et al., 2000). GSK3 was also recently reported to phosphorylate MITF on several residues in the C-

terminus, with inhibition of these phosphorylation events stabilising the protein (Ploper et al., 2015). The residues found to be phosphorylated by GSK3 (S397, S401 and S405) fit a GSK3 consensus motif in which an initial phosphorylation at S409 would serve as a priming event for GSK3, which would then consecutively phosphorylate the other residues. As S409 was found to be phosphorylated by RSK1, this is possibly an example of cross-talk between phosphorylation events mediated by different kinases (Ploper et al., 2015; Wu et al., 2000). However, it is still unclear how S409 phosphorylation would impact MITF function, with studies indicating that it may promote ubiquitination and degradation, result in activation of transcriptional activity and provide a priming event for other phosphorylation events that promote degradation (Levy et al., 2003; Ploper et al., 2015; Xu et al., 2000).

In another example of potential cross-talk between different post-translational modifications of MITF, eliminating phosphorylation at S73 with a S73A mutation resulted in a significant decrease in ubiquitination of MITF, with K201 identified as a ubiquitination target (Xu et al., 2000). Lastly, MITF was shown to be SUMOylated on two residues, K182 and K316, which resulted in alterations in MITF transcriptional activity (Miller et al., 2005; Murakami and Arnheiter, 2005). Interestingly, a mutation disrupting the consensus site for SUMOylation of K316 (E318K) was found to predispose to both melanoma and renal cell carcinoma (RCC) (Bertolotto et al., 2011; Yokoyama et al., 2011).

Two MITF phosphorylation events observed in osteoclasts and osteoclast precursor cells have yet to be observed in cells of the melanocyte lineage. First, MITF was shown to be phosphorylated on S173, promoting interaction with 14-3-3 proteins and sequestration in the cytoplasm (Bronisz et al., 2006). This is thought to be mediated by Cdc25c-associated protein kinase (C-TAK1) and was observed in

osteoclast precursor cells. Second, stimulation with RANKL also resulted in phosphorylation of MITF in cells of this lineage. This involved phosphorylation of residue S307 by p38 MAPK. These phosphorylation events had contrasting effects on MITF function, with S173 phosphorylation resulting in a decrease in transactivation potential and S307 phosphorylation resulting in an increase (Bronisz et al., 2006; Mansky et al., 2002).

1.1.1.2 Role in physiology and disease

MITF is known as the master regulator of melanocyte development, responding to multiple signalling cascades to coordinate the expression of genes involved in differentiation, survival and growth (Cheli et al., 2010). Additionally, MITF is implicated in the development of both mast cells and osteoclasts (Steingrímsson et al. 2002). The phenotype of the original *mi* mutant mouse mentioned earlier stems from a deletion of residue R216, which interrupts the normal register of the basic region within the first helix and interferes with DNA binding (Hodgkinson et al., 1993; Steingrímsson et al., 2004). This results in a failure of melanocyte development, as when MITF is absent, precursor neural crest cells are unable to differentiate into melanoblasts (Opdecamp et al., 1997).

Many *mitf* mutations have been identified in mice, with some being autosomal recessive, while others, particularly those in the bHLH domain, show a semidominant pattern of inheritance in which heterozygotes exhibit a partial phenotype (Steingrímsson et al., 2002). *Mitf* mutations manifest their pigment phenotypes through defects in neural-crest derived melanocyte development. Impairment of this lineage explains the pigment phenotype of the original *mi* mouse, with failure of development of neural

crest-derived melanocytes accounting for the white coat and impaired development of the retinal pigment epithelium resulting in the eye phenotype from which the gene derives its name.

*MITF* mutations are also found in the human conditions Waardenburg syndrome and Tietz syndrome, which involve varying degrees of hypopigmentation and deafness. The two conditions are similar, however in Tietz syndrome, hypopigmentation is more uniform rather than patchy, and the condition exhibits fully penetrant autosomal dominant inheritance (Smith et al., 2000). Waardenburg syndrome is classified into 4 types, with all involving a similar constellation of clinical features, including sensorineural hearing loss and pigmentation abnormalities of the skin, eyes and hair (Tassabehji et al., 1995). Of the different types, Waardenburg syndrome type 2 (WS2) is the mildest and does not include the facial anomalies, limb muscle hypoplasia or Hirschprung's disease observed in the other subtypes (Read & Newton, 1997; Tietz, 1963; Waardenburg, 1951). WS2 is inherited in an autosomal dominant fashion, with mutations in several genes being described (Pingault et al., 2010). Based on the nature of the genetic alteration, WS2 is then further classified into subtypes, with mutations in *MITF* resulting in type 2A (WS2A) (Baral et al., 2012; Grill et al., 2013). For example, premature incorporation of stop codons in the MITF basic region (R214*) or the second helix (R259*) resulted in truncated proteins that were not capable of dimerisation (Nobukuni et al., 1996). Moreover, these truncations were no longer able to bind DNA or transactivate the *TYR* promoter. However, being unable to dimerise, these alleles did not interfere with the function of the WT protein, providing evidence that the phenotype of WS2A caused by these mutations is due to haploinsufficiency (Nobukuni et al., 1996; Tachibana, 1997).

MITF also plays a role in melanoma, but unlike the role of MITF during development, in which a well-defined phenotype appears to result from the lack of sufficient functional MITF, how MITF impacts cancer development and progression is much less clear (Cheli et al., 2010; Hoek & Goding, 2010; Wellbrock & Arozarena, 2015). The first study to link *MITF* to melanoma found it to be a lineage addiction oncogene that was amplified in 10-20% of non-familial melanoma cases (Garraway et al., 2005). This link also appeared to apply to disease progression, as metastatic tumours exhibited more frequent *MITF* amplification than did primary tumours or benign nevi, and *MITF* amplification correlated with decreased overall survival (Garraway et al., 2005). However, MITF protein levels vary both between and within clinical specimens, and *MITF* amplifications, gain-of-function mutations and loss-of-function mutations have all been identified in melanoma, with no clear picture overall of whether MITF functions as an oncogene or a tumour suppressor (Flaherty et al., 2012; Garraway et al., 2005; Goodall et al., 2008).

Even though the exact nature of MITF's role in melanoma is still unclear, data indicates that MITF is at least partially responsible for oncogenesis mediated by other melanoma drivers (Wellbrock et al., 2008; Wellbrock & Marais, 2005). For example, *MITF* cooperates with *BRAF(V600E)* to transform primary human melanocytes (Garraway et al., 2005), and *MITF* alterations were found to correlate with mutations in the melanoma driver *BRAF (Cancer Genome Atlas Network, 2015)*. The interaction between *MITF* and the *BRAF(V600E)* oncogene was further examined recently in an elegant *in vivo* study in which oncogenic *BRAF(V600E)* was coupled with a temperature-sensitive *MITF* splice site mutation in zebrafish (Johnson et al., 2011). This experiment will be discussed in some detail, as it provides insight into the

complicated and nuanced role of MITF in melanoma development, maintenance and recurrence.

The *MITF* mutation used is temperature-sensitive and both hypomorphic and conditional. This results in decreased levels of MITF when fish are reared at a low temperature, and when fish are reared at a high temperature, MITF levels fall to the point where there is insufficient MITF activity to support melanocyte development (Johnson et al., 2011). This allowed for the conditional expression of low MITF levels alongside expression of the melanoma oncogene *BRAF(V600E)*. Importantly, neither expression of *BRAF(V600E)* in the context of wild-type (WT) *MITF* nor expression of *BRAF(V600E)* in the context of the hypomorphic *MITF* mutant raised at the higher temperature resulted in tumour formation. However, the combination of *BRAF(V600E)* and the hypomorphic *MITF* mutant resulted in formation of nevi and tumours when fish were raised at the permissive temperature, indicating that low levels of MITF (but not normal levels or absent MITF) interact with *BRAF(V600E)* expression to facilitate melanoma development *in vivo* (Lister et al., 2014).

Strikingly, if they allowed tumours to develop and then abrogated *MITF* expression by shifting fish to the prohibitive higher temperature, the tumours regressed, indicating that MITF was required for tumour maintenance as well as tumour development (Lister et al., 2014). Additionally, if fish were allowed to develop tumours, shifted to the higher temperature until the tumours regressed and then returned to the permissive temperature, *MITF* expression resumed, and tumours recurred in the same locations (Lister et al., 2014). This indicates that a population of cells capable of mediating tumour recurrence persisted despite the gross regression of tumours and that the re-expression of *MITF* was sufficient to trigger tumour recurrence.

There is also evidence indicating that, in addition to gene dosage effects, MITF point mutations are observed within the context of melanoma. Interestingly, all but one of these mutations (G244R) occur outside of the DNA binding domain, while the majority of MITF point mutations resulting in Waardenburg and Tietz syndromes lie within this domain (Cronin et al., 2009; Grill et al., 2013; Steingrímsson et al., 2004). Additionally, many of the Waardenburg mutations were unable to bind DNA or activate transcription, while this was not the case with the mutations found in melanoma (Grill et al., 2013).

The only melanoma mutation to be examined in a site-specific manner to date is E318K, which was found to increase risk of developing both familial and sporadic melanoma (Bertolotto et al., 2011; Yokoyama et al., 2011). Interestingly, this allele was also found to predispose to development of RCC, a cancer type found in cases where the other TFE family members TFEB and TFE3 are overexpressed due to chromosomal translocation (Argani, 2015; Bertolotto et al., 2011). The E318K mutation interrupts a consensus site (φKXE) for SUMOylation of neighbouring K316, resulting in impaired MITF SUMOylation, enhanced binding to target genes and increased transcriptional activity. Furthermore, this mutation appeared to comprise a gain-of-function promotion of oncogenesis, as migration and invasion were increased relative to the WT protein (Bertolotto et al., 2011).

### *1.1.2 Transcription factor EB (TFEB)*

The transcription factor EB was first identified as a protein capable of binding the major late promoter of adenovirus, with its family member TFE3 being cloned only months earlier (Beckmann et al., 1990; Carr & Sharp, 1990). Like MITF and other

bHLH-LZ factors, TFEB binds to E-box motifs to regulate gene expression. But unlike MITF-M, the predominant MITF isoform in melanocytes, the model for regulation of TFEB function involves the active maintenance of this transcription factor in the cytoplasm until a stimulus triggers its nuclear translocation (Roczniak-Ferguson et al., 2012; Settembre et al., 2011). This is mediated by a nuclear localisation signal in the bHLH domain, a sequence conserved in all isoforms of all 4 TFE family members (Kuiper et al., 2004). Mutation of this NLS prevented TFEB nuclear accumulation, even after inhibition of signals maintaining cytoplasmic sequestration (Roczniak-Ferguson et al., 2012). This general mechanism is conserved in TFE3 and the longer isoforms of MITF (Bronisz et al., 2006; Fuse et al., 1996; Martina et al., 2013; Martina et al., 2014). MITF-M does not appear to be regulated in the same way – although it harbours an identical NLS, this isoform is generally found to localise to the nucleus (Martina & Puertollano, 2013; Martina et al., 2014).

Like MITF and other TFE family members, the TFEB gene architecture is complex, with multiple unique 5' exons having been identified and leading to the designation of TFEB isoforms A-G. The initially identified TFEB was renamed TFEB-B, showing expression in a wide range of tissues that included liver, kidney and brain (Carr & Sharp, 1990; Kuiper et al., 2004). TFEB-C also showed expression in a wide range of tissues, while an isoform identified as the full-length transcript corresponded to TFEB-E (Kuiper et al., 2004; Ota et al., 2004). Despite the existence of multiple 5' exons and several alternate splicing events, only one other 5' exon harboured an in-frame ATG. If active, this would result in an extra 14 residues on the N-terminus of TFEB-A (Kuiper et al., 2004). Interestingly, most of the isoforms detected exhibited highly specific tissue expression patterns. For example, TFEB-A was expressed almost exclusively in the placenta – intriguingly, TFEB knockout mice die early in

development due to defects in placental function, possibly implicating this isoform as being important early in development (Kuiper et al., 2004; Steingrímsson et al., 1998).

Like the other TFE family members, and bHLH proteins in general, TFEB promotes the expression of target genes by binding to E-box sites in their promoters. Specifically, a ChIP-seq experiment involving ectopic expression of TFEB-3xFLAG in HeLa cells indicated that TFEB binds to a palindromic 5'-TCACGTGA-3'motif (Palmieri et al., 2011). The occurrence of these motifs in the promoter regions of lysosomal genes led the authors to term them CLEAR sites (Coordinated Lysosomal Expression and Regulation; Palmieri et al., 2011). Interestingly, they also found partial motifs (5'-TCACG-3') to be bound by TFEB, albeit at lower levels, possibly suggesting the existence of more than one class of TFEB binding site.

TFEB has been called a master regulator of the autophagy-lysosome pathway (Pastore et al., 2013). TFEB targets include genes encoding lysosomal hydrolases, proton pump subunits and lysosomal membrane proteins (Palmieri et al., 2011). Additionally, TFEB has been shown to regulate genes involved in endocytosis, autophagy, innate immunity and cellular response to stress (Martina et al., 2016; Palmieri et al., 2011; Pastore et al., 2016; Settembre et al., 2011).

Several years ago, a rheostat model was proposed to explain how MITF regulates its vast repertoire of targets, and a rheostat model has also recently been proposed for the control of TFEB level and localisation (Hoek & Goding, 2010; Marin Zapata et al., 2016). This model incorporates a time dimension – in the short-term, TFEB is negatively regulated by mTOR, with mTOR inhibition resulting in TFEB level and localisation primarily regulated by the proteasome. However, during prolonged

mTOR inhibition, TFEB becomes regulated by a long-term mTOR-independent mechanism.

#### 1.1.2.1 Transcriptional and post-translational regulation

The majority of work on TFEB has concerned its post-translational regulation and target genes, with relatively little known regarding how it is regulated at the transcriptional level. One study showed that *TFEB* expression was up-regulated in response to starvation, both *in vitro* and *in vivo* (Settembre et al., 2013). This was detected in various tissues in mice, as well as in cell culture as soon as 4 hours after withdrawal of nutrients. The authors noted that post-translational modifications caused existing TFEB to translocate to the nucleus at an earlier time point, prompting them to hypothesise that TFEB positively regulated its own transcription (Settembre et al., 2013). This positive feedback loop required the TFEB transactivation domain and was sensitive to *TFEB* copy number. TFEB had been earlier shown to bind to E-box motifs, and the authors demonstrated that TFEB bound to 4 of 6 E-box motifs present in its own promoter, leading them to conclude that in response to starvation, TFEB positively regulates its own transcription via binding to its own promoter (Settembre et al., 2013).

Unlike transcriptional regulation of TFEB, post-translational regulation of TFEB function has been studied extensively (Figure 1.2). Although this work primarily looks at regulation of TFEB localisation, some reports indicate that TFEB stability and transcriptional activity can also be regulated post-translationally (Figure 1.2a; Bao et al., 2016; Ferron et al., 2013; Roczniak-Ferguson et al., 2012; Settembre et al., 2011). TFEB has been shown to be phosphorylated by ERK (Settembre et al., 2011), mTOR (Roczniak-Ferguson et al., 2012; Settembre et al., 2012), GSK3 (Li et al., 2016;

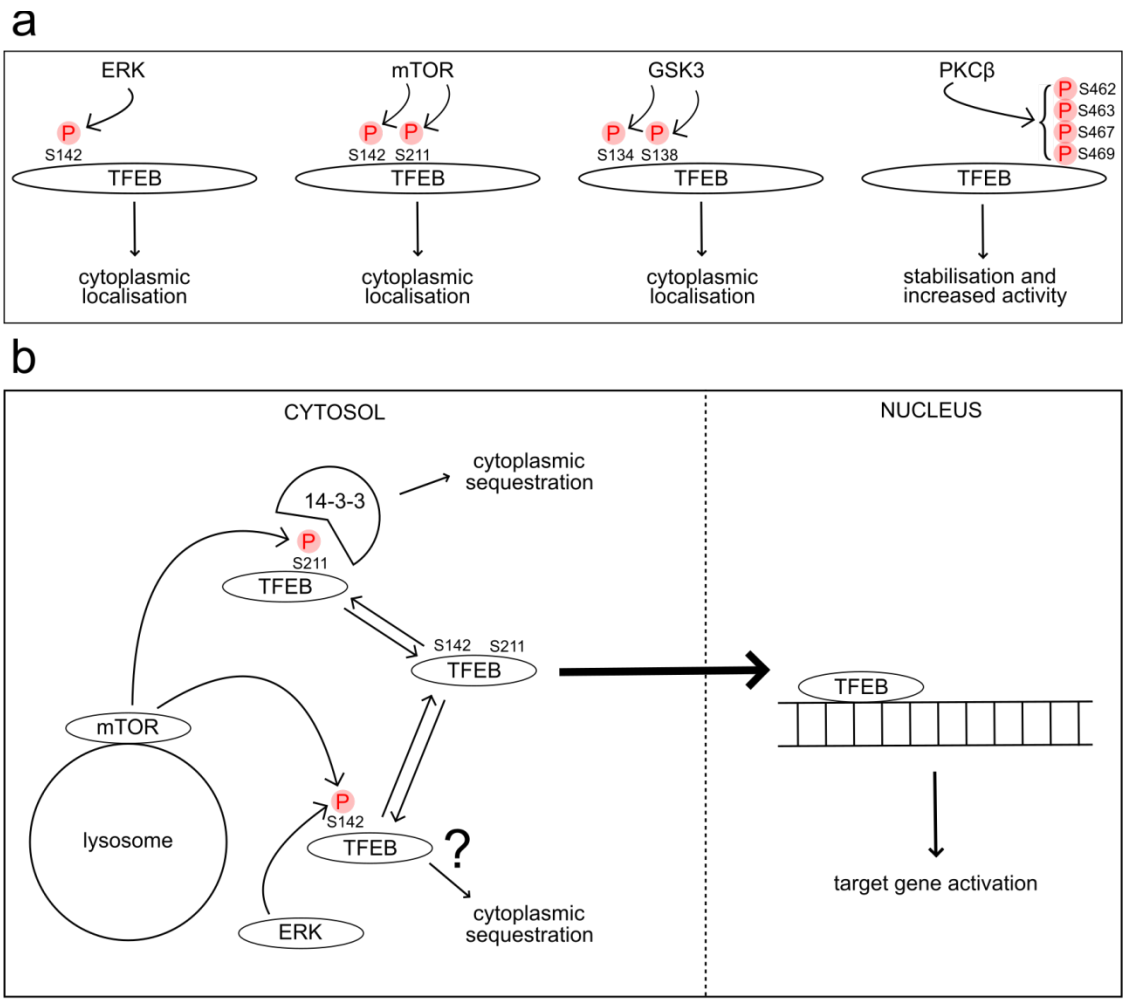



**Figure 1.2. Post-translational regulation of TFEB by phosphorylation.** TFEB function has been shown to be regulated by post-translational modification, primarily via controlling its localisation. (a) Schematic drawings depicting kinases shown to regulate TFEB function, the sites targeted by these kinases and the effect on TFEB function. (b) Schematic drawing depicting the mechanism by which mTOR and ERK phosphorylation of residues S142 and S211 is thought to control TFEB nuclear translocation and subsequent target gene activation. Although the effect of S211 phosphorylation by mTOR has been thoroughly studied and shown to be the result of 14-3-3 protein-mediated cytoplasmic sequestration, the mechanism by which phosphorylation of S142 by ERK and/or mTOR prevents nuclear translocation is currently unknown.

Marchand et al., 2015; Parr et al., 2012) and PKCβ (Ferron et al., 2013). In all, eight different phosphorylation sites have been examined with site-specific methods. These sites are shown in Figure 1.2a, along with the kinases that target them and the effect(s) on TFEB function. Interestingly, there are examples of multiple kinases modifying a single site and multiple sites being modified by a single kinase.

TFEB localisation appears to be a key determinant of its functional output and to primarily depend upon the phosphorylation state of two serine residues, S142 and S211, with phosphorylation promoting cytoplasmic localisation in both cases (Figure 1.2b). In the case of S211, mTOR phosphorylation promotes binding to 14-3-3 proteins, sequestering the protein in the cytoplasm (Marchand et al., 2015; Roczniak-Ferguson et al., 2012). To date, mTOR is the only kinase that has been shown to phosphorylate this residue, and a S211A mutation results in accumulation of TFEB in the nucleus (Martina et al., 2012; Roczniak-Ferguson et al., 2012). Both mTOR and ERK are capable of phosphorylating S142 in HeLa cells overexpressing TFEB-3xFLAG (Settembre et al., 2011; Settembre et al., 2012). As with S211, mutation of this S142 to alanine results in accumulation of TFEB in the nucleus, indicating that TFEB that is unphosphorylated at S142 and/or S211 is capable of entering the nucleus (Figure 1.2b; Roczniak-Ferguson et al., 2012; Settembre et al., 2011). Interestingly, despite S142 being the first site identified to be phosphorylated in TFEB and multiple reports that a S142A mutation promotes TFEB nuclear localisation, the mechanism by which this occurs is unknown.

No studies have directly investigated the relative influence of the S142A and S211A mutations on TFEB localisation, but the relative influence of the kinases targeting these sites has been addressed. Inhibition of ERK with the MEK inhibitor U0126 resulted in partial nuclear translocation and a partial electrophoretic mobility shift, as compared to treatment with the mTOR inhibitor Torin 1 or starvation (Settembre et al., 2012). Additionally, induction of lysosomal stress with Salicylihalamide A or chloroquine resulted both in mTOR inhibition and a pronounced TFEB nuclear translocation but left ERK signalling intact. The authors concluded that

mTOR-mediated regulation of TFEB localisation is dominant over ERK-mediated regulation (Settembre et al., 2012).

In addition to S142 and S211, other phosphorylation events have been implicated in the regulation of TFEB function. For example, PKCβ phosphorylates TFEB on several residues in the C-terminus in response to RANKL signalling in osteoclasts (Figure 1.2a; Ferron et al., 2013). The corresponding residues in MITF appear to be phosphorylated by GSK3 rather than PKCβ, although a recent report indicates that the effect of these two signalling pathways on TFEB localisation may be linked and involve the recently identified GSK3 target sites S134 and S138 (Li et al., 2016; Ploper et al., 2015).

TFEB has also been shown to be acetylated on residue K116, this being the only published study of an acetylation event in a TFE family member that has been addressed in a site-specific manner (Bao et al., 2016). Studying the ability of TFEB to promote clearance of pathogenic fibrillar Aβ and amyloid plaques in Alzheimer's disease, the authors show that ectopically expressed Flag-tagged TFEB is acetylated on K116 in HEK 293 cells upon treatment with a combination of the histone deacetylase inhibitors trichostatin A (TSA) and nicotinamide (Bao et al., 2016). This appeared to have functional consequences, as SIRT1 inhibition facilitated degradation of fibrillary Aβ in microglia, and this was dependent upon TFEB.

#### 1.1.2.2 Role in physiology and disease

*TFEB* is thought to be ubiquitously expressed, and its deletion, unlike deletion of any of the other three TFE family members, causes embryonic lethality in mice, indicating that TFEB plays an essential, non-redundant role (Steingrímsson et al., 1998;

Steingrímsson et al., 2002). Lethality appears to be due to a defect in placental vascularisation resulting in the failure of labyrinthine cells to express vascular endothelial growth factor (Steingrímsson et al., 1998). The embryo then degenerates due to embryonic vessels failing to invade the placenta. This study also made various combinatorial knockouts of one or more members of the TFE family, however because of the early lethality of *TFEB* mutation, it could only be assessed in heterozygous form. These mice showed no phenotype. The additional deletion of other TFE family members also resulted in no phenotype (Steingrímsson et al., 1998).

The only disease state in which a genetic alteration of *TFEB* has been observed is TFEB translocation RCC, in which the entire coding sequence of *TFEB* is expressed at levels approximately 50-fold higher than normal as a result of *TFEB* coming under the control of the constitutively active *ALPHA* gene promoter (Kuiper et al., 2003). These are fairly uncommon cancers that disproportionately affect younger patients. The gross features are similar to clear cell RCC, with solid tan tumours showing areas of haemorrhage, necrosis and papillary architecture (Magers et al., 2015). Differential diagnosis often involves immunohistochemical stains of melanocytic markers, with positive staining for Melan-A or HMB-45 supporting a diagnosis of TFEB translocation RCC. Also commonly used are antibodies against TFEB itself – staining is generally absent in surrounding tissue, with prominent nuclear TFEB staining observed in tumours (Argani et al., 2005; Kuiper et al., 2003).

*TFEB* expression was also noted to be elevated in lung cancer and correlated with poor prognosis, while silencing of *TFEB* in lung cancer cell lines resulted in reduced migratory capacity (Giatromanolaki et al., 2015). Likewise, *TFEB* expression was significantly elevated in pancreatic ductal adenocarcinoma (PDAC) samples (Klein et al., 2016). TFEB was seen to localise to both the cytoplasm and the nucleus in

PDAC tumour samples, although several studies indicate that TFEB is primarily nuclear in PDAC cell lines (Klein et al., 2016; Marchand et al., 2015; Perera et al., 2015).

Overexpression of *TFEB* is being studied as a means of eliminating storage material in several disease states, which fall broadly into two categories. First *TFEB* overexpression is being used to promote cellular clearance and improve proteostasis in lysosomal storage diseases including Tay-Sachs disease (Song et al., 2013), multiple sulfatase deficiency (Medina et al., 2011), Gaucher disease (Song et al., 2013) and Pompe disease (Spampanato et al., 2013). The other main therapeutic focus is neurodegenerative conditions, with *TFEB* overexpression countering toxicity in Huntington's disease and Parkinson's disease (Decressac et al., 2013; Tsunemi et al., 2012). Several studies of *TFEB* overexpression indicate that its amelioration of disease phenotypes and symptoms is likely due to its ability to transcriptionally upregulate autophagy and lysosomal biogenesis (Bao et al., 2016; Xiao et al., 2014, Xiao et al., 2015; Zhang & Zhao, 2015).

### 1.2 Post-translational modification and transcription factor function

Post-translational modifications can mediate a broad range of effects on transcription factor function and have been documented to modulate DNA binding, secondary and tertiary structure, association with co-factors, stability and localisation. These modifications, either singly or in concert, provide a means of coordinating the activity of transcription factors both temporally and spatially. The possibilities for functional regulation multiply when considering that a given post-translational modification can also influence the likelihood of subsequent post-translational modifications, each of which may have its own constellation of effects (Li et al., 2016;

Ploper et al., 2015). Additionally, a given modification is capable of inducing one or more of the above effects in one context while triggering different effects in another (Alt et al., 2000; Alt, et al., 2002). Within the context of transcription factor function, the most commonly studied post-translational modifications are phosphorylation, acetylation, methylation, glycosylation, ubiquitination and SUMOylation. Of note, some of these modifications can compete for the same residues, with serine and threonine targeted by phosphorylation and glycosylation and lysine targeted by acetylation, methylation, ubiquitination, SUMOylation and other modifications.

This thesis will examine the effect of post-translational modifications on the function of two members of the TFE transcription factor family. Overall, there does not seem to be consensus for the functional result of a given post-translational modification – e.g., acetylation and phosphorylation can promote or interfere with DNA binding and can promote or interfere with cytoplasmic localisation (Shimano, 2009; Sykes et al., 2006; Yang et al., 1998). Despite the fact that the functional effect of a given post-translational modification on a given protein will likely need to be determined empirically, several examples from the literature will be given to illustrate the spectrum and degree of post-translational modification-dependent alterations of transcription factor function. The primary focus will be on phosphorylation and acetylation as a means of modulating transcription factor DNA binding and subcellular localisation, however other modifications and functional consequences will also be mentioned.

### *1.2.1 Post-translational regulation of DNA binding*

Site-specific DNA binding factors, like those of the TFE family, exert their effects by nucleating complexes that activate, repress, silence or enhance transcription

of target genes, with their ability to carry out these functions dependent upon DNA binding. Several examples of alterations in DNA binding resulting from post-translational modification can be found in the literature and demonstrate ways in which the activity of transcription factors can be dynamically and reversibly regulated.

The tumour suppressor p53 provides an excellent example of the varied ways in which post-translational modifications can regulate transcription factor DNA binding. For example, CK2-mediated p53 phosphorylation stimulates sequence-specific DNA binding, which is thought to be mediated by a conformational change in the DNA binding domain (Hupp et al., 1995). Additionally, phosphorylation of p53 residue S20 promotes DNA binding, however this is by an indirect mechanism. This phosphorylation event facilitates interaction with the transcriptional co-activator p300, which then in turn acetylates p53 in a DNA-dependent manner (Dornan et al., 2003). It is also important to differentiate between the ability of a transcription factor to bind a DNA target and its ability to mediate downstream transcriptional effects. This was illustrated in the case of p53 when phosphorylation of S15 was shown not to be necessary for binding to the *CDKN1A* promoter but was required for subsequent histone acetylation (Loughery et al., 2014).

In addition to phosphorylation, DNA binding can also be influenced by acetylation. Modification of lysine residues by acetylation is wide-spread, with a recent mass spectrometry screen identifying 3600 acetylation sites on 1750 proteins (Gnad et al., 2010). In addition to the phosphorylation examples described above, p53 DNA binding is modified by acetylation. The authors show that residue K120 was rapidly acetylated in response to DNA damage, resulting in a modification of p53 target preference (Sykes et al., 2006). Furthermore, this residue has been found to be mutated in cancer (K120R) and appears to have functional consequences, as it was shown to

impair p53-mediated apoptosis (Sykes et al., 2006). Interestingly, p53 is also acetylated at a different location in its C-terminus by p300. This occurs in the p53 DNA binding domain and augments its sequence-specific DNA binding (Gu & Roeder, 1997).

There are other examples of acetylation altering the DNA binding of transcription factors. The Foxo1 transcription factor is also acetylated by CBP on K242, K254 and K262 – however, unlike acetylation of the p53 C-terminus, these acetylation events decrease the ability of Foxo1 to bind DNA and attenuate its transcriptional activity (Matsuzaki et al., 2005). Foxo1 also provides an example of post-translational modification cross-talk – acetylation of these residues increases PI3K-dependent Foxo1 phosphorylation on S253, possibly because DNA-bound Foxo1 is resistant to phosphorylation on this site (Matsuzaki et al., 2005). Similar to p53, acetylation of the Stat3 C-terminus stimulates its sequence-specific DNA binding and transactivation activity (Wang et al., 2005). Alternatively, acetylation of the DNA binding domain of GATA-1 by p300 attenuates the ability of GATA-1 to bind DNA, illustrating that acetylation of transcription factors is capable both of stimulating and inhibiting DNA binding (Boyes et al., 1998).

Of particular relevance for the study of the TFE family, post-translational modification of other bHLH factors has been shown to affect their DNA binding. For example, acetylation of the bHLH factor MyoD by PCAF results in augmented binding to DNA and increased transcriptional activity (Sartorelli et al., 1999). These acetylation events are constitutive and occur in the vicinity of the MyoD bHLH domain. The mutation of these residues to arginine prevents their acetylation, impairs MyoD transcriptional activity and results in a phenotype very similar to *MyoD* knockout in mice, indicating that acetylation of these residues is key for proper MyoD function both *in vitro* and *in vivo* (Duquet et al., 2006; Polesskaya et al., 2000). In another example of

acetylation of the DNA binding domain of a bHLH transcription factor, BETA2 acetylation by p300 occurs in β cells within the loop region of the bHLH domain (Qiu et al., 2004). Impairing acetylation of these sites led to impaired DNA binding and decreased transcription of the insulin (*INS*) gene.

The sterol response element-binding proteins (SREBPs) provide another example of how acetylation modulates bHLH factor function, of cross-talk between different types of post-translational modification and of multiple modifications targeting a given residue. These proteins are members of the bHLH-LZ family, placing them in the same group as the TFE family. The transcriptional activity of the SREBPs, comprising SREBP-1a, -1c and -2, is regulated by various post-translational modifications, including ubiquitination, acetylation and phosphorylation (Shao & Espenshade, 2012; Shimano, 2009). For example, the SREBP proteins are directly acetylated by p300, with SREBP-1a being acetylated on 3 lysine residues. Two of these lie within the DNA binding domain, and their status affects SREBP-1a transcriptional activity (Shimano, 2009).

### *1.2.2 Post-translational regulation of localisation*

Site-specific phosphorylation has been shown to promote nuclear export in some cases, while prohibiting it in others. One of the earlier studies of this phenomenon demonstrated that the yeast transcription factor Pho4 was exported by the nuclear export shuttle Msn5, with binding of Pho4 and subsequent export only occurring after phosphorylation (Kaffman et al., 1998). Likewise, interfering with phosphorylation of $p27^{Kip1}$ on S10 impaired both XPO1 interaction and nuclear export (Connor et al., 2003). Interestingly, the control of $p27^{Kip1}$ localisation has another layer, as

phosphorylation of another residue, T157, by Akt also promotes cytoplasmic localisation, however this is due to inhibition of importin α-mediated nuclear import (Shin et al., 2005).

Phosphorylation can also promote association with a co-factor, which is then itself responsible for mediating nuclear export. This is the case with Cdc25, where phosphorylation promotes its association with the 14-3-3 protein Rad24, which then appears to serve as an attachable nuclear export signal that mediates XPO1-dependent nuclear export of Cdc25 (Lopez-Girona et al., 1999). Cyclin D1 offers another example of phosphorylation impinging on nuclear-cytoplasmic shuttling, with phosphorylation of T286 facilitating XPO1 binding and nuclear export (Alt et al., 2000). Interestingly, later work indicated that $p21^{Cip1}$ mediated the nuclear accumulation of cyclin D1 by binding to cyclin D1 that had been phosphorylated on T286 by GSK3, preventing XPO1 binding and nuclear export (Alt et al., 2002).

In addition to earlier examples of phosphorylation of p53 affecting its DNA binding, phosphorylation also affects p53 localisation. TAF1-mediated phosphorylation of p53 residue T55 promotes interaction between p53 and the nuclear export shuttle XPO1 and subsequent p53 export and degradation (Cai & Liu, 2008). Interestingly, this phosphorylation results in an effect on p53 DNA binding, with TAF1 phosphorylation leading to dissociation of p53 from target gene promoters (Wu et al., 2014). Likewise, dephosphorylation of the transcription factor NFAT by the phosphatase calcineurin promotes its transcriptional activity by increasing its nuclear localisation. This is brought about by a conformational change that alters the exposure of nuclear localisation and nuclear export signals (NLS, NES) within NFAT (Okamura et al., 2000; Shen et al., 2005).

On the other hand, cyclin B1 offers an example of phosphorylation interfering with nuclear export, with phosphorylation of Cyclin B1 at the G2/M transition interfering with its association with the nuclear export shuttle XPO1 and resulting in nuclear accumulation (Yang et al., 1998). Another example of this is found in HDAC5, whose nuclear export is stimulated by phosphorylation by protein kinases C and D; however, phosphorylation by PKA inhibits its nuclear export, again indicating that the effects of a given post-translational modification (i.e., phosphorylation) on transcription factor function are highly dependent upon context (Ha et al., 2010; Vega et al., 2004).

Foxo1 was mentioned earlier as an example of how post-translational modifications alter DNA binding and transcriptional activity, but phosphorylation and acetylation also serve to regulate its localisation. Phosphorylation of S319 and other nearby residues cooperates with a neighbouring NES to mediate XPO1-dependent nuclear export (Zhao et al., 2004). Interestingly, Foxo1 also harbours an N-terminal NES whose function is modified by the phosphorylation status of T24 promoting cytoplasmic localisation. But the regulation of Foxo1 localisation also depends upon phosphorylation-dependent 14-3-3 protein binding, which is thought to depend on the phosphorylation status of both T24 and S256 (Zhao et al., 2004). Acetylation of Foxo1 also plays a role in regulating its localisation, as deacetylation results in Foxo1 becoming trapped in the nucleus (Frescas et al., 2005).

### 1.3 Summary and aims

Post-translational modifications have been shown to modulate the function of the TFE family members MITF and TFEB. These genes impact development, yield disease phenotypes when either absent or overrepresented and show hallmarks of

master regulators of cellular function. Understanding the mechanisms regulating their access to genomic targets is important. Previous work has focused mainly on different aspects of MITF and TFEB function. MITF is predominantly present in the nucleus, and studies have investigated how post-translational modifications might modify its stability or ability to bind DNA and activate genomic targets. Unlike MITF, TFEB exhibits marked shifts between the cytoplasmic and nuclear compartments, with its post-translational status already shown to be of great importance in mediating nuclear translocation. Our work will continue along these lines, studying the effects of post-translational modifications on MITF DNA binding and on TFEB localisation.

The literature indicates that MITF has a complicated and multifaceted role in development and disease, exerting its effects via binding various types of E-box motifs in regulatory regions of a diverse set of target genes. Confusingly, MITF is able to regulate genes involved in processes that would seem to oppose each other – MITF has been shown to promote both cell cycle arrest and proliferation, to prohibit and encourage tumour formation and to correlate with both decreased invasion and poor prognosis. That is to say that despite a significant body of work on how MITF level affects gene expression and impinges on developmental processes and oncogenesis, the nature of the subset of targets bound in different circumstances and how binding to different subsets might be restricted or facilitated is largely unknown.

TFEB is normally sequestered in the cytoplasm, preventing access to genomic targets. This appears to be primarily mediated by phosphorylation of two residues by mTOR and/or ERK, with phosphorylation promoting cytoplasmic localisation in both cases. Most work to date has focused on the acute events prompting TFEB translocation to the nucleus, as occurs during inhibition of the above kinases, starvation and stress. However, little data exists regarding whether TFEB subsequently returns to

the cytoplasm, under what circumstances this would occur and whether it might be constitutive or actively regulated. TFEB overexpression is being studied as a possible treatment for lysosomal storage diseases and neurodegenerative conditions. With its therapeutic value appearing to depend upon transcriptional activation of target genes, information regarding the influence of TFEB post-translational modifications on its localisation will be of interest.

This thesis will aim to investigate the role of post-translational modifications in regulating the function of two members of the TFE family. In the case of MITF, we aim to confirm both that this protein can be acetylated and that this occurs at particular residues within the DNA binding domain. Additionally, the consequences of such an acetylation event will be assessed *in vitro* and *in vivo*. In the case of TFEB, we will study how expression levels might impact localisation. Also, we will confirm the influence of various signalling pathways and post-translational modifications thought to modulate TFEB localisation and determine the degree to which TFEB nuclear translocation can be reversed. We will examine the mechanism(s) regulating TFEB exit from the nucleus and attempt to determine whether previously detected post-translational modifications impinge on this process.

# Chapter 2: Methods

## 2.1 Reagents

### *2.1.1 Chemicals*

All reactions were performed with autoclaved double-distilled 18 MΩ water. All buffers and solutions were made with double-distilled 18 MΩ water. All chemicals and other reagents were obtained from Sigma-Aldrich (St. Louis, USA) unless otherwise noted.

Glycerol, tris, glycine, acetic acid, sodium dodecyl sulphate (SDS), Tween, ampicillin, chloramphenicol and kanamycin were from Fisher Scientific (Waltham, USA). Triton X-100 was obtained from Merck (Darmstadt, Germany). U0126 was from Cell Signaling Technology (Danvers, USA). SAHA was a gift from Nicholas La Thangue (University of Oxford, Oxford, UK). Torin 1 was from Tocris (Bristol, UK). Paraformaldehyde (PFA) was obtained from Electron Microscopy Science (Hatfield, USA).

### *2.1.2 Antibodies*

| **Antibody** | **Immunogen** | **Source (Catalogue)** | **Dilution (Application)** |
|---|---|---|---|
| α-actin (AC-40) mouse monoclonal | C-terminus | Sigma-Aldrich A4700 | 1:1000 (WB) |
| α-acetyl-lysine rabbit polyclonal | Acetyl-lysine peptide | Cell Signaling 9441L | 1:1000 (WB) |
| α-ERK (C-14) rabbit polyclonal | C-terminus | Santa Cruz sc-154 | 1:10000 (WB) |
| α-FLAG (M2) mouse monoclonal | DYKDDDDK | Sigma-Aldrich F1804 | 1:20000 (WB) |
| α-GAPDH rabbit polyclonal | Residues 314-333 | Sigma-Aldrich G9545 | 1:20000 (WB) |
| α-GFP rabbit polyclonal | Full-length GFP | Abcam ab290 | 1:20000 (WB)<br>1:1000 (IF) |
| α-H3 rabbit polyclonal | Residue 100 to C-terminus | Abcam ab1791 | 1:2000 (WB) |

| | | | |
|---|---|---|---|
| α-MITF mouse polyclonal | C-terminus | Generated in house | 1:5000 (WB) 1:500 (IF) |
| α-p70 S6 Kinase (C-18) rabbit polyclonal | C-terminus | Santa Cruz sc-230 | 1:1000 (WB) |
| α-phospho ERK1/2 (T202/Y204) rabbit polyclonal | Region surrounding T202/Y204 | Cell Signaling 4377 | 1:1000 (WB) |
| α-phospho p70 S6 Kinase (T389) rabbit polyclonal | Region around T389 | Cell Signaling 9205 | 1:1000 (WB) |
| α-TFEB goat polyclonal | Residues 2-14 of human TFEB | Abcam ab2636 | 1:1000 (WB) |
| α-TFEB (3E1-G6) mouse monoclonal | Full-length TFEB | Abnova 7942-M01 | 1:1000 (WB) |
| α-TFEB rabbit polyclonal | Residues 325-375 of human TFEB | Bethyl A303-672A | 1:1000 (WB) |
| α-TFEB rabbit polyclonal | Residues 426-476 of human TFEB | Bethyl A303-673A | 1:1000 (WB) |
| α-TFEB rabbit polyclonal | Region surrounding G412 | Cell Signaling 4240 | 1:1000 (WB) 1:250 (IF) |
| α-tyrosinase mouse monoclonal | Full-length human tyrosinase | Santa Cruz sc-20035 | 1:1000 (WB) |

*2.1.3 Purified Proteins*

Purified GSK3 was obtained from New England Biolabs (NEB; Ipswich, USA).

*2.1.4 Oligonucleotides*

All oligonucleotides were made by Integrated DNA Technologies (Leuven, Belgium).

| **Use** | **Details** | **Sequence** |
|---|---|---|
| Cloning | Clone full-length human MITF into pNIC, forward | TACTTCCAATCCATGCTGGAAAT GCTAGAATATAATCACTATCAGG |
| Cloning | Clone full-length human MITF into pNIC, reverse | TATCCACCTTTACTGCTAACAAG TGTGCTCCGTCTCTTCCATG |

| | | |
|---|---|---|
| Cloning | Clone full-length human TFEB into p3xFLAG-CMV-14, BamHI, forward | AGACGGATCCATGGCGTCACGCATAG |
| Cloning | Clone full-length human TFEB into p3xFLAG-CMV-14, BamHI, reverse | AGACGGATCCGCACAGCACATCGCCC |
| Cloning | Clone full-length human TFEB into pHTN-HaloTag-CMV, EcoRI, forward | AGACGAATTCATGGCGTCACGCATAG |
| Cloning | Clone full-length human TFEB into pHTN-HaloTag-CMV, EcoRI, reverse | AGACGAATTCTCACAGCACATCGCCC |
| Cloning | Clone human TFEB residues 1-159 into nlsCARGO, AgeI, forward | CTAGACCGGTGCCACCATGGCGTCACGCATAGGGTTGCG |
| Cloning | Clone human TFEB residues 1-159 into nlsCARGO, AgeI, reverse | CTAGACCGGTATATCATCCAACTCCCTCTCAGGGTTGG |
| Cloning | Clone human TFEB residues 129-152 into nlsCARGO, EcoRI, forward | CTAGGAATTCACACGTGCTGTCCTCCTCCGCTG |
| Cloning | Clone human TFEB residues 129-152 into nlsCARGO, KpnI, reverse | CTAGGGTACCGTTGGAGCCAATGTGCAGCATGG |
| Cloning | Clone MITF-3xFLAG into pPB-iCMV-MCS, SacII, forward | CTAGCCGCGGGCCACCATGCTGGAAATG |
| Cloning | Clone MITF-3xFLAG into pPB-iCMV-MCS, NotI, reverse | CTAGGCGGCCGCTTACTTGTACAGCTCG |
| Cloning | Clone TFEB-GFP into pPB-iCMV-MCS, SacII, forward | CTAGCCGCGGGCCACCATGGCGTCACGC |
| Cloning | Clone TFEB-GFP into pPB-iCMV-MCS, NotI, reverse | CTAGGCGGCCGCTCACAGCACATCGCCC |
| Cloning | Clone shTFEB1 into pSUPER, BglII, forward | GATCCCCAGACCTATGGGAACAAGTTTGTTCAAGAGACAAACTTGTTCCCATAGGTCTTTTTTA |
| Cloning | Clone shTFEB1 into pSUPER, HindIII, reverse | AGCTTAAAAAAGACCTATGGGAACAAGTTTGTCTCTTGAACAAACTTGTTCCCATAGGTCTGGG |
| Cloning | Clone shTFEB2 into pSUPER, BglII forward | GATCCCCGAGACGAAGGTTCAACATCAATTCAAGAGATTGATGTTGAACCTTCGTCTCTTTTTA |

| | | |
|---|---|---|
| Cloning | Clone shTFEB2 into pSUPER, HindIII reverse | AGCTTAAAAAGAGACGAAGGTTCAACATCAATCTCTTGAATTGATGTTGAACCTTCGTCTCGGG |
| Cloning | Clone shTFEB3 into pSUPER, BglII forward | GATCCCCCCTTGGCTACATCAATCCTTTCAAGAGAAGGATTGATGTAGCCAAGGTTTTTA |
| Cloning | Clone shTFEB3 into pSUPER, HindIII reverse | AGCTTAAAAACCTTGGCTACATCAATCCTTCTCTTGAAAGGATTGATGTAGCCAAGGGGG |
| Site-directed mutagenesis | MITF K206Q mutagenesis forward | AGCATTGGCTAAAGAGAGGCAGAAAC |
| Site-directed mutagenesis | MITF K206Q mutagenesis reverse | ATCAAGTTGTGATTGTCCTGTTTCTGC |
| Site-directed mutagenesis | MITF K206R mutagenesis forward | AGCATTGGCTAAAGAGAGGCAGAAAA |
| Site-directed mutagenesis | MITF K206R mutagenesis reverse | ATCAAGTTGTGATTGTCCCTTTTCTGC |
| Site-directed mutagenesis | mitfa K201Q mutagenesis forward | GCAAAAGAGAGACAAAAGCAGGACAA |
| Site-directed mutagenesis | mitfa K201Q mutagenesis reverse | GAGGTTGTGGTTGTCCTGCTTTTGTCT |
| Site-directed mutagenesis | mitfa K201R mutagenesis forward | CCTGGCAAAAGAGAGACAAAAGAGGG |
| Site-directed mutagenesis | mitfa K201R mutagenesis reverse | GTTGTGGTTGTCCCTCTTTTGTCTCTCT |
| Site-directed mutagenesis | TFEB S138A mutagenesis forward | CCTCCGCTGGCAACGCTGCTCCCAATAGCC |
| Site-directed mutagenesis | TFEB S138A mutagenesis reverse | GGCTATTGGGAGCAGCGTTGCCAGCGGAGG |
| Site-directed mutagenesis | TFEB S138D mutagenesis forward | TCCTCCGCTGGCAACGATGCTCCCAATAGCCC |
| Site-directed mutagenesis | TFEB S138D mutagenesis reverse | GGGCTATTGGGAGCATCGTTGCCAGCGGAGGA |
| Site-directed mutagenesis | TFEB S138E mutagenesis forward | CTCCTCCGCTGGCAACGAGGCTCCCAATAGCCCCA |
| Site-directed mutagenesis | TFEB S138E mutagenesis reverse | TGGGGCTATTGGGAGCCTCGTTGCCAGCGGAGGAG |
| Site-directed mutagenesis | TFEB S142A mutagenesis forward | TGGCAACAGTGCTCCCAATGCCCCCATG |
| Site-directed mutagenesis | TFEB S142A mutagenesis reverse | GGCCATGGGGGCATTGGGAGCACTGTTG |
| Site-directed mutagenesis | TFEB M144A mutagenesis forward | GCTCCCAATAGCCCCGCGGCCATGCTGCACAT |
| Site-directed mutagenesis | TFEB M144A mutagenesis reverse | ATGTGCAGCATGGCCGCGGGGCTATTGGGAGC |
| Site-directed mutagenesis | TFEB M146A mutagenesis forward | CAATAGCCCCATGGCCGCGCTGCACATTGGCTCC |
| Site-directed mutagenesis | TFEB M146A mutagenesis reverse | GGAGCCAATGTGCAGCGCGGCCATGGGGCTATTG |

| | | |
|---|---|---|
| Site-directed mutagenesis | TFEB L147A mutagenesis forward | GCCCCATGGCCATGGCGCACATTGGCTCCA |
| Site-directed mutagenesis | TFEB L147A mutagenesis reverse | TGGAGCCAATGTGCGCCATGGCCATGGGGC |
| Site-directed mutagenesis | TFEB I149A mutagenesis forward | CATGGCCATGCTGCACGCTGGCTCCAACCCTGAG |
| Site-directed mutagenesis | TFEB I149A mutagenesis reverse | CTCAGGGTTGGAGCCAGCGTGCAGCATGGCCATG |
| Site-directed mutagenesis | TFEB S211A mutagenesis forward | GTCACCAGCAGCGCCTGCCCTGCGG |
| Site-directed mutagenesis | TFEB S211A mutagenesis reverse | CCGCAGGGCAGGCGCTGCTGGTGAC |
| ChIP | Human *CDH4* promoter forward | CATGGGTTCACAGAGTCACG |
| ChIP | Human *CDH4* promoter reverse | GGTTGAGTGACTGACCTTCCT |
| ChIP | Human *CDK4* promoter forward | GGAGGAGGGCGAAGAGTGTA |
| ChIP | Human *CDK4* promoter reverse | TCAGAGCAATGTCAAGCGGT |
| ChIP | Human *HDAC4* promoter forward | TGTCTGCGAGCCTAATTCGC |
| ChIP | Human *HDAC4* promoter reverse | AGTATCCAAGATGGACGCCG |
| ChIP | Human *HEXA* promoter forward | CACCCTGCCCTTTGACTTCC |
| ChIP | Human *HEXA* promoter reverse | CTCTACTGGGCCCGTGAAC |
| ChIP | Human *LAMP1* promoter forward | CGTGTCGGCCTGCATCA |
| ChIP | Human *LAMP1* promoter reverse | CTTGTCACGTGAGCTGCG |
| ChIP | Human *PMEL* promoter forward | ATCCCCCAGAGCCCTTTCAT |
| ChIP | Human *PMEL* promoter reverse | GATGGGTACGGGTGAACACA |
| ChIP | Human *PPARGC1* promoter forward | CCCCAGTCACATGACAAAGC |
| ChIP | Human *PPARGC1* promoter reverse | TGACGTCACGAGTTAGAGCAG |
| ChIP | Human *SLC2A1* promoter forward | AAGGCTAAGGGGAGAACCCT |
| ChIP | Human *SLC2A1* promoter reverse | TGGCCCAGCATTCTCATTAGG |
| ChIP | Human *TYR* enhancer forward | CGAGAACATAGAAAAGAATTATGAAA |
| ChIP | Human *TYR* enhancer reverse | CTCTGGCTGGAATCAGGAAG |

| | | |
|---|---|---|
| EMSA | Human *LAMP1* promoter WT forward | CTAGCGCGGCGCAGCTCACGTG ACAAGCGCTGCCGGCCG |
| EMSA | Human *LAMP1* promoter WT reverse | CTAGCGGCCGGCAGCGCTTGTC ACGTGAGCTGCGCCGCG |
| EMSA | Human *LAMP1* promoter C-to-T forward | CTAGCGCGGCGCAGCTCATGTGA CAAGCGCTGCCGGCCG |
| EMSA | Human *LAMP1* promoter C-to-T reverse | CTAGCGGCCGGCAGCGCTTGTC ACATGAGCTGCGCCGCG |
| EMSA | Human *TYR* enhancer WT forward | CTAGACTTGTGGAGATCATGTGA TGACTTCCTGATTCCT |
| EMSA | Human *TYR* enhancer WT reverse | CTAGAGGAATCAGGAAGTCATC ACATGATCTCCACAAGT |
| EMSA | Human *TYR* enhancer mut forward | CTAGACTTGTGGAGATCTCTCTA TGACTTCCTGATTCCT |
| EMSA | Human *TYR* enhancer mut reverse | CTAGAGGAATCAGGAAGTCATAG AGAGATCTCCACAAGT |
| EMSA | Human *TYR* enhancer T-to-C forward | CTAGACTTGTGGAGATCACGTGA TGACTTCCTGATTCCT |
| EMSA | Human *TYR* enhancer T-to-C reverse | CTAGAGGAATCAGGAAGTCATC ACGTGATCTCCACAAGT |
| Gene expression | Human *TFEB*, set 1, forward | TGTTGAAGGTGCAGTCCTACC |
| Gene expression | Human *TFEB*, set 1, reverse | TGATGTGGGCAGCAAACTTG |
| Gene expression | Human *TFEB*, set 4, forward | AGTTGGGAATGCTGATCCC |
| Gene expression | Human *TFEB*, set 4, reverse | ATCCTCCGGATGTAATCCAC |

*2.1.5 Plasmids*

| **Construct** | **Comments** |
|---|---|
| p3xFLAG-CMV-14 | Sigma-Aldrich; mammalian 3xFLAG expression vector |
| p3xFLAG-MITF | Available in the lab |
| p3xFLAG-MITF(K206R) | Available in the lab |
| p3xFLAG-MITF(K206Q) | Available in the lab |
| p3xFLAG-MITF(K225R) | Available in the lab |
| p3xHA-MITF | Available in the lab; used to make 501mel MITF-3xHA stable line |
| p3xHA-MITF(K206R) | Prepared by the candidate; MITF(K206R)-3xHA |
| p3xHA-MITF(K206Q) | Prepared by the candidate; MITF(K206Q)-3xHA |
| pcDNA-p300-HA | Available in the lab; p300-HA |
| pCD-NLBH | Available in the lab; vector containing Rev/Gag/Pol for lentiviral production |

| | |
|---|---|
| pDestTol2CG2-mitfa | Elizabeth Patton, University of Edinburgh; zebrafish expression vector with mitfa under control of the *mitfa* promoter |
| pDestTol2CG2-mitfa(K201R) | Prepared by the candidate; mitfa(K201R) |
| pDestTol2CG2-mitfa(K201Q) | Prepared by the candidate; mitfa(K021Q) |
| p3xFLAG-CMV-14-TFEB | Prepared by the candidate; full-length human flag-tagged TFEB |
| pEGFP-C1-TFE3 | Addgene; GFP-tagged human TFE3 |
| pEGFP-C1-TFEB | Addgene; GFP-tagged human TFEB |
| pEGFP-C1-TFEB(S211A) | Prepared by the candidate; TFEB(S211A)-GFP |
| pEGFP-C1-TFEB(S142A) | Prepared by the candidate; TFEB(S142A-GFP |
| pEGFP-C1-NLS-GST | Available in the lab; GFP-NLS-GST cargo (nlsCARGO) |
| pEGFP-C1-NLS-GST-NES | Available in the lab; nlsCARGO with PKI NES (nlsCARGO-NES) |
| pEGFP-C1-NLS-GST-TFEB(1-159) | Prepared by the candidate; nlsCARGO with TFEB residues 1-159 |
| pEGFP-C1-NLS-GST-TFEB(129-152) | Prepared by the candidate; nlsCARGO with TFEB residues 129-152 |
| pEGFP-C1-NLS-GST-TFEB(1-159)(S142A) | Prepared by the candidate; TFEB(1-159)(S142A)-nlsCARGO |
| pEGFP-C1-NLS-GST-TFEB(129-152)(S142A) | Prepared by the candidate; TFEB(129-152)(S142A)-nlsCARGO |
| pEGFP-C1-TFE3 | Addgene; full-length human GFP-tagged TFE3 |
| pEGFP-C1-TFEB | Addgene; full-length human GFP-tagged TFEB |
| pET28a-MITF(180-296)-His | Available in the lab; His-tagged MITF DNA binding domain for bacterial expression |
| pET28a-MITF(K205Q)(180-296)-His | Available in the lab; K205Q mutation in pET28a-MITF(180-296)-His |
| pET28a-MITF(K205R)(180-296)-His | Available in the lab; K205R mutation in pET28a-MITF(180-296)-His |
| pET28a-MITF(K205Q/K206Q)(180-296)-His | Available in the lab; K205Q/K206Q mutations in pET28a-MITF(180-296)-His |
| pET28a-MITF(K205Q/K206R)(180-296)-His | Available in the lab; K205Q/K206R mutations in pET28a-MITF(180-296)-His |
| pET28a-MITF(K205R/K206Q)(180-296)-His | Available in the lab; K205R/K206Q mutations in pET28a-MITF(180-296)-His |
| pET28aMITF(K205R/K206R)(180-296)-His | Available in the lab; K205R/K206R mutations in pET28a-MITF(180-296)-His |
| pET28a-MITF(K206Q)(180-296)-His | Available in the lab; K206Q mutation in pET28a-MITF(180-296)-His |
| pET28a-MITF(K206R)(180-296)-His | Available in the lab; K206R mutation in pET28a-MITF(180-296)-His |
| pGL3-TYR | Available in the laboratory; -300/+80 bp of the human *TYR* promoter driving luciferase |

| | |
|---|---|
| pHTN-HaloTag-CMV-Neo | Promega; mammalian expression vector with N-terminal HaloTag |
| pHTN-HaloTag-TFEB | Prepared by the candidate; full-length human TFEB with N-terminal HaloTag |
| pMDG-VSV-G | Available in the lab; vector containing VSV for production of lentivirus |
| pNIC28-bsa4 | Available in the lab; His-tagged vector for bacterial expression |
| pNIC28-hMITF-His | Prepared by the candidate; His-tagged full-length human MITF for bacterial expression |
| pNIC28-hMITF(198-302)-His | Sarah Picaud, SGC, University of Oxford; His-tagged human MITF DNA binding domain for bacterial expression |
| pNIC28-hMITF(198-302) (K206Q)-His | Sarah Picaud, SGC, University of Oxford; His-tagged human MITF DNA binding domain with (K206Q) for bacterial expression |
| pPB-iCMV-MCS | Available in the laboratory; piggyBac vector with Tet-On inducible system |
| pPB-iCMV-MITF-3xFLAG | Prepared by the candidate; MITF-3xFLAG in Tet-On with piggyBac transposon elements |
| pPB-iCMV-MITF(K206R)-3xFLAG | Prepared by the candidate; MITF(K206R)-3xFLAG in Tet-On with piggyBac transposon elements |
| pPB-iCMV-MITF(K206Q)-3xFLAG | Prepared by the candidate; MITF(K206Q)-3xFLAG in Tet-On with piggyBac transposon elements |
| pPB-iCMV-TFEB-GFP | Prepared by the candidate; TFEB-GFP in Tet-On with piggyBac transposon elements |
| pPB-iCMV-TFEB(S138A)-GFP | Prepared by the candidate; TFEB(S138A)-GFP in Tet-On with piggyBac transposon elements |
| pPB-iCMV-TFEB(S138D)-GFP | Prepared by the candidate; TFEB(S138D)-GFP in Tet-On with piggyBac transposon elements |
| pPB-iCMV-TFEB(S138E)-GFP | Prepared by the candidate; TFEB(S138E)-GFP in Tet-On with piggyBac transposon elements |
| pPB-iCMV-TFEB(S142A)-GFP | Prepared by the candidate; TFEB(S142A)-GFP in Tet-On with piggyBac transposon elements |
| pPB-iCMV-TFEB(M144A)-GFP | Prepared by the candidate; TFEB(M144A)-GFP in Tet-On with piggyBac transposon elements |
| pPB-iCMV-TFEB(M146A)-GFP | Prepared by the candidate; TFEB(M146A)-GFP in Tet-On with piggyBac transposon elements |
| pPB-iCMV-TFEB(L147A)-GFP | Prepared by the candidate; TFEB(L147A)-GFP in Tet-On with piggyBac transposon elements |

| | |
|---|---|
| pPB-iCMV-TFEB(I149A)-GFP | Prepared by the candidate; TFEB(I149A)-GFP in Tet-On with piggyBac transposon elements |
| pPB-iCMV-TFEB(S211A)-GFP | Prepared by the candidate; TFEB(S211A)-GFP in Tet-On with piggyBac transposon elements |
| pPB-iCMV-TFEB(S142A) (S211A)-GFP | Prepared by the candidate; TFEB(S142A/S211A)-GFP in Tet-On with piggyBac transposon elements |
| pSUPER | Available in the lab; entry vector for shRNA cloning into pTRIP- EF1α-GFP |
| pTRIP-EF1α-GFP | Available in the lab; vector for lentiviral expression of shRNA with GFP selection |
| pTRIP-shTFEB1-GFP | Prepared by the candidate; lentiviral expression vector harbouring shTFEB1, GFP selection |
| pTRIP-shTFEB2-GFP | Prepared by the candidate; lentiviral expression vector harbouring shTFEB2, GFP selection |
| pTRIP-shTFEB3-GFP | Prepared by the candidate; lentiviral expression vector harbouring shTFEB3, GFP selection |

## 2.2 Nucleic Acid Methods

### *2.2.1 Plasmid Purification*

Bacterial cultures were prepared by picking a single colony and inoculating 3 ml of Lysogeny broth (LB) containing the appropriate antibiotic(s). After growing overnight at 37°C with shaking at 225 rpm, the bacteria were pelleted by centrifuging for 3 minutes at 6800 g. Bacterial pellets were processed with a QIAprep Spin Miniprep Kit (QIAGEN, Hilden, Germany), DNA was eluted in water and concentration was measured with a NanoDrop 2000 spectrophotometer (Thermo Scientific, Waltham, USA).

*2.2.2 Agarose gel electrophoresis*

DNA was resolved by size using agarose gels. Agarose (Web Scientific, Crewe, UK) was dissolved in TBE buffer (Invitrogen, Carlsbad, USA; 100 mM Tris, 90 mM boric acid, 1 mM EDTA) and heated in a microwave. The intercalating dye peqGREEN (PEQLAB, Erlangen, Germany) was added to a final concentration of 1:25000, and gels were poured and allowed to cool. Samples were added at the appropriate ratio to 6X Purple Gel Loading Dye (NEB) and run at 120 V in TBE buffer. Migration was monitored with either Hyperladder 1 kb or Hyperladder 50 bp (Bioline, London, UK). Bands were visualised with UV light using a UVIdoc (UVItec, Cambridge, UK). The QIAquick Gel Extraction Kit (QIAGEN) was used to purify excised fragments when necessary.

*2.2.3 Polymerase chain reaction*

Accuprime *Taq* DNA Polymerase High Fidelity (Invitrogen) was used to amplify DNA fragments when high fidelity was necessary. A reaction consisted of 5 ng of template along with 20 pmol of each primer, 5 µl 10x Accuprime PCR Buffer I, 1 unit Accuprime *Taq* High Fidelity enzyme and water to bring the final volume to 50 µl. A T100 Thermal Cycler (Bio-Rad, Hercules, USA) was programmed with an initial step of 94°C for 2 minutes, followed by 35 cycles of a denaturation step (94°C, 20 s), an annealing step (primer-dependent annealing temperature, 20 s) and an extension step (68°C for 1 min/kb of product). After a final extension step of 68°C for 2 min/kb of product, samples were visualised on an agarose gel and purified using the QIAquick Gel Extraction Kit (QIAGEN).

When high fidelity was not needed, MyTaq Red (Bioline) was used. A reaction consisted of 3 ng of template, 5 pmol of each primer, 5 µl of 2x MyTaq Red Mix and water to bring the total volume to 10 µl. Reactions were processed in a T100 Thermal Cycler with the following steps: an initial step of 95°C for 5 minutes, 40 cycles of denaturation (95°C, 15 s), annealing (primer-dependent temperature, 20 s) and extension (72°C, 15 s) and a final extension step of 72°C for 3 minutes. An agarose gel was then used to analyse the PCR products.

*2.2.4 Site-directed mutagenesis*

Mutations were introduced with the QuikChange Lightning Site-Directed Mutagenesis Kit (Agilent, Santa Clara, USA) using primers designed with the QuikChange Primer Design Program (http://www.genomics.agilent.com). Reactions used 20 ng of plasmid DNA, 125 ng of each primer, 1 µl dNTP mix, 1.5 µl QuikSolution, 5 µl 10x buffer, and 1 µl QuikChange Lightning enzyme in a total volume of 50 µl. Samples were then incubated in a T100 Thermal Cycler using the following program: 95°C denaturation for 2 minutes followed by 25 cycles of denaturation (95°C; 15 s), annealing (58°C; 15 s) and extension (68°C; 30 s/kb of plasmid), and a final extension step (68°C; 10 m). Samples were then incubated with 2 µl DpnI at 37°C for 1 hour, followed by transformation into XL10-Gold ultracompetent cells (Agilent). Sanger sequencing was used to screen colonies for successful insertion of point mutations.

*2.2.5 Restriction enzyme digest*

All restriction enzymes were sourced from New England Biolabs. Digests used 2 µg of DNA in a total reaction volume of 20 µl. This included 5 units of enzyme and 2 µl of a suitable 10x reaction buffer, which was found with the NEB Double Digest Finder online tool (https://www.neb.com/tools-and-resources/interactive-tools/double-digest-finder). Digests were performed at 37°C for 2 hours, and samples were analysed by agarose gel electrophoresis. Where required, this was followed by DNA purification with the QIAquick PCR Purification Kit or the QIAquick Gel Extraction Kit (QIAGEN).

*2.2.6 DNA ligation*

Insert and vector DNA were mixed at a molar ratio of (10:1), which was calculated using the online Ligation Calculator tool (http://www.insilico.uni-duesseldorf.de/Lig_Input.html). Ligation reactions used 1 µl of 10x T4 DNA Ligase Buffer and 250 units of T4 DNA Ligase (NEB) in a total volume of 10 µl. Samples were incubated at 16°C overnight, followed by transformation into DH5α chemically competent bacteria (Invitrogen). Colony PCR was used to screen colonies for successful insertion. Hits obtained from the colony PCR were then verified by Sanger sequencing.

*2.2.7 Purification of mRNA*

Cells were grown to 75% confluence, rinsed with cold phosphate-buffered saline (PBS; 137 mM NaCl, 2.7 mM KCl, 10mM $Na_2HPO_4$, 1.8 mM $KH_2PO_4$, pH 7.4) and

scraped from dishes directly in buffer RLT from the RNeasy Mini Kit (QIAGEN). Lysates were homogenised by passing 10x through a 20-gauge needle. Samples were then processed at room temperature according to the manufacturer's instructions. RNA was eluted from the included RNeasy spin columns in water and quantified with a Nandrop 2000 spectrophotometer.

*2.2.8 qPCR*

RNA was obtained as described above, and cDNA was generated from 1 µg of the resulting RNA with the QuantiTect Reverse Transcription Kit (QIAGEN) according to the manufacturer's instructions. Primers for qPCR were chosen to span introns and amplify a region of 100-200 bp. Reactions were performed in duplicate in a total volume of 15 µl using the 2x SensiMix SYBR reagent (Bioline). One reaction contained 7.5 µl of the 2x SensiMix SYBR reagent, 0.5 µl of cDNA, 5 pmol of forward and reverse primers and water to bring the reaction to 15 µl. A Rotor Gene 6000 (Corbett Life Sciences, Sydney, Australia) thermocycler was used to analyse samples according to the following program: initial denaturation (95°C; 10 m), 55 cycles of denaturation (95°C; 5 s), annealing (60°C; 10 s) and extension (72°C; 10 s) and a final melt-curve step where the temperature was raised 1°C every 5 seconds from 72°C to 95°C. Expression levels were obtained by normalising to a housekeeping gene according to the 2-ΔΔC(T) method (Livak and Schmittgen, 2001). This method states that:

$$\text{Relative fold change of target} = 2^{-\Delta\Delta C(T)}$$

where $\Delta\Delta C(T) = (\Delta C(T)[\text{sample}] - \Delta C(T)[\text{reference}])$

and $\Delta C(T) = \Delta C(T)[\text{target}] - \Delta C(T)[\text{housekeeper}]$

## 2.3 Protein Methods

### *2.3.1 Cell extracts*

#### 2.3.1.1 Whole cell extracts

Whole cell extracts were made by the direct addition of 1x Laemmli sample buffer (62.5 mM Tris [pH 6.8], 2% SDS, 10% glycerol, 0.02% bromophenol blue, 5% 2-mercaptoethanol) to the cells in the culture vessel. Cells were scraped with a cell scraper (TPP, Trasadingen, Switzerland), and lysates were collected and sonicated twice for 3 seconds with a probe sonicator (Sonics, Newton, USA). Where samples were prepared by some other means, 2x or 4x Laemmli sample buffer was added to yield a final concentration equating to 1x Laemmli sample buffer. Samples were then incubated at 95°C for 5 minutes and stored at -20°C until use.

#### 2.3.1.2 Subcellular fractionation

To obtain nuclear and cytoplasmic fractions, an adaptation of the Rapid Efficient And Practical method was used (REAP; Suzuki et al., 2010). Briefly, cells were rinsed with cold PBS and scraped in 500 µl of 0.1% NP-40 in PBS. One third of the sample was taken as a whole cell lysate, while the remainder was spun at 13,000 g for 30 seconds. From the supernatant, 150 µl was taken as a cytoplasmic fraction, while the remainder was discarded. The pellet was then washed with 1 ml of 0.1% NP-40 in PBS. After centrifugation at 13,000 g for 30 seconds, the supernatant was discarded. The pellet was resuspended in 1x Laemmli buffer and processed as the nuclear fraction.

*2.3.2 Protein purification*

2.3.2.1 Immunoprecipitation

To detect MITF acetylation, a denaturing immunoprecipitation protocol was used to increase the solubility of MITF-3xFLAG. Cells were first rinsed and scraped in cold PBS, followed by suspension in 200 µl of deep extraction buffer (5 mM EDTA, 10 mM 2-mercaptoethanol, 10 mM nicotinamide, 10 mM sodium butyrate, 1% SDS) supplemented with 1x Complete Protease Inhibitor (PIC; Roche, Basel, Switzerland) and 1x PhosSTOP Phosphatase Inhibitor (Roche). Samples were vortexed for 10 seconds and boiled at 95°C for 5 minutes, followed by dilution 10x in dilution buffer (20 mM Tris [pH 8.0], 137 mM NaCl, 2 mM EDTA, 10 mM nicotinamide, 10 mM sodium butyrate, 1% NP-40) supplemented with 1x PIC and 1x PhosSTOP Phosphatase Inhibitor. After being passed 10x through a 25G needle, samples were incubated for 10 minutes on ice and centrifuged at 10,000 g for 10 minutes at 4°C. An input fraction was taken from the supernatant (5% of the sample), the remainder of which was then incubated with 25 µl of anti-FLAG M2 Magnetic Beads (Sigma-Aldrich) overnight at 4°C with rotation. After washing 3x with ice-cold dilution buffer, bound proteins were eluted by boiling beads for 5 minutes directly in 1x Laemmli sample buffer. Samples were stored at -20°C until analysis.

2.3.2.2 His-tagged protein purification

As for immunoprecipitation, all steps were carried out on ice or at 4°C. For purification of His-tagged murine MITF constructs, pellets of frozen bacteria were thawed on ice and suspended in 10 ml native lysis buffer (50 mM $NaH_2PO_4$, 300 mM NaCl, 10 mM imidazole, 10% glycerol, pH 7.4) supplemented with 1x PIC. After a 10-

minute incubation on ice, lysozyme (0.2 mg/ml) was added, followed by 6 rounds of sonication on ice (12 s on, 18 s off). Lysates were centrifuged at 10,000 g for 30 minutes, and clarified samples were incubated with 50% Ni-NTA slurry in native lysis buffer for 30 minutes at 4°C. This mixture was loaded onto a polypropylene chromatography column (Bio-Rad) that had been equilibrated in native lysis buffer. The column was then washed 2x in wash buffer (50 mM $NaH_2PO_4$, 300 mM NaCl, 20 mM imidazole, 10% glycerol, pH 7.4), followed by elution of bound material with 3 washes of native elution buffer (50 mM $NaH_2PO_4$, 300 mM NaCl, 250 mM imidazole, 10% glycerol, pH 7.4). The fractions were screened by SDS-PAGE, and those containing the target protein were pooled. Glycerol (30%) was added, and the samples were stored at -20°C.

For purification of optimised human His-tagged MITF fragments, samples were again kept at 4°C, and buffers were kept ice-cold. Pellets were thawed on ice, weighed, suspended in 1 volume of lysis buffer (50 mM Tris [pH 9.0], 1 M NaCl, 10 mM imidazole, 5% glycerol), and broken 3x in a constant cell disruptor at 25 Kpsi. Lysates were cleared by centrifugation at 12,000 g for 45 minutes. Supernatants were then passed first over a pre-equilibrated DE-52 column to bind DNA and then over a Ni-NTA column to bind His-tagged proteins. Ni-NTA columns were then washed sequentially with 20 ml lysis buffer, 20 ml wash buffer (50 mM Tris [pH 9.0], 1 M NaCl, 30 mM imidazole, 5% glycerol), and 5 ml of each elution buffer (50 mM Tris [pH 9.0], 1 M NaCl, 100 – 500 mM imidazole, 5% glycerol) in order of increasing concentration of imidazole (100 mM, 150 mM, 250 mM, 500 mM). All fractions were saved and analyzed by SDS-PAGE. Selected elution fractions were pooled and incubated overnight at 4°C with 100 µl of TEV protease (3 mg/ml; provided by SGC, University of Oxford). Samples were concentrated to 5 ml and subjected to gel

filtration. All fractions were collected, analyzed by SDS-PAGE and selected fractions were pooled and analysed by time-of-flight mass spectrometry (TOFMS). Protein was then concentrated to approximately 10 mg/ml, flash-frozen in liquid nitrogen and stored at -80°C in 50 or 100 µl aliquots.

*2.3.3 SDS-PAGE*

SDS polyacrylamide gel electrophoresis (SDS-PAGE) was used to separate proteins by molecular weight. After cleaning the system components (Bio-Rad) in ethanol, 1 mm thick gels were poured. Resolving gels consisted of an appropriate percentage of acrylamide (37.5:1 acrylamide:bis-acrylamide; Severn Biotech, Kidderminster, UK) in a solution of 150 mM Tris (pH 8.8) and 1% SDS to which we added 0.1% APS and TEMED to catalyse polymerisation. A thin layer of isopropanol was layered over this until the resolving gel had polymerised. After removing the isopropanol, the stacking gel was poured. This contained 3.75% acrylamide, 125 mM Tris (pH 6.8), 1% SDS, 0.1% APS and 0.1% TEMED. Samples were prepared as described above (Section 2.3.1.1) and loaded onto gels. Gels were run at 150 V for 60-90 minutes or until the dye front was just leaving the bottom of the resolving gel. The protein ladder Precision Plus Protein All Blue Protein Standard (Bio-Rad) was used to indicate molecular weight.

*2.3.4 Coomassie staining*

Proteins were visualised after SDS-PAGE by Coomassie staining. Briefly, gels were heated in a microwave for 30 seconds in Coomassie staining solution (0.05% Coomassie Brilliant Blue R-250 in 50% methanol and 10% glacial acetic acid). Gels

were then incubated for 10 minutes at room temperature with agitation. After rinsing once with Coomassie destaining solution (25% methanol, 10% glacial acetic acid), gels were placed in the same for 1 hour at room temperature with agitation. The Coomassie destaining solution was periodically replaced, and gels were destained for 1 hour to 18 hours, followed by imaging on a Gel Doc (Bio-Rad).

*2.3.5 Western blotting*

Proteins were transferred from gels onto a Protran nitrocellulose membrane (Whatman, Kent, UK) by electroblotting at 150 mA for 90 minutes on ice. The transfer buffer consisted of 25 mM Tris, 192 mM glycine and 20% methanol. Ponceau staining (0.1% Ponceau S in 5% acetic acid; 5 minutes) was used to assess the efficacy of the transfer and to facilitate cutting the membrane when probing the same membrane with multiple antibodies.

After rinsing off the Ponceau staining solution, membranes were incubated with agitation at room temperature for 1 hour in 5% milk in 0.1% Tween in PBS (PBST) or 5% bovine serum albumin (BSA) in 0.1% Tween in TBS (TBST), depending on the antibody. Primary antibodies are then diluted (see Section 2.1.2 for details) into either 5% milk in PBST or 5% BSA in TBST to match the blocking solution and incubated with membranes overnight at 4°C with agitation. Membranes were then washed 3x in PBST or TBST and incubated with the appropriate horseradish peroxidase (HRP)-conjugated secondary antibody (Bio-Rad) diluted 1:10,000 in 5% milk in PBST or 5% BSA in TBST for 1 hour at room temperature with agitation. After 3 washes in PBST or TBST, membranes were incubated with enhanced chemiluminescence (ECL) reagent

(Amersham, Uppsala, Sweden). X-ray film (Fujifilm, Tokyo, Japan) was exposed to the membranes and developed in a dark room.

*2.3.6 Electrophoretic mobility shift assay (EMSA)*

To investigate the ability of a protein to bind a double-stranded DNA probe, a mixture of the protein and radiolabelled probe of interest were incubated together and run on a native gel. If the protein interacted with the probe, migration through the gel was slowed, resulting in a shift of the band observed after exposing the gel to X-ray film.

Oligonucleotide probes (20 µg each) were annealed in 1x React buffer 3 (Invitrogen) using the following PCR program: 94°C, 2 minutes; 65°C, 10 minutes; 37°C, 10 minutes; 25°C, 10 minutes. The annealed probe (200 ng) was then labelled for 1 hour at 25°C in 1x React buffer 1 (Invitrogen) supplemented with 200 µg/ml BSA, 2 µM dithiothreitol (DTT), 200 µM each of dATP, dTTP, and dGTP, 1µl Klenow polymerase (Invitrogen), and 1.5 µl [α-32P]-dCTP (15 µCi; Perkin Elmer, Waltham, USA). Glycogen (20 µg) was then added, and the reaction brought up to 50 µl with water. Probes were extracted twice through 1 volume of phenol-chloroform and precipitated overnight in 1 volume ammonium acetate (5 M) and 6 volumes ethanol at -20°C. The probe was then recovered by centrifugation (16,000 g; 30 m) and suspended in water.

Purified protein (1 µl) was then added to 14 µl of band shift buffer (25 mM HEPES [pH 7.4], 150 mM KCl, 200 µg/ml BSA, 5 µM DTT) on ice. Where competing unlabelled oligonucleotides were used, these were added to the reaction at this point in a total volume of 1 µl. These samples were then incubated at room temperature for 15

minutes with 1 µl of labelled probe and loaded on a native gel containing 6% acrylamide (44% stock solution; 29:1 acrylamide:bis-acrylamide), 0.5x TBE (Gibco, Waltham, USA), 0.09% APS and 0.09% TEMED. After running for 90 minutes at 180V, gels were dried under vacuum for 1 hour at 80°C. Dried gels were then exposed to autoradiography film, which was developed after exposure for 18-96 hours at -80°C.

*2.3.7 Chromatin immunoprecipitation (ChIP)*

Cells were grown in 15 cm dishes to approximately 75% confluency, followed by rinsing 3x in cold PBS and fixation for 15 minutes in 0.4% paraformaldehyde with agitation at room temperature. The fixation reaction was then quenched with glycine (200 mM) for 15 minutes at room temperature with agitation. After again washing 3x in cold PBS, cells were scraped, collected and centrifuged at 1500 g for 5 minutes. After discarding the supernatant, the cell pellets were suspended in ChIP lysis buffer (50 mM Tris [pH 8.0], 10 mM EDTA and 1% SDS) supplemented with 1x PIC and sonicated for 15 minutes in a Covaris S220 focused ultrasonicator (Covaris, Woburn, USA). An aliquot of each sample was taken to evaluate the sonication, while the remainder of the sample was stored at -80°C. This was also used to quantify the chromatin and was used as an input fraction.

Chromatin was processed by diluting into ChIP dilution buffer (16.7 mM Tris [pH 8.0], 167 mM NaCl, 1.2 mM EDTA, 0.01% SDS and 1% Triton X-100). This was then incubated at 4°C with rotation for 1 hour with 25 µl of 50% protein G sepharose slurry (Roche) that had been blocked with 0.5 mg/ml BSA and 0.5 mg/ml sonicated salmon sperm DNA. This was followed by incubation with 25 µl of FLAG-conjugated dynabeads (for FLAG-tagged proteins) or 3 µg of anti-HA antibody (for HA-tagged

proteins) at room temperature for 1 hour with rotation. For HA-tagged proteins, this was followed by another incubation with 25 µl of 50% protein G sepharose slurry at 4°C with rotation for 1 hour. Beads were washed twice for 15 minutes in each of the following solutions in sequence: low salt buffer (20 mM Tris [pH 8.0], 150 mM NaCl, 2 mM EDTA, 0.1% SDS and 0.1% Triton X-100), high salt buffer (20 mM Tris [pH 8.0], 500 mM NaCl, 2 mM EDTA, 0.1% SDS and 0.1% Triton X-100), LiCl wash buffer (250 mM LiCl, 10 mM Tris [pH 8.0], 1 mM EDTA, 1% NP-40 and 1% sodium deoxycholate) and TE buffer (10 mM Tris [pH 8.0], 1 mM EDTA). Elution buffer (100 mM $NaHCO_3$) was added (250 µl) to the beads for 15 minutes at room temperature to elute chromatin. This was repeated a second time, and elution fractions were pooled.

To reverse crosslinks, the same protocol was used for both the small evaluation sample and the larger bulk of the sample, which was only processed after verifying proper sonication. Briefly, samples were incubated at 65°C overnight in 300 mM NaCl supplemented with 10 µg RNAse A (Invitrogen). The next day samples were brought to a final concentration of 4 mM Tris (pH 8.0) and 10 mM EDTA and incubated with 20 µg Proteinase K (Fermentas, Waltham, USA) at 42°C for one hour. Samples were extracted through phenol-chloroform and then through chloroform. DNA was then precipitated by bringing samples to a final concentration of 300 mM sodium acetate and adding 1 µg glycogen. To this we added 2 volumes 100% ethanol and incubated samples overnight at -20°C. The next day, samples were centrifuged at 13,000 g for 30 minutes, and pellets were resuspended in 50 µl water after being washed in 70% ethanol. Samples were then processed for qPCR as detailed previously. The enrichment of a given PCR product was calculated relative to the amount of that target in the input sample.

*2.3.8 Peptide SPOT kinase assay*

Peptides 19 amino acids long were synthesised on cellulose membranes using SPOT technology (Winkler et al., 2009; membranes provided by Sarah Picaud, SGC, Oxford, UK). First, membranes were rinsed with 95% ethanol, followed by washing 5x with TBST. GSK3 kinase (NEB) was then prepared in a reaction mixture comprising 50 ng of kinase, 200 μM ATP (Sigma-Aldrich) and 8 μCi [γ-32P]-ATP (Perkin Elmer) in 1.5 ml of 1x NEBuffer for Protein Kinases (NEB). The reaction mixture was then placed on the membrane, which was incubated at 30°C for 30 minutes. The membrane was then washed 15x with NaCl (1 M), followed by washing 10x with water. Next, the membrane was washed with stripping buffer (1% SDS, 8 M urea, 0.5% 2-mercaptoethanol) for 1 hour at 40°C. This was followed by washing 10x in water and a final wash in 95% ethanol. After air drying the membrane for 10 minutes, it was exposed to a phosphor screen overnight for 3 hours. Images were acquired with a PMI phosphorimager (Bio-Rad).

## 2.4 Bacterial Methods

*2.4.1 Growth Conditions*

Unless otherwise indicated, liquid bacterial cultures were grown at 37°C with shaking at 225 rpm overnight in LB consisting of 1% bactotryptone, 1% NaCl and 0.5% yeast extract (pH 7.5). This was supplemented with one or more of the following antibiotics: ampicillin (100 μg/ml), kanamycin (30 μg/ml), chloramphenicol (50 μg/ml). For solid cultures, bacteria were streaked on agar plates made by dissolving 1.5% agar in LB supplemented with the appropriate antibiotics and poured into 10 cm Petri dishes (Sterilin, Newport, UK). After storage at 4°C, plates were warmed for one hour at 37°C

before streaking with bacteria. They were then incubated at 37°C upside down overnight before colonies were picked the following day.

*2.4.2 Bacterial Strains*

Unless otherwise noted, bacterial work was conducted with *E. coli* strain DH5α (F- Φ80lacZΔM15 Δ[lacZYA-argF] U169 recA1 endA1 hsdR17[rk-, mk+] phoA supE44 thi-1 gyrA96 relA1 λ-) sourced from Invitrogen. For site-directed mutagenesis, *E. coli* strain XL-10 Gold ultracompetent cells (TetrΔ(mcrA)183 Δ(mcrCB-hsdSMR-mrr)173 endA1 supE44 thi-1 recA1 gyrA96 relA1 lac Hte [F' proAB lacIqZ ΔM15 Tn10 (Tetr) Amy Camr]) were obtained from Agilent.

Expression of recombinant proteins was done in either *E. coli* strain BL21(DE3) with genotype F- ompT hsdSB (rB-mB-) gal dcm (DE3) (Invitrogen) or *E. coli* strain Rosetta(DE3)pLysS with genotype F-ompT hsdSB (rB-mB-)gal dcm(DE3) pRARE (CamR) (P. Filippakopoulos, University of Oxford, UK).

*2.4.3 Transformation of competent bacteria*

Chemically competent bacteria were transformed by thawing on ice and aliquoting 20 µl into pre-chilled 1.5 ml Eppendorf tubes. DNA was added to the bacteria, and samples were incubated on ice for 20 minutes. Cells were then heat shocked at 42°C for 30 seconds, followed by incubation on ice for 5 minutes. A volume of 180 µl of S.O.C. medium (2% tryptone, 0.5% yeast extract, 10 mM $MgSO_4$, 10 mM $MgCl_2$, 10 mM NaCl, 2.5 mM KCl and 20 mM glucose) was then added to the samples,

which were incubated at 37°C in a shaking incubator with rotation at 225 rpm. Samples were then spread on pre-warmed plates containing the appropriate antibiotics.

*2.4.4 Expression of recombinant protein*

For initial expression of murine His-tagged MITF fragments, BL21(DE3) were transformed, and bacteria were streaked on plates containing the appropriate antibiotics. The following day, 3 colonies were pooled and grown overnight in 3 ml LB. The next day this culture was inoculated into 100 ml LB containing the appropriate antibiotics and grown until $OD_{600}$ ~ 0.8. Isopropyl β-D-1-thiogalactopyranoside (IPTG) was added to a final concentration of 500 μM to induce protein expression. After another 6 hours, bacteria were harvested by centrifugation, and pellets were frozen at -20°C until purification.

For expression of optimised human His-tagged MITF fragments, constructs were transformed into Rosetta (Novagen, Kenilworth, USA). After streaking plates and incubating them overnight, 3 colonies were selected, pooled and inoculated into 12 ml LB. The following morning a portion of this was diluted 100x into Terrific Broth (TB; 17 mM $KH_2PO_4$, 72 mM $K_2HPO_4$, 1.2% tryptone, 2.4% yeast extract, 0.4% glycerol) containing the appropriate antibiotics and grown until $OD_{600}$ ~ 2.3. Cultures were induced with IPTG (500 μM) overnight at 18°C. Bacteria were then pelleted by centrifugation and frozen until purification at -20°C.

## 2.5 Cell Biology Methods

### *2.5.1 Flow cytometry*

A BD FACSCanto flow cytometer (BD Biosciences, San Jose, USA) was used to process cells for flow cytometry. For analysis of GFP expression, cells were trypsinised, centrifuged at 500 g for 5 minutes, resuspended in FACS staining solution (5% foetal bovine serum [FBS], 0.1% sodium azide in PBS) and processed on the flow cytometer. Between 5,000 and 20,000 events were counted for each sample. Analysis was done with BD FACSDiva software (BD Biosciences).

### *2.5.2 Luciferase reporter assay*

We used a vector harbouring luciferase under the control of the *TYR* promoter to measure MITF transcriptional activity. Cells were plated in 24-well plates and transfected when they had reached 50-75% confluence. After 24 hours, cells were lysed with Passive Lysis Buffer (Promega, Madison, USA) for 30 minutes on a rocking platform at 4°C. Plates were centrifuged at 100 g for 1 minute to pellet cell debris, and 20 µl of cell lysate was carefully aspirated from the 24-well plate and mixed with 50 µl of Luciferase Assay Reagent (Promega) in a 96-well plate. For measurement of luminescence, these plates were then fed into a GloMax-Multi Microplate Multimode Reader machine (Promega).

### *2.5.3 Fluorescence live cell imaging*

Cells were plated in 6-well or 12-well plates. If the experimental setup did not involve altering the culture medium during the experiment, plates were then placed on

the stage of a Nikon TE 2000-E Eclipse inverted microscope in a climate-controlled (37°C; 10% $CO_2$) incubation chamber. After being allowed to acclimate for 1 hour, images were acquired with a Hamamatsu Orca-ER C4742-95 camera and Metamorph software (Molecular Devices, Sunnyvale, USA). If a timelapse series was needed, this image served as the initial timepoint, with subsequent imaging being automated via the Metamorph software. The multidimensional acquisition option was used to capture DAPI, GFP and RFP channels as required, with the system set to autofocus for every exposure.

If the experimental design required altering the culture medium during the course of the experiment, this was done by pausing the system, carefully opening the doors of the incubator and lifting the lid off the plate. Where medium was exchanged for medium lacking a factor, existing medium was aspirated, cells rinsed once with the medium to be added, the new medium added and the plate replaced on the stage. After restarting the machine, two cycles of imaging were observed to ensure that the field of view and focus had not drifted. Where a factor was added or replenished, as in experiments involving addition of inhibitors or replenishment of nutrients, the lid of the plate was removed and the plate left in position on the stage. Medium containing the factor at 10x the final concentration was then carefully added dropwise to the medium. The lid was then replaced, and imaging was observed for two cycles as before to ensure that the field of view and focus had not drifted.

Images were acquired with Metamorph software and processed in ImageJ. Background correction was done in an automated batch fashion using a macro written by Mark Shipman (LICR, University of Oxford). For quantification of TFEB localisation, cells were classified into two groups according to whether TFEB was primarily nuclear or not. This was done by opening acquired images in ImageJ and

using the region of interest (ROI) tool to select nuclear and cytoplasmic regions. If the mean signal intensity in the nuclear ROI was greater than that in the cytoplasmic ROI, the cell was classified as having primarily nuclear TFEB. Multiple fields of view were counted, and results were expressed as the percentage of cells assayed that had primarily nuclear TFEB.

*2.5.4 Immunofluorescence*

Cells were grown to 75% confluency on circular glass coverslips (VWR, Radnor, USA) in 24-well plates. At this point cells were either transfected or treatments were administered. For transfected cells, treatments were administered 18 hours after transfection unless otherwise noted. To process coverslips for imaging, cells were fixed in 3.7% formaldehyde in PBS for 10 minutes at room temperature with agitation, followed by permeabilisation in 0.2% Triton X-100 in PBS for 20 minutes at room temperature with agitation. Coverslips were then blocked in 4% BSA in PBS at room temperature for 20 minutes with agitation. Primary antibodies were diluted 1:500 unless otherwise noted (see Section 2.1.2) into 4% BSA in PBS and added to coverslips for 20 minutes at room temperature upside down on PARAFILM M (Sigma-Aldrich). After washing for 3x in PBS for 3 minutes each, secondary antibodies were added (1:500) in a solution of 4% BSA in PBS for 20 minutes at room temperature upside down on PARFILM M in the dark. DAPI was added to the secondary antibody solution to stain nuclei (1:2000). Coverslips were then mounted on glass microscope slides (VWR) with Mowiol mounting medium (Sigma-Aldrich). A Zeiss LSM710 and accompanying Zen software were used to acquire confocal images (Zeiss, Oberkochen, Germany).

## 2.6 Mammalian Cell Methods

### *2.6.1 Cell culture*

All cell lines were available from laboratory stocks and were grown in monolayers at 37°C in humidified air containing 10% CO2. Human melanoma lines were grown in Roswell Park Memorial Institute Medium-1640 (RPMI; Gibco) supplemented with 10% foetal bovine serum (FBS), while all other cell lines were grown in Dulbecco's Modified Eagle Medium (DMEM; Gibco) supplemented with 10% FBS. For studies of glucose starvation, 10% dialysed FBS was substituted for 10% FBS. For general maintenance, cells were grown to 90% confluence and passaged by trypsinisation. This involved aspirating the medium, rinsing the culture vessel with PBS and adding 0.05% trypsin-EDTA. After incubating at 37°C for 5 minutes, two volumes of complete medium were added to inactivate trypsin. The cell suspension was then centrifuged at 100 g, supernatant was aspirated and discarded and cells were resuspended and plated in an appropriately sized culture vessel at a density that would result in approximately 75% confluence at the time of harvesting or analysis.

For storage, cells were trypsinised as detailed above and resuspended in FBS supplemented with 10% dimethyl sulfoxide (DMSO). Cells were then aliquoted into Cryovials (Thermo Scientific, Waltham, USA), placed into a Mr Frosty (Thermo Scientific) and stored at -80°C for 24 hours. Cells were then transferred to liquid nitrogen. Cells were thawed by incubating at room temperature, followed by plating into an appropriate culture vessel containing complete medium. After several hours, this medium was carefully aspirated and replaced with fresh complete medium to remove residual DMSO.

*2.6.2 Transient transfection of DNA*

Cells were plated and grown for at least 24 hours before transfection using FuGENE 6 (Promega) or Lipofectamine 2000 (Fisher Scientific). Cells were transfected at 50-75% confluence in serum-free Opti-MEM (Invitrogen) according to the manufacturer's instructions. First, FuGENE 6 or Lipofectamine 2000 was incubated at room temperature in Opti-MEM for 5 minutes, followed by the addition of DNA and a further incubation of 15 minutes. The transfection mixture was then added drop-wise to cells. Cells were analysed within the next 72 hours.

*2.6.3 Stable transfection of DNA*

Low-passage cells were transfected as described above and 48 hours later were trypsinised. For the generation of polyclonal pools stably expressing ectopic MITF or TFEB, cells were plated at a confluency of 25% in appropriate selection medium, which consisted of complete medium with the addition of puromycin (300 ng/ml) and/or neomycin (1 mg/ml). Medium was replaced every 2 days for 14 days, and cells were then analysed. For GFP-tagged proteins, this consisted of administering a range of doxycycline concentrations, followed by evaluation of ectopic protein expression by Western blotting and live cell fluorescence imaging. For FLAG-tagged proteins, a range of doxycycline concentrations was again administered, and ectopic protein expression was assessed by Western blotting. For the generation of monoclonal cell lines, cells were again plated at approximately 25% confluency, transfected, and allowed to reach confluency. At this point, cells were trypsinised and plated in 10 cm dishes at several different dilutions, ranging from 1:1000 to 1:100,000. Selection medium was replaced every 3 days until colonies were visible. A dish containing

colonies that were well-separated was chosen, and colonies were aspirated with a pipet tip and plated in selection medium in 24-well plates. Clones were expanded until sufficient cells for analysis were available. Analysis consisted of induction with a range of doxycycline concentrations followed by Western blotting to evaluate the level of ectopic protein expression and immunofluorescence studies to evaluate clonality. . Acceptable clones were expanded, frozen and stored in liquid nitrogen.

*2.6.4 Lentiviral transduction*

Phoenix cells were seeded in 15 cm dishes that had been coated in poly-L-lysine. Cells were transiently transfected at approximately 50% confluency using Lipofectamine 2000. The transfection mixture contained an shRNA-harbouring pTRIP vector (5 μg) and the two lentiviral packaging vectors pCD-NLBH (4 μg) and pMDG-VSV-G (3 μg). The next day the medium was replaced, with virus-containing medium collected on both of the next two days. This was filtered through a 0.45 μm syringe, diluted into Hank's Balanced Salt Solution (HBSS; Gibco) containing 4 μg/ml polybrene and added to cells that had been seeded in a 24-well plate. Cells were assessed for GFP expression by FACS 48 hours after transduction.

**2.7 Animal Methods**

*2.7.1 Zebrafish melanocyte rescue assay*

Zebrafish were cared for by standard methods (Westerfield, 2000). The zebrafish *mitfa* cDNA was placed under control of a 2.1 kb fragment of the zebrafish *mitfa* promoter in the Gateway Tol2 vector pDestTol2CG2 (Kwan et al., 2007).

Constructs (50 pg) were injected along with mRNA encoding the *Tol2* transposase (70 pg) into *mitfa*$^{w2}$ (*nacre*) mutant embryos at the one-cell stage (Lister et al., 1999). Embryos were then incubated at 28.5°C. At 3 dpf, embryos were dechorionated, anesthetised in tricaine (160 μg/ml) and imaged under a stereomicroscope. Embryos were then fixed and stored in 4% PFA for melanocyte counting.

# Chapter 3: MITF mutant K206Q has altered function

## 3.1 Introduction

The bHLH-LZ transcription factor MITF has been shown to regulate a plethora of genes involved in diverse and, sometimes, seemingly opposing processes. A rheostat model has been proposed to explain how MITF might be able to accomplish this, with a spectrum of MITF activity resulting in a spectrum of transcriptional outputs (Carreira et al., 2006). Although MITF protein level affects the expression of its target genes, this single variable might not be sufficient to understand how MITF mediates transcription of its many targets. Post-translational modifications have been posed as an additional means by which MITF activity might be fine-tuned (Carreira et al., 2006; Cheli et al., 2010; Hoek & Goding, 2010). Indeed, previous studies have shown the functional output of MITF to depend both on protein level and qualitative alterations to the protein itself via post-translational modifications (Carreira et al., 2005; Lister et al., 2014; Miller et al., 2005; Murakami & Arnheiter, 2005).

In a survey of dozens of MITF targets, two very similar motifs were highly represented in the regulatory regions of genes regulated by MITF – 5'-CATGTG-3' and 5'-CACGTG-3' (Cheli et al., 2010).One of these, the 5'-CATGTG-3' motif, lies at the core of the M-box motif found in the promoters and enhancers of several genes involved in melanocyte differentiation (Lowings, 1992). For example, the promoter of the mouse *tyrosinase* gene was found to contain 2 instances of the 5'-CATGTG-3' motif, one approximately 70 bp upstream of the TATA box and one near the initiator site (Bentley et al., 1994; Bertolotto et al., 1996). MITF binds to both of these sites to stimulate transcription, and also binds to another 5'-CATGTG-3' motif approximately 2 kb upstream in an enhancer region (Bentley et al., 1994; Bertolotto et al., 1996; Yasumoto et al., 1994). M-box motifs also play a crucial role in the regulation of the *TYRP1* and *TYRP2* genes, as MITF binds to 5'-CATGTG-3' elements in the promoters

of these genes to stimulate transcription (Bertolotto et al., 1998b). Another gene involved in melanosome biogenesis, *GPR143*, also harbours a 5'-CATGTG-3' motif, which was shown to mediate MITF binding and transcriptional activation of this gene (Vetrini et al., 2004).

This would seem to indicate that by steering MITF towards or away from the 5'-CATGTG-3' motif, genes involved in melanocyte differentiation could be differentially targeted. The 5'-CATGTG-3' motif falls within the larger category of E-box motifs (5'-CANNTG-3'), which are bound by many bHLH transcription factors. If the combination of the 5'-CATGTG-3' motif and specific flanking residues permitted binding by MITF but precluded binding by other bHLH-LZ factors, this could provide a way to prevent widespread activation of genes involved in melanocyte differentiation by other bHLH factors (Aksan & Goding, 1998).

However, other variants of the E-box (5'-CANNTG-3') play functional roles in the expression of pigmentation genes. For example, the effects of MITF on transcription of the melanocyte-specific gene *MLANA* depended on both a 5'-CATGTG-3' motif and a 5'-CACGTG-3' motif, the latter comprising the other main class of MITF binding motif (Du et al., 2003). On the other hand, 5'-CATGTG-3' motifs are also present in MITF targets not directly involved in melanocyte differentiation. MITF was shown to target cyclin-dependent kinase 2 (*CDK2*), activating its expression and promoting melanoma growth. This was dependent upon the same 5'-CATGTG-3' motif that regulates expression of *PMEL*, another gene involved in melanosome biogenesis (Du et al., 2003; Du et al., 2004).

Thus, it is unclear if the MITF binding motif 5'-CATGTG-3' demarcates a functional "category" of genes involved in melanocyte differentiation. Moreover, the

regulation of MITF target specificity is likely to depend on many factors in addition to the sequence of the binding site. For example, as MITF binds DNA as a dimer, the nature of its binding partner could modulate its preference for a given target motif. MITF has been shown to heterodimerise with the other 3 members of the TFE family, and it is possible that different heterodimers could exhibit altered target specificity. Alternatively, asymmetric post-translational modification of one member of an MITF hetero- or homodimer could impact its DNA binding. Additionally, directing MITF to a subset of its possible target genes could be accomplished in other ways – by varying the nature of the target (e.g., methylation or chromatin state) or the nature of MITF co-factors, (e.g., amount or post-translational status).

This chapter will attempt to extend the MITF rheostat model by examining the effect of an acetylation-mimicking mutation on the ability of MITF to bind two motifs commonly observed in its target genes. Additionally, we will study the functional consequences of this mutation in cell culture and *in vivo*.

## 3.2 Results

### *3.2.1 MITF can be acetylated in melanoma cells*

Initial studies in our laboratory indicated that MITF ectopically expressed in HEK 293 cells could be acetylated on multiple sites by p300/CBP. To confirm these findings in the context of a melanoma cell line, we attempted to demonstrate acetylation of endogenous MITF. Unfortunately, after multiple attempts, we failed to immunoprecipitate sufficient endogenous MITF from 501mel or SK-MEL-28 cells to assess MITF acetylation (data not shown). This is possibly because MITF is poorly extractable from the nucleus, with over 90% being retained in an insoluble pellet after

extraction using nuclear extraction buffer (20 mM HEPES [pH 7.9], 420 mM NaCl, 1.5 mM MgCl2, 0.2 mM EDTA, 0.5 mM DTT, 25% glycerol), followed by chromatin digestion with Lysonase (Merck) bioprocessing reagent (Pakavarin Louphrasitthiphol, personal communication). As we had struggled to find an antibody against MITF that was suitable for immunoprecipitation, we used MITF-negative IGR39 melanoma cells to generate a cell line stably expressing tetracycline-inducible MITF-3xFLAG (IGR39 iMITF-3xFLAG). This would allow us to take advantage of the high affinity and specificity of the FLAG tag system (Lichty et al., 2005). A stable cell line expressing 3xFLAG (IGR39 i3xFLAG) was generated for use as a negative control. We screened for those clones showing the least leakiness in the absence of doxycycline induction and a progressive increase in expression in response to increasing doses of doxycycline (data not shown).

Figure 3.1 shows the most promising clone expressing inducible MITF-3xFLAG. These cells were induced with increasing doses of doxycycline and assessed by Western blotting and immunofluorescence. Probing with a FLAG antibody showed that MITF-3xFLAG ran as a doublet just under the 75 kDa marker (Figure 3.1a). This migration pattern has been noted in previous studies, which have indicated that these two bands may correspond to differentially phosphorylated species of MITF (Hemesath et al., 1998). These bands progressively increased in intensity with increasing doses of doxycycline, indicating that the inducible feature of our system was working properly. It should be noted that MITF-3xFLAG was expressed at low levels in the absence of doxycycline; other reports have also seen that tetracycline-inducible systems often suffer from leakiness (Urlinger et al., 2000).

To further verify that the bands detected by the FLAG antibody indeed corresponded to MITF-3xFLAG, we probed lysates with an antibody against MITF,

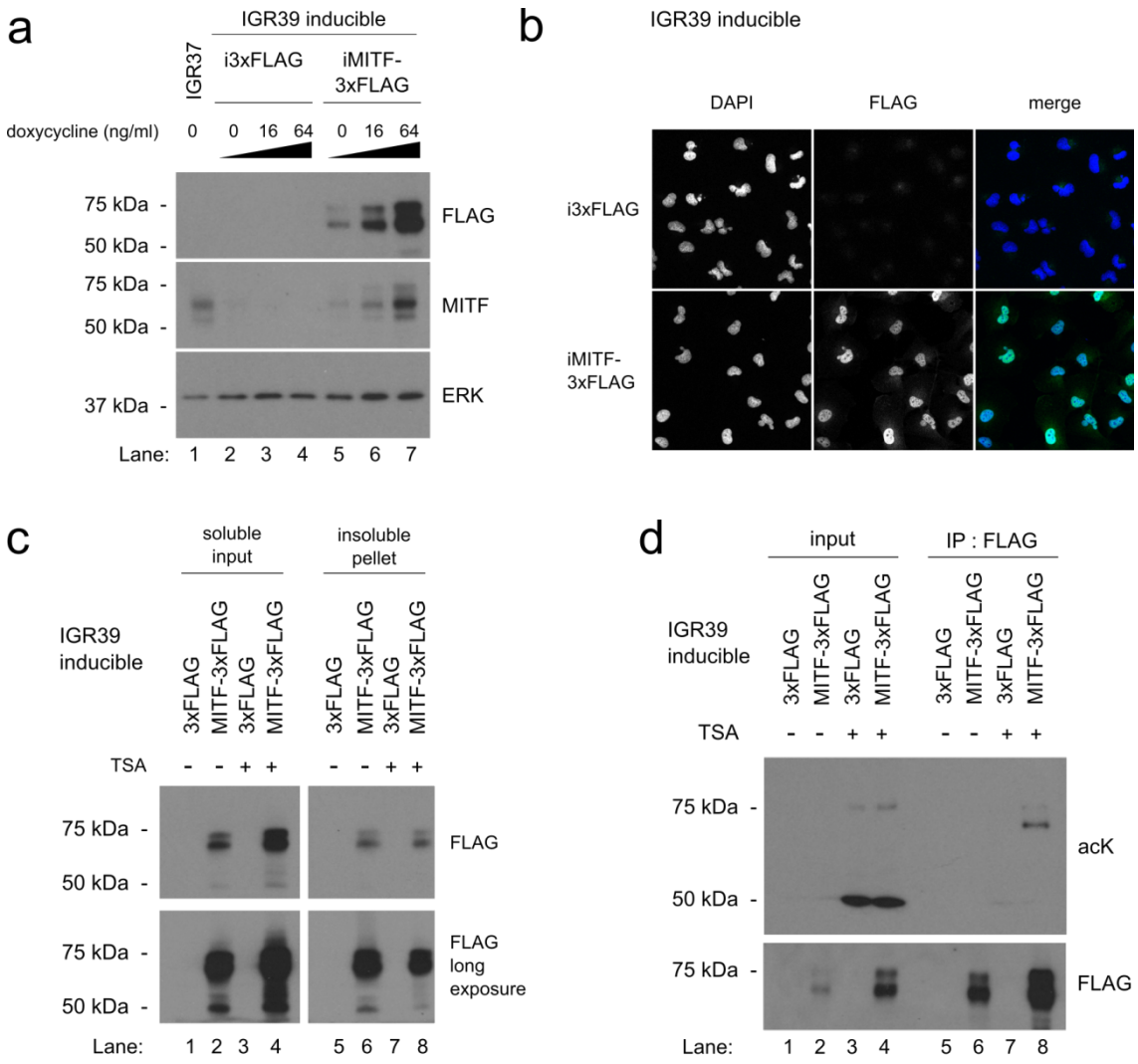



**Figure 3.1. MITF-3xFLAG is acetylated in IGR39 melanoma cells during HDAC inhibition.** FLAG-tagged murine MITF was inducibly overexpressed in IGR39 melanoma cells, immunoprecipitated and probed with an antibody against pan-acetyl-lysine. (a) IGR39 cells expressing inducible 3xFLAG or inducible MITF-3xFLAG were either left uninduced or induced with 16 or 64 ng/ml doxycycline for 24 hours. Whole cell lysates were blotted with antibodies against FLAG and MITF, with ERK serving as a loading control. (b) The same cell lines as in (a) were plated on glass coverslips and induced with 16 ng/ml doxycycline for 24 hours. Cells were then fixed and stained with an antibody against FLAG and with DAPI to label nuclei. Images were acquired by confocal microscopy. (c) The same cell lines as in (a) were induced as before in the presence or absence of trichostatin A (TSA; 400nM, 6 hours) and processed for FLAG immunoprecipitation. The soluble input and insoluble pellet fractions were then screened with an antibody against FLAG to determine the degree to which MITF-3xFLAG was solubilised. (d) The input and FLAG immunoprecipitation (IP) fractions from the same experiment as in (c) were probed with antibodies against pan-acetyl-lysine (acK) and FLAG.

including the MITF-expressing IGR37 melanoma cell line as a positive control (Figure 3.1a; lane 1). We noted that the IGR39 cell line expressed a very low level of

endogenous MITF, consistent with what has been reported by others (Sáez-Ayala et al., 2013). Although the two bands likely comprising the MITF-3xFLAG doublet seen with the FLAG antibody appeared to also be detected by the MITF antibody, there is a third, minor species detected that appeared lower, just over the 50 kDa marker (Figure 3.1a; lane 7). This band increased in intensity with higher doses of doxycycline, making it possible that it corresponded to either a MITF-3xFLAG degradation product, a species arising via internal ribosome entry, or a differentially modified species that is more efficiently detected with the MITF antibody than with the FLAG antibody (Figure 3.1a). Alternatively, comparison with the migration of endogenous MITF (Figure 3.1a; lane 1) in IGR37 cells indicates that this could represent endogenous MITF whose expression has been activated in IGR39 cells by ectopic MITF-3xFLAG. It is also possible that endogenous MITF was induced in IGR39 iMITF-3xFLAG cells by doxycycline treatment alone; however, doxycycline did not activate expression of endogenous MITF in IGR39 i3xFLAG cells (lanes 2-4), making this explanation less likely.

To verify the localisation of MITF-3xFLAG, we plated IGR39 i3xFLAG and IGR39 iMITF-3xFLAG cells on glass coverslips, induced them with doxycycline (16 ng/ml; 24 hours), fixed them and stained them with an antibody against FLAG and with DAPI. The majority of cells showed primarily nuclear staining with the FLAG antibody, which is consistent with the localisation of endogenous MITF (Figure 3.1b; Carreira et al., 2006). Having confirmed that MITF-3xFLAG was of the expected migration pattern on Western blot and localised to the nucleus as assessed by immunofluorescence, we used these cells to determine if MITF could be acetylated in this context.

We planned to immunoprecipitate FLAG-tagged MITF and probe the IP fractions with an antibody raised against pan-acetyl-lysine (acK) to detect MITF acetylation. We treated cells with either DMSO or trichostatin A (TSA), an inhibitor of many histone deacetylases (Matsuyama et al., 2002). An initial immunoprecipitation with a relatively gentle lysis resulted in a large portion of MITF-3xFLAG remaining in the insoluble fraction (data not shown). Accordingly, we used a denaturing lysis protocol and assessed the amount of MITF-3xFLAG that was solubilised and the amount that stayed insoluble in the pellet, loading volumes that corresponded to 1% of each sample (Figure 3.1c). Although a significant amount of MITF-3xFLAG remained in the insoluble pellet, the majority appeared to be solubilised by the denaturing lysis protocol (Figure 3.1c; lanes 6, 8 vs. lanes 4, 2). This also showed that TSA treatment (400 nM; 6 hours) resulted in an increase in the amount of MITF-3xFLAG that was solubilised (Figure 3.1c; lane 4 vs. lane 2). Whether this was through increased transcription, stabilisation or another mechanism is unclear, however a previous report has indicated that MITF transcript level decreased in response to HDAC inhibition (Yokoyama et al., 2008). It is important to note that the portion of MITF-3xFLAG that remained insoluble was unable to be assessed for acetylation by this protocol – it is possible that acetylated MITF-3xFLAG is disproportionately present in or absent from this fraction.

Having verified that MITF-3xFLAG was adequately solubilised, we immunoprecipitated MITF-3xFLAG from the soluble input fractions (Figure 3.1c; lanes 1-4) and probed both input and FLAG IP fractions with an antibody against FLAG and an antibody raised against pan-acetyl-lysine (acK; Figure 3.1d). For the acK blot, a lower percentage of acrylamide was used in the hope of increasing resolution of various species – this likely accounts for why there is more separation between the 50 kDa and

75 kDa markers than on previous blots (Figure 3.1a, c, d). Looking at the input fractions, treatment with TSA resulted in the appearance of a band detected by the acK antibody at approximately 50 kDa. This would be consistent with the migration of tubulin, acetylation of which has been shown to increase with TSA treatment (Matsuyama et al., 2002). Notably, the acK antibody detects a doublet just under 75 kDa in the FLAG IP fraction of the TSA-treated sample (Figure 3.1d; lane 8). No such bands were seen in the 3xFLAG controls or in the MITF-3xFLAG sample that was not treated with TSA. This migration pattern is highly similar to that observed with the FLAG and MITF antibodies and is consistent with these bands representing acetylated MITF-3xFLAG.

The lower band appeared to be acetylated to a greater extent than did the upper band, although this pattern was also evident in the FLAG blot of the input fraction (lane 4), meaning that this may have resulted from there being more of the faster-migrating species in total rather than differential acetylation (Figure 3.1d). The fact that both bands were detected by the acK antibody was consistent with a report that the p300 acetylase interacted with both hypo- and hyperphosphorylated MITF (Sato et al., 1997), although another report found that p300 preferentially interacted with hyperphosphorylated MITF (Price et al., 1998). We note that regardless of the preference of p300 for interacting with hypo- or hyperphosphorylated MITF, this interaction would not necessarily correspond to MITF being acetylated.

Thus, MITF-3xFLAG can be acetylated in a melanoma cell line, but we only detected acetylation during treatment with the HDAC inhibitor TSA. We noted that the level of MITF-3xFLAG was lower in the IP fraction from the control condition than in the TSA-treated condition, however Figure 3.1d shows a long exposure of the acK

antibody blot – if acetylation of MITF-3xFLAG occurred in control conditions, it was below the limit of detection of this assay.

### *3.2.2 MITF can be acetylated on multiple sites*

The first stages of this work were carried out by Alex Schepsky (former lab member) and involved overexpressing Myc epitope-tagged MITF and HA-tagged p300 in HEK 293 cells, immunoprecipitating Mitf-Myc and identifying acetylation sites by mass spectrometry (Figure 3.2). Several sites were identified (highlighted in purple), with two main clusters being found in the N-terminus and the bHLH region of the DNA binding domain. Note that no sites were found to be acetylated in the absence of p300 overexpression. To validate this work, Rob Siddaway (former lab member) overexpressed MITF-3xFLAG and HA-p300 in Phoenix cells. MITF-3xFLAG was either WT or harboured a single lysine-to-arginine point mutation corresponding to one of the sites previously found to be acetylated. Unlike lysine, arginine cannot be acetylated, permitting an assessment of the contribution of each site to MITF-3xFLAG acetylation. For each mutant, the signal was then normalised to the total amount of MITF-3xFLAG present, which was gauged by the signal from a FLAG antibody.

He found that mutation of many of the sites identified in the previous mass spectrometry experiment indeed impaired acetylation of MITF-3xFLAG (Figure 3.3a, b). Overall, the sites in the N-terminus decreased acetylation to a lesser extent than those in the DNA-binding domain, with the K33R mutant apparently demonstrating increased acetylation as compared to the WT. The greatest effects were seen for the K206R and K225R point mutants, decreasing acetylation to approximately 25% of that seen with WT MITF-3xFLAG (Figure 3.3a, b). As seen in the mass spectrometry

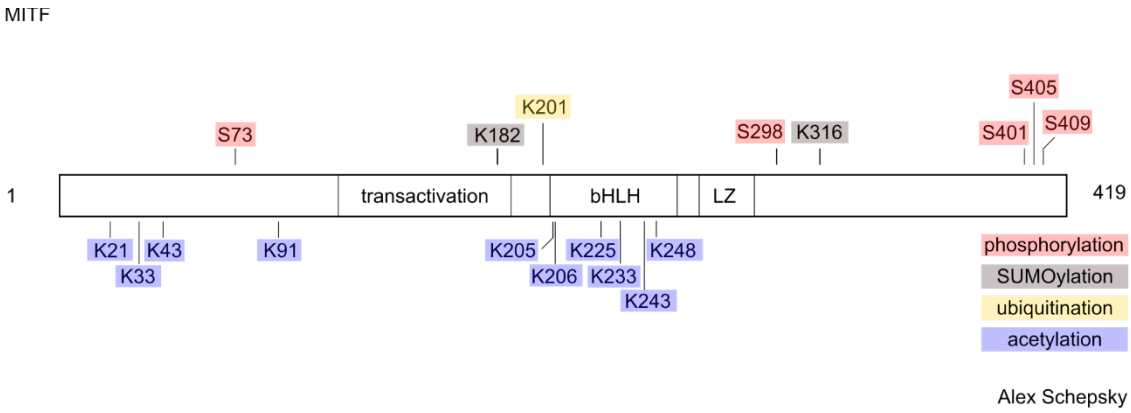



**Figure 3.2. MITF can be acetylated on multiple residues.** This schematic depicts sites identified by mass spectrometry to be acetylated in murine Myc epitope-tagged MITF in HEK 293 cells overexpressing the p300 acetylase. Spacing is drawn to scale, with acetylation events shown in purple. Other previously identified post-translational modifications of MITF are also indicated, as are the locations of the putative transactivation, bHLH and LZ domains. This experiment was done by Alex Schepsky, a former member of the laboratory.

experiment (see Figure 3.2), no acetylation of MITF was observed in the absence of ectopic p300 (Figure 3.3a; lane 3).

The two sites exhibiting the greatest reduction in acetylation were then included in another experiment to confirm their contribution to MITF acetylation. Phoenix cells were co-transfected with HA-p300 and MITF-3xFLAG that was either WT or contained the K206R or K225R mutations. After immunoprecipitating MITF-3xFLAG, samples were probed with an antibody against acK and an antibody against FLAG. Again, we see that in the absence of p300, MITF-3xFLAG is not acetylated, however expression of MITF-3xFLAG was low in this condition, possibly complicating detection of acetylation (Figure 3.3c, lane 1). We noted that even long exposures did not result in saturation of bands with the acK antibody, possibly indicating that low levels of acetylation might be difficult to detect with this assay. Co-transfection with HA-p300 resulted in a moderate increase in MITF-3xFLAG level, and the acK antibody detected two bands, similar to the pattern detected with the FLAG antibody (Figure 3.3c, lane 2).

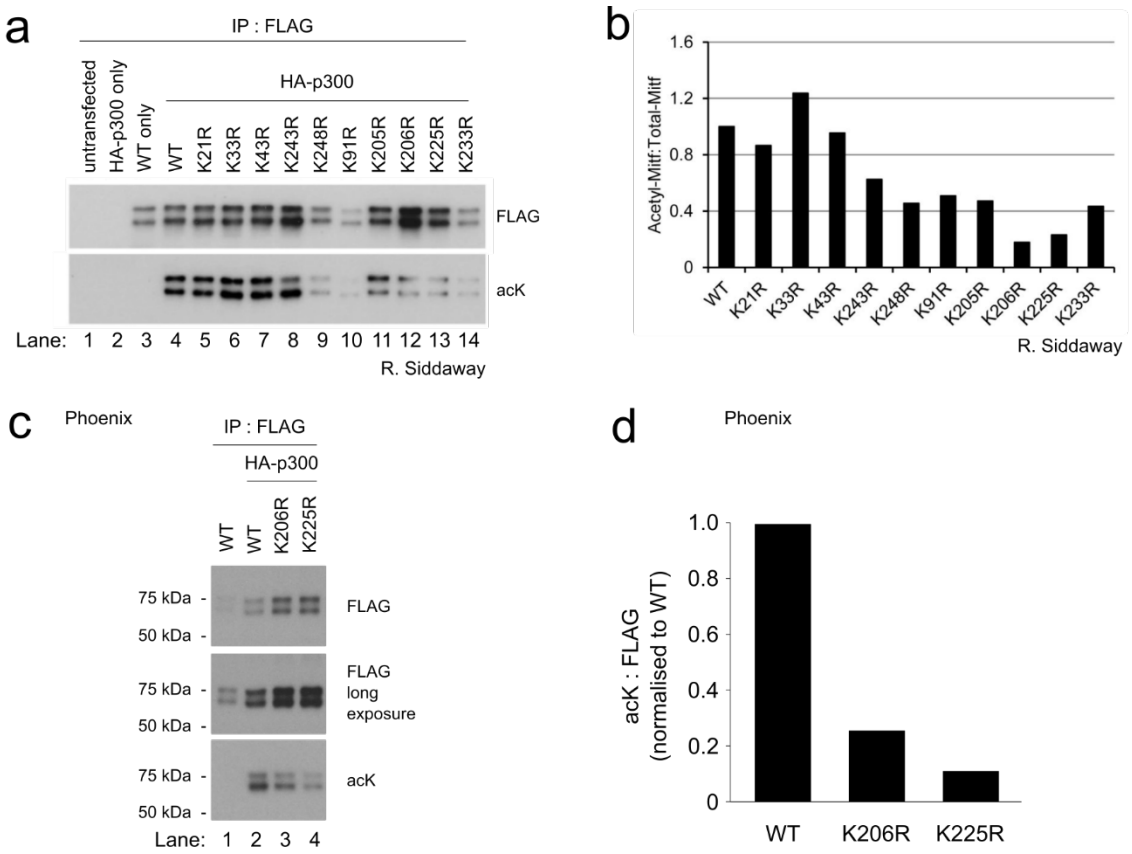



**Figure 3.3. Mutation of residues K206 and K225 impairs acetylation of MITF-3xFLAG.** Western blotting and quantification of the ratio of signal from a pan-acetyl-lysine (acK) antibody to a FLAG antibody. (a) Phoenix cells were transiently transfected with HA-p300, MITF-3xFLAG or both. MITF-3xFLAG was either WT or harboured a single lysine-to-arginine point mutation. MITF-3xFLAG was then immunoprecipitated, and samples were probed with antibodies against FLAG and pan-acetyl-lysine. (b) Quantification of the data in (a) using ImageJ to normalise the signal from the pan-acetyl-lysine antibody to that of the FLAG antibody, followed by normalising each mutant to the WT. (c) The experiment shown in (a) was repeated with MITF-3xFLAG being either WT or harbouring a K206R or K225R mutation. (d) Quantification of the data shown in (c) using the shorter FLAG blot exposure. Data shown in (a) and (b) are courtesy of Rob Siddaway.

As it has been shown that these bands correspond to differentially phosphorylated species (Hemesath et al., 1998), our data indicated that, as we had seen with HDAC inhibition (see Figure 3.1d), p300 overexpression resulted in the acetylation of both of these species.

We note that unlike in the previous experiment (Figure 3.3a), but similar to MITF-3xFLAG acetylation in a melanoma stable line (see Figure 3.1d), the lower band

appeared to be acetylated to a higher degree than the upper band (Figure 3.3c). Importantly, both mutations resulted in lower levels of acetylation, as judged relative to the WT after normalising to the signal from the FLAG antibody to account for differences in expression among the constructs (Figure 3.3c, lanes 3-4 vs. lane 2). Although both the K206R and K225R mutants showed acetylation levels less than 25% that observed with the WT, the K225R mutant showed a stronger effect than the K206R mutant (Figure 3.3c, d). Thus, multiple studies have indicated that overexpression of p300 results in acetylation of MITF-3xFLAG. Given that p300 has been documented to interact with MITF (Sato et al., 1997), these data would be consistent with p300 directly acetylating MITF.

To confirm the importance of K206 for MITF acetylation, we studied whether an arginine mutation at this residue could impair MITF-3xFLAG acetylation during stable expression in a melanoma cell line. We generated 501mel cell lines expressing inducible 3xFLAG and MITF-3xFLAG that was either WT or harboured the K206R mutation. In an experiment analogous to that conducted with the IGR39 cell lines, we planned to induce expression of WT and mutant MITF-3xFLAG, immunoprecipitate FLAG-tagged proteins and blot these fractions with the acK antibody used previously (see Figure 3.1). Figure 3.4a shows endogenous MITF expression in 501mel 3xFLAG cells, seen as a doublet between 50 and 75 kDa. Doxycycline did not appear to affect endogenous MITF expression at the doses used.

Although the band pattern cannot be completely resolved, samples from the induced 501mel iMITF-3xFLAG cell lines showed slower-migrating species that were detected with the MITF antibody and corresponded in size to the bands detected by the FLAG antibody (Figure 3.4a; lanes 5-6, 8-9). This indicated that the slower-migrating species detected by the MITF antibody in the induced 501mel iMITF-3xFLAG cell

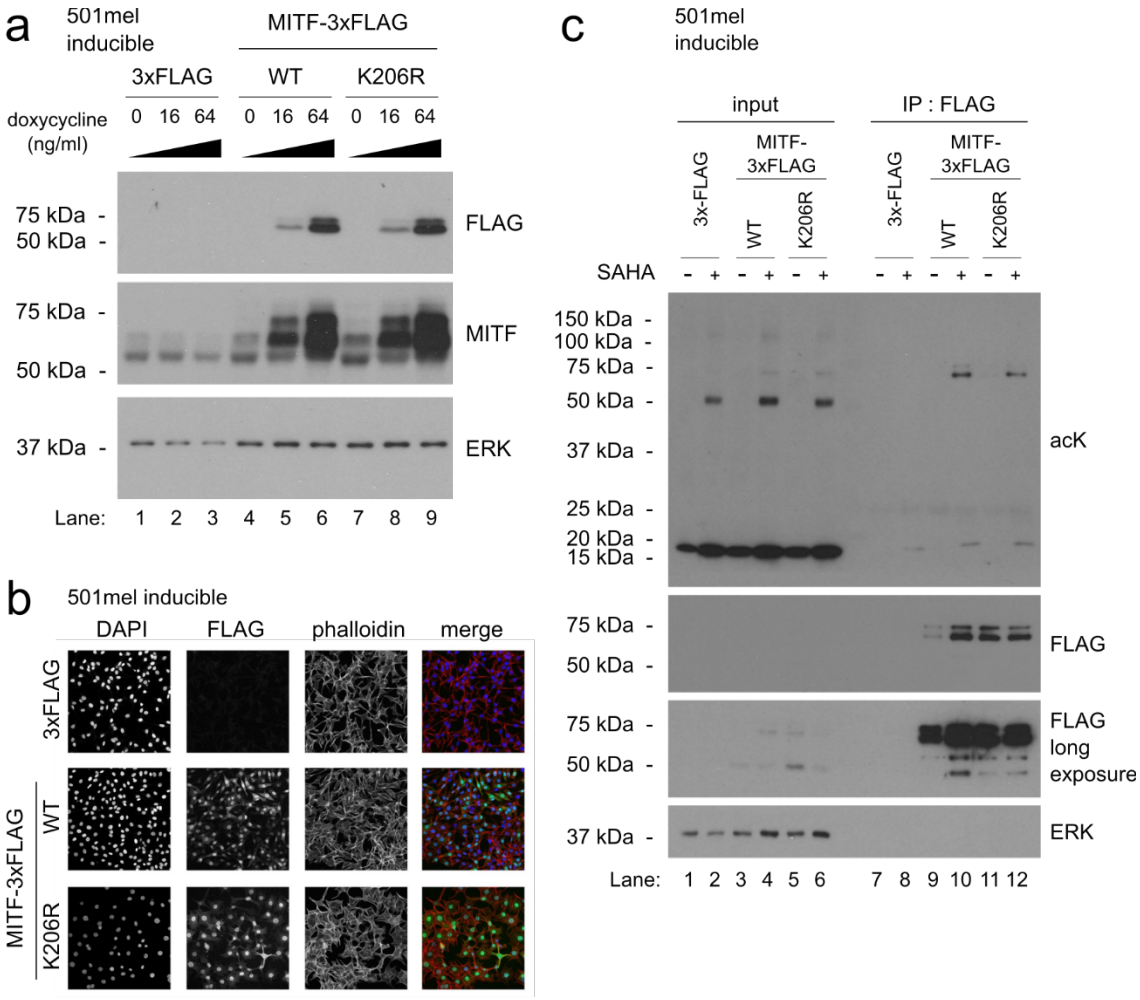



**Figure 3.4. The K206R mutation does not significantly impair MITF-3xFLAG acetylation in 501mel melanoma cells.** FLAG-tagged murine MITF was inducibly overexpressed in 501mel melanoma cells, immunoprecipitated and probed with an antibody against pan-acetyl-lysine (acK). (a) 501mel cells expressing inducible 3xFLAG or MITF-3xFLAG that is either WT or K206R mutant were either left uninduced or induced with 16 or 64 ng/ml doxycycline for 24 hours. Whole cell lysates were blotted with antibodies against FLAG and MITF, while ERK served as a loading control. (b) The same cell lines as in (a) were plated on glass coverslips and induced with 16 ng/ml doxycycline for 24 hours. Cells were then fixed and stained with an antibody against FLAG. Fluorescent phalloidin and DAPI were used to stain actin and nuclei, respectively. Images were acquired by confocal microscopy. (c) The same cell lines as in (a) were induced (16 ng/ml doxycycline, 24 hours) in the presence or absence of the HDAC inhibitor suberoylanilide hydroxamic acid (SAHA; 2 μM, 3 hours) and processed for FLAG immunoprecipitation. The inputs and IP fractions were then probed with antibodies against acK and FLAG. ERK served as a loading control.

lines were the ectopic MITF-3xFLAG. This enabled us to compare the levels of endogenous and ectopic MITF, hoping to keep any overexpression artefacts to a minimum. We judged 16 ng/ml doxycycline to be a dose that resulted in MITF-

3xFLAG expression at a level comparable to endogenous MITF (Figure 3.4a, lanes 5, 8). Lastly, we noted that assessment of the intensity of the two doublet bands relative to one another is complicated in the induced samples – resolution was not good enough to differentiate the bands thought to represent the upper endogenous MITF band and the lower MITF-3xFLAG band.

We assessed these same cell lines by immunofluorescence to verify that MITF-3xFLAG was localised to the nuclear compartment. 501mel iMITF-3xFLAG cell lines were plated on glass coverslips, induced with 16 ng/ml doxycycline, fixed and stained with an antibody against FLAG. We also stained cells with fluorescent phalloidin to label actin and DAPI to label nuclei. The majority of cells expressed MITF-3xFLAG primarily in the nuclear compartment (Figure 3.4b), a localisation pattern consistent with what we had seen for MITF-3xFLAG in the IGR39 iMITF-3xFLAG cell line (see Figure 3.1b).

Having determined the localisation pattern and expression level of MITF-3xFLAG in the 501mel inducible cell lines, we used the acK antibody to assess the effect of the K206R mutation on MITF acetylation. As no acetylated MITF peptides were identified in earlier mass spectrometry experiments in the absence of ectopic p300, we again decided to include both a control condition and a condition in which we attempted to boost global acetylation. To test whether MITF could be acetylated when HDACs were inhibited with a different compound, cells were treated with suberoylanilide hydroxamic acid (SAHA; 2 μM, 3 hours; Richon et al., 1998), an inhibitor of class I, II and IV HDACs (Xu et al., 2007).

Previously, we had seen that HDAC inhibition resulted in increased expression of MITF-3xFLAG (see Figure 3.1). This was not the case with this experiment –

although the level of MITF-3xFLAG is very low in the input fractions, SAHA treatment did not appear to increase the level of MITF-3xFLAG or MITF(K206R)-3xFLAG (Figure 3.4c; lanes 3-6). However, the acK blot indicated that SAHA treatment was indeed increasing protein acetylation. As we saw with TSA treatment, SAHA treatment resulted in the appearance in the input fractions of a band running just above the 50 kDa marker, consistent with the migration pattern of acetylated tubulin (Figure 3.4c; lane 1 vs. lane 2). Also, the acK antibody detected a strong signal between 15 and 20 kDa in the input fractions of each sample, a migration pattern consistent with histones. Treatment with SAHA to inhibit HDACs resulted in this band increasing in intensity, consistent with increased histone acetylation (Figure 3.4c; lane 1 vs. lane 2). Thus, it appeared that, like TSA treatment, SAHA treatment was resulting in higher levels of acetylated proteins in the input fractions. This indicated that SAHA was functioning as intended, and the acK antibody was detecting acetylated proteins.

Turning to the FLAG immunoprecipitation (IP) fractions, probing with a FLAG antibody showed that no bands were visible in the control or SAHA-treated 501mel i3xFLAG samples (Figure 3.4c, lanes 7-8), while a doublet of the expected size appeared in both WT and K206R mutant MITF-3xFLAG samples (Figure 3.4c, lanes 9-12). This indicated that the FLAG immunoprecipitation successfully isolated MITF-3xFLAG. Although a long exposure was again necessary, probing with the acK antibody revealed a doublet consistent with the MITF-3xFLAG migration pattern in the SAHA-treated 501mel iMITF-3xFLAG WT sample (Figure 3.4c, lane 10). Importantly, this indicated that ectopic MITF-3xFLAG expressed at near-endogenous level can be acetylated during HDAC inhibition in 501mel melanoma cells.

As we had seen before in IGR39 iMITF-3xFLAG cells, the lower band appeared to be acetylated to a greater extent than the upper band (Figure 3.4c, lane 10; also see

Figure 3.1d). However, the FLAG antibody revealed that this band was stronger than the top band, making it unclear if the faster migrating species was preferentially acetylated or merely present at a higher level. The acK antibody did not detect bands consistent with the MITF-3xFLAG migration pattern in the control condition (lane 9), however the FLAG blot showed that the level of immunoprecipitated WT MITF-3xFLAG in this sample was much lower than in the SAHA-treated sample. Thus, it could be that that MITF-3xFLAG can be acetylated in control conditions, but we failed to detect this due to the low level of immunoprecipitated MITF-3xFLAG in the control sample (Figure 3.4c, lane 9 vs. lane 10).

The K206R mutant was also acetylated in the SAHA-treated sample (Figure 3.4c, lane 12). It showed a pattern similar to the WT in which the lower band is preferentially acetylated, but again, the FLAG antibody revealed the lower band was also present at a higher level. Importantly, the K206R mutation did not appear to impair MITF-3xFLAG acetylation in these conditions – although the doublet seen in the acK blot may be slightly fainter, the FLAG blot showed that there is slightly less total protein (Figure 3.4c, lane 12 vs. lane 10). Interestingly, the acK antibody gave a very faint signal in the IP fraction of the untreated K206R mutant sample (lane 11), possibly indicating that this protein could be acetylated in the absence of HDAC inhibition. Whether this is unique to the K206R mutant is unclear, as the WT is present at a much lower level in the IP fraction of the untreated sample (Figure 3.4c, lane 11 vs. lane 9).

We note that use of a “pan” antibody to detect a post-translational modification could raise concerns of false positive results, and we were unable to directly confirm that the species detected by this antibody at the migration of MITF-3xFLAG in IP fractions represented acetylated MITF-3xFLAG. However, the migration patterns of the 50 kDa and 15-20 kDa bands detected by this antibody in the input fractions

corresponded to the expected migration patterns of proteins known to be acetylated in response to HDAC inhibition (tubulin and histones, respectively). Additionally, the intensity of these bands increased during HDAC inhibition, indicating that the antibody was detecting acetylated proteins in a quantitative manner and increasing our confidence that the acK antibody was indeed detecting acetylation of MITF-3xFLAG.

### *3.2.3 MITF(K206Q) shows altered DNA binding*

We chose to focus on K206, as our studies in Phoenix cells had indicated that K206 was a primary acetylation target, and this residue is conserved from humans to fruit flies (Figure 3.5a). Additionally, it is conserved among all members of the 4-member TFE family. Interestingly, outside of the TFE family, a lysine at this position is uncommon in bHLH transcription factors in general. We conducted an alignment of the 113 human bHLH proteins annotated in the Uniprot database (http://www.uniprot.org) and saw that only 18% had a lysine at this position, with the majority having an arginine (Figure 3.5a). The high percentage of human bHLH proteins that harbour a lysine or an arginine residue at this position (81%, n = 113) may imply that a basic side chain at this location in the DNA binding domain is structurally important. This notion is supported by the recently published co-crystal structure of MITF bound to DNA (Pogenberg et al., 2012), which showed that this residue was appropriately positioned for the amino group of the lysine side chain to form a hydrogen bond with the negatively charged DNA phosphate backbone (Figure 3.5b).

Assessment of the influence of acetylation on MITF DNA binding was complicated by the fact that conditions used to induce MITF acetylation also increased MITF levels (Rob Siddaway, former lab member). This was also evident in our

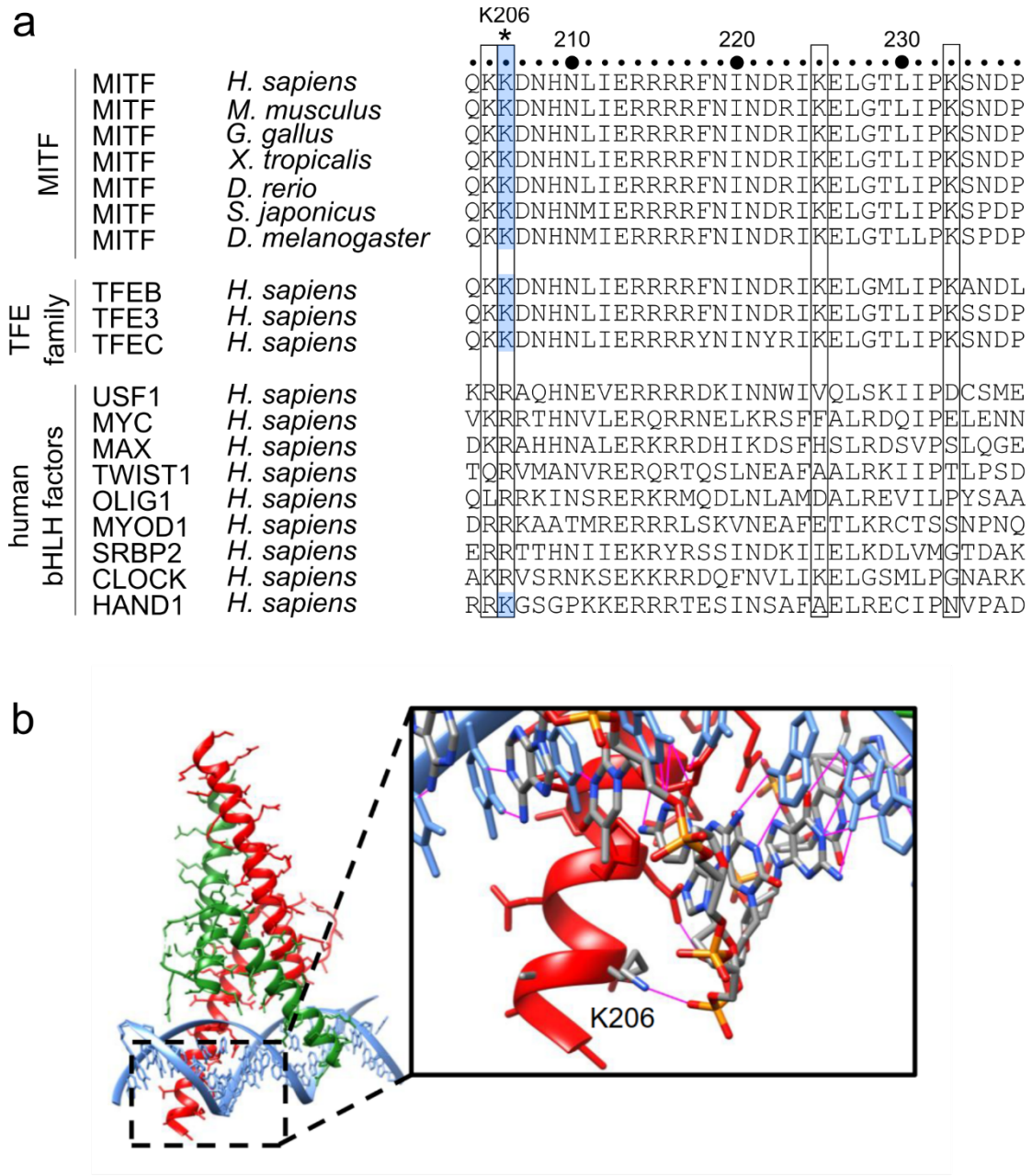



**Figure 3.5. K206 is conserved within the TFE family and positioned to interact with DNA.** A protein alignment and co-crystal structure demonstrate the conservation and positioning of MITF K206. (a) An alignment of the basic region and first helix of the MITF DNA binding domain is shown. Human MITF is aligned against MITF from other species, other human TFE family members and other human bHLH proteins. Numbering is according to human MITF, with residues found to acetylated boxed in black. Conservation of a lysine residue at the position corresponding to human MITF K206 is indicated by blue highlighting. (b) A co-crystal structure of the MITF DNA binding domain bound to an M-box (5'-CATGTG-3') motif is shown (Pogenberg et al., 2012). Atomic coordinates were downloaded from the Protein Data Bank and visualised in Chimera v1.11. MITF protomers are shown in green and red, while DNA is blue. The inset shows the hypothesised hydrogen bond (pink) formed between the amino group of the K206 side chain and the phosphate group of the DNA backbone, with hydrogen bonds among the DNA bases also visible. Atomic structure is shown for the lysine side chain and DNA, with nitrogen as blue, oxygen as red and phosphate as orange.

assessment of acetylation in MITF-3xFLAG stable cell lines, where MITF levels were increased when acetylation was induced with either an HDAC inhibitor (see Figure 3.1) or p300 overexpression (see Figure 3.3). Additionally, MITF binds DNA as a dimer and can dimerise with itself or with other members of the TFE family (Hemesath et al., 1994). Accordingly, ascertaining the effects of K206 status on MITF function would be simplified if we adopted a system in which both the composition of the dimers and the status of K206 were known.

In light of these considerations, we opted to purify bacterially-expressed MITF for use in DNA binding assays. This would also have the advantage of providing large quantities of protein that could then be used in future biochemical studies. We first attempted to purify full-length human MITF from *E. coli*. We cloned the *MITF* coding sequence into the pNIC vector, which is designed for expression of His-tagged proteins in bacteria. Screening a lysate from bacteria induced to express MITF-His in a small-scale test batch revealed a prominent band just over 50 kDa, which is consistent with the projected migration pattern of MITF (Figure 3.6a, # in lane 2). We then repeated the induction and processed the sample for purification of His-tagged proteins. Note that we saw high variability from experiment to experiment in the proteins present in induced fractions from bacteria transformed with this construct, with some inductions showing a single predominant band and others showing many bands of comparable intensity (Figure 3.6a; lane 2 vs. lane 4). After purification, the predominant band in the elution fractions appeared to be a faster-migrating species (Figure 3.6a; * in lanes 6, 7). We repeated the entire purification and again saw that the predominant band in the elution fractions migrated faster than the band seen in the original test expression.

As the predicted weight of MITF-His was 49.5 kDa, it was unclear which, if either, of these bands represented our target protein. We excised the two bands (Figure

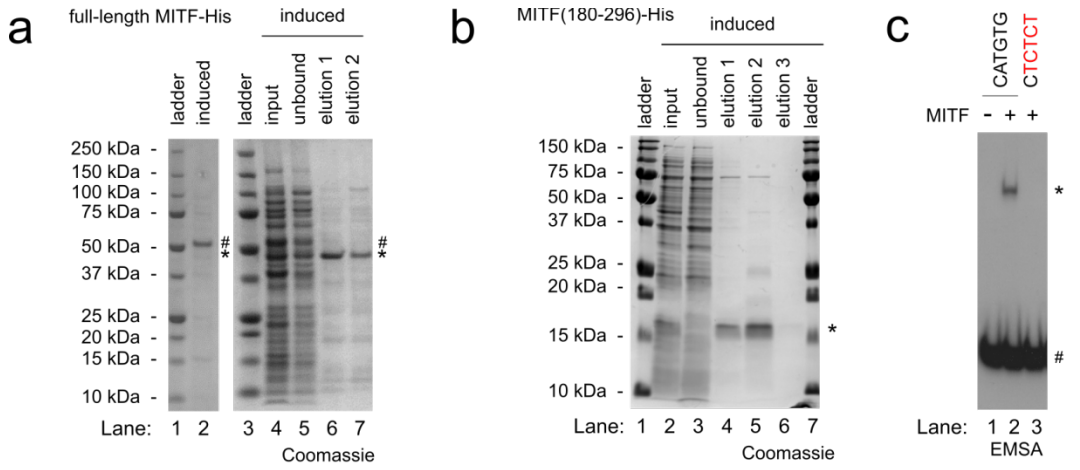



**Figure 3.6. Binding of MITF to the *TYR* enhancer is mediated by a CATGTG motif.** His-tagged MITF was expressed in *E. coli*, and binding to the *TYR* enhancer was examined in an electrophoretic mobility shift assay (EMSA). (a) Coomassie staining of the indicated fractions from a purification of full-length human MITF, which was cloned into a prokaryotic expression vector. Expression was induced with IPTG (lane 2, #). Subsequent purification resulted in a predominant species of different mobility (lane 7, *). (b) Coomassie staining of fractions from purification of His-tagged MITF(180-296), comprising the DNA binding domain. Expression was induced as in (a), with purification resulting in a species of approximately 15-20 kDa (lane 7, *). (c) EMSA assay in which the protein in (b; lane 4) is incubated with a radiolabelled DNA probe comprising approximately 40 bp of the *TYR* enhancer. This sequence was either WT, containing the central motif 5'-CATGTG-3' (lanes 1-2), or harboured a mutated motif (5'-CTCTCT-3', lane 3). Unbound probe (#) and shifted probe (*) are indicated. (d) Schematic depicting the sense strand of the EMSA probes used in (c). The 5'-CATGTG-3' motif is underlined. A mutated version of the probe is also shown with mutations in red.

3.6a; lanes 2, 7) and sent them for identification by mass spectrometry (Structural Genomics Consortium, University of Oxford). This revealed that the species in the original (pre-purification) lysate was indeed MITF, running over the 50 kDa marker despite the predicted molecular weight of 49.5 kDa (Figure 3.6a, # in lane 2). However, the species present in the elution fraction was identified as *E. coli* elongation factor Tu 1, which has a predicted molecular weight of 43.3 kDa (Figure 3.6a, * in lanes 6, 7). Despite several modifications made to the buffer solutions, we did not see the slower-migrating band that corresponded to MITF (Figure 3.6a; # in lane 2) in any of the

elution fractions, indicating that despite being expressed, we were unable to purify full-length MITF-His in the conditions tested.

We instead elected to express only the DNA binding domain of MITF, a fragment that our collaborators had recently successfully expressed and crystallised (Pogenberg et al., 2012). A vector encoding the murine MITF DNA binding domain (residues 180-296) with an N-terminal His-tag was generously provided, and a small-scale purification was conducted. The predicted molecular weight of MITF(180-296)-His was 17.3 kDa, so we were concerned when we did not see significant induction of a species at this migration (Figure 3.6b; lane 2). However, a species migrating just over the 15 kDa marker was detectable in the elution fraction (Figure 3.6b; * in lane 6). This band was excised and identified by mass spectrometry as MITF, so we proceeded to test this elution fraction in an electrophoretic mobility shift assay (EMSA). This entails incubating a protein sample with a radiolabelled oligonucleotide probe and running the sample on a native gel. If the protein binds the probe, the probe's mobility will be retarded, resulting in a shift of the band observed upon exposing the gel to X-ray film. If no binding occurs, the oligonucleotide probe will move faster through the gel, and no band shift will be observed.

We chose the *TYR* enhancer to test MITF binding. This is a well-validated MITF target, and binding has been shown to be mediated by a 5'-CATGTG-3' motif, which is one of two motifs often found in validated MITF target genes (Cheli et al., 2010). A radiolabelled double-stranded DNA probe containing approximately 40 bp of the *TYR* enhancer was designed, with the 5'-CATGTG-3' motif in the centre. Incubating bacterially purified MITF(180-296)-His (Figure 3.6c, lane 4) with this probe resulted in a shift of the probe's mobility, indicating that this fragment of MITF is capable of binding the *TYR* enhancer (Figure 3.6c; * in lane 2). When no protein was

added (lane 1), the probe migration was not retarded (unbound probe indicated by #). Lastly, if the centrally-located 5'-CATGTG-3' motif in the probe was mutated from 5'-CATGTG-3' to 5'-CTCTCT-3', the mobility of the probe did not shift (Figure 3.6c; lane 3; Figure 3.6d). This indicated that MITF binding of the probe appeared to be dependent upon the 5'-CATGTG-3' motif, as mutation of this motif eliminated the MITF-dependent shift of the radiolabelled probe.

We were now ready to test the effect of K206 acetylation on MITF DNA binding using the EMSA system described above. Having confirmed that the fragment of MITF comprising the DNA binding domain was capable of binding the *TYR* enhancer, we introduced an acetyl-lysine mimicking glutamine mutation or an unacetylated lysine mimicking arginine mutation at residue K206 (Lv et al., 2013; Shogren-Knaak et al., 2006). Earlier experiments had indicated that MITF could also be acetylated on K205 (see Figure 3.2), so this residue was also mutated to glutamine or arginine. As we were interested in possible interactions between these two acetylation events, all of the possible arginine and glutamine mutant combinations of residues K205 and K206 were made, comprising 8 mutants in all (vectors provided by Rob Siddaway). We note that glutamine and arginine mutations are not perfect mimics, in that they differ structurally from acetyl-lysine and lysine, respectively. This consideration will be discussed further in a later section.

We first performed a small-scale purification of each of the vectors mutated at K205 and/or K206, using the same conditions as were used to prepare the WT protein. Screening of fractions from this purification showed that, for each mutant, the predominant species present in the elution fractions migrated at just over 15 kDa (Figure 3.7a). This was consistent with the migration of the WT protein seen previously. We conducted an EMSA using the same WT *TYR* enhancer as had been

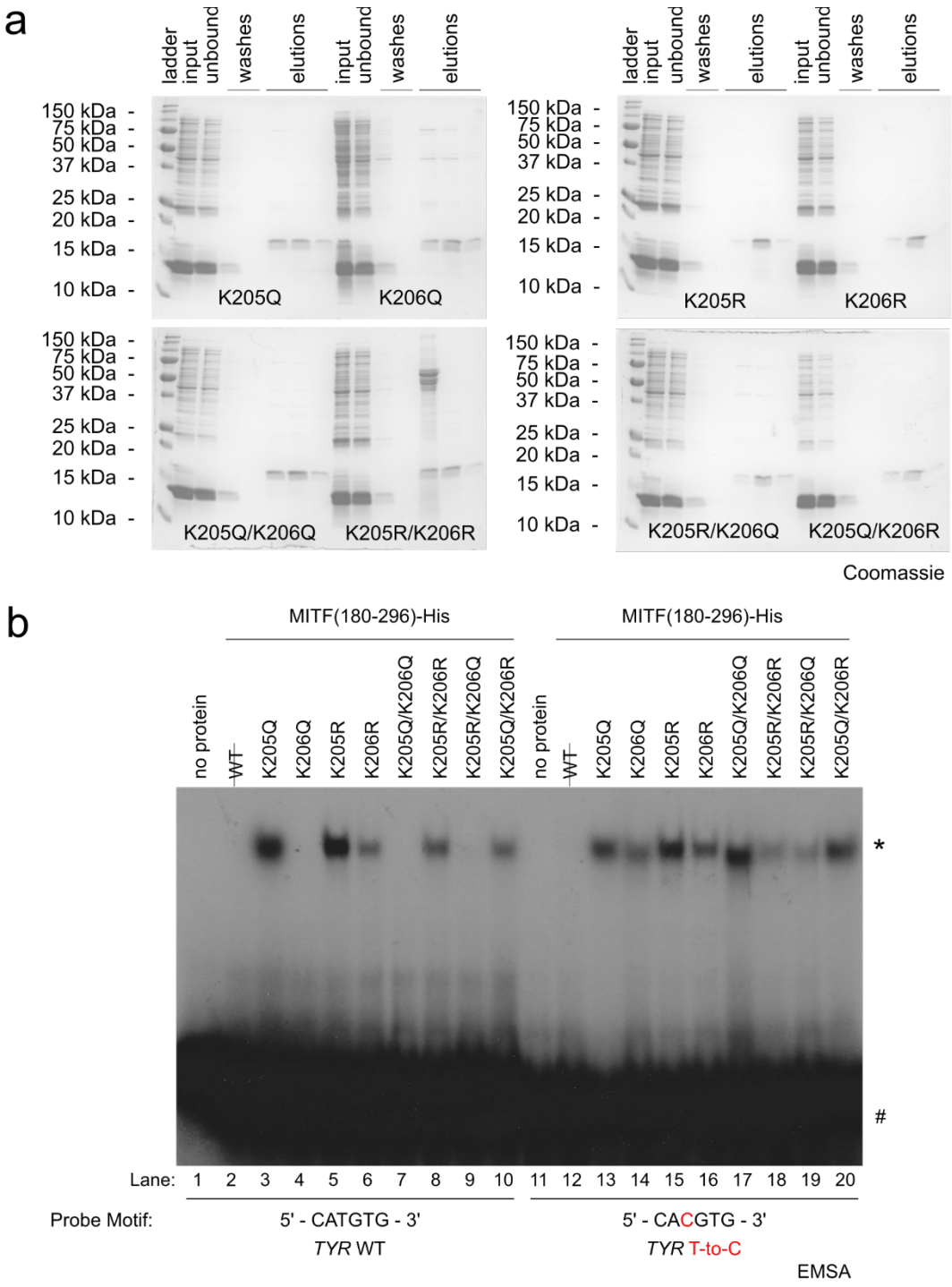



**Figure 3.7. K206 status impacts MITF DNA binding.** WT or mutated His-tagged MITF was expressed in *E. coli* and used in an electrophoretic mobility shift assay (EMSA) to examine the effect of K205 and K206 mutations on MITF DNA binding. (a) Coomassie staining of fractions from purification of the indicated MITF DNA binding domain mutants. The second elution faction for each protein was used in EMSA studies. (b) EMSA in which the protein from (a) is incubated with a radiolabelled DNA probe comprising approximately 40 bp of the *TYR* enhancer, which was either WT or had the central M-box motif mutated from 5'-CATGTG-3' (*TYR* WT) to 5'-CACGTG-3' (*TYR* T-to-C), as indicated. Shifted probe (*) and free probe (#) are indicated. Note that the WT protein is indicated with a strike-through, as this protein was later found to have degraded.

used to test the WT protein (see Figure 3.6c). We were surprised to see that the WT protein did not bind to this probe (Figure 3.7b; lane 2, indicated by strike-through text) as it had done before. This fraction was again screened against the mutant elution fractions and found to have degraded (data not shown). After consulting with collaborators in the SGC (Structural Genomics Consortium, University of Oxford) who are expert in bacterial protein purification, it was determined that the WT protein had been improperly stored. All future studies used protein stored according to their recommendations.

The newly prepared K205 and K206 mutant proteins had not been subjected to the storage conditions that likely resulted in the degradation of the WT protein and bound the WT *TYR* enhancer probe to varying degrees (Figure 3.7b). First, while the K205Q mutant was capable of binding to the 5'-CATGTG-3' probe, the K206Q mutant was not (Figure 3.7b; lane 4 vs. lane 3). Next, both K205R and K206R bound the probe, though the K205R mutant appeared to bind better. Lastly, the K205Q/K206Q double mutant and the K205R/K206Q double mutant showed no binding to the probe, while the K205R/K206R and the K205Q/K206R double mutants were able to bind the probe at moderate levels. Strikingly, no protein containing the K206Q mutation, irrespective of the status of K205, was able to bind the WT *TYR* enhancer element, and all proteins containing the K206R mutation bound at a similar level (Figure 3.7b). This indicated that the K206Q mutation (and possibly K206 acetylation) interfered with the ability of MITF to bind an enhancer element of the *TYR* gene.

However, only a subset of MITF binding sites harbour a 5'-CATGTG-3' motif – the other motif most commonly found in MITF target genes differs by one base (5'-CACGTG-3'; Cheli et al., 2010). In fact, unpublished data from a ChIP-seq experiment in melanoma cells expressing HA-tagged MITF indicated that MITF binding sites

primarily harboured 5'-CACGTG-3' motifs (Rob Siddaway, unpublished data). With these two major MITF binding motifs in mind, we mutated the *TYR* enhancer probe from the WT sequence (5'-CATGTG-3') to 5'-CACGTG-3' (Figure 3.7b; *TYR* T-to-C). The remainder of the probe was not changed, so as to compare the effect of changing a single base in the centre of the 5'-CATGTG-3' motif. This greatly altered the DNA binding of some mutants, while leaving that of others relatively intact (Figure 3.7b). Importantly, mutation of the central 5'-CATGTG-3' motif to a 5'-CACGTG-3' motif permitted binding of the K206Q mutant (Figure 3.7b; lane 14). Additionally, binding of the other mutants harbouring a K206Q was also detected with the mutant probe (Figure 3.7b; lanes 17, 19). Binding of the K206R-containing mutants was largely unaffected, although the K205R/K206R mutant bound slightly worse to the mutated probe (Figure 3.7; lane 18). Thus, the K206Q mutation appears to abrogate binding to the 5'-CATGTG-3' motif but permit binding to the 5'-CACGTG-3' motif. These results suggest that, regardless of the status of K205, K206 status may have a role in determining the relative preference of MITF for 5'-CACGTG-3' and 5'-CATGTG-3' motifs.

Having seen that the K206Q mutant may show altered target specificity, we prepared two new batches of WT and K206Q mutant protein. New probes were annealed and labelled, and we again tested the ability of the WT and K206Q mutant MITF(180-296) DNA binding domains to bind probes harbouring either the WT *TYR* enhancer 5'-CATGTG-3' motif or the same probe mutated to 5'-CACGTG-3' (*TYR* T-to-C). Figure 3.8 shows two different experiments using independently prepared proteins and probes – note that the loading of the WT and K206Q proteins is reversed in the two experiments. First, the elution fractions from bacteria induced to express either WT or K206Q mutant MITF were normalised by Coomassie (Figure 3.8a, c). Then, the

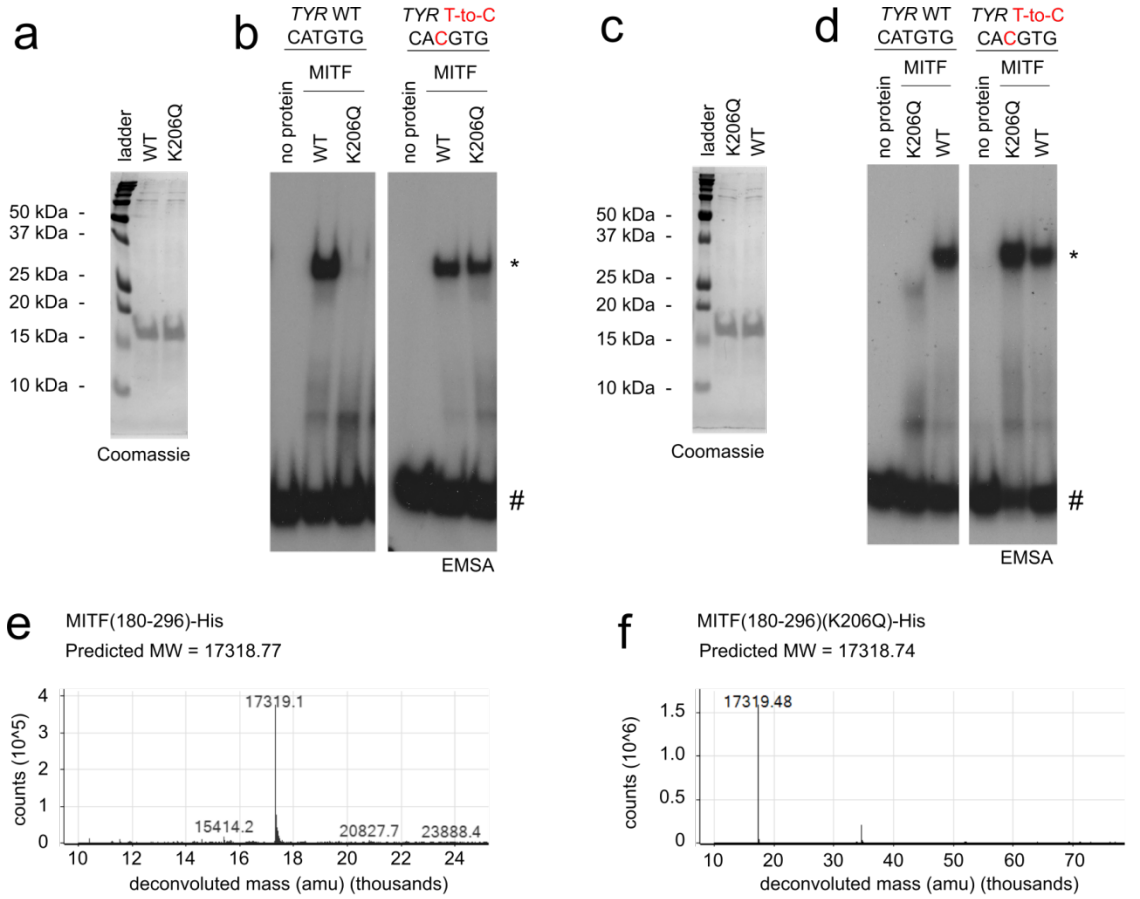



**Figure 3.8. The K206Q mutation impairs MITF(180-296)-His binding to a 5'-CATGTG-3' motif.** WT or mutated His-tagged MITF was expressed in *E. coli* and used in an electrophoretic mobility shift assay (EMSA) to examine the effect of the K206Q mutation on MITF DNA binding. (a) Coomassie staining of normalised elution fractions from WT and K206Q mutant MITF. The second elution fraction for each protein was used in EMSA studies. (b) EMSA in which the protein in (a) is incubated with a radiolabelled DNA probe comprising approximately 40 bp of the *TYR* enhancer, which was either WT or had the central M-box motif mutated from 5'-CATGTG-3' to 5'-CACGTG-3', as indicated. The shifted probe (*) and free probe (#) are indicated. (c) Repeat of (a) using separate batch of proteins and probes. (d) Repeat of (b) using separate batch of proteins and probes. (e, f) The elution fractions shown in (a) were analysed by time-of-flight mass spectrometry (TOFMS), with the molecular weight of the predominant species shown for the WT (e) and K206Q mutant (f) protein samples.

elution fractions shown in Figure 3.8a were analysed by time-of-flight mass spectrometry (TOFMS; Figure 3.8e, f). This verified that the MITF fragments were not truncated or modified post-translationally, as both the WT and K206Q mutant were measured to weigh within 1 Da of the predicted molecular weight. Lastly, the proteins were assessed for their ability to bind 5'-CATGTG-3' and 5'-CACGTG-3' motifs

(Figure 3.8b, d). As we had seen previously, the K206Q mutant was able to bind the mutated *TYR* enhancer probe (5'-CACGTG-3') but not the WT *TYR* enhancer probe (5'-CATGTG-3'; Figure 3.8b, d). The WT protein was able to bind both probes, with a preference for the WT probe in the first experiment and the mutated T-to-C probe in the other.

To increase the yield of purified protein for *in vitro* applications, we collaborated with colleagues in the SGC, where, after analysing the protein sequence, several different fragments of MITF were generated and tested. The best-expressing construct resulted from shifting the borders of the fragment from residues 180-296 to residues 198-302. A further modification to the expression and purification protocol was made after an *in silico* analysis of the protein sequence indicated that the DNA binding domain of MITF contained a high frequency of codons rarely used in *E. coli*, potentially complicating expression (http://nihserver.mbi.ucla.edu/RACC). Our collaborators provided us with the Rosetta strain of bacteria (Novagen, Madison, USA), which harbours genes encoding tRNAs for these rare codons. A full-scale purification of this fragment is shown in Figure 3.9a, with MITF(198-302)-His indicated (*).

Unfortunately, gel filtration revealed that the protein was aggregating during purification (data not shown), and spectrophotometric analysis showed that the elution fractions were contaminated with a large amount of DNA despite passage over a DNA-binding resin at an earlier step in the protocol (Figure 3.9b). In fact, contaminating DNA was present at a level that prohibited quantification of purified protein – the absorbance at 280 nm was judged to be a result of the large peak at 260nm and not reflective of the actual protein concentration (Figure 3.9b; purple line). Importantly, we tested elution fractions from earlier purifications of the 180-296 fragment of MITF, and these samples showed similar levels of contaminating DNA (data not shown). The

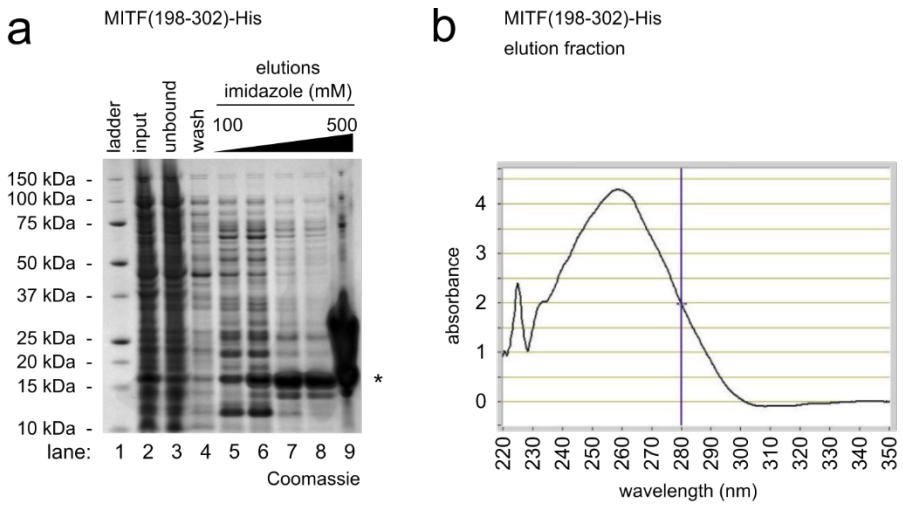



**Figure 3.9. MITF(198-302)-His purifies with DNA.** A fragment of MITF that had been optimised for high expression in *E. coli* was used in a large-scale purification. (a) Coomassie staining of input, unbound, wash and elution fractions, with MITF(198-302)-His indicated (*). (b) Spectrophotometric analysis of an elution fraction, with a purple line indicating absorbance at 280 nm.

presence of large quantities of bacterial DNA of unknown sequence would be an important consideration for applications in which we wish to compare the effects of MITF point mutations on DNA binding to different target motifs.

Accordingly, we began optimizing purification conditions in cooperation with our colleagues in the SGC, eventually developing a protocol resulting in a high yield of protein and significantly lowered levels of contaminating DNA (Figure 3.10). We first attempted purifying the MITF fragment in a range of buffers of varying pH (Figure 3.10a). MITF was detected during purification with buffers of pH greater than 7.0, and roughly equal amounts were purified from buffers with pH of 8.0-9.0 (Figure 3.10a). However, all conditions tested showed high levels of contaminating DNA, with the spectrophotometric analysis of the pH 9.0 buffer condition shown in Figure 3.10b.

Our collaborators then suggested elevating the concentration of NaCl, so we tested three of the pH conditions showing the highest levels of eluted MITF in combination with varying salt concentrations. Both the 0.5 M and 1.0 M NaCl

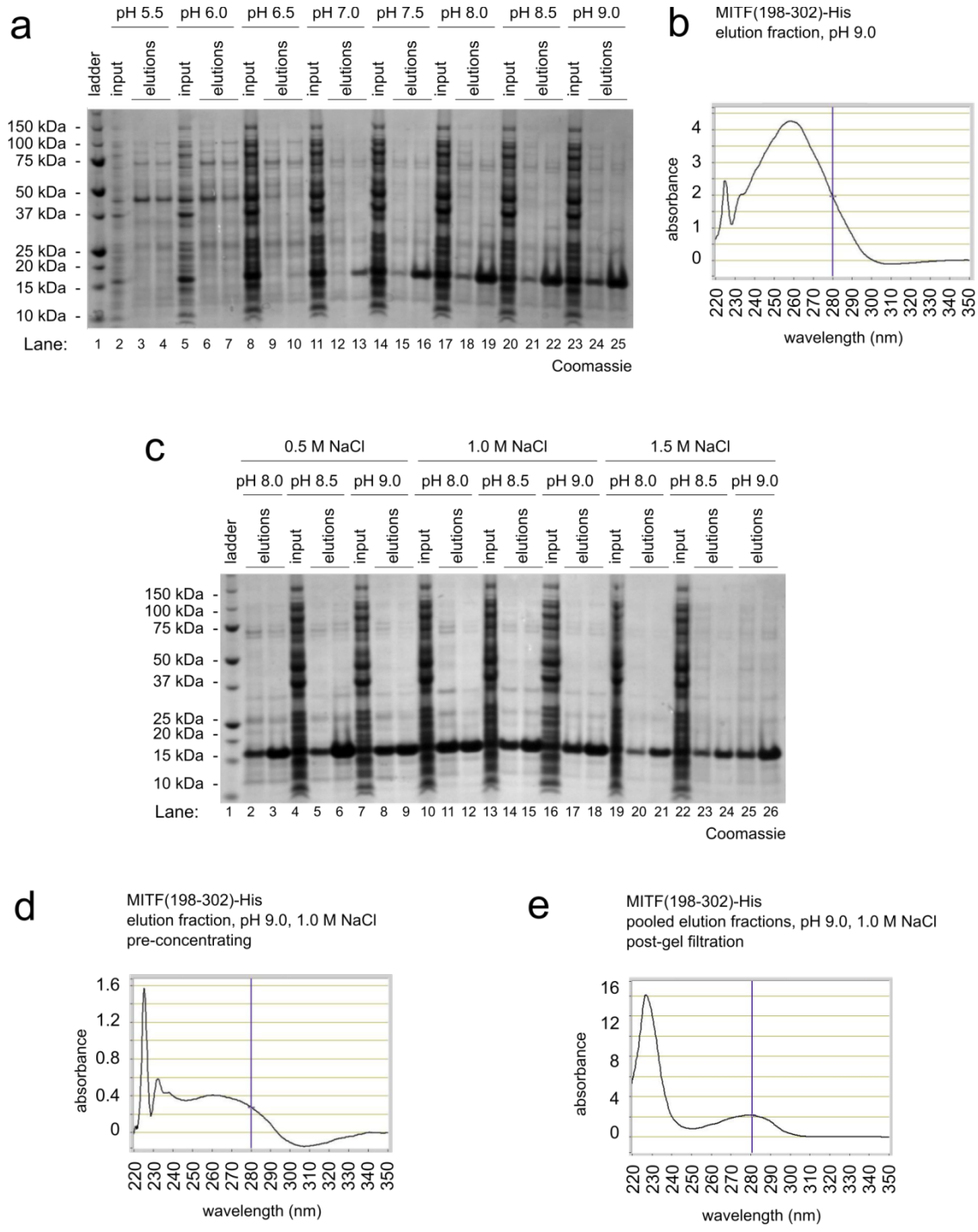



**Figure 3.10. Optimisation of MITF(198-302) purification.** WT or mutated His-tagged MITF was expressed in *E. coli* using a range of buffer conditions in an attempt to eliminate contaminating DNA. (a) Coomassie staining of input and elution fractions from small-scale purifications using buffers with different pH values. (b) Spectrophotometric analysis of an elution fraction from the pH 9.0 condition, with a purple line indicating absorbance at 280 nm. (c) Coomassie staining of input and elution fractions using buffers with pH of 8.0, 8.5 or 9.0 combined with NaCl concentrations of 0.5 M, 1.0 M or 1.5 M. (d) Spectrophotometric analysis of an elution fraction from a purification using buffers with pH 9.0 and 1.0 M NaCl. (e) Spectrophotometric analysis of a final purified protein fraction after His tag cleavage and gel filtration. Note that the scale of the y-axes (absorbance) varies among (b), (d) and (e).

conditions showed roughly equivalent levels of purified MITF, while the 1.5 M NaCl condition showed slightly lower levels (Figure 3.10c). Spectrophotometric analysis revealed that the 0.5 M conditions retained high levels of contaminating DNA (data not shown). However, the 1.0 M NaCl conditions showed reduced absorbance at 260 nm, with the pH 9.0 buffer showing the lowest level of contaminating DNA (Figure 3.10d) while still purifying a high level of MITF (Figure 3.10c; lanes 17-18).

Note that the axes of Figures 3.10b and 3.10d differ – the absorbance at 260 nm has decreased roughly 10-fold as a result of buffer optimisation, while the level of MITF purified remains comparable. Although the absorbance at 260 nm was still higher than that at 280 nm, after pooling the elution fractions, cleaving the His-tag and subjecting elution fractions to gel filtration and concentration, the spectrophotometric profile showed a higher 280/260 ratio (Figure 3.10e). This indicated lower levels of contaminating DNA and permitted us to normalise the amount of protein in elution fractions by spectrophotometric means. All future EMSAs of MITF DNA binding used purified protein prepared according to this optimised protocol.

It is worth noting that the absorbance spectrum shown in Figure 3.10e depicts a final elution fraction. These were from large-scale protein preparations and had to be diluted heavily (approximately 20,000-fold) for use in EMSAs, likely resulting in a very low concentration of contaminating DNA compared to earlier assays (see Figures 3.6, 3.7 and 3.8). Lastly, mass spectrometry revealed the final elution fraction from purification of the optimised WT MITF(198-302) fragment to predominantly contain a species of molecular weight 12,787.19 Da (predicted MW = 12786.79 Da), while the K206Q mutant final elution fraction primarily harboured a species weighing 12,787.17 Da (predicted MW = 12786.74 Da). Both proteins were within 1 Da of their predicted weights, indicating that His-tag cleavage occurred as expected and that the proteins

were not post-translationally modified or truncated during bacterial expression or purification.

As this was the first time we had used the shorter MITF(198-302) fragment in a DNA binding assay, we ran an EMSA comparing the magnitude of the shifts produced by the two different fragments (Figure 3.11a). In addition to confirming that the MITF(198-302) fragment was capable of binding the *TYR* enhancer, this indicated that the shorter fragment was indeed resulting in a lesser shift of the radiolabelled probe (*), as compared to MITF(180-296)-His (Figure 3.11a). In addition to confirming that the optimised fragment was capable of binding this sequence, this experiment indicated that the His-tag was dispensable for DNA binding, as this EMSA used MITF(198-302) protein from which the His-tag was cleaved during purification (Figure 3.11a; lane 2). Another benefit of the more recent purification protocol was that, in the absence of a large spectrophotometric absorbance peak at 260 nm, we were able to quantify the protein by spectrophotometry and load known amounts. Coomassie staining indicated that the protein migrated as expected for a protein weighing approximately 13 kDa and confirmed the spectrophotometric normalisation (Figure 3.11b).

We next compared the ability of the normalised WT and K206Q MITF(198-302) fragments to bind the *TYR* enhancer. A dilution series in which known amounts of the two proteins were incubated with a given amount of probe confirmed earlier experiments in which the K206Q mutant showed impaired binding to the *TYR* enhancer (Figure 3.11c; also see Figure 3.8). Although binding of the K206Q mutant could be detected, this was at higher protein concentrations, with 10 ng of the K206Q mutant only capable of achieving a level of binding equivalent to between 313 pg and 625 pg of the WT protein – a difference of 16- to 32-fold (Figure 3.11c; lane 19 vs. lanes 4-5). Under these conditions, the assay was highly sensitive to the amount of purified protein,

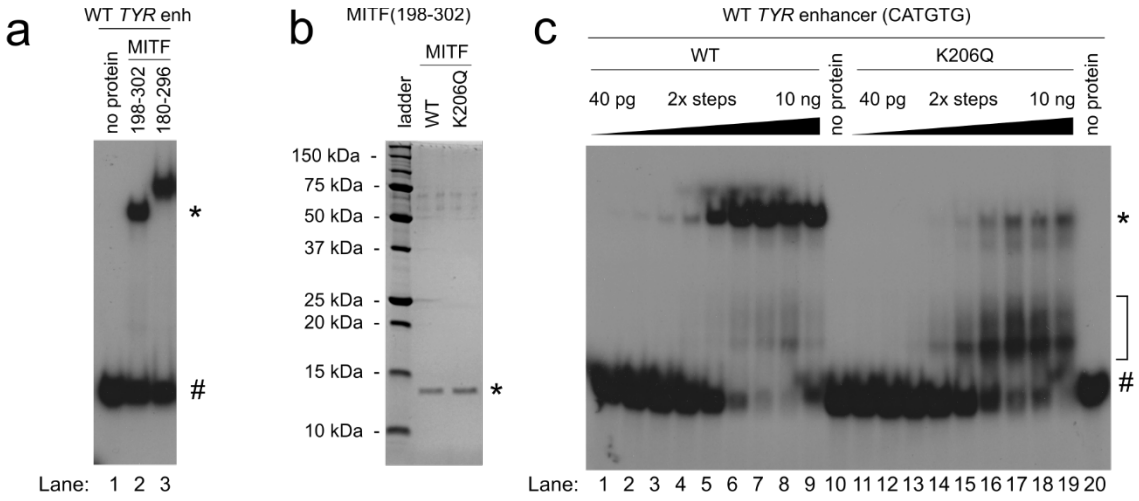



**Figure 3.11. The K206Q mutation impairs binding of MITF(198-302) to the *TYR* enhancer.** WT or mutated His-tagged MITF was expressed in *E. coli* using an optimised protocol to eliminate contaminating DNA, normalised and used in an EMSA. (a) EMSA comparing the binding ability of MITF(180-296)-His and MITF(198-302) using a radiolabelled *TYR* enhancer probe. The shifted probe in the MITF(198-302) condition (*) and free probe (#) are indicated. (b) Coomassie staining showing normalisation of MITF(198-302) that is either WT or K206Q mutant. (c) EMSA comparing the ability of the WT and K206Q mutant proteins shown in (b) to bind the WT *TYR* enhancer probe. Increasing amounts of the proteins (2-fold steps from approximately 40 pg to 10 ng) are incubated with a given amount of the probe. Shifted probe (*) and free probe (#) are indicated. Probe shifted to intermediate levels is indicated by a bracket.

as essentially no probe was shifted with 313 pg of WT protein (lane 4), and the majority of the probe was shifted with 4-fold more protein (1.25 ng, lane 6). We noted that this same trend was observed at similar concentrations of the K206Q mutant when concentrating on the level of free probe (Figure 3.11c, # in lanes 15-17). However, in samples with the K206Q mutant showing lower levels of free probe, the probe was shifted to an intermediate level, rather than the migration pattern we had seen with the WT protein and the longer MITF(180-296)-His protein (Figure 3.11c; bracket, lanes 16-19). It should be noted that the WT protein also showed a small amount of probe with this intermediate migration pattern at higher concentrations of protein, but the majority of shifted probe showed the slower migration pattern observed earlier (Figure 3.11c, lanes 6-8; compare to Figure 3.11a, * in lane 2). Upon reviewing our earlier

experiments, we saw that a small amount of probe was shifted to the same intermediate migration pattern with the WT MITF(180-296)-His protein (see Figure 3.8).

Given the Coomassie staining (Figure 3.11b) and mass spectrometry characterisations of the proteins used in these experiments, it seemed unlikely that this shift was resulting from a shorter protein (e.g., degradation product) binding the probe and resulting in an intermediate shift. As the intermediately shifted band was much more prominent for the K206Q mutant than the WT protein, one possibility was that the K206Q mutant was binding the probe but then dissociating at some point during the protocol. This would most likely be during electrophoresis, as dissociation before the gel began running should not result in an intermediate migration pattern. Several modifications of the protocol were attempted, including varying the incubation temperatures and times, running the gel at 4°C, altering the concentrations of various components of the band shift buffer and altering the concentration of acrylamide and other gel components. However, none of these modifications eliminated or accentuated the bands with an intermediate shift pattern (data not shown). Regardless, this data indicated that although the K206Q mutant was capable of some degree of binding to the *TYR* enhancer, its ability to bind this sequence was impaired relative to the WT protein under the conditions tested.

To verify the earlier results with the MITF(180-296)-His protein prepared with the un-optimised protocol (see Figures 3.7, 3.8), we again compared the ability of the MITF(198-302) fragment to bind the WT *TYR* enhancer 5'-CATGTG-3' motif and the *TYR* T-to-C enhancer 5'-CACGTG-3' motif. We had seen earlier that mutation of one of the central bases to alter the motif from 5'-CATGTG-3' to 5'-CACGTG-3' had augmented the ability of the K206Q mutant to bind while not greatly affecting the binding of the WT protein (see Figure 3.8). The present experiment used a slightly

different portion of the MITF DNA binding domain and an optimised protocol, resulting in several orders of magnitude less contaminating bacterial DNA when compared with the earlier experiments.

This experiment was done twice, using independently prepared proteins and probes – each EMSA panel in Figure 3.12 depicts one of these experiments. The only difference was that the second experiment used double the amount of probe as the first. As we had seen before, the K206Q protein showed little binding to the WT *TYR* enhancer probe, even at higher protein concentrations (Figure 3.12, lanes 8-9), while the WT protein was capable of binding to this motif in a manner dependent on protein concentration (Figure 3.12, lanes 3-5). Mutation of the motif to 5'-CACGTG-3' resulted in K206Q binding, although it never achieved the same level of binding as the WT protein (Figure 3.12, lanes 17-18 vs. lanes 13-14). Although the WT protein was capable of binding both probes, binding to the mutated T-to-C probe was stronger. This indicated that in this context, both the WT and K206Q proteins bound better to the 5'-CACGTG-3' motif. The present study differs from previous experiments in that the binding of the K206Q mutant protein to the *TYR* T-to-C enhancer probe (5'-CACGTG-3'; lanes 15-18) was clearly less than that of the WT protein (lanes 11-14).

Thus, it was unclear to what extent the lack of K206Q mutant binding to the WT *TYR* enhancer probe was due to a selective impairment in binding to the 5'-CATGTG-3' motif. It was also possible that the K206Q mutant merely suffered from globally diminished DNA binding capacity and that the preference of MITF in general for the 5'-CACGTG-3' motif over the 5'-CATGTG-3' motif (seen with the WT protein; Figure 3.12, lanes 13-14 vs. lanes 4-5) was preserved in the K206Q mutant. When coupled with a lower DNA binding ability in general, this could result in the K206Q mutant

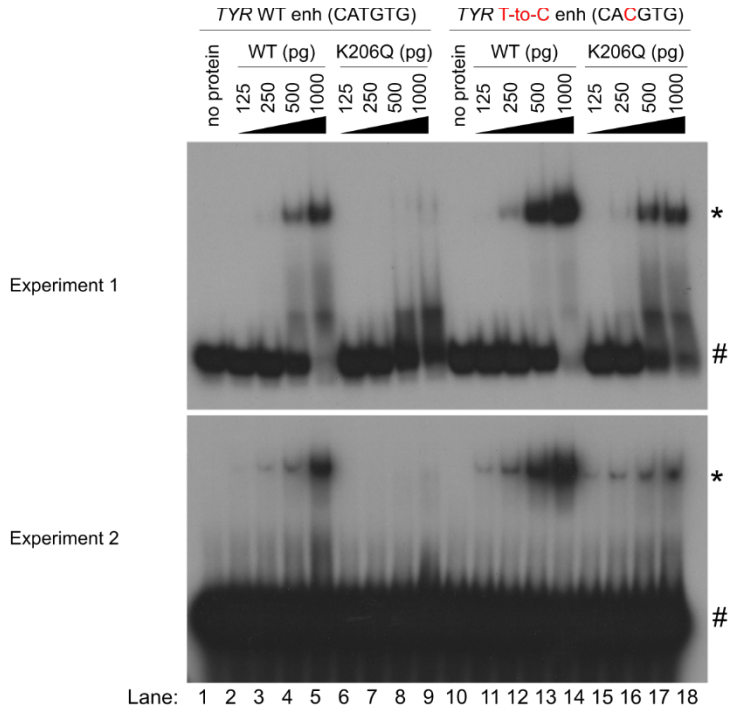



**Figure 3.12. MITF(K206Q) shows impaired binding to E-box and M-box motifs.** WT or K206Q mutant MITF(198-302) were expressed in *E. coli* and purified in buffers with pH 9.0 and 1 M NaCl to eliminate contaminating DNA. Shown are two replicates of the same experiment, which use independently prepared protein and probes. The experiments were conducted identically, save for double the amount of radiolabelled probe being used in the second experiment. Several different dilutions of protein were incubated with the labelled probe that comprised either the WT *TYR* enhancer (*TYR* WT enh) or the same with a T-to-C mutation in the central 5'-CATGTG-3' motif (*TYR* T-to-C enh). Shifted (*) and free probe (#) are indicated.

failing to bind the 5'-CATGTG-3' motif while retaining some binding to the 5'-CACGTG-3' motif.

To further address this, we decided to test MITF binding in another context. We chose the *LAMP1* promoter, a binding site identified by an MITF-3xHA ChIP-seq experiment (Rob Siddaway, unpublished data). Unlike the *TYR* enhancer 5'-CATGTG-3' motif, the *LAMP1* promoter harbours a 5'-CACGTG-3' motif – the motif that, according to our data, is preferred by the K206Q mutant and comprises the other major class of MITF binding sites (Cheli et al., 2010). The motif is flanked 5' by a T and 3' by an A, identical to the flanking bases found in the *TYR* enhancer sequence,

eliminating the potential confounding influence of these bases on MITF binding (Aksan and Goding, 1998). This experiment was in some ways the reverse of the *TYR* enhancer experiment, in that we again included probes with 5'-CATGTG-3' and 5'-CACGTG-3' motifs, however the WT *TYR* enhancer probe used earlier harboured the former, whereas the WT *LAMP1* promoter used presently harbours the latter. As we had done before with the *TYR* enhancer, we tested both the WT *LAMP1* promoter and a version of the same in which the central 5'-CACGTG-3' motif was mutated to a 5'-CATGTG-3' motif with a single C-to-T point mutation (Figure 3.13a). As done previously, varying amounts of the WT and K206Q mutant proteins were then incubated with one or the other of the radiolabelled probes, the amount of which was held constant. Also, note that we chose to use the higher of the two concentrations of probes tested earlier in Figure 3.12 (second panel).

Both the WT and K206Q mutant MITF(198-302) proteins bound the WT *LAMP1* promoter with roughly equal affinity (Figure 3.13b). This was different from what we had observed with these proteins when examining binding to the *TYR* T-to-C enhancer probe (5'-CACGTG-3'; see Figure 3.12) but similar to earlier studies of this same probe using protein preparations containing high levels of contaminating DNA (see Figure 3.8). Mutation of the *LAMP1* promoter 5'-CACGTG-3' motif to a 5'-CATGTG-3' motif impaired the binding of WT MITF(198-302), resulting in approximately 4-fold more protein being required to observe a similar level of binding (Figure 3.13b, lanes 4-6). The K206Q mutant protein binding was also impaired when the 5'-CACGTG-3' motif was mutated to a 5'-CATGTG-3'motif. However, the loss of binding observed for the K206Q was more significant than seen with the WT, with the highest protein concentration of 500 pg only achieving binding equivalent to that achieved by approximately 16-fold less protein with the WT *LAMP1* promoter probe

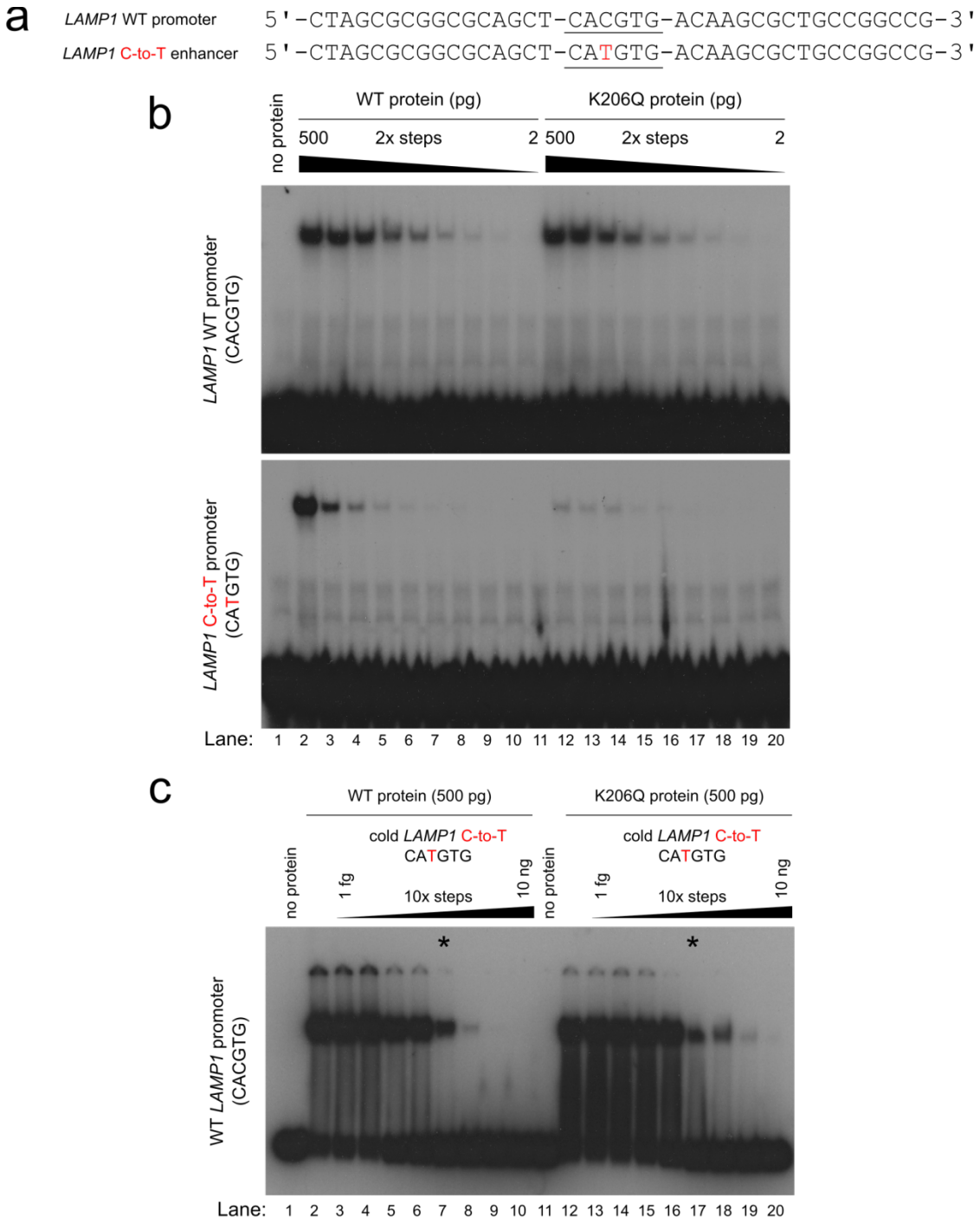



**Figure 3.13. MITF(K206Q) binding to the *LAMP1* promoter is impaired by a C-to-T mutation.** WT or K206Q mutant MITF(198-302) was expressed in *E. coli* and purified in buffers with pH 9.0 and 1 M NaCl to eliminate contaminating DNA. (a) The sequence of the two EMSA probes used in (b) and (c) is shown. These probes contained approximately 40 bp of either the WT *LAMP1* promoter or the same in which the central E-box motif (underlined) was mutated (shown in red). (b) EMSAs using a dilution series of the WT and K206Q mutant proteins and either the WT *LAMP1* promoter probe (top panel) or the mutated *LAMP1* promoter probe (lower panel). (c) A competition EMSA in which the WT *LAMP1* promoter probe is incubated with 500 pg of either WT or K206Q mutant MITF. Samples received either no cold competitor DNA (lanes 2 and 12) or increasing amounts of unlabelled *LAMP1* C-to-T promoter probe, according to a 10-fold dilution series. Asterices (*) indicate samples with 10 pg of cold competitor DNA, the level at which competitor DNA begins to compete with the labelled probe.

(Figure 3.13b, lane 12 vs. lane 16). This indicated that, in the context of the *LAMP1* promoter, the K206Q mutation primarily affected binding to the *TYR* C-to-T mutant 5'-CATGTG-3' motif while leaving binding to the WT 5'-CACGTG-3' motif virtually entirely intact.

The relative binding preferences of a protein for different motifs can also be assessed with a competition EMSA. This involves incubating the protein with radiolabelled probe as done previously, but unlabelled probe of known sequence is then added to determine the ability of this sequence to compete with the radiolabelled probe for protein binding. We made use of this system to address the preference of K206Q mutant MITF for 5'-CACGTG-3' and 5'-CATGTG-3' motifs. MITF(198-302) that was either WT or K206Q mutant was incubated with radiolabelled WT *LAMP1* promoter probe (5'-CACGTG-3') as before. We then added increasing concentrations of unlabelled *LAMP1* C-to-T promoter probe (5'-CATGTG-3') to assess the ability of this sequence to compete with the radiolabelled 5'-CACGTG-3'-containing probe.

The WT protein began to be competed away from the labelled WT *LAMP1* promoter probe in the presence of approximately 10 pg of unlabelled C-to-T (5'-CATGTG-3') *LAMP1* promoter probe (Figure 3.13c, * in lane 7). The K206Q protein was competed away from the labelled probe by the same amount of unlabelled probe (Figure 3.13c, * in lane 17). However, binding of the WT protein was no longer detectable at 1 ng of competing probe (lane 9), while binding of the K206Q protein to the labelled 5'-CACGTG-3' probe could still just be detected with 10 ng of competing unlabelled 5'-CATGTG-3' probe (lane 20). That is to say, roughly equivalent binding to the labelled 5'-CACGTG-3' probe was seen with approximately 100 pg of competing 5'-CATGTG-3' probe for the WT protein and approximately 1 ng of competing 5'-CATGTG-3' probe for the K206Q mutant (Figure 3.13b, lane 8 vs. lane 19). This

indicated that, compared to the WT protein, the K206Q mutant required approximately 10-fold more unlabelled *LAMP1* C-to-T promoter probe (5'-CATGTG-3') to fully compete it away from the WT *LAMP1* promoter probe.

Taken together, our data indicated that, under the limited conditions tested, WT MITF has more affinity for 5'-CACGTG-3' motifs than 5'-CATGTG-3' motifs. The same appeared to be true of the K206Q mutant. Whether MITF(K206Q) binding was impaired in general was unclear as binding to a 5'-CACGTG-3' motif in the context of the *TYR* enhancer was impaired, while binding to the 5'-CACGTG-3' motif in the *LAMP1* promoter was not. The data were consistent with the K206Q mutant protein exhibiting a greater degree of preference for the 5'-CACGTG-3' motif over the 5'-CATGTG-3' motif than did the WT protein. Put another way, the K206Q mutation altered MITF motif preference, resulting in a severe impairment of binding to 5'-CATGTG-3' motifs while leaving binding to 5'-CACGTG-3' motifs intact to varying degrees, depending on the context.

### *3.2.4 MITF(K206Q) shows altered function in vitro*

#### 3.2.4.1 Effect of K206 status on genomic target binding

MITF(K206Q) had shown an impairment in DNA binding assays, and we wondered whether this impairment extended to the full-length protein in a cellular context. To investigate this, we used a 501mel cell line stably expressing triple HA-tagged MITF (MITF-3xHA) that was available in the lab. The vector used to generate this cell line was also available. This vector was mutated to K206R or K206Q and used to generate 501mel stable cell lines expressing these mutants for comparison to the existing cell line expressing the WT protein. The first two rounds of screening failed to

yield any clones stably expressing MITF(K206Q)-3xHA (data not shown). We increased the number of clones screened from 24 to 72 for each construct and were able to isolate clones stably expressing MITF(K206R)-3xHA and MITF(K206Q)-3xHA, although only one clone expressing levels comparable to the WT stable cell line was found for the K206Q mutant (Figure 3.14a, lane 9). After expansion and further screening, MITF(K206R)-3xHA clone 6 and MITF(K206Q)-3xHA clone 41 (the only positive clone) were chosen, as they showed levels of MITF-3xHA similar to the WT protein (Figure 3.14b). These clones were then examined by immunofluorescence with an antibody against HA to assess clonality. Each of the three cell lines showed more than 95% of cells positive for HA staining in the nucleus, a distribution consistent with MITF overexpressed in non-melanoma cell lines and with endogenous MITF in 501mel cells (see Figures 3.1b, 3.4b; Bismuth et al., 2006; Carreira et al., 2006).

Initially, we planned to use ChIP-seq to compare the binding of WT and mutant MITF, however the resulting DNA was neither of sufficient quantity nor quality, as judged by Bioanalyzer (data not shown). We turned to ChIP, with the aim of analysing the binding of WT and mutant MITF to several MITF targets, which included a combination of targets taken from the literature and from an MITF ChIP-seq experiment done in 501mel cells expressing WT MITF-3xHA (Figure 3.14d; Rob Siddaway, unpublished data). These were chosen to include binding sites containing both 5'-CACGTG-3' and 5'-CATGTG-3' motifs, analogous to the two motifs tested with EMSAs in the previous section.

Two plates of each cell line were grown in parallel, harvested, pooled and processed for ChIP, using an antibody against HA to immunoprecipitate MITF-3xHA. The 501mel parental cell line served as a negative control, with each sample being normalised to the signal from its own input. The ChIP protocol appeared to have

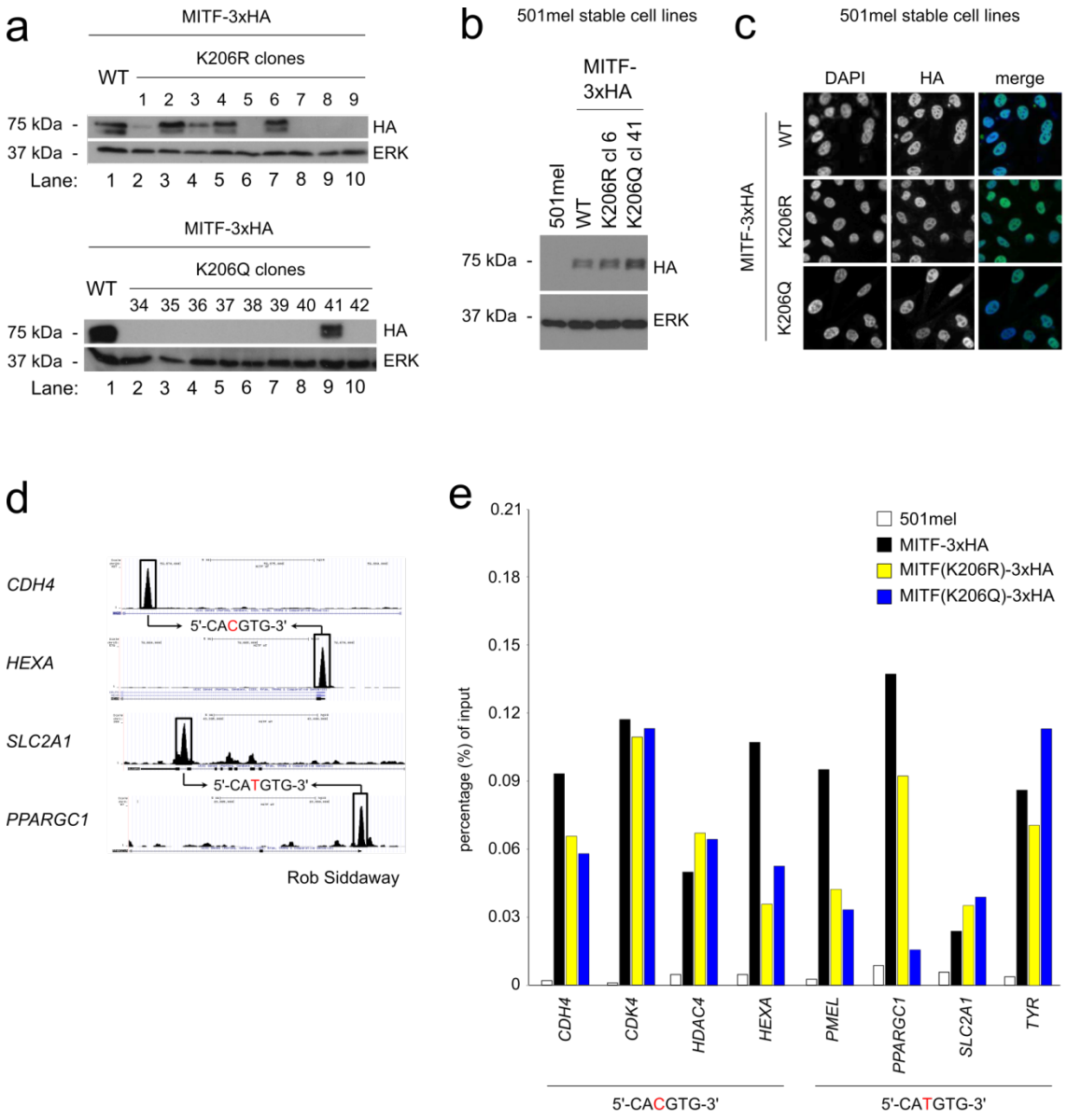



**Figure 3.14. Initial investigation of MITF-3xHA binding to targets in 501mel melanoma cells.** 501mel cells stably expressing MITF-3xHA that is either WT or mutated to K206R or K206Q were used to examine the effect of K206 mutations on MITF binding to genomic targets. (a) Western blotting showing a subset of clones during screening for expression of MITF(K206R)-3xHA or MITF (K206Q)-3xHA. The WT cell line is shown in lane 1 for comparison. Whole cell lysates were probed with antibodies against FLAG and ERK. (b) Selected clones were re-tested to verify comparable levels of MITF-3xHA expression among the different clones. (c) Cells were plated on glass coverslips. After 48 hours, they were fixed and stained with an antibody against HA and with DAPI to visualise nuclei. Images were acquired by confocal microscopy. (d) Screenshots from the UCSC genome browser showing raw read density of MITF-3xHA for several genomic targets harbouring either 5'-CACGTG-3' motifs or 5'-CATGTG-3' motifs. Data is courtesy of Rob Siddaway. (e) Cells were processed for ChIP using primers flanking previously identified MITF binding sites near the indicated genes. Results are shown relative to the signal given by the input from the corresponding sample. Values shown are the mean of duplicate biological replicates that were processed in parallel.

worked as intended – the 501mel parental cell line gave very low signal compared to the MITF-3xHA-expressing cell lines (Figure 3.14e). The K206R and K206Q mutants did not consistently bind better or worse than the WT to the tested 5'-CACGTG-3' or 5'-CATGTG-3' motifs. Overall, the *HEXA*, *PMEL* and *PPARGC1* promoters showed the greatest difference between the binding of the WT and one of the mutant proteins. There was also no clear pattern discernible when comparing the K206R and K206Q mutant proteins (Figure 3.14e).

We were unable to repeat this experiment – upon thawing the cells, MITF(K206Q)-3xHA expression had fallen to such low levels as to no longer be comparable to the WT and K206R proteins. Although we began a new round of selection for a replacement K206Q mutant cell line, we had recently received a tetracycline-inducible piggyBac transposon system (see Figures 3.1, 3.4). We chose to use this to generate new cell lines, rather than attempting to use conventional methods to remake the K206Q stable cell line. Additionally, the 501mel cell line we had been using harboured a relatively high level of endogenous MITF. We were concerned that this might obscure the effect of the K206 mutations – MITF binds DNA as a dimer, and heterodimerisation of ectopic mutant MITF with endogenous MITF of unknown K206 status could complicate interpretation of results.

Accordingly, we turned to the IGR39 cell line, which expresses very low levels of endogenous MITF (see Figure 3.1a). We had already generated an IGR39 cell line stably expressing inducible MITF-3xFLAG (see Figure 3.1), so the vector used to make this cell line was mutated to either K206R or K206Q and then used to generate cell lines stably expressing these mutants. Clones were screened, and those that did not induce well or showed high levels of MITF-3xFLAG expression in the absence of doxycycline were discarded. Figure 3.15a depicts selected clones for the WT and

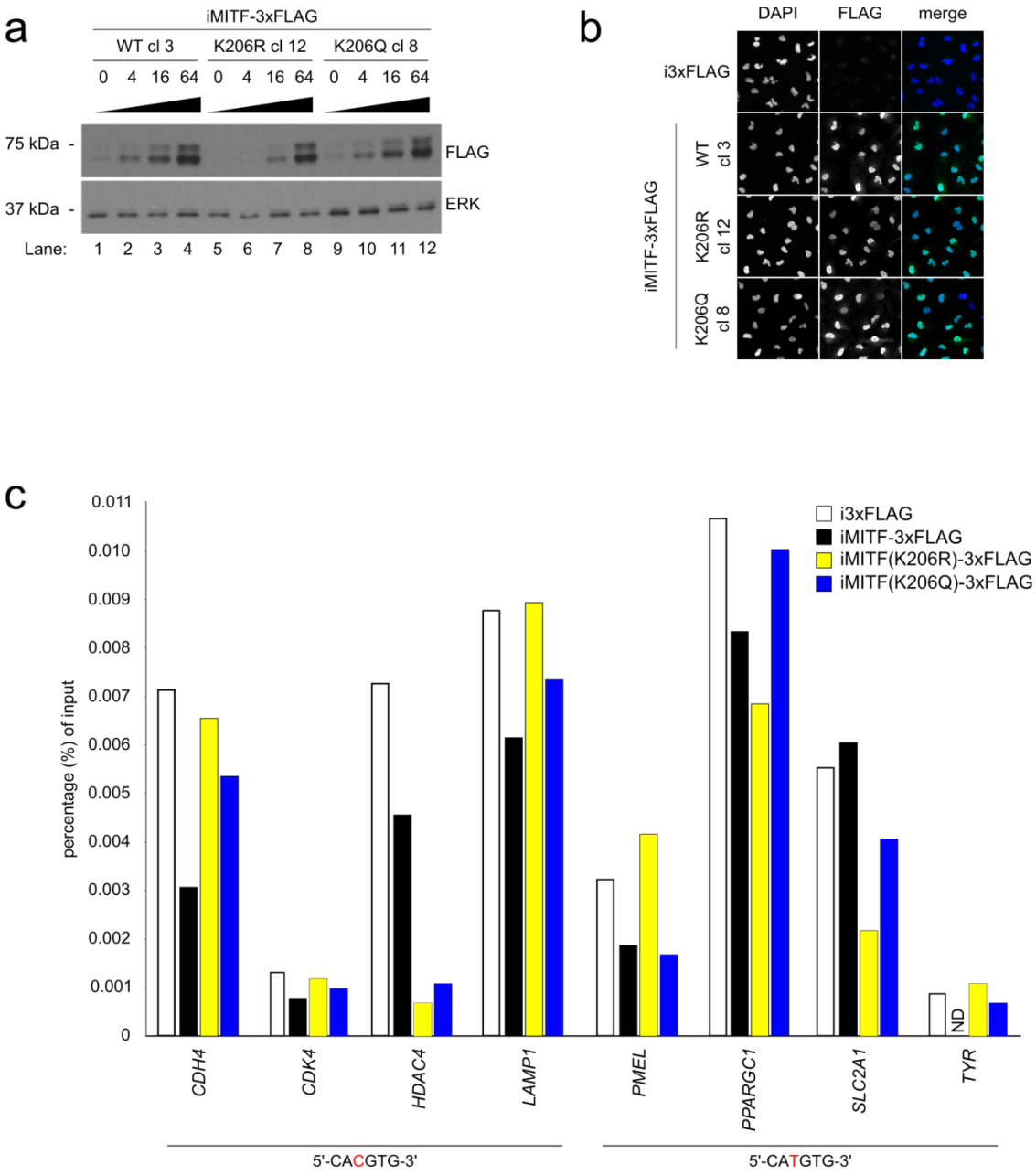



**Figure 3.15. Effect of K206 status on MITF-3xFLAG binding in IGR39 cells.** IGR39 cells stably expressing inducible MITF-3xFLAG that is either WT or mutated to K206R or K206Q were used to examine the effect of K206 mutations on MITF binding to genomic targets. (a) IGR39 iMITF-3xFLAG cell lines expressing MITF that was either WT or mutated at K206 were induced with doxycycline as indicated, and whole cell lysates were probed with antibodies against FLAG and ERK. (b) The same cell lines as in (a) were plated on glass coverslips and induced with doxycycline for 24 hours. Cells were then fixed and stained with an antibody against FLAG and with DAPI to visualise nuclei. Images were acquired by confocal microscopy. (c) Cells were induced with doxycycline and processed for ChIP using primers flanking previously identified MITF binding sites near the indicated genes. Results are shown relative to the signal given by the input from the corresponding samples. Values shown are the mean of duplicate biological replicates that were processed in parallel. ND indicates no signal was detected. Note that the data shown in the top two rows of (b) also appears in Figure 3.1b.

mutant proteins, showing that expression of WT and mutant MITF-3xFLAG increased in response to higher doses of doxycycline. In an attempt to normalise the levels of ectopic MITF, we chose to induce the WT and K206Q cell lines with 16 ng/ml of doxycycline, while the K206R cell line was induced with 32 ng/ml of doxycycline (Figure 3.15a). Immunofluorescence studies indicated that, for each of the MITF-3xFLAG-expressing cell lines, the majority of cells showed MITF-3xFLAG to be primarily localised to the nucleus (Figure 3.15b). IGR39 i3xFLAG cells served as a negative control. Note that the immunofluorescence images for the IGR39 i3xFLAG and WT iMITF-3xFLAG also appeared in Figure 3.1b when these lines were used to assess MITF acetylation.

We then used the same ChIP experimental setup employed with the 501mel MITF-3xHA cell lines to investigate the effect of K206 status on MITF binding to genomic targets in the IGR39 cell line. We included the *LAMP1* promoter as an MITF target site in place of the *HEXA* promoter examined in the previous ChIP study, as we had recently obtained the EMSA results assessing WT and K206Q mutant MITF binding to the *LAMP1* promoter (see Figure 3.13) and wanted to assess MITF binding to this motif in a cellular context. Also, note that the other motif analysed in EMSAs, the *TYR* enhancer, was included in the panel of ChIP target sites. This experiment was done in duplicate biological replicates that were processed in parallel, with the mean signal normalised to the signal given by the input fraction from the same sample (Figure 3.15c).

We first noted that, when compared to the previous 501mel ChIP experiment, the values were very low – approximately 10-fold lower than those seen in 501mel MITF-3xHA cells (Figure 3.15c vs. Figure 3.14e). This could be due to several different factors and would not have precluded analysis, however the high signal given

by the IGR39 i3xFLAG negative control cell line relative to the WT and mutant IGR39 iMITF-3xFLAG cell lines complicated interpretation of this experiment (Figure 3.15c, white bars). The negative control cell line gave high values for every primer set tested, indicating that the signal was non-specific and unlikely to be resulting from binding of MITF-3xFLAG proteins. Shortly after this experiment was conducted, a report was published indicating that melanoma cell lines expressing low levels of MITF showed methylation of MITF target promoters and impaired upregulation of MITF targets in response to ectopic MITF (Lauss et al., 2015). This indicated that perhaps the binding of ectopic MITF-3xFLAG to our chosen targets sites may be impaired in IGR39 cells, providing a possible explanation for both the low values in general and the failure of MITF-3xFLAG-expressing cell lines to return values greater than those seen in the negative control cell line (Figure 3.15c).

Fortunately, the piggyBac system facilitated relatively rapid generation of stable cell lines. After realising that the 501mel MITF(K206Q)-3xHA cell line (see Figure 3.14) was no longer suitable due to loss of expression of ectopic MITF and that the IGR39 cell line may prove a difficult context in which to assess MITF-3xFLAG binding to endogenous targets, we generated stable inducible 501mel cell lines. The lines expressing the WT and K206R mutant proteins have already been discussed in the context of MITF acetylation (see Figure 3.4). The new K206Q mutant cell line was induced with a doxycycline titration curve alongside the WT and K206R mutant lines for normalisation of the amount of ectopic MITF-3xFLAG (Figure 3.16a). The K206Q mutant cell line was also assessed by immunofluorescence, using an antibody against FLAG, fluorescent phalloidin to label actin and DAPI to label nuclei.

The 501mel iMITF(K206Q)-3xFLAG cell line showed a level of ectopic MITF roughly equivalent both to endogenous MITF and to the level of ectopic MITF in the

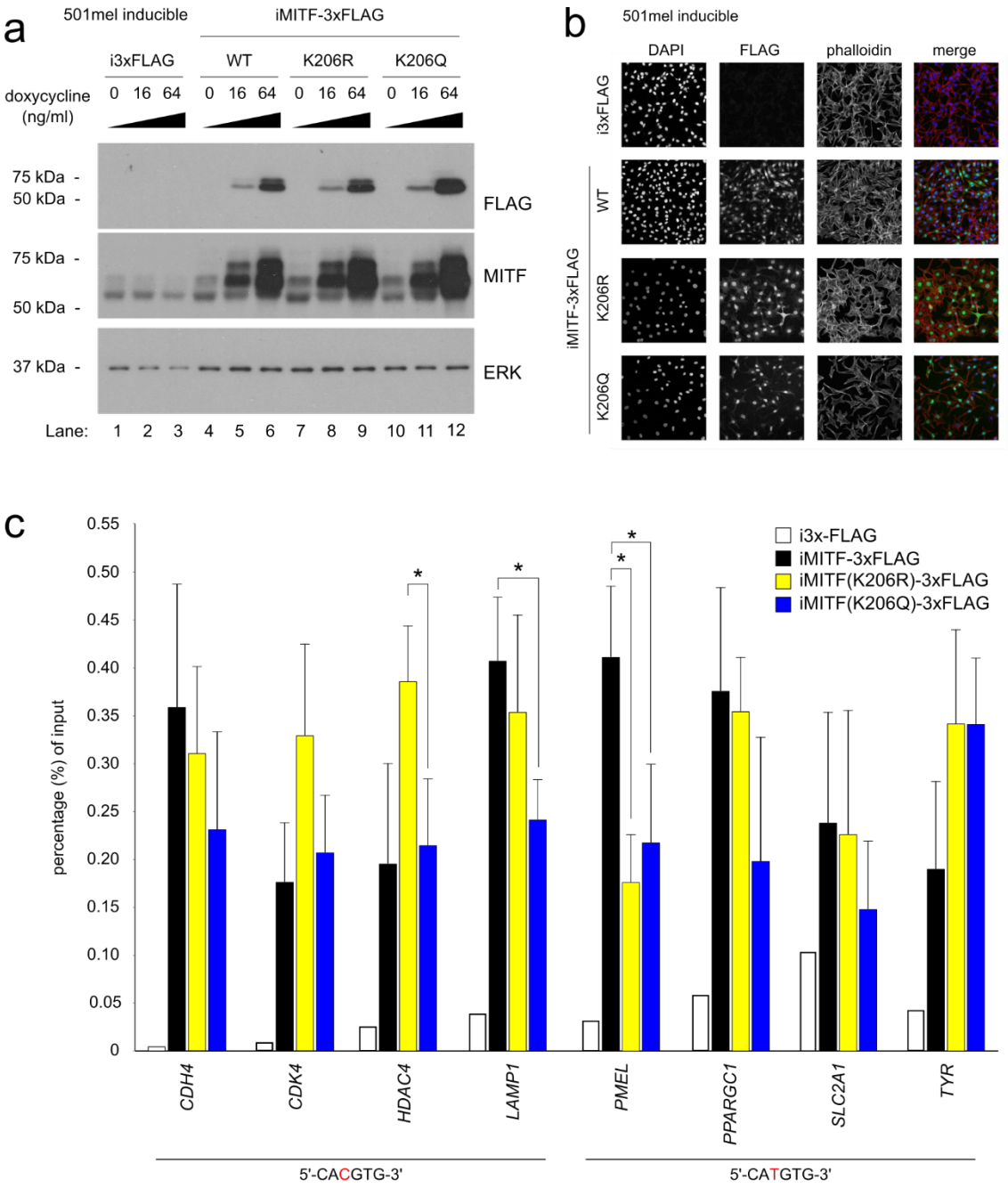



**Figure 3.16. K206 status slightly alters MITF binding to some targets in 501mel melanoma cells.** 501mel cell lines stably expressing inducible MITF-3xFLAG that is either WT or mutated to K206R or K206Q were used to examine the effect of K206 status on MITF binding to genomic targets. (a) 501mel iMITF-3xFLAG cell lines expressing MITF that was either WT or mutated at K206 were induced with doxycycline (16 ng/ml) as indicated, and whole cell lysates were probed with antibodies against FLAG, MITF and ERK. (b) The same cell lines as in (a) were plated on glass coverslips and induced with 16 ng/ml doxycycline for 24 hours. Cells were then fixed and stained with an antibody against FLAG, fluorescent phalloidin to visualise actin and DAPI to visualise nuclei. Images were acquired by confocal microscopy. (c) Cells were induced as in (a) and processed for ChIP using primers flanking previously identified MITF binding sites in the indicated genes. Results are shown relative to the signal given by the input from the corresponding samples. Values are the mean of three experiments, with error bars indicating standard deviation. Changes were not statistically significant, except where indicated with asterices (*, $p < 0.05$). Note that some of the data in (a) and (b) appears in Figure 3.4 in the context of another experiment.

WT and K206R mutant cell lines (Figure 3.16a). We observed that the lower band of the MITF-3xFLAG doublet was more intense than the upper band for each of the MITF-3xFLAG constructs, possibly indicating that ectopic MITF is primarily dephosphorylated. This was similar to the pattern seen for the doublet representing endogenous MITF in the 501mel i3xFLAG cell line (Figure 3.16a, lanes 1-3). Additionally, MITF(K206Q)-3xFLAG was primarily localised to the nucleus, again consistent with the localisation pattern seen in the WT and K206R mutant cell lines (Figure 3.16b). Note that some of the data shown in Figure 3.16a and Figure 3.16b. also appears in Figure 3.4 – the K206Q line was not depicted in the earlier figure, as this line was not included in studies of MITF acetylation.

These cell lines were then used in an attempt to clarify data from earlier ChIP experiments done in 501mel and IGR39 cells (see Figures 3.14, 3.15). MITF-3xFLAG was expressed at levels comparable to the level of endogenous MITF by inducing cells with 16 ng/ml doxycycline (Figure 3.16a, MITF blot). Importantly, each of the cell lines used appeared to have roughly equivalent levels of endogenous MITF (Figure 3.16a, lanes 4, 7 and 10). This could be an important consideration when assessing the effects of a given point mutant, as MITF binds to DNA as a dimer. The potential implications of the influence of MITF hetero- and homodimer formation on our results will be discussed further in later sections.

This ChIP experiment was done in triplicate, with cell plating staggered across three days. Each sample was induced for 48 hours with 16 ng/ml doxycycline. As before, the signal was normalised to the signal from the input of the same sample. Results are shown in Figure 3.16c, with the same colour scheme as used in Figure 3.15c. As we had seen with the non-inducible 501mel MITF-3xHA stable lines (see Figure 3.14e), the normalised signal from the 501mel i3x-FLAG negative control cell

line was lower than the normalised signal for each MITF-3xFLAG-expressing cell line, and this was true for each target examined (Figure 3.16c; white bars). We noted that the absolute values of the normalised signals for the 501mel iMITF-3xFLAG cell lines were higher than observed with the non-inducible 501mel MITF-3xFLAG stable cell lines and the IGR39 inducible stable cell lines in the previous experiments (Figure 3.16c vs. Figures 3.14e, 3.15c).

There was no consistent difference in binding to targets harbouring 5'-CACGTG-3' motifs as compared to targets harbouring 5'-CATGTG-3' motifs among the WT, K206R mutant or K206Q mutant proteins. That said, neither of the mutants bound significantly better than the WT to any of the 8 targets examined, while three targets showed that at least one of the K206 mutants bound more poorly than the WT (Figure 3.16c). The K206Q mutant showed impairment in binding to the *HDAC4*, *LAMP1* and *PMEL* promoters, relative either to the WT (*LAMP1*, *PMEL*) or the K206R mutant (*HDAC4*). The only other significant difference was seen with the *PMEL* promoter, where the K206R mutant also bound worse than the WT (Figure 3.16c). Thus, it appeared that the status of K206 influenced binding of full-length FLAG-tagged MITF to a subset of genomic targets in the 501mel melanoma cell line. However, this was variable and target-dependent – neither the mutational status (WT vs. K206R vs. K206Q) nor the nature of the genomic target motif (5'-CACGTG-3' vs. 5'-CATGTG-3') consistently affected MITF binding in a cellular context.

3.2.4.2 Effect of K206 status on *TYR* activation

DNA binding assays had indicated that the K206Q mutation may impair the ability of MITF to bind to a 5'-CATGTG-3' motif present in the *TYR* enhancer.

However, this was done with only the DNA binding region of MITF and a short oligonucleotide. Moreover, binding of MITF to the endogenous *TYR* enhancer in 501mel cells was not affected by the K206Q mutation (see Figure 3.16c). To determine if the K206Q mutation resulted in an impairment of full-length MITF's ability to activate expression from the *TYR* promoter in a cellular context, , we used the stable inducible melanoma cell lines described in the previous sections.

We began by inducing expression of MITF-3xFLAG, MITF(K206R)-3xFLAG or MITF(K206Q)-3xFLAG in 501mel cells for 2 days, collecting whole cell lysates and using an antibody against tyrosinase to assess endogenous tyrosinase expression. Prior reports indicated that better induction of tyrosinase expression was achieved by plating cultures sparsely and allowing them to grow to confluency (Wade & Burkart, 1978), so we conducted another experiment in parallel in which the same cell lines were plated sparsely and induced for 6 days (fresh doxycycline was added every 2 days) until they reached confluency. These cells were then lysed and processed for Western blotting alongside the 2-day samples.

Figure 3.17a shows the results of the 2-day and 6-day MITF-3xFLAG inductions. We were surprised to see that induction of MITF-3xFLAG over the course of 2 days resulted in a lower level of tyrosinase than the corresponding uninduced sample (Figure 3.17a, lane 4 vs. lane 3). However, doxycycline treatment also resulted in a lower level of tyrosinase expression in all cell lines tested. Importantly, doxycycline decreased tyrosinase levels in the negative control 501mel i3x-FLAG cell line, indicating that although the dose of doxycycline used was quite low (16 ng/ml), it appeared to be sufficient to impair endogenous tyrosinase expression. None of the stable inducible lines appeared to have elevated levels of tyrosinase at baseline, as compared to the 501mel i3x-FLAG cell line (Figure 3.17a). We noted that the WT and

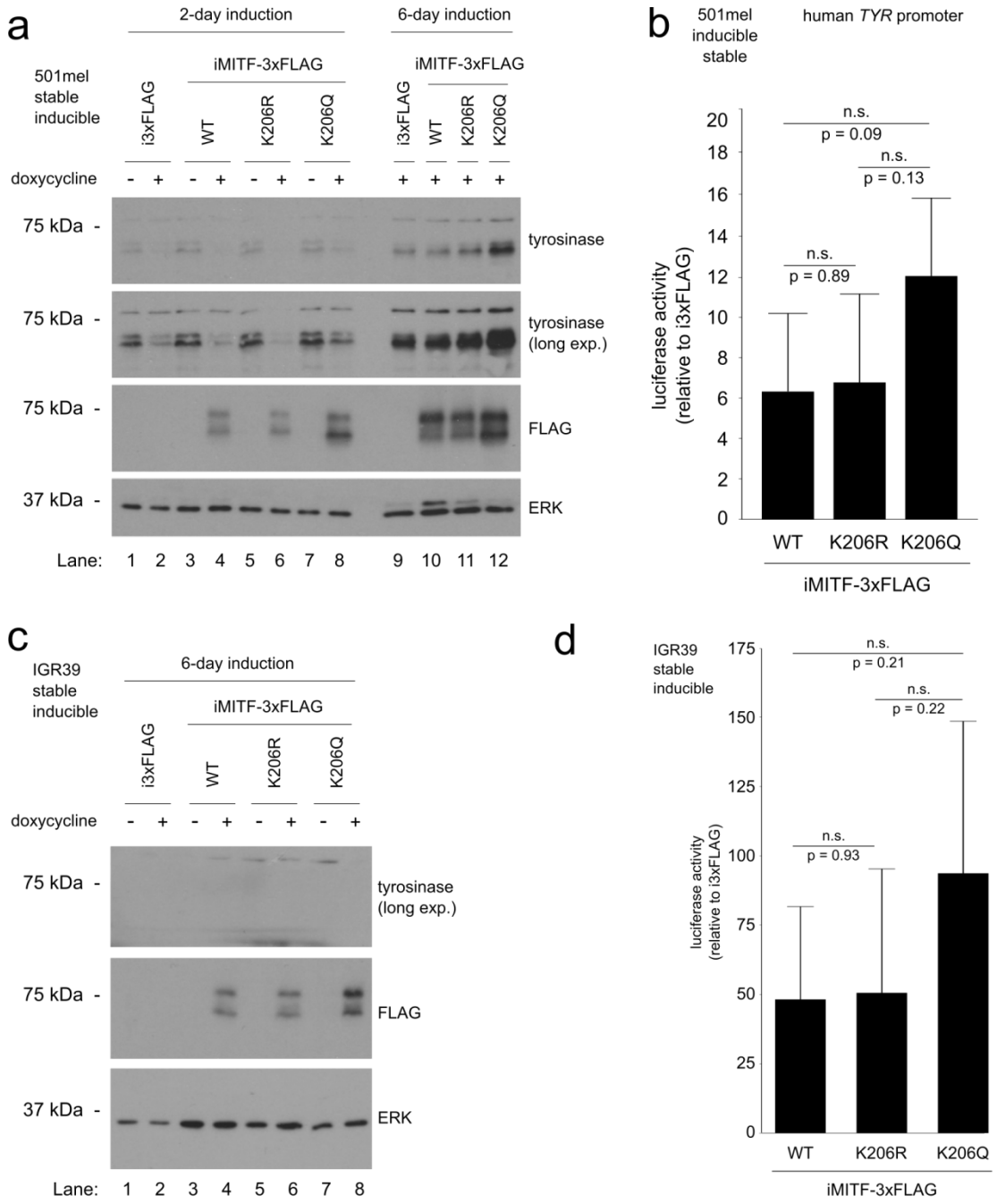



**Figure 3.17. MITF(K206Q) does not show impaired *TYR* activation *in vitro*.** The ability of MITF-3xFLAG to activate expression of *TYR* was examined by Western blotting and luciferase assay. (a) 501mel iMITF-3xFLAG cell lines expressing MITF that was either WT or mutated at K206 were induced with doxycycline (16 ng/ml) as indicated, and whole cell lysates were probed with an antibody against tyrosinase. Expression of MITF constructs was assessed by probing with a FLAG antibody, while ERK served as a loading control. (b) The same cell lines as in (a) were transfected with a vector in which luciferase expression was driven by the human *TYR* promoter. These cells were then induced 24 hours later as in (a), and luciferase activity was assessed 48 hours later. (c) IGR39 WT and mutant iMITF-3xFLAG cells were treated as in (a), and samples were probed with antibodies against tyrosinase, FLAG and ERK. (d) IGR39 WT and mutant iMITF-3xFLAG cells were treated as in (b) and used in a luciferase reporter assay. Luciferase assays (b, d) show the average luciferase activity for each condition (technical triplicates) relative to that seen in the i3xFLAG cell lines. Error bars represent standard deviation (n = 4). Comparisons consisted of unpaired t-tests, and p-values are shown.

K206R mutant cell lines showed a greater decrease in tyrosinase levels than did the i3x-FLAG cell line. This is contradictory to published reports in which ectopic MITF promoted tyrosinase expression (Schepsky et al., 2006). Also surprising was that the K206Q mutant appeared to show a smaller decrease in tyrosinase expression in response to doxycycline than any of the other cell lines (Figure 3.17a, lane 8 vs. lane 7), however we note that the FLAG immunoblot indicated this mutant was present at a higher level than the WT or K206R proteins.

Turning to the samples induced for 6 days, we saw that coupling sparse plating with a long induction time resulted in elevated levels of both MITF-3xFLAG proteins and tyrosinase, as compared to the analogous 2-day induction samples (Figure 3.17a, lane 10 vs. lane 4 and lane 11 vs. lane 6). The most notable difference was again seen with the K206Q mutant, which exhibited a marked increase in tyrosinase level, compared to both the 6-day induction 3x-FLAG control and the 2-day induction MITF(K206Q)-3xFLAG samples (Figure 3.17a, lane 12 vs. lane 9 and lane 8). Lastly, the iMITF(K206Q)-3xFLAG cell line showed a significantly higher level of tyrosinase than did the WT or K206R mutant cell lines after a 6-day induction with doxycycline (Figure 3.17a, lane 12 vs. lanes 10 and 11), although we again note that the level of MITF(K206Q)-3xFLAG was slightly higher than the levels of the WT or K206R mutant proteins, particularly when comparing the fastest-migrating species. Taken together, these data indicate that full-length MITF harbouring the K206Q mutation promotes higher levels of endogenous tyrosinase than WT MITF or MITF harbouring the K206R mutation. This was true for the 501mel melanoma cell line with two different experimental designs.

In an attempt to ascertain whether this effect was transcriptionally mediated, we made use of a *TYR* promoter luciferase construct. This construct consisted of luciferase

under the control of the -300 bp to +80 bp region relative to the human *TYR* transcription start site (available in the lab). Note that this construct does not include the *TYR* enhancer motif tested in EMSAs – the enhancer lies 1.8 kb upstream of the *TYR* promoter, and its inclusion would necessitate incorporating a large region of DNA harbouring many potential binding sites. This construct was transiently transfected into the same 501mel iMITF-3xFLAG cell lines as in Figure 3.17a. Cells were then induced for 48 hours, and luciferase activity was quantified by normalising relative to the 501mel i3xFLAG cell line. All MITF-3xFLAG cell lines showed an increase in luciferase activity of between 5-fold and 10-fold relative to the i3x-FLAG cell line (Figure 3.17b). The WT protein showed the lowest activation (6.32-fold), and the K206Q protein showed the highest activation (12.03-fold), however a one-way ANOVA showed that there was no significant difference among any of the cell lines expressing MITF-3xFLAG, $F(2, 9) = 2.31$, $p = 0.155$. Although the experiment was conducted 4 times, the high variation among experiments complicated interpretation. That said, the trend in the luciferase assay data was consistent with the data from the Western blot (Figure 3.17a) and indicated that rather than showing impaired activation of the *TYR* gene, if anything, MITF(K206Q)-3xFLAG exhibited greater *TYR* activation.

Our other inducible system was used to confirm what we had seen in the 501mel cell lines. The IGR39 iMITF-3xFLAG cell line and the counterpart cell lines expressing the K206R and K206Q mutants were subjected to the same experimental setup as described above for the 501mel cell lines. As we had seen higher tyrosinase levels in 501mel cells after a 6-day induction, this time point was chosen for analysis in the IGR39 cell lines. Surprisingly, tyrosinase was not expressed in any of the MITF-3xFLAG-expressing cell lines tested, neither in control conditions nor when expression of MITF-3xFLAG was induced for 6 days (Figure 3.17c). Although we were not aware

of this at the time, reports have since emerged that indicate that melanoma lines that express low levels of MITF (e.g., IGR39) are more likely to show methylation of the *TYR* promoter and are resistant to ectopic MITF-induced upregulation of pigmentation targets (Lauss et al., 2015).

We attempted to address this by using the *TYR* promoter luciferase construct in the IGR39 stable cell lines to assess the influence of K206 status on MITF activation of the *TYR* promoter. As had been done for the 501mel cell lines, we conducted a luciferase assay, using the *TYR* promoter region to drive expression of luciferase. We first noted that the luciferase activity fold-change in the IGR39 iMITF-3xFLAG cell line compared to the negative control i3xFLAG cell line was much greater than in the 501mel cells (Figure 3.17d). This is possibly due to the fact that the 501mel cells harbour endogenous MITF, which may have been capable of activating luciferase expression from the *TYR* promoter in the 501mel i3x-FLAG negative control cell line in the absence of ectopic MITF. The IGR39 i3x-FLAG negative control cell line, having very low levels of endogenous MITF, may have failed to activate the *TYR* promoter construct, resulting in higher luciferase activity in the IGR39 iMITF-3xFLAG cell lines in comparison to the negative control.

However, despite the greater absolute value of the activation of the *TYR* promoter relative to the control, analysis of the data with a one-way ANOVA again demonstrated no difference among the cell lines expressing WT, K206R mutant or K206Q mutant versions of MITF-3xFLAG, $F(2, 9) = 1.42$, $p = 0.29$. The general trend was in the same direction as for the 501mel cell lines, with the K206Q showing the greatest fold activation (94.62) and the WT showing the lowest (48.69). The fact that WT MITF-3xFLAG was capable of robustly activating expression from a plasmid-based *TYR* promoter but not capable of binding to (see Figure 3.15c) or activating

expression from (Figure 3.17c) the endogenous locus was consistent with the hypothesis that the endogenous TYR locus is methylated in IGR39 cells (Lauss et al., 2015).

### *3.2.5 MITF K206Q shows altered function in vivo*

To study the possible influence of MITF acetylation on K206 *in vivo*, we used a melanocyte development assay to assess the effect of the acetyl-lysine mimicking K206Q mutation. This was done in zebrafish and made possible by the existence of a line that harboured a homozygous mutation in *mitfa*, a zebrafish homologue of human *MITF* that governs development of neural crest-derived pigment cells (Lister et al., 1999). Expression of ectopic *mitfa* in this line (*mitfa* -/-) can rescue melanocyte development, which can be observed and quantified in the transparent embryos during the first 5 days post fertilisation (dpf). Moreover, the influence of mutations on MITF function can be assessed by comparing the degree of melanocyte rescue achieved by a given mutant to that achieved by the WT.

This work was done in collaboration with Elizabeth Patton and Zhiqiang Zeng at their facility and under their supervision (University of Edinburgh, UK). They also generously provided the construct required for the experiment, which is illustrated in Figure 3.18a. This construct harbours a portion of the zebrafish *mitfa* promoter, followed by the zebrafish *mitfa* coding sequence, which is then followed by a poly(A) sequence. This entire cassette was flanked with Tol2 sites to mediate insertion into the zebrafish genome (Kawakami et al., 2000). This construct was then injected along with Tol2 mRNA into single-celled *mitfa* -/- zebrafish embryos. We also included a small amount of phenol red as a tracking dye to gauge the efficacy of injections.

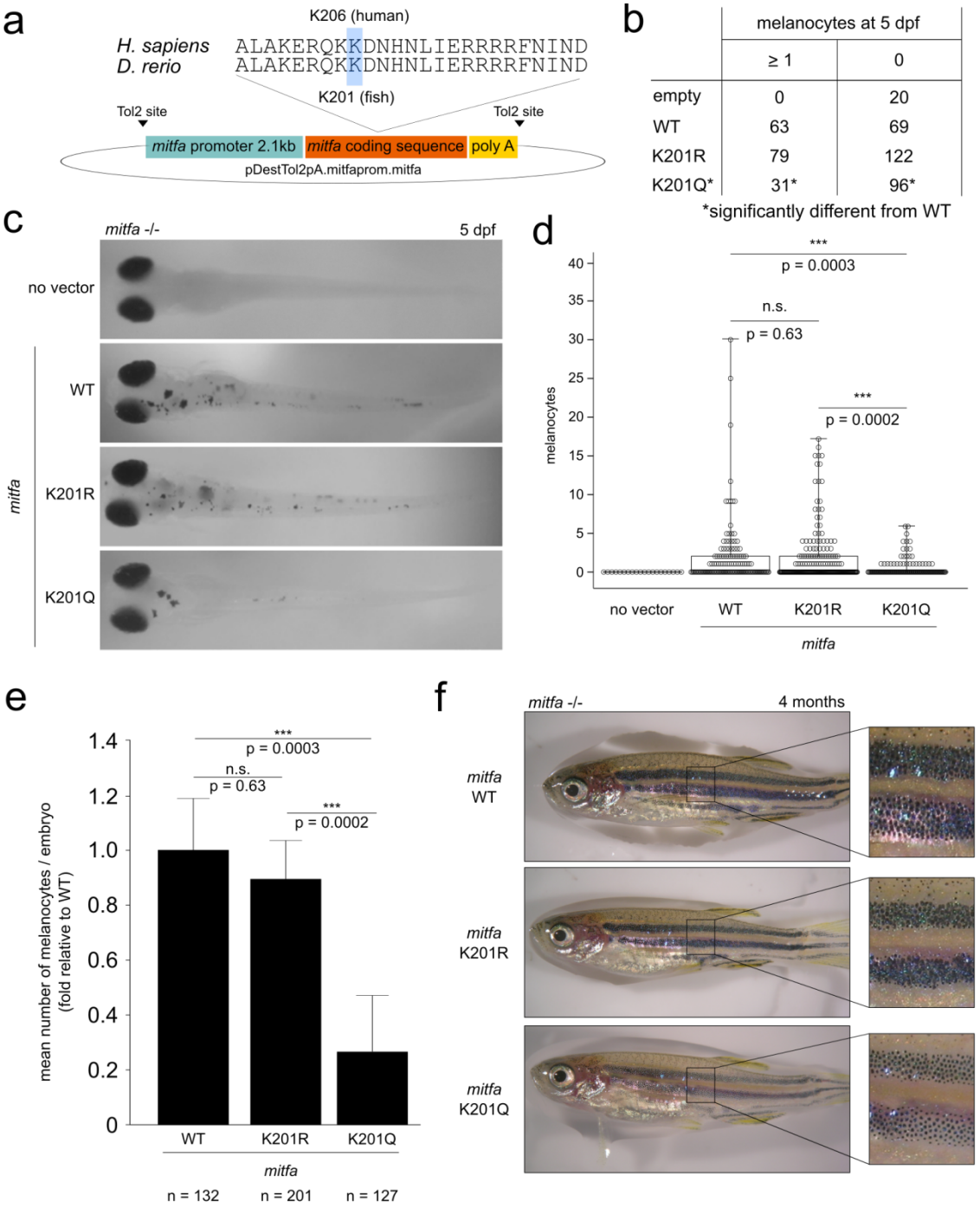



**Figure 3.18. Mitfa(K201Q) has impaired function *in vivo*.** *Mitfa* -/- zebrafish were used to compare the ability of *mitfa* mutants to rescue melanocyte development. (a) Schematic showing the Tol2-based construct injected into *mitfa* -/- zebrafish embryos. A 2.1 kb fragment of the zebrafish *mitfa* promoter, the zebrafish *mitfa* coding sequence and the SV40 late poly(A) sequence are flanked by Tol2 sites. An alignment of the basic region of the human and zebrafish MITF coding sequences shows K206 (K201 in zebrafish) highlighted in blue. (b) The vector detailed in (a) is either left as WT or mutated to K201R or K201Q and injected with Tol2 mRNA into *mitfa* -/- zebrafish embryos. After 5 days, embryos are collected, melanocytes are counted and a chi-square test showed the K201Q to be significantly different from the WT (*, see text for description). (c) An example of each condition in which some melanocytes were rescued is shown. (d) Quantification of the data shown as a box plot. (e) The same data as in (d) are shown as the number of melanocytes rescued per embryo relative to the WT. Error bars represent standard deviation, and p-values derived from unpaired t-tests are shown. (f) *Mitfa* -/- zebrafish were injected as in (b) and imaged at 4 months of age. The panels to the right show an enlarged region of pigmented stripes on the flank. Work was done in collaboration with Zhiqiang Zeng. Data in (f) is courtesy of Zhiqiang Zeng.

Figure 3.18a shows the basic region of human MITF and zebrafish mitfa, with the residue corresponding to K206 in human MITF highlighted (K201 in zebrafish; Figure 3.18a). MITF is highly conserved between humans and zebrafish, with particularly high conservation in the DNA binding domain. We injected *mitfa* -/- embryos with the construct shown in Figure 3.18a harbouring the *mitfa* coding sequence that was either WT or mutated at residue K201 to arginine or glutamine. Embryos were injected according to four conditions (Figure 3.18b, c). The control condition consisted of an injection of only Tol2 mRNA and phenol red tracking dye, while the other 3 conditions included Tol2 mRNA, phenol red tracking dye and the vector containing *mitfa* (WT, K201R or K201Q) under control of the zebrafish *mitfa* promoter (see Figure 3.18a). Embryos were injected over the course of 5 days – two experimenters injected embryos, with each injecting embryos for each condition on each day. The number of melanocytes were counted at 5 dpf for each injected embryo that had survived. It was noted that the number of embryos injected with WT *mitfa* that did not show any melanocyte rescue was higher than our collaborators normally observed (Figure 3.18b; Zhiqiang Zeng, personal communication).

We first treated the data as categorical, with embryos counted as either having melanocytes or not having melanocytes (Figure 3.18b). The WT showed the best melanocyte rescue in terms of the percentage of embryos that had at least one melanocyte (47.7%, n = 132; Figure 3.18b). Of embryos injected with the K201R mutant, 39.3% had at least one melanocyte after 5 days (n = 201). The K201Q mutant showed the worst rescue of melanocyte development in terms of the percentage of embryos with at least one melanocyte (24.4%; n = 127). These groups were significantly different, as judged by the chi-square test, $X^2$ (2, N = 457) = 14.36, $p$ = 0.0008. Next, post hoc pairwise comparisons were done with the Bonferroni correction

– this showed that embryos injected with WT and K201R mutant *mitfa* did not differ significantly in terms of the percentage of embryos with 1 or more melanocytes, $X^2$ (1, N = 333) = 2.31, $p$ = 0.13 (Figure 3.18b). However, the K201Q mutant differed significantly from both the WT, $X^2$ (1, N = 259) = 15.22, $p$ = 0.0001, and the K201R mutant, $X^2$ (1, N = 328) = 7.75, $p$ = 0.0054. Thus, injection of the K201Q mutant resulted in a lower percentage of embryos showing rescue of melanocyte development than did injection with either the WT or the K201R mutant (Figure 3.18b).

The K201Q (but not the K201R) mutant was also significantly worse than the WT at rescuing melanocyte development when comparing the number of rescued melanocytes per embryo, rather than just comparing the percentage of embryos that showed any degree of melanocyte rescue. Figure 3.18c shows examples of embryos from each condition that displayed melanocyte rescue – note that these are not representative, as the median number of rescued melanocytes for all conditions was zero (Figure 3.18b, d). Figure 3.18d shows a box and whisker plot in which each embryo is depicted as a data point. This illustrates two factors that potentially limited the utility of this assay. The first is that the number of embryos (across all conditions) showing no melanocyte rescue was relatively high. The second is the variation in the number of melanocytes rescued, climbing to 30 in an embryo injected with WT *mitfa*. However, in spite of these limitations, a one-way ANOVA revealed that the effect of *mitfa* K201 status on the mean number of melanocytes rescued per embryo was significant, F (3, 499) = 7.72, $p < 0.0001$. Post hoc comparison testing showed that the average number of melanocytes rescued per embryo was lower for the K201Q mutant than for the WT (0.51 vs. 1.92, $p < 0.0005$; Figure 3.18e). This was also true when comparing the K201Q mutant to the K201R mutant, with the K201Q mutant rescuing significantly fewer melanocytes per embryo (0.51 vs 1.72, $p < 0.0005$). For

comparison, the WT and the K201R mutant were not significantly different (1.92 vs. 1.72, p = 0.63). Thus, the K201Q mutant rescued approximately 4-fold fewer melanocytes per embryo than did the WT or the K201R mutant (Figure 3.18e).

The impairment in function of the K201Q that was evident in embryos at 5 dpf was also evident in older fish. Fish injected with the same constructs as used for the melanocyte rescue assay were allowed to grow for 4 months. Images of *mitfa* -/- siblings injected with the WT, K201 and K201Q versions of the construct outlined in Figure 3.18a are shown in Figure 3.18f (images courtesy of Zhiqiang Zeng, University of Edinburgh). Although no quantification was done and images were only taken for a very small number of fish, this could indicate that whatever the nature of the defect caused by the K201Q mutation during melanocyte development, its effects may not be limited to early developmental stages. This defect appeared to manifest in older fish as decreased density of pigmentation in the horizontal stripes (Figure 3.18f, magnified views), but a larger sample would be needed before making any conclusions about the effect of K201 status on mitfa function in older zebrafish.

### 3.3 Discussion

MITF was shown to be acetylated in melanoma cells, with K206 being identified as an acetylation site using site-specific methods in Phoenix cells. We used bacterially expressed MITF to study the influence of K206 status on the ability of MITF to bind DNA, showing that the K206Q mutation impaired binding to a motif found in many MITF targets (5'-CATGTG-3'). However, MITF also binds to targets containing a 5'-CACGTG-3' motif. We found binding of the K206Q mutant to this motif may also be impaired, but not to the same degree as binding to the 5'-CATGTG-3' motif. We

then tested the ability of MITF(K206Q)-3xFLAG to bind these motifs in cell culture, however we were unable to demonstrate a consistent effect of the K206Q mutant on MITF motif preference in terms of its DNA binding or gene activation. Lastly, we examined the influence of the K206Q mutation on MITF function *in vivo*, using a zebrafish line lacking *mitfa*, which is the functional equivalent of *MITF* in zebrafish. These fish do not develop melanocytes, but by injecting embryos with *mitfa* that is WT or harbours the K206R or K206Q mutations, we can compare the degree to which these proteins are able to rescue melanocyte development. We observed that the K206Q mutant rescued significantly fewer melanocytes than did the WT or the K206R mutant, indicating that the K206Q mutation interferes with MITF function *in vivo* during development.

We showed that MITF can be acetylated in multiple cell lines. MITF has been reported to run as a doublet on Western blot, with the two species being differentially phosphorylated on S73, and we saw that both of these species were capable of being acetylated (Sato et al., 1997). Previous work in the lab indicated that MITF can be acetylated on multiple residues, and we confirmed two of those that showed the largest contribution to total MITF acetylation, K206 and K225. We were unable to confirm acetylation of K206 when MITF-3xFLAG was stably expressed in 501mel melanoma cells, as the K206R mutant was acetylated to the same extent as the WT protein. It could be that K206 is acetylated in Phoenix cells but not melanoma cells or that acetylation of this residue requires overexpression of the p300 acetylase and does not occur during HDAC inhibition. Alternatively, it could be that K206 is acetylated in this context but that this site accounts for only a small portion of total MITF acetylation, making evaluation of acetylation of a single site with the acK antibody difficult. Accordingly, we also attempted to evaluate acetylation of K206 by mass spectrometry,

however two runs using independently prepared samples showed that no peptides corresponding to MITF could be detected (data not shown).

We only detected acetylation of MITF during HDAC inhibition or p300 overexpression, but it is not clear if our failure to detect MITF acetylation in control conditions is due to a lack of sensitivity of our assay or if MITF is not acetylated in cell culture under control conditions. We note that our collaborators have observed acetylation of endogenous MITF in SK-MEL-28 cells under control conditions, however this occurs on a residue that was not identified as an acetylation site in our studies (José Rodríguez-López, personal communication).

MITF acetylation has not been previously described. However, a recent study provided the first report of acetylation of a TFE family member (Bao et al., 2016). TFEB was found to be acetylated on residue K116, a residue not conserved in MITF. As in our experiments, acetylation was primarily detected under conditions in which HDACs were inhibited. They noted that deacetylation of this residue correlated with increased transcription of TFEB target genes, which could operate via many possible mechanisms, including changes in DNA binding, association with co-factors, protein stability or nuclear-cytoplasmic shuttling. Of note, each of the 6 lysine residues we found to be acetylated in the MITF DNA binding domain are conserved in TFEB, TFE3 and TFEC and show some conservation among other bHLH factors. It would be interesting to see whether these residues can be acetylated in other bHLH transcription factors and, if so, if these acetylation events affect DNA binding in a manner similar to what we have seen for MITF.

MITF targets appear to largely contain one of two motifs that differ at one central base, 5'-CATGTG-3' and 5'-CACGTG-3' (Cheli et al., 2010; Rob Siddaway,

unpublished data). It is unclear how binding to these two slightly different motifs is modulated, but there is evidence for differential MITF binding, and post-translational modifications have been cited as one possible way by which this might be accomplished (Aksan & Goding, 1998; Cheli et al., 2010). Indeed, ChIP-seq data from our lab indicate that acetylation of another DNA backbone-contacting lysine residue within the second helix of the DNA binding domain affects binding of MITF to its target motifs, supporting the notion that acetylation of this region could modify MITF DNA binding (Rob Siddaway, unpublished data). Although beyond the scope of this thesis, this data set also confirms earlier work indicating that the identity of the residues flanking the 6-nucleotide core E-box motifaffects MITF binding to targets (Aksan and Goding, 1998).

MITF residue K206 was found to be acetylated in response to p300 overexpression, prompting us to examine the influence of K206 status on MITF function. This residue is of interest due to the positioning of its side chain in a co-crystal structure of MITF bound to a DNA target motif (Pogenberg et al., 2012), its significant contribution to total MITF acetylation during p300 overexpression and the fact that it has been observed to be mutated (K206Q) in a family with Waardenburg syndrome (Léger et al., 2012). Using the Waardenburg mutant K206Q to mimic acetylation of this residue, we studied the ability of MITF to bind to an enhancer region upstream of the *TYR* gene, which is activated by MITF and harbours a 5'-CATGTG-3' motif. Neighbouring K205 was also found to be acetylated in earlier studies, and although we were primarily interested in the influence of K206 on MITF function, we tested various combinations of K205 and K206 mutations meant to mimic acetylated lysine (Q) or unacetylated lysine (R). After establishing that MITF binding to the *TYR* enhancer was mediated by the 5'-CATGTG-3' motif, we found that the acetylation-

mimicking K206Q mutation greatly impaired MITF binding. Interestingly, this was true regardless of the status of K205. Subsequent experiments confirmed these results using a slightly modified fragment of the MITF DNA binding domain, altered expression and purification protocols and an additional MITF target motif. Despite some variation in our results, the EMSA data is consistent with the K206Q mutation resulting in a significant impairment of binding to 5'-CATGTG-3' motifs and a milder impairment of binding to 5'-CACGTG-3' motifs, a result that is consistent with another report examining MITF(K206Q) function (Grill et al., 2013). The end result of this may be a shifting of MITF target preference – if the K206Q mutation adequately mimics K206 acetylation, this would provide a dynamic and reversible means of steering MITF from one set of targets to another.

Optimization of the purification protocol for bacterially expressed MITF(198-302) increased yield and decreased contaminating DNA, permitting attempts to use this purified protein to obtain co-crystal structures of MITF bound to DNA target motifs. Although crystals have been obtained, they are not yet of sufficient quality to generate high resolution structures (Sarah Picaud, personal communication).

At this point, it is important to mention that it is unclear to what extent the point mutants K206R and K206Q faithfully represent the unacetylated and acetylated states of K206 (Fujimoto et al., 2012). Glutamine is the most similar to acetyl-lysine among the amino acids, however glutamine has a significantly shorter carbon chain, and the amide carbonyl group is at a different position, making it far from a perfect mimic of acetyl-lysine (Kamieniarz & Schneider, 2009). Aside from the question of whether or not glutamine adequately mimics acetyl-lysine, the introduction of lysine-to-glutamine mutations opens up another possible confound. Lysine is targeted by multiple post-translational modifications. Even if a glutamine mutation adequately mimics acetyl-

lysine and an arginine mutation mimics unacetylated lysine, both of these mutations would likely affect the ability of the residue in question to be ubiquitinated, methylated, hydroxylated, SUMOylated, succinylated or malonylated (Du et al., 2011; Peng et al., 2011). With arginine and glutamine mutations of a given lysine potentially affecting all of these modifications, great care must be taken when making conclusions based upon lysine point mutants as mimics of post-translational modifications.

To support and extend our conclusions regarding MITF acetylation and DNA binding based on the K206R and K206Q mutants, we planned to mimic acetyl-lysine in a different way. A group in the Department of Chemistry (University of Oxford, UK) developed a system in which the lysine residue to be examined is mutated to cysteine, followed by derivatisation of the thiol side chain to yield an acetyl-lysine mimic (Chalker et al., 2012). Although the required mutant was made, another system became available that would potentially offer a better solution. This involved using the amber stop codon to genetically encode acetyl-lysine, allowing for the incorporation of acetyl-lysine residues in bacterially-expressed proteins in a site-specific manner (Neumann et al., 2009). Although this system required significant optimisation, our colleagues in the SGC have successfully produced MITF(198-302) that harbours acetyl-lysine at position 206 (K206ac). By comparing the ability of MITF(WT), MITF(K206Q) and MITF(K206ac) to bind 5'-CATGTG-3' and 5'-CACGTG-3' motifs, we should be able to more thoroughly evaluate the influence of K206 status on MITF DNA binding. Additionally, this system will possibly allow us to make a broader statement about the suitability of glutamine as a mimic of acetyl-lysine in the study of bHLH factor DNA binding.

Although we saw that the K206Q mutant impaired MITF function in EMSAs and in a zebrafish melanocyte rescue assay, we were unable to confirm these results in

melanoma cell lines. We noted that the K206Q mutant demonstrated slightly impaired binding to some targets and may show altered activation of endogenous *TYR* expression, however we saw no consistent impairment in binding to either 5'-CATGTG-3' or 5'-CACGTG-3' motifs. It is possible that this is due to the presence of endogenous MITF at a level roughly equivalent to the ectopic mutant MITF. Another explanation could be that the K206Q mutation does not result in the same functional impairments in the full-length protein as in a smaller fragment comprising only the DNA binding domain. Also, the 3xFLAG tag could interfere with the function of ectopic MITF in cell lines, or the presence of co-factors could result in discrepancies between the influence of the K206Q mutation in EMSAs and in cell culture.

Expression of the K206Q alongside WT MITF also occurs naturally. A French family diagnosed with Waardenburg syndrome, which involves defects in pigmentation, was found to have a heterozygous germline K206Q mutation in MITF, indicating that this mutation has a phenotype when present alongside the WT allele (Léger et al., 2012). The proband has a relatively mild phenotype within the spectrum of Waardenburg syndrome, with congenital sensorineural hearing loss, a white forelock and blue irides, but no skin pigmentation abnormalities. The regulatory elements for many MITF targets contain 5'-CATGTG-3' motifs (Aksan & Goding, 1998; Cheli et al., 2010), and it is possible that the impaired ability of MITF(K206Q) to bind this sequence could underlie the symptoms observed in this family.

Interestingly, we do not see a consistent effect of the K206Q mutation on DNA binding or activation of the *TYR* promoter when it is expressed alongside endogenous MITF in 501mel melanoma cells. This situation could be somewhat analogous to that in the Waardenburg patient described above, where mutant and WT MITF are co-expressed, and no skin pigmentation phenotype is seen. On the other hand, we see a

functional impact of the K206Q mutation on binding to 5'-CATGTG-3' motifs and melanocyte development when it is effectively present in homozygous form. This is the case in our work with EMSAs, which demonstrate impaired 5'-CATGTG-3' binding in the context of truncated MITF(K206Q) homodimers in the absence of post-translational modifications, protein cofactors and chromatin architecture. It is also the case in the zebrafish melanocyte rescue assay, where full-length mitfa(K201Q) is expressed *in vivo* in the absence of endogenous mitfa.

Provided that the inability of MITF(K206Q) homodimers to bind 5'-CATGTG-3' elements in EMSAs *in vitro* is recapitulated *in vivo* and that this impairment would be sufficient to affect some stage of melanocyte development or function, the fact that there is no functional impact of this mutation in melanoma cells in culture and no skin phenotype in the Waardenburg patient harbouring a heterozygous K206Q mutation could be due to haplosufficiency. This could indicate that the WT/K206Q heterodimers retain at least some degree of functionality and would argue against the K206Q mutation functioning in a dominant-negative manner, at least in the context of the targets we examined in melanoma cells in culture and in the context of skin pigmentation in humans. Alternatively, WT/K206Q heterodimers could exhibit functional alterations, but the number of WT/WT homodimers is sufficient for normal MITF function.

Of course, this is further complicated by the fact that the endogenous protein is not a known entity in terms of its post-translational status – an unknown fraction of the pool of endogenous MITF could be acetylated on K206 or decorated with other post-translational modifications that have functional implications. This is unlikely to have been an issue in the EMSAs, where purified bacterially expressed protein was verified to be free of post-translational modifications before incubation with oligonucleotides of

known composition. The influence of this particular complication was also probably somewhat lessened in the assays utilising the IGR39 cell line and the *mitfa* -/- zebrafish line, as neither of these scenarios involve appreciable amounts of endogenous MITF.

However, MITF has been shown to be capable of binding to other members of the 4-member TFE family (Hemesath et al., 1994), some of which are thought to have ubiquitous expression (Kuiper et al., 2004). Thus, even in the absence of endogenous MITF, the effect of a given point mutant may be difficult to discern due to the presence of an unknown amount of TFEB, TFE3 and TFEC binding partners. It seems likely that the pool of binding partners would be limited to the TFE family, as a "kink" in the leucine zipper domain present exclusively in the 4-member TFE family renders them unable to pair with other members of the larger Myc bHLH-LZ superfamily (Pogenberg et al., 2012).

We saw a significant number of embryos in the zebrafish melanocyte rescue assay that did not develop any pigmented melanocytes, even when injected with WT *mitfa*. It was difficult to judge the cause of this failure to develop pigmented melanocytes – this could have been due to failed injections, successful injections in which the construct was not incorporated or failed to express the intended protein or successful injections in which the protein was expressed as intended but was incapable of supporting the development of neural crest-derived pigmented melanocytes. The other aspect that our current system lacked was a way to detect any melanocytes that might be unpigmented. As the K206Q mutant may impair pigmentation, we wanted a way to detect melanocytes present in 5 dpf embryos that did not rely on the presence of pigment.

Accordingly, we designed two new systems in an attempt to address these shortcomings – namely, that there was no internal control by which to gauge expression from the injected *mitfa* constructs and that we could not differentiate between the complete lack of melanocytes and the presence of unpigmented melanocytes. The first of the new systems used the same Tol2-based vector as in our previous experiments but incorporated two modifications. First, a 3x-FLAG tag was added to the *mitfa* coding sequence to facilitate staining zebrafish embryos with a FLAG antibody. This would serve both to verify expression from the construct and as a means of detecting *mitfa*-expressing cells independent of their pigmentation. This system also including EGFP under the control of the cardiac myosin light chain promoter between the flanking Tol2 sites. In this way, successful injections could be tracked by viewing fish under a fluorescent microscope during anaesthesia.

The second system employed a similar strategy but used the ac/ds transposon system (provided by Tatjana Sauka-Spengler, University of Oxford, UK), rather than the Tol2 transposon system. Our collaborators had indicated that if we were designing a system *de novo*, the ac/ds transposon would be the better choice, as they had observed higher efficiency of incorporation of injected constructs (Tatjana Sauka-Spengler, personal communication). This system was designed to again incorporate 3x-FLAG-tagged mitfa for immunohistochemistry purposes. However, in place of the EGFP marker driven by the cardiac myosin light chain promoter, this system placed EGFP C-terminal to the *mitfa* coding sequence, separated from it by the P2A self-cleaving peptide (Szymczak-Workman et al., 2012). This short sequence mediates cleavage of EGFP from mitfa, labelling mitfa-expressing cells but also mitigating concerns regarding the EGFP tag interfering with mitfa function. This should allow us to track mitfa-expressing cells under a fluorescent microscope and facilitate the identification of

any unpigmented melanocytes. The appearance of green cells would also provide qualitative evidence that the injection was successful.

These systems have been cloned and verified by sequencing. Additionally, the K201R and K201Q mutations (the zebrafish equivalent of K206R and K206Q, respectively) have been incorporated. Before the project started, we had taken steps to do the work within the University under the supervision of our collaborator (Tatjana Sauker-Spengler), bringing in the required *mitfa* -/- zebrafish line in anticipation of repeating and extending the experiments done in Elizabeth Patton's lab (University of Edinburgh). Unfortunately, this line did not breed well. Help was sought from personnel within the animal facility and from neighbouring labs expert in zebrafish work, but the line has thus far failed to produce sufficient embryos to conduct meaningful studies. That said, we were able to obtain and inject several *mitfa* -/- embryos, verifying that mitfa-3xFLAG can mediate melanocyte rescue and that EGFP can be detected in the heart for the system containing EGFP under the expression of the cardiac myosin light chain promoter. We are still having difficulty detecting EGFP in the mitfa-3xFLAG-P2A-EGFP system, as the pigment in melanocytes appears to interfere with detection of EGFP. However, this system should be appropriate for assessing the presence of unpigmented melanocytes, provided the *mitfa* promoter remains active in these cells.

What the present studies indicate is that the K206Q mutant shows alterations in function, both in terms of DNA binding *in vitro* and ability to support development of pigmented melanocytes *in vivo*. Whether or not MITF that is acetylated on K206 shows the same functional alterations is unclear, but future studies using MITF(K206Q) and MITF(K206ac) could clarify this. Provided K206 is acetylated *in vivo* and that K206Q is indeed faithfully mimicking this acetylation event, the fact that the K206Q mutation

has been observed naturally and causes an impairment in MITF function is interesting. It is possible that the protein product of this allele is effectively "locked in" to the acetylated state, indicating that the ability to dynamically regulate acetylation of this residue is important for proper functioning of MITF.

The mechanism by which K206 status might impact MITF DNA binding is unclear, but the co-crystal structure of MITF bound to DNA may provide clues (Pogenberg et al., 2012). Given that the K206 side chain is predicted to contact the phosphate backbone of DNA during MITF binding, it is perhaps not surprising that the K206Q mutation leads to changes in DNA binding. However, the differential effect observed in which binding to 5'-CATGTG-3' is impaired more than binding to 5'-CACGTG-3' is unexpected. According to published structural data, certain residues within the first helix make base-specific contacts (e.g., H209, E213, R217), however K206 is not among them (Pogenberg et al., 2012). Interestingly, R217 is predicted to make a base-specific contact with a central base in the motif (Pogenberg et al, 2012), the same base that we observed was responsible for either allowing (5'-CACGTG-3') or impairing (5'-CATGTG-3') binding of MITF(K206Q). Thus, even though K206 does not make a base-specific contact with the central (C/T) base that differentiates the two major MITF target motifs, another residue does. Elimination of the K206 electrostatic interaction with the DNA phosphate backbone could alter the positioning of the first helix within the DNA major groove. The K206Q mutant's preference for one motif over the other might then be hypothesised to result from an alteration in the positioning of residues in the major groove that make base-specific contacts (e.g., R217).

Another residue we found to be acetylated, K225, is at the other end of the first helix on the same face as K206 and reaches toward the phosphate backbone of the DNA (Pogenberg et al., 2012). Shifting of the first helix in response to K206 acetylation

could bring K225 closer to the phosphate backbone, facilitating an attractive electrostatic interaction. Interestingly, K225 is also a major acetylation target, as mutation to arginine resulted in a significant decrease in p300-mediated MITF acetylation, second only to the impairment observed with a K206R mutant. Perhaps acetylating one, the other or both of these sites could fine tune the positioning of the first helix in the major groove to influence MITF DNA binding.

It is also interesting that K206 and K225 are conserved throughout evolution within the 4-member TFE transcription factor family but are uncommon among bHLH factors in general. Many bHLH proteins are capable of binding identical or near-identical target motifs, and the "rocker-switch" hypothesis outlined above would be a means of targeting TFE factors while leaving the binding of other bHLH proteins unaffected. In fact, the 4 proteins of the TFE family are the only factors out of 117 human bHLH proteins analysed that harbour lysine residues both at position 206 and position 225. Future studies could attempt to address any interplay between K206 and K225 status in TFE family members by making single and double mutant combinations and testing their ability to bind different target motifs. However, we note that consensus motifs derived from ChIP-seq data indicate that both TFE3 and TFEB exhibit a marked preference for 5'-CACGTG-3' motifs over 5'-CATGTG-3' motifs (Betschinger et al., 2013; Palmieri et al., 2011). Even if it occurs in other TFE family members, this could limit the influence of acetylation of the K206-equivalent residues in these proteins on DNA binding – as they appear to primarily bind the 5'-CACGTG-3' motif, a decrease in binding to 5'-CATGTG-3' motifs may have limited functional consequences.

# Chapter 4: TFEB is subject to nuclear export

## 4.1 Introduction

The regulation of TFEB localisation appears to be complex. It is dependent upon multiple factors, including nutritional state, cell line and the status of at least 4 signalling pathways (Marchand et al., 2015; Martina et al., 2012; Perera et al., 2015; Settembre et al., 2011). Already, 26 sites have been reported to be phosphorylated in human TFEB, with methylation and acetylation also having been identified (Bao et al., 2016; Dephoure et al., 2008; Mayya et al., 2009; Yu et al., 2011). The fact that at least 2 of the kinases known to modify TFEB do so on multiple sites complicates attempts to pharmacologically dissect regulation of TFEB localisation. Likewise, the fact that individual sites are targeted by multiple kinases complicates studying TFEB nuclear translocation by genetic approaches. Additionally, cell lines commonly used in culture can harbour mutations in one or more of the pathways that impinge on TFEB post-translational status.

Many of the studies examining TFEB localisation have involved transient or stable overexpression and find TFEB to be localised to the cytoplasm in cell culture (Medina et al., 2015; Roczniak-Ferguson et al., 2012; Settembre et al., 2011). How the level of TFEB protein in these systems compares to the level of the endogenous protein is often unclear. One study found that ectopic TFEB was present in the nucleus of hippocampal neurons when overexpressed *in vivo* to levels 6-fold above that of the endogenous protein (Xiao et al., 2014). Additionally, TFEB is nuclear in *TFEB*-overexpressing RCC, where *TFEB* expression was approximately 50-fold that of adjacent normal tissue (Kuiper et al., 2003). It is unknown whether the marked discrepancies observed for TFEB localisation *in vivo* and in cell culture indicate that *TFEB* expression level correlates with its nuclear localisation or that the conditions in

cell culture prompt TFEB to adopt a cytoplasmic localisation pattern regardless of expression level.

Most work on TFEB localisation has aimed to elucidate the mechanisms by which it can be induced to enter the nucleus, to identify its target genes and to determine the downstream consequences of activating these genes (Martina & Puertollano, 2013; Palmieri et al., 2011; Sardiello et al., 2009; Xiao et al., 2015). Whether or not TFEB nuclear import is constitutive or regulated has not been directly addressed, although there is evidence that importin 8 plays a role in mediating the nuclear import of TFE family members (Perera et al, 2015). Additionally, although TFEB has been shown to re-establish cytoplasmic localisation after being induced to translocate to the nucleus in response to amino acid starvation, the mechanisms underlying this shift in localisation have not been investigated (Settembre et al., 2012).

This chapter will examine whether TFEB expression level influences its localisation in cell culture. Additionally, the mechanisms governing TFEB nuclear-to-cytoplasmic shifts in localisation will be studied, as will the influence of signalling pathways and post-translational modifications already known to regulate TFEB nuclear translocation.

## 4.2 Results

### *4.2.1 TFEB expression level and localisation*

We began our initial studies of TFEB with a TFEB-GFP fusion obtained commercially, since although several commercial anti-TFEB antibodies were available, these needed validation. HeLa cells (cervical carcinoma) were seeded in 6-well plates, transfected with TFEB-GFP and imaged 48 hours later using fluorescence live cell

imaging. Surprisingly, TFEB-GFP was predominantly nuclear in the majority of cells (Figure 4.1a). We lowered the amount of vector transfected and used another transfection method, but TFEB-GFP remained primarily nuclear. Rarely, cells exhibiting a predominantly cytoplasmic distribution were seen (Figure 4.1a, arrowhead). As TFEB is normally reported to localise to the cytoplasm in control conditions (Roczniak-Ferguson et al., 2012), we repeated this study with a small panel of NCI-60 cell lines. Again, TFEB-GFP was localised to the nucleus in the vast majority of cells (Figure 4.1b).

As TFEB is actively held in the cytoplasm by phosphorylation events, we reasoned that perhaps in our hands the level of transiently overexpressed TFEB-GFP was sufficient to saturate cytoplasmic retention mechanisms, allowing TFEB to translocate to the nucleus even in the fed state. To investigate this possibility, we generated MCF7 and HS578T cell lines that stably expressed ectopic TFEB-GFP, either under the control of the CMV promoter (TFEB-GFP) or in a Tet-On inducible system (iTFEB-GFP). In stark contrast to transient overexpression, TFEB-GFP that was stably expressed was predominantly localised to the cytoplasm in both cell lines (Figure 4.2a), a distribution pattern that is consistent with the majority of the reports in the literature.

Interestingly, our initial assessment of MCF7 iTFEB-GFP and HS578T iTFEB-GFP inducible stable lines (100 ng/ml doxycycline, 18 hours; Figure 4.2b) showed TFEB-GFP to again be primarily localised to the nucleus. However, titration of the dose of doxycycline revealed that the doxycycline dose correlated with the degree of TFEB-GFP nuclear localisation (Figure 4.2b) and the level of TFEB-GFP as assessed by Western blotting with an antibody against GFP (Figure 4.2c). By lowering the dose of doxycycline, we saw that TFEB-GFP was present predominantly in the cytoplasm (Figure 4.2b) and expressed at lower levels (Figure 4.2c). In our inducible system,

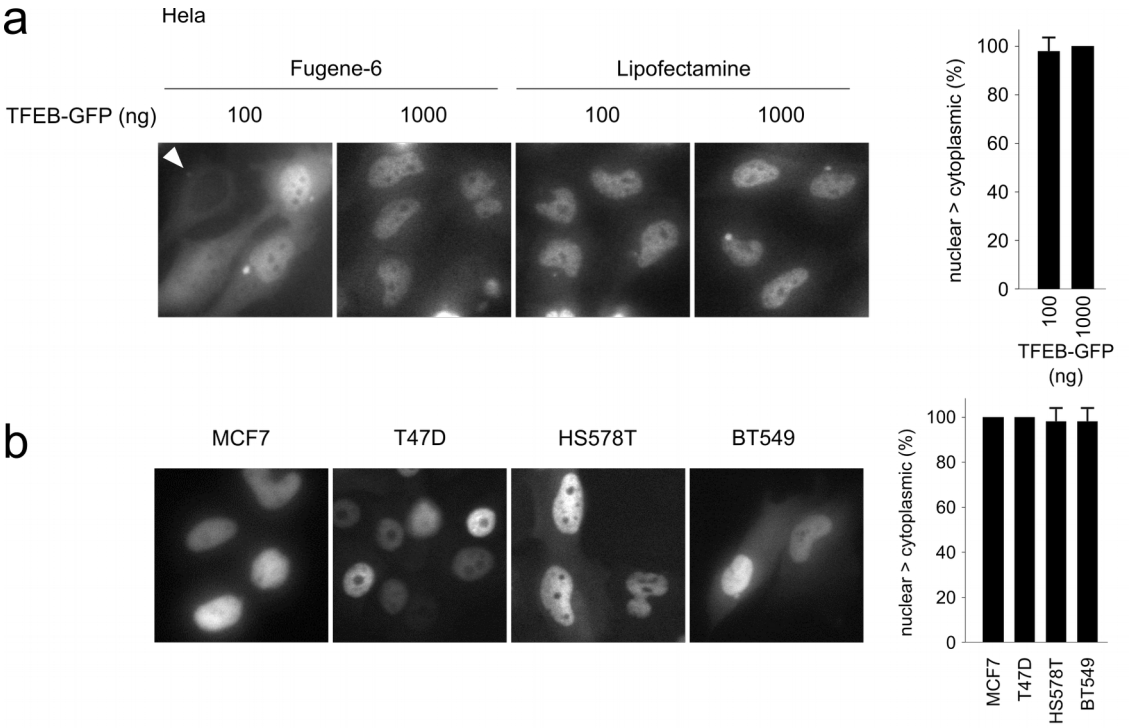



**Figure 4.1. Transiently overexpressed TFEB-GFP localises to the nucleus.** Cell lines were allowed to grow to 50% confluency, transfected with TFEB-GFP and imaged 48 hours later by fluorescence live cell imaging. Multiple fields of view were imaged, images were opened in ImageJ, cytoplasmic and nuclear signal intensity were measured and cells were classified as having primarily nuclear GFP or not. (a) HeLa cells were transfected with two different amounts of TFEB-GFP using two different transfection methods, as indicated. An arrowhead indicates a rare cell with primarily cytoplasmic TFEB-GFP. A quantification of cells with primarily nuclear TFEB-GFP for those transfected with Fugene-6 is shown. (b) Several other cell lines were transfected with TFEB-GFP using Fugene-6, imaged and quantified as in (a). Error bars represent the standard deviation of multiple fields, with fifty cells counted for each condition.

TFEB-GFP was also detectable without adding doxycycline to the medium, which was perhaps not surprising given reports of leakiness in these systems (Hosoda et al., 2011). Additionally, we cultured our inducible lines in certified tetracycline-free FBS and saw no alteration in the baseline expression of TFEB-GFP as compared to culture in normal FBS (data not shown), indicating that the leakiness was inherent to our system and not due to doxycycline present in the serum.

Although the doses of doxycycline we used were relatively low compared to those normally employed with Tet-On systems (Heinz et al., 2013), it was possible that

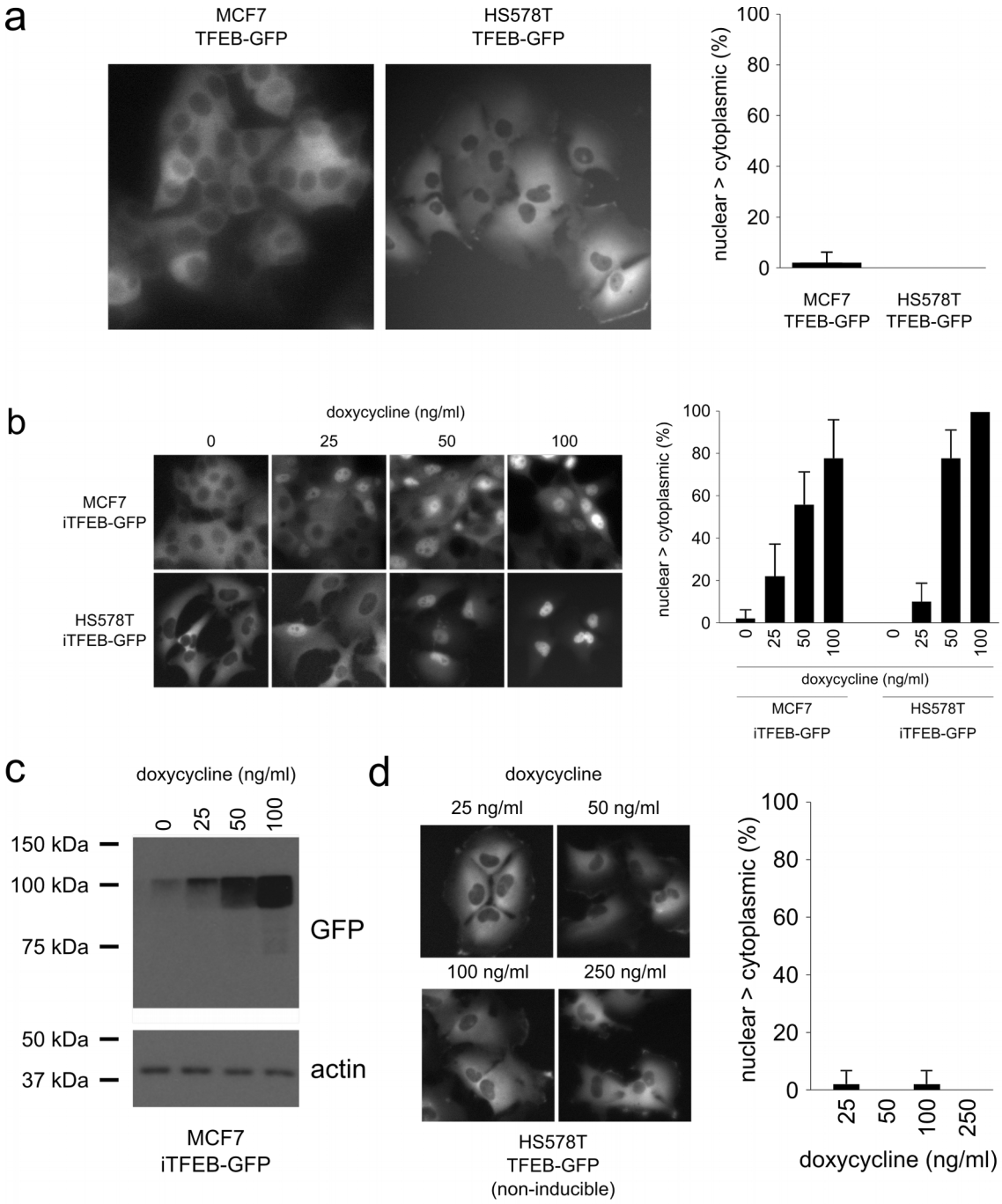



**Figure 4.2. TFEB-GFP level correlates with localisation.** Assessment of localisation of TFEB-GFP in MCF7 and HS578T cells stably overexpressing TFEB-GFP under control of either the CMV promoter or as part of a Tet-On inducible system. (a) Cells were plated in 6-well plates and imaged using fluorescence live cell imaging. Multiple fields of view were imaged, images were opened in ImageJ, cytoplasmic and nuclear signal intensity were measured and cells were classified as having primarily nuclear GFP or not. (b) The indicated inducible stable lines were induced for 18 hours with the indicated doses of doxycycline, imaged and TFEB-GFP localisation was quantified as for (a). (c) MCF7 iTFEB-GFP cells were induced with doxycycline as for (b) at the dose indicated and processed for Western blotting using an antibody against GFP to detect TFEB-GFP. Loading was assessed by probing for actin. (d) Doxycycline was added to the non-inducible HS578T TFEB-GFP stable line as indicated. After 18 hours the cells were imaged, and TFEB-GFP localisation was quantified as for (a). For all quantifications shown, error bars represent the standard deviation of multiple fields, with 50 cells counted for each condition.

doxycycline itself was inducing TFEB-GFP nuclear translocation. Recent studies have noted that doxycycline can induce significant alterations to cellular metabolism, even when present at dosages lower than those often used experimentally (Ahler et al., 2013). To rule out a doxycycline off-target effect resulting in TFEB-GFP nuclear translocation, we treated the non-inducible HS578T TFEB-GFP stable cell line with increasing concentrations of doxycycline and assessed TFEB-GFP localisation. TFEB-GFP stably overexpressed under control of the non-inducible CMV promoter in HS578T cells did not change localisation with any doxycycline dose tested (Figure 4.2d), indicating that doxycycline per se was unlikely to be responsible for TFEB nuclear translocation in our system.

As TFEB-GFP levels increased, faster migrating species appeared and became progressively more prominent, seen as a smear located below the band found at the lowest concentration of doxycycline (Figure 4.2c). This effect has been observed in reports investigating the effect of various types of starvation and stress on TFEB migration, with faster migrating species correlating both with TFEB nuclear translocation and TFEB dephosphorylation (Peña-Llopis et al., 2011; Settembre et al., 2012). Taken together, these data are consistent with higher levels of TFEB-GFP saturating the mechanisms responsible for actively retaining it in the cytoplasm, resulting in a portion of TFEB-GFP being dephosphorylated and localising to the nucleus.

As we saw different localisation patterns depending on the level of expression, we were interested in how the expression levels seen in our stable lines compared to endogenous expression levels. Several antibodies against TFEB were commercially available, so we began by validating these against tagged TFEB constructs. First, we used the MCF7 iTFEB-GFP stable line and its negative control counterpart expressing

inducible GFP (MCF7 iGFP) to determine whether the antibodies could recognise TFEB-GFP and to see if they could detect quantitative differences in TFEB-GFP level at different doses of doxycycline. Figure 4.3a shows that 2 (Abcam, Bethyl) of the 3 antibodies tested successfully detected TFEB-GFP in a quantitative manner. As the Abnova antibody failed to detect TFEB-GFP, it was omitted from further testing. Note that the blots are overexposed in an attempt to detect endogenous TFEB in the MCF7 iGFP samples shown in the first 3 lanes. Endogenous TFEB would be expected to run between 50 and 75 kDa, however no signal was detected with any of the antibodies (Figure 4.3a). This indicated that either the antibodies could recognise TFEB-GFP but not endogenous TFEB, or the level of endogenous TFEB was below the threshold of detection for these antibodies.

To determine the specificity of the antibodies, we assembled a panel of constructs comprising several members of the TFE family with various tags (Figure 4.3b). As the 4-member TFE family exhibits a high degree of homology and are expressed in a diverse range of tissues (Kuiper et al., 2004; Merrell et al., 1997), we were concerned about antibody cross-reactivity. Before the arrival of the TFEB-GFP fusion protein expression vector described above, we had cloned TFEB from MCF7 breast cancer cells and tagged the coding sequence with either an N-terminal Halo tag or a C-terminal 3xFLAG tag. Together with the TFEB-GFP vector, this gave us a panel of TFEB constructs with various tags in different positions (Figure 4.3b). The negative control constructs contained TFE3-GFP and MITF-3xHA, both of which were available in the lab. The constructs were then transiently transfected into MCF7 cells, and the Abcam and Bethyl antibodies against TFEB were tested.

Specificity was poor for the Abcam antibody, which reacted with all constructs tested, including TFEB, TFE3 and MITF (Figure 4.3c). The Bethyl antibody reacted

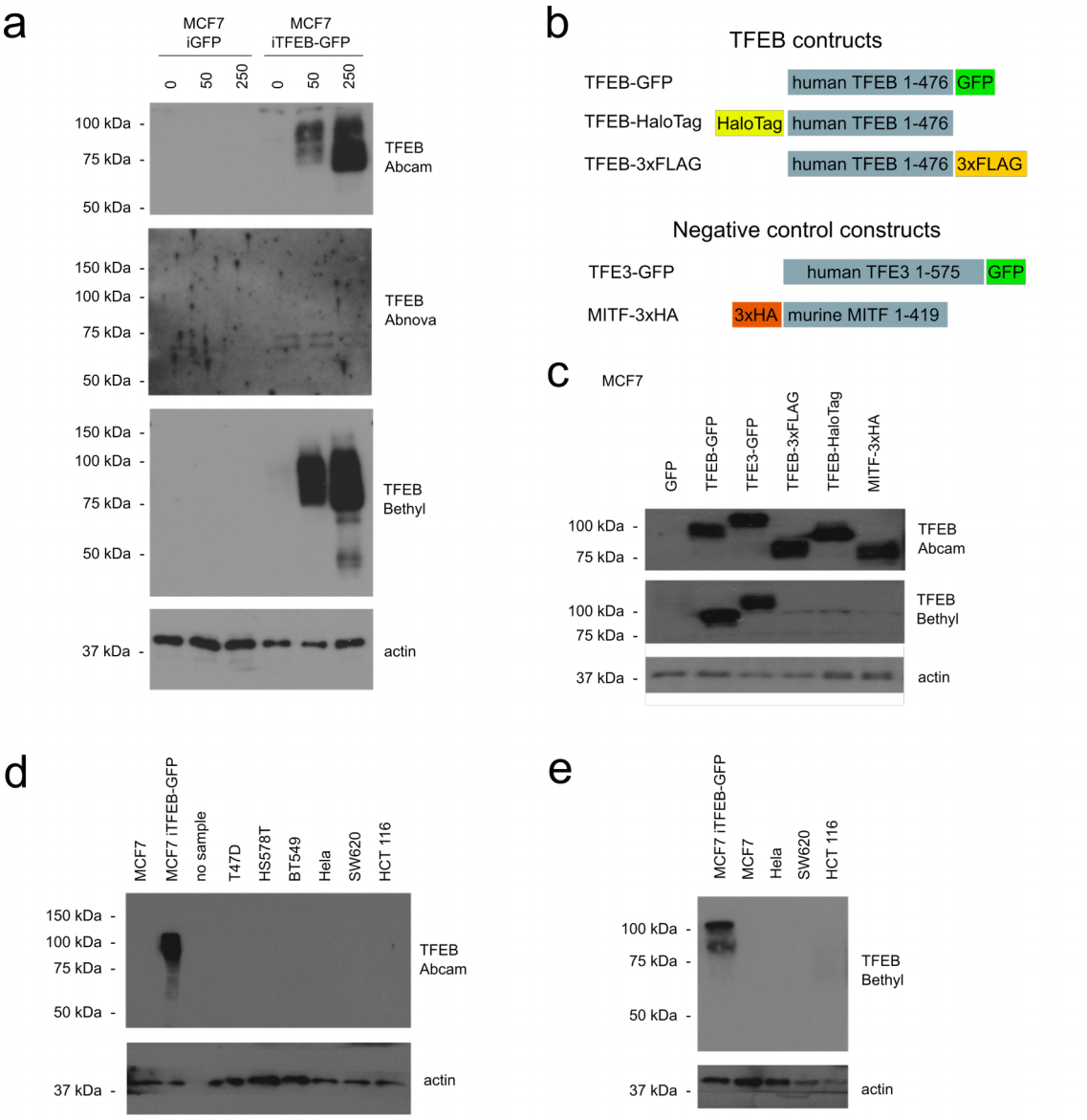



**Figure 4.3. TFEB antibodies exhibit poor sensitivity and specificty.** The sensitivity and specificity of TFEB antibodies were tested using stable and transient overexpression of TFE family fusion proteins. (a) MCF7 iGFP or iTFEB-GFP stable cell lines were treated overnight with different doxycycline doses and processed for Western blotting. Samples were probed with 3 different antibodies raised against TFEB. (b) A schematic drawing of the various fusion proteins used shows the location of tags relative to the coding sequences. (c) MCF7 cells were transfected with the constructs shown in (b) and after 48 hours were processed for Western blotting. The Abcam (d) and Bethyl (e) antibodies were tested against a panel of whole cell extracts from various cell lines. MCF7 iTFEB-GFP cells were used as a positive control for TFEB while actin was used as a loading control.

with both TFEB-GFP and TFE3-GFP but failed to detect any of the other constructs (Figure 4.3c). The TFEB fusions not detected by the Bethyl antibody have the tag

positioned on different termini (Figure 4.3b), so it is unclear why this antibody detects only some of the TFEB fusions. Finally, we broadened our testing with a larger panel of cell lines, attempting to detect endogenous TFEB with the Abcam (Figure 4.3d) and Bethyl (Figure 4.3e) antibodies. Although both antibodies were again able to detect stably overexpressed TFEB-GFP, no signal was visible at the expected molecular weight for endogenous TFEB in any cell line tested, despite the use of very long exposures (Figure 4.3d, e). In summary, the antibodies available against TFEB detected overexpressed TFEB with varying degrees of success, however none were able to reliably detect overexpressed TFEB with both high sensitivity and specificity. Moreover, the antibodies did not appear suitable for the detection of endogenous TFEB under the conditions tested.

Being unable to detect endogenous TFEB by Western blotting, we used qPCR to examine expression levels. First, several primer sets were ordered and tested against a dilution series of TFEB-GFP vector DNA to determine their linear ranges of detection (Figure 4.4a). We included TFE3-GFP vector DNA as a negative control to test specificity. Also, two different amounts of TFEB-GFP vector DNA were spiked into cDNA isolated from MCF7 cells to verify that the primers could specifically and sensitively detect TFEB transcript in the context of a complex cDNA pool. Of the primer sets tested, sets 1 and 4 showed the best correlation through a linear range of approximately 10 pg to 1 fg of TFEB-GFP vector DNA, the latter of which corresponds to roughly 150 copies of TFEB cDNA (Figure 4.4a). These primer sets exhibited a significant preference for TFEB-GFP target DNA over TFE3-GFP non-target DNA, requiring 10,000 to 1,000,000 times the amount of TFE3-GFP DNA to return a

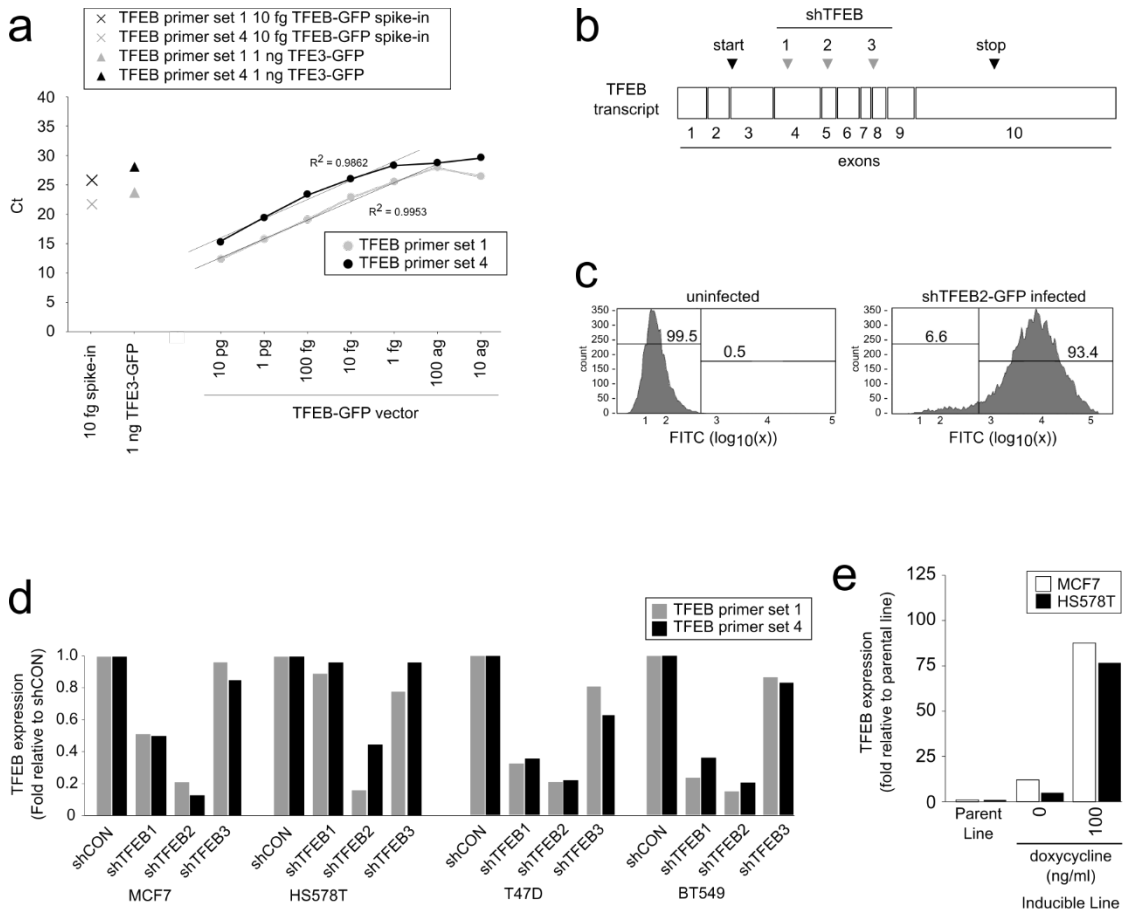



**Figure 4.4. Validation of TFEB qPCR primers and TFEB shRNA constructs.** Results of qPCR assays using primers directed against TFEB. (a) Two primer sets (set 1 shown in gray; set 4 shown in black) directed against human TFEB are used to detect a dilution series of TFEB-GFP vector DNA ranging from 10 ag to 10 pg (circles). Pearson correlations for the region between 1 fg and 10 ng are shown. The left side of the chart shows the signal returned by the 2 primer sets for 10 fg of TFEB-GFP vector DNA spiked into MCF7 cDNA (X symbols) and the signal returned by the 2 primer sets for 1 ng of TFE3-GFP non-target vector DNA (triangles). (b) Shown is a schematic of the human TFEB transcript with exons and start and stop codons indicated. Also shown are the target locations of three shRNA constructs against TFEB. These were cloned into a lentiviral system that included GFP expression to assess and select for infected cells. (c) FACS of MCF7 cells that were either uninfected (left) or infected with GFP-expressing lentivirus harbouring shTFEB2 (right). The percentages of cells in GFP-negative and GFP-positive gates are shown. (d) Four different cell lines are infected with either lentivirus harbouring a scrambled shRNA sequence (shCON) or one of the 3 shRNA sequences against TFEB as indicated in (b), and cDNA is subjected to qPCR with two primer sets against TFEB (see (a)). TFEB expression is shown as fold expression relative to cells infected with shCON virus after normalising to actin. Values are the average of duplicate experiments. (e) MCF7 and HS578T iTFEB-GFP cell lines were either left uninduced or induced with 100 ng/ml doxycycline and processed for qPCR analysis. TFEB expression is shown as fold relative to the respective parental cell lines after normalising to actin. Values are the average of the two primer sets.

comparable Ct value (Figure 4.4a). Also, both primer sets detected 10 fg of TFEB-GFP when spiked into MCF7 cDNA with little difference in the Ct value compared to the same amount of TFEB-GFP amplified alone (e.g. primer set 4 returned a Ct of 25.71 for 10 fg of target spiked into MCF7 cDNA and a Ct of 25.93 when 10 fg of target was amplified alone; Figure 4.4a). We noted that although this spike-in experiment indicated that the primers were specific, it also implied that the level of endogenous TFEB transcript may be very low in these cells.

In anticipation of future studies, we also generated a lentiviral system for the introduction of shRNA directed against TFEB. These constructs could also serve to confirm that our qPCR assays and Western blots were indeed measuring TFEB. Figure 4.4b shows a schematic of the human TFEB transcript illustrating the regions targeted by 3 different shRNA sequences. Each of these was cloned into the GFP-expressing pTRIP lentiviral vector. The same vector harbouring a scrambled shRNA sequence was provided by Johannes Schmidt, a previous student in the lab, and used as a negative control. Phoenix cells were used to generate lentivirus, which was collected in the medium and used to infect MCF7 cells. Over 90% of cells infected with pTRIP(shTFEB2)-GFP expressed GFP as assessed by FACS (Figure 4.4c), with other pTRIP shRNA constructs achieving similar infection efficiencies.

We then proceeded to infect HS578T, T47D and BT549 cells with lentivirus harbouring one of 3 shRNA sequences directed against *TFEB* (shTFEB1, shTFEB2, shTFEB3; Figure 4.4b) or a scrambled control sequence (shCON). When compared to cells that were infected with the shCON virus, 3 of the 4 cell lines displayed knock-down of *TFEB* expression to some extent with shTFEB1 (Figure 4.4d). As shTFEB3 did not appear to knock-down *TFEB* expression reliably in any of the cell lines tested, it was omitted from further studies. The most consistent knockdown of *TFEB* expression

was achieved with shTFEB2, which achieved approximately 75% knock-down on average (Figure 4.4d). Thus, we concluded that the qPCR TFEB primer sets were both sensitive and specific for the detection of endogenous *TFEB*. Additionally, shTFEB1 and shTFEB2 showed consistent knockdown of endogenous *TFEB* across several cell lines, as determined by our validated qPCR primers.

These primers were then used to compare the levels of endogenous *TFEB* and overexpressed TFEB-GFP. MCF7-iTFEB-GFP cells were either left uninduced or induced with 100 ng/ml doxycycline and processed for qPCR, with parental MCF7 cells processed in parallel. After normalising to actin expression, *TFEB* expression relative to MCF7 parental cells was calculated (Figure 4.4e). Averaging the results from the two primer sets, the MCF7 and HS578T iTFEB-GFP stable cell lines express *TFEB* at levels roughly 12-fold and 5-fold higher than the respective parental lines. If these cells are induced with 100 ng/ml doxycycline, *TFEB* expression climbs to just over 85-fold that of endogenous expression in MCF7 cells and approximately 77-fold of endogenous *TFEB* expression in HS578T cells (Figure 4.4e).

When a new rabbit polyclonal antibody against TFEB (Cell Signalling) became available, we used the same shRNA system to determine whether it could detect endogenous TFEB in our cell lines. Figure 4.5a shows that this antibody detects overexpressed TFEB-GFP (lane 8) in the MCF7 iTFEB-GFP stable cell line. Notably, in MCF7 and HS578T lines infected with a scrambled shRNA sequence (shCON), endogenous TFEB could be detected around 75 kDa in both cell lines. Moreover, the two shRNA sequences knocked-down endogenous *TFEB* at the transcript level (see Figure 4.4d), resulting in lower endogenous TFEB protein levels (Figure 4.5a). This also indicates that this antibody is not cross-reacting with other members of the TFE family. As was seen for transcript levels, shTFEB2 shows a greater knock-down of

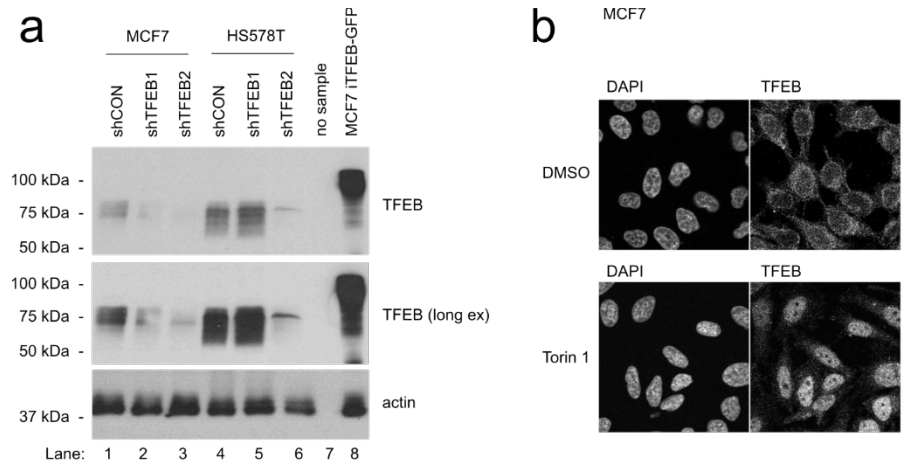



**Figure 4.5. Detection and knock-down of endogenous TFEB.** An antibody against TFEB is validated using Western blotting and immunofluorescence. (a) Whole cell lysates of MCF7 and HS578T cells infected with lentivirus expressing shRNA targeting a scrambled sequence (shCON) or TFEB (shTFEB1, shTFEB2) were probed with an antibody against TFEB. Cells overexpressing TFEB-GFP are used as a positive control for TFEB while actin serves as a loading control. (b) Immunofluorescence images of MCF7 cells that were treated with DMSO or the mTOR inhibitor Torin 1 (250 nM, 1 hour), fixed and stained with an antibody against TFEB and DAPI to label nuclei. Images were acquired by confocal microscopy.

TFEB protein than shTFEB1. By contrast, shTFEB1 did not knock-down TFEB protein levels in HS578T cells, which is consistent with what was seen at the transcript level previously (Figure 4.4d). HS578T cells appear to express a higher level of TFEB than MCF7 cells, which is also consistent with what was seen previously when comparing the ratio of overexpressed *TFEB* to endogenous *TFEB* (Figure 4.4e).

To further validate the Cell Signalling rabbit antibody and evaluate the localisation of endogenous TFEB, MCF7 and HS578T cells were plated on glass coverslips and examined by immunofluorescence. MCF7 cells showed TFEB to be primarily localised to the cytoplasm (Figure 4.5b), which is consistent with the localisation pattern reported previously and with our low-level TFEB-GFP stable overexpression (Roczniak-Ferguson et al., 2012; see Figure 4.2). Additionally, we treated cells with the mTOR inhibitor Torin 1, as this has been reported to shift TFEB

from the cytoplasm to the nucleus (Settembre et al., 2012). In agreement, we observed TFEB nuclear translocation after 1 hour of Torin 1 (250 nM) treatment (Figure 4.5b).

Now that we could see that endogenous TFEB was localised to the cytoplasm and that TFEB-GFP was localised to the nucleus in both transient overexpression and at higher levels of induction during inducible stable overexpression, we took efforts to avoid overexpression-induced alterations in TFEB localisation. Our inducible stable cell lines showed a degree of leakiness in the absence of doxycycline that resulted in TFEB-GFP being expressed at a level several fold higher than the endogenous level (see Figure 4.4e). This level of TFEB-GFP seemed sufficient for detection by imaging, Western blotting and qPCR and showed a localisation pattern similar to endogenous TFEB. In light of the apparent dependence of TFEB-GFP localisation in MCF7 and HS578T cells on expression level and the low levels of endogenous TFEB compared to our overexpression systems, we made use of low-level stable overexpression whenever possible. However, as time did not permit stable lines to be generated for all constructs, transient overexpression was used where indicated.

Having observed that TFEB-GFP expression level influenced its localisation, we turned to other stimuli shown to modulate TFEB subcellular distribution. We used fluorescence live cell imaging to study changes in localisation of stably overexpressed inducible TFEB-GFP in HS578T cells, beginning by verifying that the TFEB-GFP fusion protein responded to signals already shown to influence TFEB localisation. Inhibition of mTOR with Torin 1 (250 nM, 1 hour) shifted TFEB-GFP from the cytoplasm to the nucleus, as we had observed with endogenous TFEB and as has been seen by other groups when mTOR signalling is inhibited (Figure 4.6a, b; Settembre et al., 2011). Torin 1 treatment also induced a downward shift in TFEB-GFP electrophoretic mobility (Figure 4.6c, d), as we saw earlier when increasing the level of

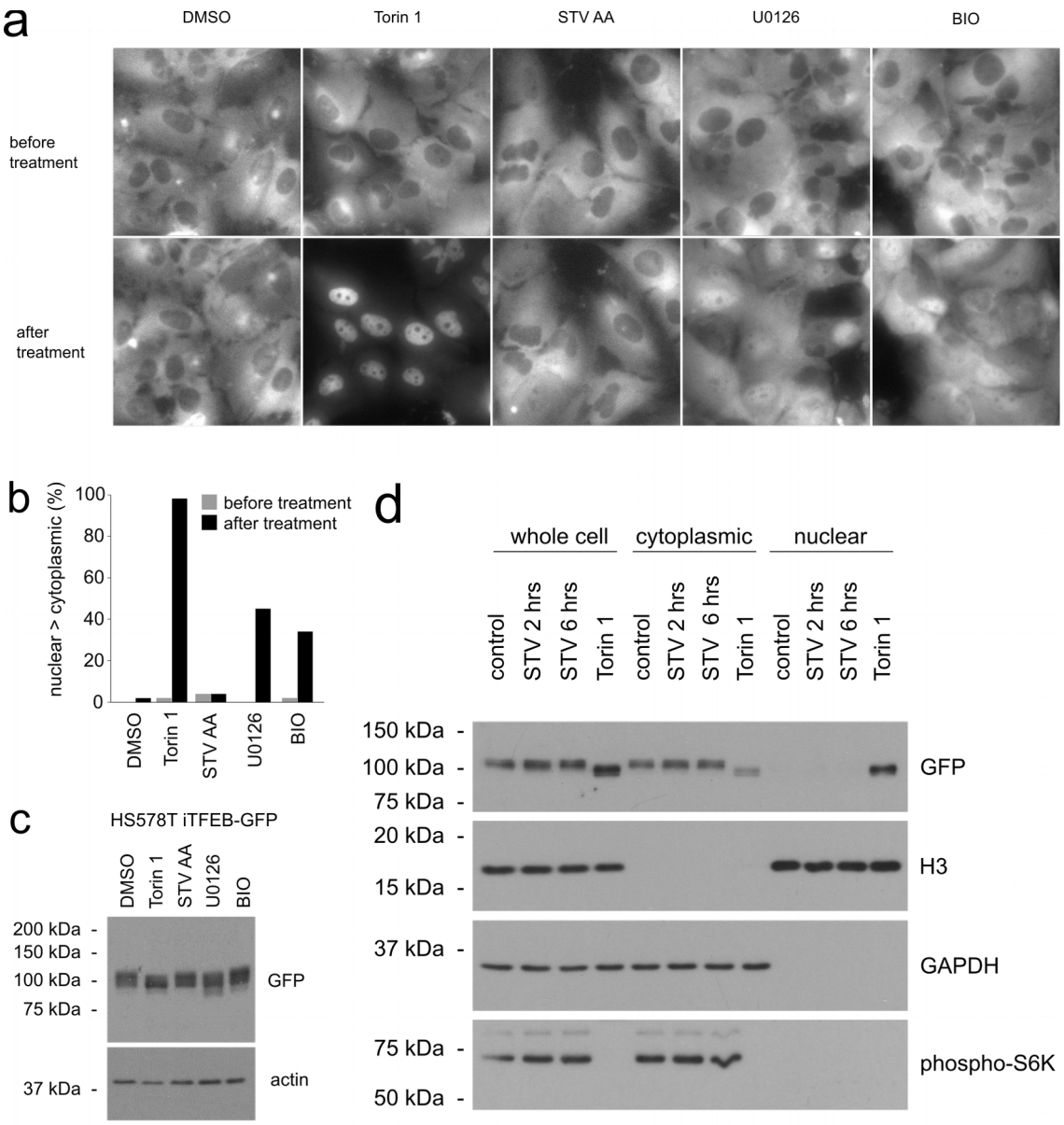



**Figure 4.6. TFEB-GFP nuclear translocation in response to treatments targeting mTOR, MAPK and GSK3 pathways.** HS578T cells stably expressing TFEB-GFP were treated as indicated, and the locasliation and electrophoretic mobility of TFEB-GFP were examined. (a) Fluorescence time lapse microscopy was used to image a given field of cells before and after being treated with DMSO, Torin 1 (250 nM; 1 hour), U0126 (20 μM; 3 hours), BIO (2 μM; 6 hours) or starved of amino acids in HBSS supplemented with 10% dialysed FBS (STV AA; 2 hours). (b) Quantification of TFEB localisation, with the same cells in multiple fields of view being followed for each treatment. As done previously, multiple fields of view were imaged, images were opened in ImageJ, cytoplasmic and nuclear signal intensity were measured and cells were classified as having either primarily nuclear GFP or not. Error bars indicate standard deviation. (c) Western blotting of whole cell extracts from cells treated in parallel with those in (a) probed with an antibody against TFEB. Cells were treated as indicated. Actin is shown as a loading control. (d) Western blotting of subcellular fractions from HS578T iTFEB-GFP cells treated as in (a). Whole cell, cytoplasmic and nuclear fractions were loaded as shown and probed with the indicated antibodies. Histone H3 and GAPDH were used as nuclear and cytoplasmic markers, respectively. The status of mTOR signalling was assessed with a phospho-S6K antibody.

TFEB-GFP in an inducible system (Figure 4.2c). This mobility shift has been noted in previous studies and was ascribed to a loss of phosphorylation at S142, S211 and/or other residues (Marchand et al., 2015; Settembre et al., 2012, Roczniak-Ferguson et al., 2012).

Other signalling pathways and treatments have also been shown to influence TFEB localisation and migration on Western blotting. Inhibition of MAPK signalling was one of the first pathways shown to influence TFEB localisation, although other reports have brought this finding into question (Settembre et al., 2011; Peña-Llopis et al., 2011). In our hands, treatment of uninduced HS578T iTFEB-GFP cells with the MEK inhibitor U0126 (20 μM, 3 hours) and the GSK3 inhibitor BIO (1.5 μM, 6 hours) both resulted in a partial nuclear translocation after 3 hours, however this was not as marked as the shift seen with Torin 1 (Figure 4.6a, b). To determine whether U0126 or BIO treatment altered the electrophoretic mobility of TFEB-GFP, we treated cells as above and probed whole cell lysates with an antibody against GFP. Torin 1 and U0126 treatment, but not BIO treatment, resulted in the appearance of faster migrating species (Figure 4.6c). We also deprived cells of amino acids by incubating them for 2 hours in HBSS supplemented with 10% dialysed FBS, a treatment that has been shown to induce TFEB nuclear translocation (Perera et al., 2015). Surprisingly, we did not observe an alteration in TFEB-GFP localisation or migration on Western blot (Figure 4.6a-c).

To further investigate this, we used subcellular fractionation to separate the cytoplasmic and nuclear compartments of HS578T iTFEB-GFP cells that were grown either in complete medium (control) or starved (STV) of amino acids in HBSS for 2 hours or 6 hours (Figure 4.6d). Torin 1 (250 nM; 1 hour) treatment was used as a positive control for nuclear translocation. Fractionation of the cells appeared to be successful, as GAPDH was absent from the nuclear fraction, and histone H3 was absent

from the cytoplasmic fraction. Again, Torin 1 treatment results in a faster migrating TFEB-GFP species when compared to control conditions (Figure 4.6d, lane 4 vs. lane 1). We checked the efficacy of mTOR inhibition by probing phospho-S6K, using an antibody that recognises S6K phosphorylated on mTOR target site T389 (Dufner & Thomas, 1999). Although inhibition of mTOR with Torin 1 effectively abolishes phosphorylation of S6K on this residue, neither starvation condition showed evidence of TFEB-GFP nuclear translocation or inhibition of S6K phosphorylation (Figure 4.6d). This indicates that in contrast to reports using HeLa cells and pancreatic ductal epithelial cells (Settembre et al., 2012; Perera et al., 2015) the starvation conditions used are not sufficient to inhibit mTOR or prompt TFEB-GFP to shift to the nucleus in HS578T cells.

Lastly, it is perhaps worth noting that although Torin 1 treatment apparently converts virtually all TFEB-GFP to the faster migrating form (Figure 4.6d, lanes 4, 8, 12), some of this species remains in the cytoplasm (Figure 4.6d; lane 8). This may indicate that dephosphorylation is necessary but not sufficient for entry into the nucleus – or that it is sufficient but the nuclear import machinery has been overwhelmed. Another explanation would be that dephosphorylation is sufficient for nuclear translocation and the nuclear import machinery is not limiting, but TFEB can cycle back out of the nucleus.

### *4.2.2 TFEB nuclear translocation is reversible*

Amino acid starvation is not the only stimulus thought to affect TFEB phosphorylation status or localisation. For example, glucose and serum starvation have been reported to affect TFEB electrophoretic mobility, however their effect on TFEB

localisation has not been addressed (Peña-Llopis et al., 2011). We subjected MCF7 iTFEB-GFP cells to glucose or serum starvation by incubating them for 90 minutes in either complete medium lacking serum (no serum) or complete medium lacking glucose (no glucose) and followed TFEB-GFP localisation for a given group of cells before and after the starvation conditions using time lapse fluorescence live cell imaging (Figure 4.7). Nuclei were visualised by incubating all cells in Hoechst 33342 dye before the addition of the various treatments (Figure 4.7; lower panels). Cells receiving fresh complete medium were used as a negative control (control), while cells incubated with the mTOR inhibitor Torin 1 (250 nM) served as a positive control (Torin 1). Both serum and glucose starvation resulted in a shift of TFEB from the cytoplasm to the nucleus, with nuclear translocation being more marked with glucose starvation than serum starvation (Figure 4.7).

Interestingly, after increasing the temporal resolution of our imaging, we noted that at early time points in several of the treatments, a small portion of cells exhibited transient shifts in TFEB-GFP localisation between the cytoplasm and the nucleus. This occurred in the absence of any intentionally administered stimulus and could be observed sporadically in clusters of cells in both control and starvation conditions. We observed that TFEB-GFP in cells cultured in complete medium appeared to begin entering the nucleus within the first 2 minutes, with the most pronounced nuclear localisation being around 5 minutes (Figure 4.8). Five minutes later, TFEB-GFP was already becoming less nuclear, and after 15-20 minutes, TFEB-GFP was once again predominantly cytoplasmic (Figure 4.8). These cells were imaged for a further 40 minutes, and no change was observed in localisation as compared to the 20-minute time point (data not shown). This was intriguing, but these events were variable and unpredictable. We decided to use conditions already shown to prompt TFEB nuclear

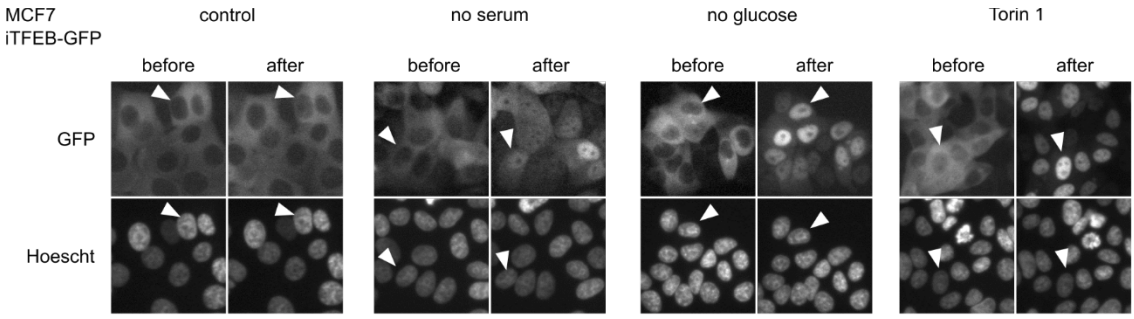



**Figure 4.7. Serum and glucose starvation result in TFEB-GFP nuclear translocation.** Time lapse fluorescence live cell imaging showing TFEB-GFP localisation in MCF7 cells. To visualise nuclei, cells were incubated with Hoechst 33342 (100 ng/ml) for 30 minutes prior to the indicated treatments. Cells were then washed twice with complete medium, imaged (before), incubated in the indicated conditions for 90 minutes and imaged again (after). A representative field of cells is shown for each condition before and after treatment. The conditions consisted of complete medium (control), complete medium lacking serum (no serum), complete medium lacking glucose with 10% dialysed FBS substituted for 10% FBS (no glucose) and complete medium supplemented with Torin 1 (250 nM). White arrowheads indicate the same cell before and after treatment.

translocation in an attempt to better observe this cytoplasmic-nuclear-cytoplasmic transition under more controlled conditions. Also, as the rapid alterations in TFEB-GFP localisation appeared to occur soon after placing the plate in the time-lapse microscope, future studies were allowed to acclimate for 1 hour before applying treatments or capturing images.

We began by using glucose starvation and subsequent refeeding to investigate the reversibility of TFEB nuclear translocation. As we saw before, starving both MCF7 and HS578T cells of glucose resulted in TFEB-GFP adopting a primarily nuclear localisation (Figure 4.9). MCF7 iTFEB-GFP cells starved for serum also showed relocalisation of TFEB-GFP to the nucleus, although we again saw that this effect was not as pronounced as that observed with glucose starvation (Figure 4.9a). We were unable to assess the effect of serum starvation on TFEB-GFP localisation in HS578T iTFEB-GFP cells, as these rounded up and lifted off the plate (data not shown). Importantly, we found that refeeding with complete medium after the cells had been

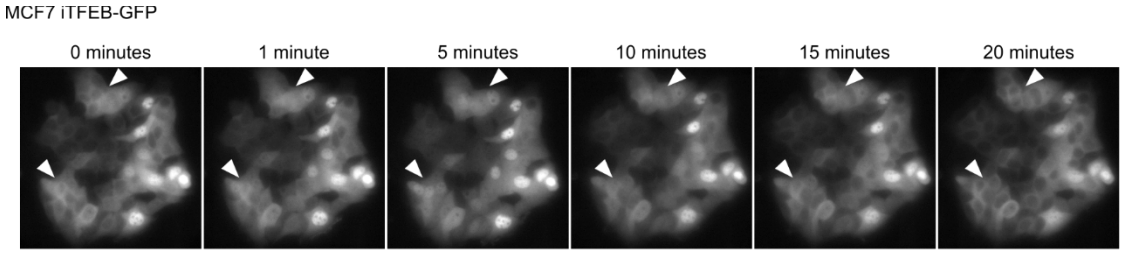



**Figure 4.8. TFEB-GFP rapidly and transiently changes localisation.** Time lapse fluorescence live cell imaging showing TFEB-GFP localisation in MCF7 iTFEB-GFP cells. Cells were incubated in complete medium, and images were taken every minute. Selected time points are shown for one cluster of cells imaged over the course of 20 minutes. White arrowheads indicate goups of cells demonstrating a rapid shift of TFEB-GFP to the nucleus, followed by re-establishment of cytoplasmic localisation.

starved of glucose or serum resulted in a shift of TFEB back to a predominantly cytoplasmic distribution (Figure 4.9a, b).

We also tested other stimuli known to induce TFEB translocation, treating MCF7 iTFEB-GFP cells with inhibitors of the mTOR, MAPK and GSK3 pathways. TFEB-GFP shifted from a cytoplasmic distribution to a nuclear distribution in response to treatment with each of the drugs and then returned to a predominantly cytoplasmic distribution when the drug was washed out with fresh complete medium (Figure 4.9c). This effect was the most pronounced with mTOR inhibition. U0126 treatment resulted in a more moderate effect, and BIO treatment only resulted in a portion of cells shifting TFEB-GFP to the nucleus and back to the cytoplasm (Figure 4.9c). This indicated that for a diverse set of stimuli that promote TFEB-GFP nuclear translocation, cytoplasmic localisation is re-established after the stimulus is no longer active.

### *4.2.3 TFEB nuclear export depends upon XPO1*

To further investigate the nature of TFEB redistribution, we fused TFEB to the C-terminus of Dendra2, a green-to-red photoconvertible variant of GFP (Chudakov et

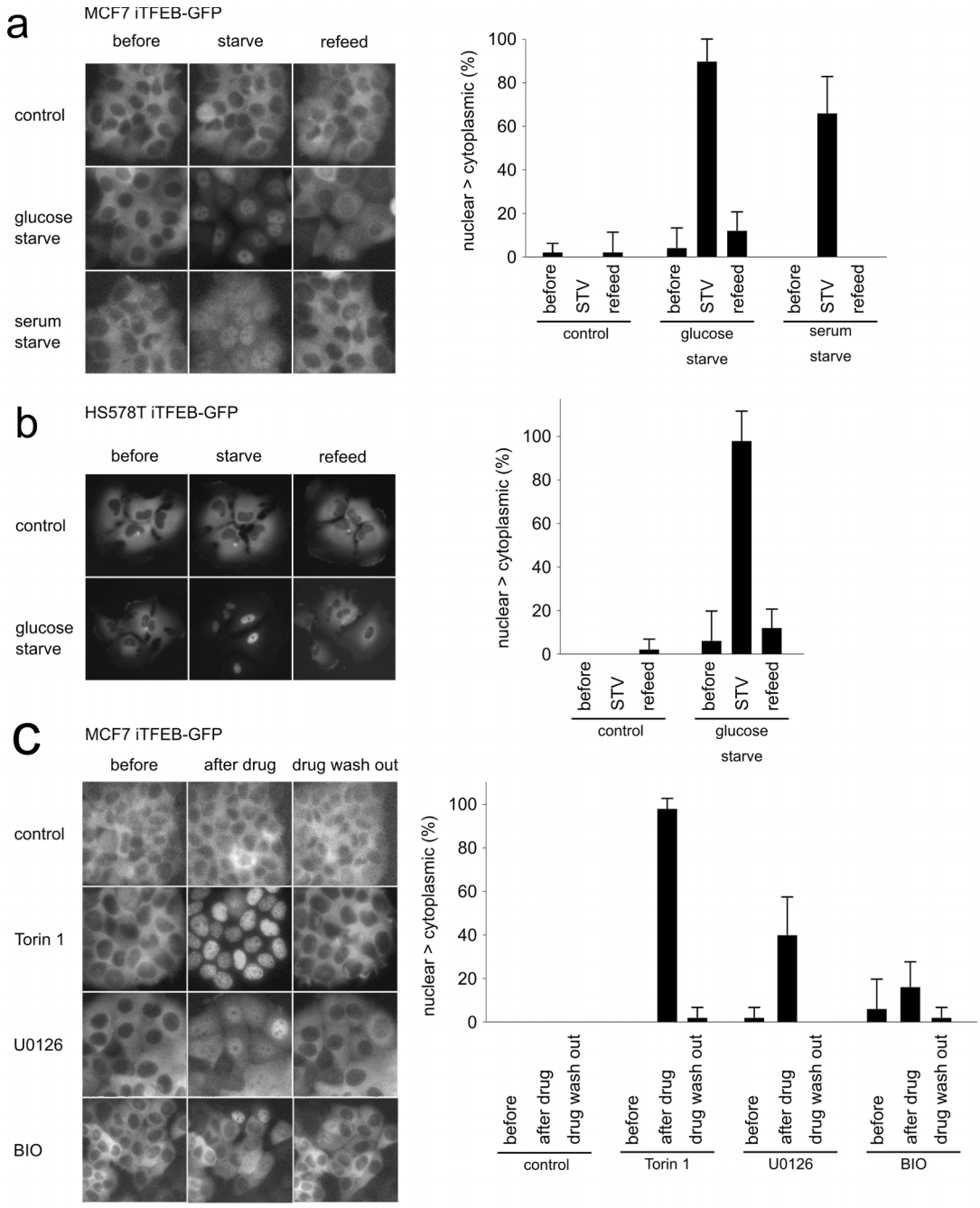



**Figure 4.9. TFEB-GFP nuclear translocation in response to diverse stimuli is reversible.** Time lapse fluorescence live cell imaging showing TFEB-GFP localisation in MCF7 and HS578T cells. (a) MCF7 iTFEB-GFP cells were incubated in complete medium, and images were taken (before). Cells were then incubated in complete medium supplemented with DMSO (control), complete medium lacking glucose (glucose starve) or complete medium lacking serum (serum starve). Images were taken after 90 minutes (starve). All cells were then given fresh complete medium and imaged after 2 hours (refeed). Multiple fields of view were followed over time and imaged, images were opened in ImageJ, cytoplasmic and nuclear signal intensity were measured and cells were classified as having primarily nuclear GFP or not. (b) HS578T iTFEB-GFP cells were treated, imaged and quantified as in (a). (c) MCF7 iTFEB-GFP cells were incubated in complete medium, and images were taken (before). Cells were then incubated in complete medium supplemented with DMSO (control) or complete medium supplemented with Torin 1 (250 nM, 1 hour), U0126 (40 μM, 3 hours) or BIO (1.5 μM, 6 hours) and imaged (after drug). Cells were then washed once with complete medium, incubated in complete medium for 2 hours, imaged (drug wash out) and quantified as in (a). Error bars represent the standard deviation of multiple fields, with 50 cell counted for each condition.

al., 2007). Similar to GFP, this protein is excited by light of 490 nm and emits at 507 nm in the green channel. However, UV light (e.g. 405 nm) will stably and irreversibly convert the tag, shifting the excitation and emission spectra to 553 nm and 573 nm, respectively and resulting in emission in the red channel rather than the green channel. In this way we could convert TFEB-Dendra2 from green to red, permitting us to track a given pool of TFEB-Dendra2 as it shifts between subcellular compartments. As with several other TFEB constructs, transient overexpression of TFEB-Dendra2 resulted in a predominantly nuclear localisation pattern (Figure 4.10a; upper left panel), complicating analysis of cytoplasmic redistribution. Accordingly, we generated an inducible MCF7 stable line, as was done for the TFEB-GFP construct. Although we did not necessarily plan to make use of the inducible feature of this system, our previous data indicated that this inducible system gave an expression level similar to endogenous TFEB when left uninduced (see Figure 4.4e). Surprisingly, this cell line also displayed predominantly nuclear localisation, the first TFEB construct that had been observed to localise to the nucleus when stably overexpressed in uninduced conditions (Figure 4.10a; lower left panel).

Noting that the Dendra2 tag was on the N-terminus of TFEB and the TFEB-GFP construct used for previous experiments contained a C-terminal tag, we relocated the Dendra2 tag to the C-terminus (TFEB-Dendra2 will refer to this construct from here on). Although transient overexpression of this construct again showed a nuclear localisation pattern (Figure 4.10a; upper right panel), low-level stable overexpression of inducible C-terminally tagged TFEB-Dendra2 in MCF7 cells showed the protein to be cytoplasmic (Figure 4.10a; lower right panel). This was consistent with the TFEB literature and with what we had observed in MCF7 cells stably overexpressing low levels of TFEB-GFP. It is possible that placement of the Dendra2 tag at the N-terminus

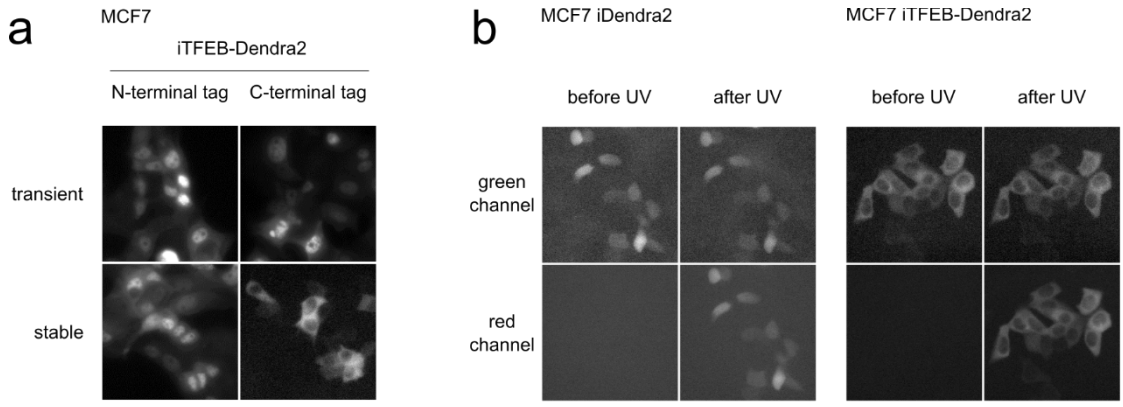



**Figure 4.10. Optimisation of TFEB-Dendra2.** Fluorescence live cell imaging showing Dendra2 and TFEB-Dendra2 localisation in MCF7 cells before and after photoconversion with UV light. (a) The Dendra2 tag is placed either N-terminal or C-terminal of the *TFEB* coding sequence and expressed either transiently or stably in MCF7 cells. Images of the green channel show the localisation of the fusion proteins. (b) MCF7 cells stably expressing either the Dendra2 tag only (MCF7 iDendra2) or *TFEB* with a C-terminal Dendra2 tag (MCF7 iTFEB-Dendra2) were cultured in complete medium, and the same group of cells was followed with time lapse fluorescence live cell imaging. Cells were imaged in both the red and green channels before and after UV light was used to photoconvert Dendra2 and TFEB-Dendra2.

interferes with targeting of TFEB to the lysosome where it is subject to post-translational modifications that promote cytoplasmic localisation (Medina et al., 2015; Roczniak-Ferguson et al., 2012; Settembre et al., 2012).

To verify that the Dendra2 tag was functional in this context, we again used time lapse fluorescence live cell imaging to analyse Dendra2 photoconversion in response to UV light. The MCF7 iDendra2 and MCF7 iTFEB-Dendra2 stable cell lines were imaged both before and after a 1 minute UV light exposure (Figure 4.10b). No signal was apparent in the red channel before UV light exposure for either cell line, while signal was detected in the red channel after photoconversion. Importantly, photoconversion did not appear to alter the distribution of either Dendra2 (pancellular) or TFEB-Dendra2 (cytoplasmic) (Figure 4.10b). Lastly, we noted that despite a clear signal in the red channel after photoconversion, (Figure 4.10b; lower right panels), the intensity of fluorescence in the green channel appeared largely unchanged. In light of

this, we tested longer UV light exposures in an effort to photoconvert a greater portion of the TFEB-Dendra2. We exposed fields of cells to UV light for up to 10 minutes, with little increase in red channel signal intensity or decrease in green channel intensity compared to the 1-minute exposure used in our experiments (data not shown).

Having verified that TFEB-Dendra2 was localised to the cytoplasm and that the Dendra2 tag appeared to be functioning properly, we studied TFEB-Dendra2 nuclear-cytoplasmic shuttling. Using the MCF7 iTFEB-Dendra2 stable cell line and its counterpart control cell line (MCF7 iDendra2), we verified that the TFEB-Dendra2 fusion protein responded to glucose starvation and subsequent refeeding in the same fashion as TFEB-GFP. We saw that after 90 minutes of glucose starvation, TFEB-Dendra2 had shifted from a primarily cytoplasmic localisation pattern to a primarily nuclear one; Dendra2 remained pancellular throughout (Figure 4.11a, b; before vs. glucose starve). At this point, cells were exposed to UV light for 1 minute to photoconvert Dendra2 and TFEB-Dendra2. The third panel of Figure 4.11 shows both the green and red channels immediately after photoconversion (Figure 4.11). We then refed cells with complete medium and followed both unconverted (green channel) and photoconverted (red channel) Dendra2 and TFEB-Dendra2. As can be seen in Figure 4.11b, the red channel shows converted TFEB-Dendra2 in the nucleus after starvation. Upon refeeding, the signal in the nucleus decreases, and the signal in the cytoplasm increases (white arrowheads). The same pattern is also evident in the green channel (Figure 4.11b; top panels) and is similar to that observed in earlier experiments with TFEB-GFP (see Figure 4.9). The fact that photoconverted TFEB-Dendra2 decreases in the nucleus while increasing in the cytoplasm (Figure 4.11b; white arrowhead in red channel) is consistent with TFEB moving from the nucleus to the cytoplasm upon refeeding after starvation-induced nuclear translocation.

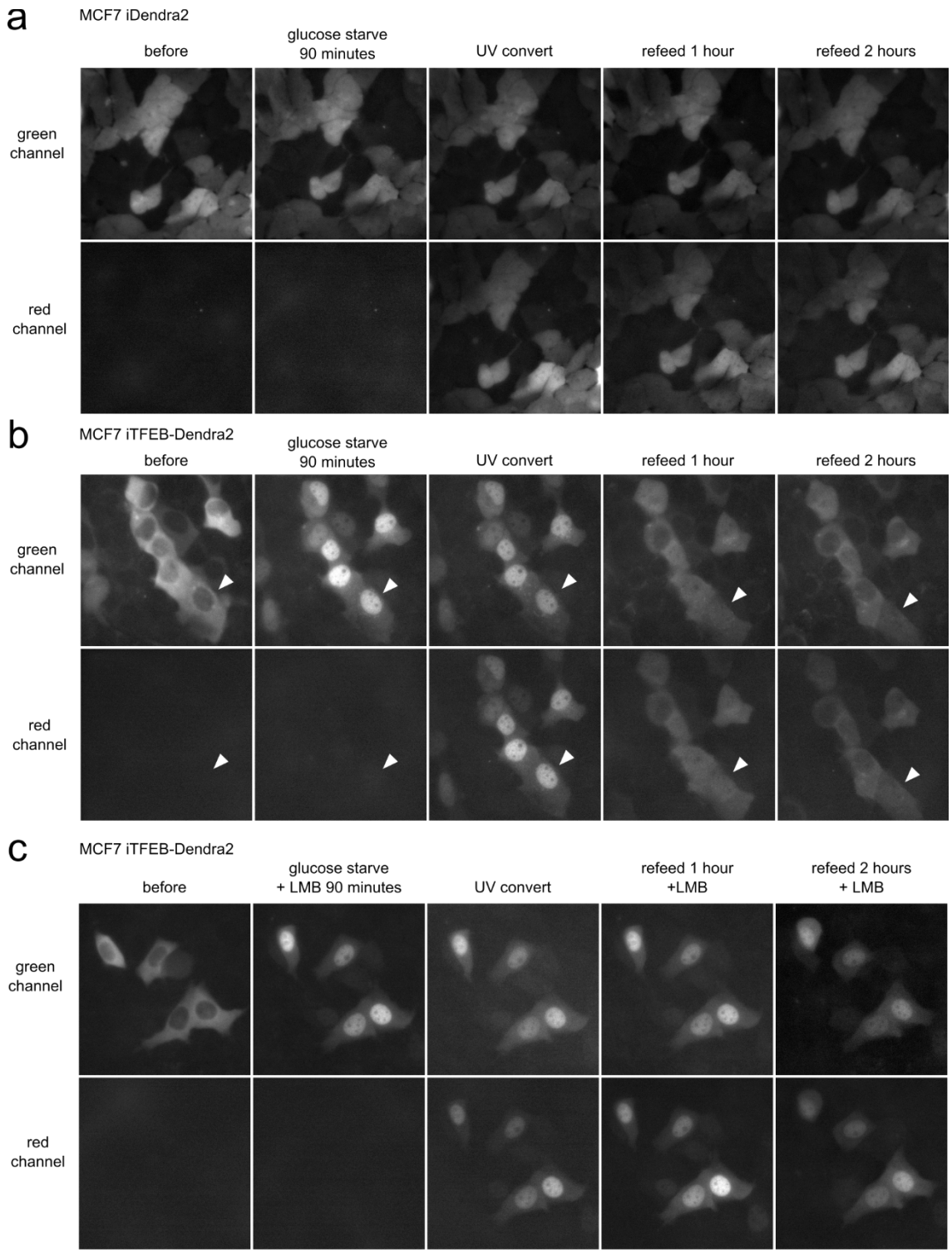



**Figure 4.11. TFEB-Dendra2 exit from the nucleus after refeeding requires nuclear export.** Time lapse fluorescence live cell imaging showing Dendra2 and TFEB-Dendra2 localisation during stable expression in MCF7 cells before and after photoconversion from green to red with UV light. MCF7 iDendra2 (a) and MCF7 iTFEB-Dendra2 (b) were cultured in complete medium and imaged (before). Cells were then incubated in complete medium lacking glucose for 90 minutes and again imaged (glucose starve 90 minutes). At this point, the field was exposed to UV light for 1 minute to convert the Dendra2 from green to red (UV convert). Cells were then refed with complete medium and imaged after 1 hour and after 2 hours. (c) MCF7 iTFEB-GFP cells were treated as in (b), but each media replacement consisted of the indicated medium supplemented with leptomycin B (LMB, 20 nM).

When taken together with the data concerning TFEB-GFP cytoplasmic-nuclear-cytoplasmic shifts, this may indicate that the reappearance of TFEB in the cytoplasm after nuclear translocation is at least partially due to the nuclear pool of TFEB exiting the nucleus. We note that other mechanisms could also contribute to this effect. For example, the pool of TFEB in the nucleus following starvation could be degraded upon refeeding. To further investigate this, we starved MCF7 iTFEB-Dendra2 cells of glucose as before. This time, we included leptomycin B (LMB, 20 nM) in the starvation medium. This compound binds to exportin 1 (XPO1) and interferes with nuclear export mediated by this protein (Fornerod et al., 1997). Cells were then refed with complete medium supplemented with LMB. The inclusion of LMB during starvation and refeeding resulted in TFEB-Dendra2 being maintained in the nucleus, whereas in the absence of this drug, TFEB-Dendra2 disappeared from the nucleus in response to refeeding (Figure 4.11b, c). This pattern was the same for both photoconverted and unconverted TFEB-Dendra2. This indicates that the reversal of TFEB nuclear localisation following reintroduction of glucose after starvation at least partly depends on XPO1-mediated nuclear export. We note that even when nuclear export is inhibited, the intensity of the TFEB-Dendra2 protein in the nucleus in both red and green channels diminishes by the 2-hour refeeding time point, leaving open the possibility that degradation contributes to the loss of nuclear TFEB following refeeding.

To determine if nuclear export of TFEB was limited to scenarios following an acute episode of nuclear translocation, as is seen with mTOR inhibition or starvation, we incubated MCF7 iGFP or MCF7 iTFEB-GFP cells with LMB without any prior treatment and observed them by time lapse fluorescence live cell imaging. Neither drug treatment affected the localisation of GFP in an MCF7 iGFP stable cell line. By contrast, treatment with LMB (20 nM, 2 hours) resulted in accumulation of TFEB-GFP

in the nucleus of MCF7 cells, similar to that observed with the mTOR inhibitor Torin 1 (Figure 4.12a). We then blotted subcellular fractions prepared from these cells and noticed several things. First, TFEB-GFP stably expressed in MCF7 cells was present almost exclusively in the cytoplasm and appeared to comprise only the slower migrating species (Figure 4.12b). Next, Torin 1 treatment resulted in virtually all TFEB-GFP being converted to the faster migrating form, and although a portion of this remained in the cytoplasm, the majority was present in the nucleus. Also, inhibition of nuclear export with LMB resulted in accumulation of TFEB-GFP in the nucleus, although not to the same extent as treatment with Torin 1 (Figure 4.12b). In contrast to Torin 1, LMB treatment did not appear to alter the migration of TFEB-GFP observed in the cytoplasm.

However, as for Torin 1 treatment, the portion present in the nucleus showed a faster migration pattern compared to the control condition (Figure 4.12b). Taken together, this indicates that TFEB-GFP is constitutively cycling through the nucleus, with XPO1 being responsible for mediating its nuclear export. Note that this does not rule out that an off-target effect of LMB is responsible for these observations – it is possible that LMB is inhibiting the export of a protein that is responsible for maintaining TFEB in the cytoplasm and that XPO1 is not directly responsible for exporting TFEB. This will be further addressed in later sections.

To determine whether endogenous TFEB behaves in the same fashion as TFEB-GFP, we used the antibody against TFEB that we had previously validated (see Figure 4.5) to conduct similar studies in MCF7 cells (Figure 4.12c, d). Although TFEB was seen to be more pancellular in control conditions than in previous experiments, Torin 1, LMB and U0126 all resulted in TFEB shifting to the nucleus, with Torin 1 and U0126 having stronger effects (Figure 4.12c). Blotting of subcellular fractionation samples

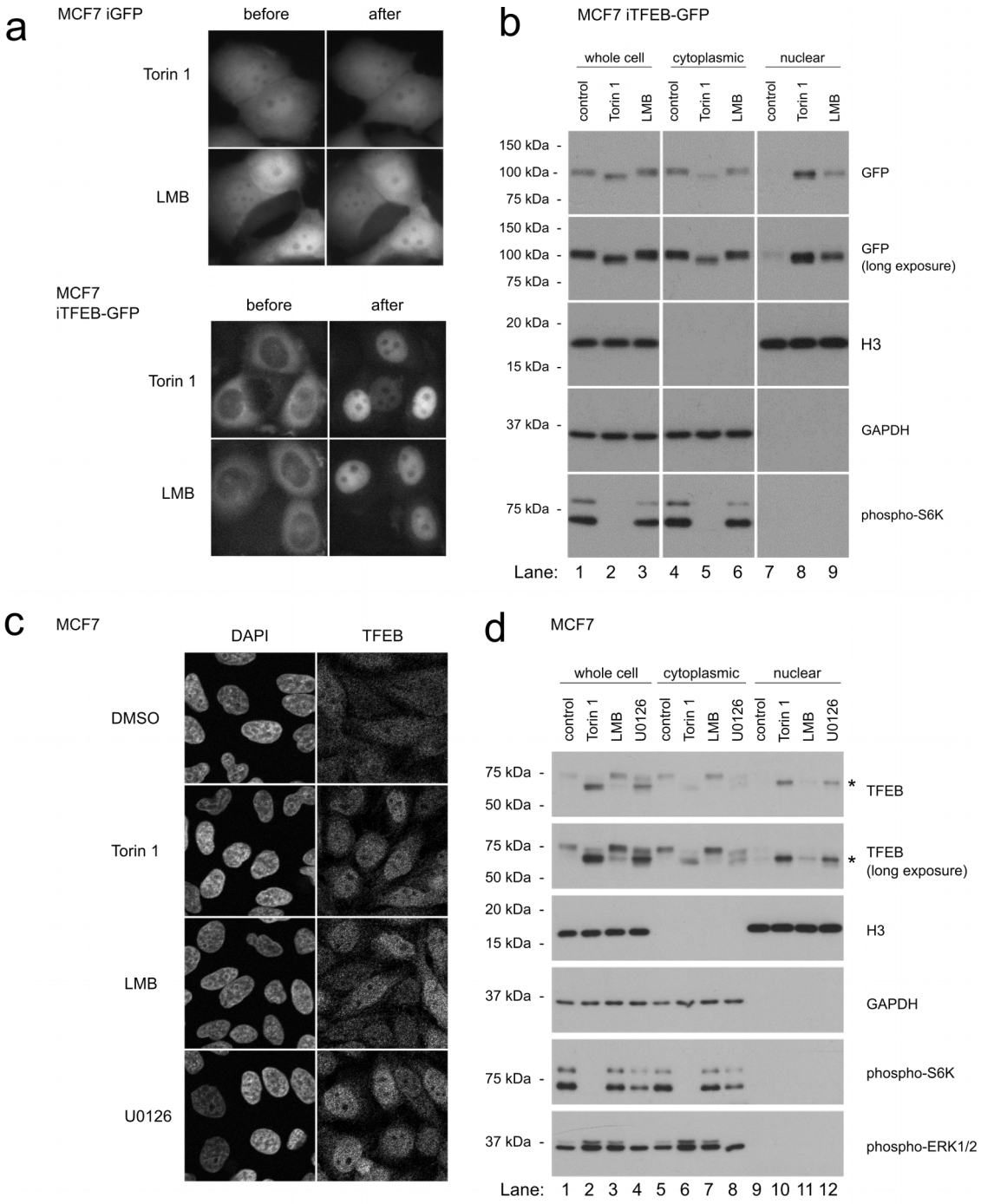



**Figure 4.12. Inhibition of nuclear export induces nuclear accumulation of TFEB-GFP and TFEB.** Localisation of TFEB-GFP and TFEB is examined by fluorescence imaging and Western blotting. (a) Time lapse fluorescence live cell imaging of MCF7 iGFP and iTFEB-GFP stable cell lines before and after treatment with either Torin 1 (250 nM, 1 hour) or LMB (20 nM, 2 hours). (b) Western blotting of subcellular fractions from MCF7 iTFEB-GFP cells treated as in (a). (c) Immunofluorescence images of MCF7 cells treated with DMSO, Torin 1 (250 nM, 1 hour), LMB (20 nM, 2 hours) or U0126 (20 μM, 3 hours). (d) Western blotting of subcellular fractions from MCF7 cells treated as in (c). Whole cell, cytoplasmic and nuclear fractions were loaded as shown and probed with the indicated antibodies. An asterisk (*) indicates a faster migrating TFEB species. Histone H3 and GAPDH are used as nuclear and cytoplasmic markers, respectively. The status of mTOR and MAPK signalling is assessed with phospho-S6K and phospho-ERK1/2 antibodies, respectively.

showed that, as for TFEB-GFP, TFEB is essentially absent from the nuclear fraction in control conditions (Figure 4.12d). Torin 1 treatment resulted in an acceleration of TFEB electrophoretic mobility, with the faster-migrating band highlighted by an asterisk. Possibly due to its lower molecular weight as compared to TFEB-GFP, it was easier to resolve different species when blotting endogenous TFEB. This experiment identified at least 3 different migration patterns, which are perhaps easiest seen in the whole cell lysate samples with the long exposure TFEB blot (Figure 4.12d, lanes 1-4). In control conditions, TFEB existed primarily as the slowest-migrating band and was present in the cytoplasmic fraction (top band). Torin 1 treatment resulted in the disappearance of this top band, and TFEB instead ran as two faster-migrating species, with the majority comprising the bottom band (bottom band), and a small portion showing a migration pattern intermediate between the bottom band and the top band (middle band; Figure 4.12d, lane 2). This same pattern was also evident with U0126 treatment (lane 4).

As seen with TFEB-GFP, treatment with LMB resulted in two things. First, TFEB appeared in the nuclear fraction, running as the bottom band. Note that the amount of TFEB present in the nuclear fraction in the LMB-treated sample appeared lower than was observed for TFEB-GFP in the LMB-treated sample (Figure 4.12b, d), possibly indicating that endogenous TFEB is not cycling through the nucleus as rapidly as stably overexpressed TFEB-GFP. Second, lanes 3 and 7 showed that the majority of TFEB is maintained in the cytoplasm as the top band. This is interesting, as this is the only treatment resulting in accumulation of TFEB in the nucleus while apparently leaving most TFEB present in the top band, as it is in control conditions.

We also note that Torin 1 treatment, LMB treatment and U0126 treatment all result in an elevation of TFEB level (Figure 4.12d). For Torin 1 and U0126 treatment,

the majority of TFEB ran as the bottom band, possibly indicating that loss of post-translational modifications stabilises TFEB. Another explanation would be that this TFEB bottom band, present largely in the nuclear compartment, is shielded from degradation. Interestingly, LMB treatment also appeared to increase TFEB levels slightly, but this was present mainly as the top band. Again, this could mean that nuclear TFEB is shielded from degradation and that inhibition of nuclear export increases the amount of time that the pool of TFEB spends in the nuclear compartment as it cycles between the cytoplasm and the nucleus. Alternatively, LMB treatment could interfere with the function of factors responsible for TFEB degradation by preventing them or their co-factors from exiting the nucleus.

### *4.2.4 The TFEB N-terminus mediates nuclear export*

Studies have consistently found that TFEB post-translational status influences its nuclear-cytoplasmic shuttling. Specifically, phosphorylation of S142 and S211 by mTOR and phosphorylation of S142 by ERK are reported to promote cytoplasmic localisation, as serine-to-alanine mutations at either of these locations result in TFEB localising to the nucleus in control conditions (Settembre et al., 2011; Settembre et al., 2012; Martina et al., 2012). We have found that impairing nuclear export with LMB also results in TFEB accumulating in the nucleus in control conditions. Given these findings, we wondered whether either of the two phosphorylation sites already known to modulate TFEB nuclear localisation affected its nuclear export. To determine how these mutations influenced TFEB shuttling in our system, S142A and S211A mutations were introduced into TFEB-GFP, either singly or in combination. As we had seen that transient overexpression resulted in constitutively nuclear localisation, these mutants

were stably overexpressed in MCF7 cells using the same inducible system as has been outlined previously.

The first column of panels in Figure 4.13 shows the influence of these mutations on TFEB localisation in control conditions. Like other groups, we saw that S142A and S211A mutations resulted in an increase in TFEB nuclear localisation in fed conditions, however we observed that these two mutations affected TFEB localisation in different ways. The iTFEB-GFP WT cell line showed a localisation pattern consistent with previous experiments, with almost all cells displaying primarily cytoplasmic localisation (Figure 4.13). The S142A mutant showed a high degree of heterogeneity, with some cells showing primarily nuclear localisation, some cells showing cytoplasmic localisation in a pattern similar to the WT and others displaying an intermediate phenotype. The S211A mutant showed a pancellular localisation in the majority of cells, with very little cell-to-cell variability (Figure 4.13). The most striking phenotype was observed with the S142A/S211A double mutant, which was uniformly nuclear in control conditions (Figure 4.13). As the S142A/S211A double mutant resulted in a markedly nuclear localisation that was more pronounced than either single mutation alone, it appears that these two mutations promote TFEB nuclear localisation in an additive manner. This indicates that either both mutations affect the same pathway with each only partially responsible for mediating cytoplasmic localisation, or that the S142A and S211A mutations interfere with cytoplasmic localisation through distinct mechanisms.

To further dissect the influence of these two residues on TFEB localisation, we treated each of these mutants with various drugs. First, we incubated each mutant with Torin 1 to determine the degree to which each site contributed to mTOR-dependent cytoplasmic localisation (Figure 4.13, third column). We found that the WT, the S142A

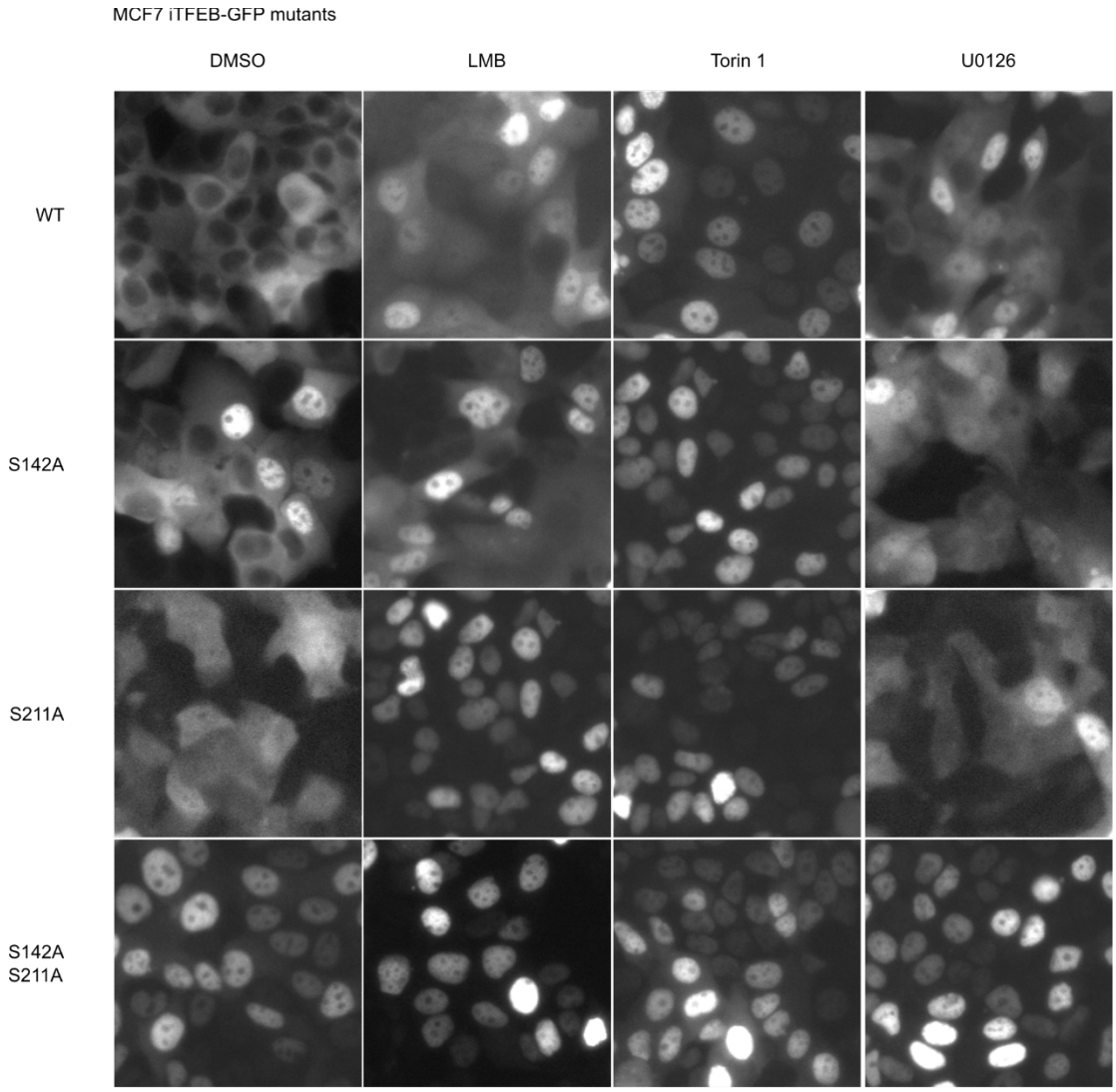



**Figure 4.13. The S142A mutation renders TFEB-GFP insensitive to LMB.** Fluorescence live cell imaging showing localisation of TFEB-GFP mutants during stable overexpression in MCF7 cells in response to various drug treatments. Cells expressing the indicated mutants were incubated in complete medium that was supplemented with DMSO (DMSO), LMB (20 nM, 2 hours), Torin 1 (250 nM, 1 hour) or U0126 (20 μM, 3 hours).

mutant and the S211A mutant showed increased nuclear localisation in response to mTOR inhibition (Figure 4.13). The S142A/S211A double mutant did not change localisation in response to mTOR inhibition, however it was already very nuclear in control conditions, and it is possible that a further increase in nuclear localisation would not be detected with this setup. The fact that the phenotype of the S142A/S211A double mutant so closely resembles the phenotype seen with the WT after Torin 1 treatment is

consistent with mTOR mediating its effects on TFEB localisation via these two residues.

We next treated the same cell lines with U0126 to inhibit MAPK signalling, which is thought to target only S142. This drug promoted some degree of nuclear translocation of WT TFEB-GFP, but did not appear to affect any of the mutants (Figure 4.13). The fact that U0126 does not seem to promote nuclear translocation of the S211A mutant could be due to mTOR still being able to phosphorylate S142 in the absence of MAPK signalling. It is also consistent with mTOR being the kinase predominantly responsible for phosphorylating this residue in our system.

Lastly, we used LMB to inhibit nuclear export. The WT again showed an increase in nuclear localisation, confirming our earlier results. Aside from the WT, the most noticeable effect of LMB was seen in the S211A mutant, where inhibition of nuclear export resulted in a marked shift to the nucleus (Figure 4.13, second column). Interestingly, the S142A mutant did not appear to change localisation in response to LMB treatment. The S142A/S211A double mutant also did not change localisation. This indicates that phosphorylation of S211 and nuclear export function additively to maintain TFEB-GFP in the cytoplasm. Intriguingly, the S142A mutation and inhibition of nuclear export did not complement each other to promote TFEB nuclear localisation in the same way as the S211A and LMB treatment did. The fact that the S142A mutation results in LMB having no effect on TFEB-GFP localisation could imply that this site and nuclear export are linked.

Noting that TFEB(S211A)-GFP accumulated in the nucleus in response to inhibition of nuclear export and that TFEB(S142A)-GFP did not, we focused our studies on S142. Although the S211A mutation influenced TFEB localisation, the

mechanism by which it does this has been thoroughly investigated, with multiple reports implicating 14-3-3 binding and cytoplasmic sequestration following mTOR-mediated phosphorylation (Martina et al., 2012; Martina & Puertollano, 2013; Roczniak-Ferguson et al., 2012). Additionally, our data indicated that the influence of S211 and LMB on TFEB localisation may act via separate mechanisms (see Figure 4.13).

Accordingly, we designed a construct incorporating a portion of the TFEB N-terminus that included S142 but excluded S211. This fragment is below the size cut-off generally accepted for passive diffusion through nuclear pores, which is thought to be around 50 kDa (Weis, 2003). Consequently, we made a cargo protein by fusing GFP to GST and attached the TFEB N-terminus to this fusion (Figure 4.14a). The GFP-GST fusion localised to the cytoplasm when transiently overexpressed in MCF7 cells, indicating that it was sufficiently bulky to be excluded from the nucleus (Figure 4.14a). Fusing TFEB residues 1-159 to the N-terminus did not alter its localisation. Also, treatment with the nuclear export inhibitor LMB or the mTOR inhibitor Torin 1, both of which normally result in translocation of full-length TFEB to the nucleus, did not alter the localisation of either construct, indicating that they are not subject to nuclear export or capable of nuclear translocation during mTOR inhibition. Lastly, inclusion of the S142A mutation in the TFEB(1-159)-GFP-GST construct did not alter its primarily cytoplasmic localisation in control conditions or with LMB or Torin 1 treatment (Figure 4.14a). Thus, it does not appear that this fragment of TFEB is capable of mediating nuclear localisation in control conditions, when mTOR or nuclear export are inhibited or when harbouring the S142A mutation known to modulate localisation of full-length TFEB. Also, note that this is the first instance in which transient overexpression of a TFEB construct has not led to primarily nuclear localisation.

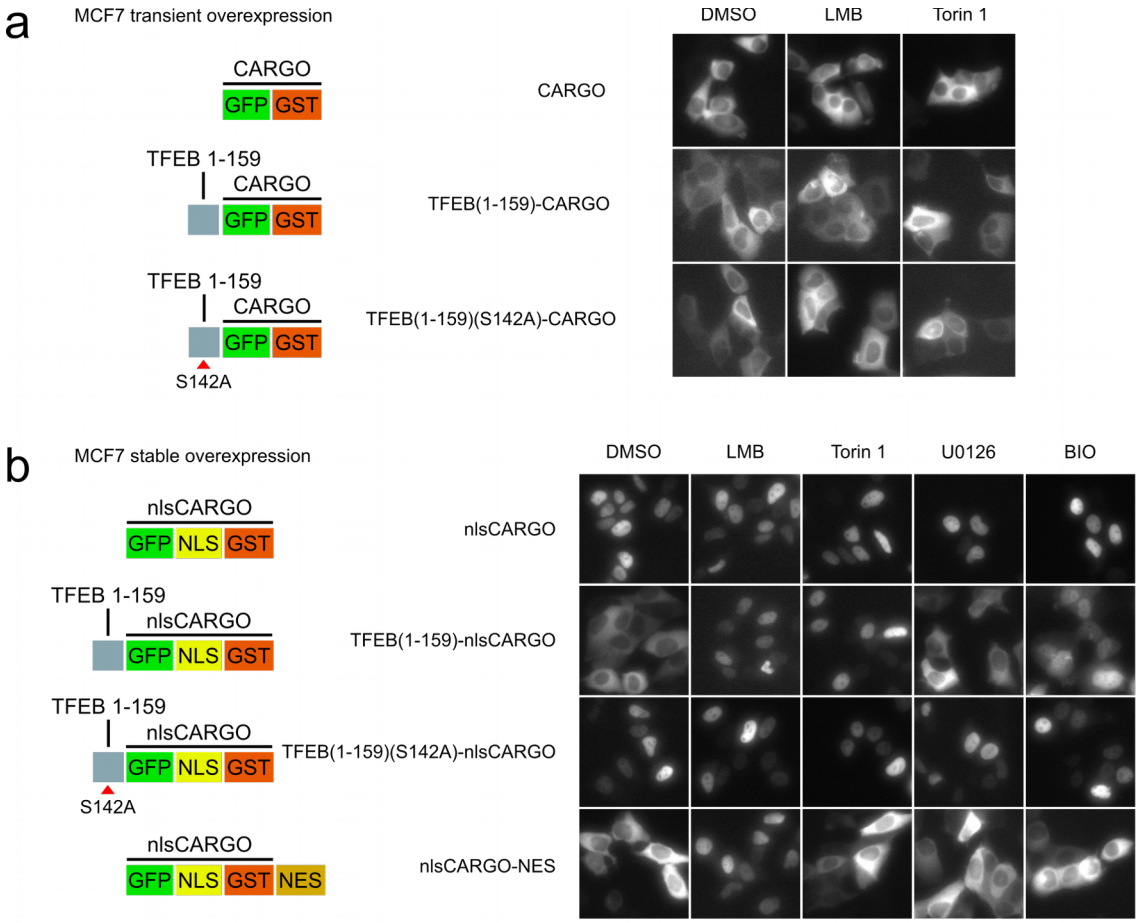



**Figure 4.14. The TFEB N-terminus directs nuclear export and mediates responses to mTOR and GSK3 signalling in a S142-dependent manner.** Fluorescence live cell imaging showing localisation of different fusion proteins during overexpression in MCF7 cells in response to various drug treatments. (a) A schematic shows the design of constructs based on the GFP-GST (CARGO) fusion protein. Panels to the right show fluorescence live cell imaging of these same constructs. MCF7 cells were transiently transfected, and 48 hours later were treated with DMSO, LMB (20 nM, 2 hours) or Torin 1 (250 nM, 1 hour) and imaged. (b) A schematic shows modified cargo constructs, all of which are based on the addition of a NLS to the GFP-GST (CARGO) protein to make the GFP-NLS-GST nuclear cargo (nlsCARGO). To this we added either TFEB residues 1-159, the same but with the S142A mutation or a canonical NES. MCF7 cells stably overexpressing these constructs were incubated in complete medium supplemented with DMSO, LMB (20 nM, 2 hours), Torin 1 (250 nM, 1 hour), U0126 (20 μM, 3 hours) or BIO (1.5 μM, 6 hours). Cells were then imaged, with representative fields shown for each condition.

However, TFEB harbours a nuclear localization signal (NLS) in the DNA binding domain (Roczniak-Ferguson et al., 2012) and to study the ability of the N-terminus to promote cytoplasmic localisation, the fusion protein must be capable of entering the nucleus. Accordingly, a classical NLS comprising the residues PKKKRKV from the simian virus 40 T-antigen (Kalderon et al., 1984) was added to the GFP-GST

fusion protein. This new GFP-NLS-GST nuclear cargo protein (nlsCARGO) localised to the nucleus of MCF7 cells (Figure 4.14b). We next attempted to examine whether the addition of TFEB residues 1-159 altered the localisation of nlsCARGO. We began by using transient overexpression, as had been done for the 3 vectors in the CARGO system (Figure 4.14a). However, this resulted in a high percentage of cells displaying nuclear localisation (data not shown), as had been observed with transient expression of full-length TFEB constructs. Accordingly, we again turned to stable overexpression, and MCF7 cells were used to make inducible stable lines expressing the various nlsCARGO constructs shown in Figure 4.14b. Fluorescence live cell imaging revealed that the addition of TFEB residues 1-159 to the N-terminus of nlsCARGO was sufficient to shift the constitutively nuclear nlsCARGO to the cytoplasm (Figure 4.14b). This indicated that the first 159 residues of TFEB harbour a sequence capable of competing with a classical NLS to redistribute a heterologous cargo protein from the nucleus to the cytoplasm.

To investigate if this change in localisation was due to the TFEB N-terminus promoting nuclear export, we cultured these cell lines in the presence of LMB (20 nM, 2 hours) to inhibit XPO1-mediated nuclear export. To serve as a control, we made a new construct (nlsCARGO-NES) by adding to nlsCARGO the residues LALKLAGLDI, comprising a nuclear export signal (NES) from the cAMP-dependent protein kinase inhibitor PKI (Wen et al., 1995). This construct should be subject to nuclear export via XPO1. In the absence of LMB, nlsCARGO was nuclear, and the nlsCARGO-NES showed a predominantly cytoplasmic localisation, indicating that the NES in our control construct was capable of competing with the NLS present in the nlsCARGO protein (Figure 4.14b).

Inhibition of nuclear export with LMB had no effect on the predominantly nuclear localisation of nlsCARGO, but nlsCARGO-NES and TFEB(1-159)-nlsCARGO both showed a pronounced nuclear translocation, indicating that the cytoplasmic localisation of nlsCARGO-NES and TFEB(1-159)-nlsCARGO was at least partially due to nuclear export and that the LMB treatment we used was sufficient to inhibit nuclear export of these proteins (Figure 4.14b). Importantly, when we mutated the mTOR and ERK target site S142 [TFEB(1-159)(S142A)-nlsCARGO], the TFEB N-terminus was no longer capable of localising the nlsCARGO protein to the cytoplasm (Figure 4.14b, third row). This indicates that either this residue must be phosphorylated in order for export to occur, or that mutation of this residue interferes with some other mechanism that is promoting cytoplasmic localisation of TFEB(1-159)-nlsCARGO.

We were curious to see if TFEB(1-159)-nlsCARGO was capable of mediating shifts in localisation in response to other signals that change the localisation of full-length TFEB. Specifically, as we observed that the S142A mutation rendered full-length TFEB and TFEB(1-159)-nlsCARGO insensitive to LMB, we began by investigating kinases already thought to target this residue. As mTOR and ERK2 have been shown to phosphorylate S142, the mTOR and MAPK pathways were individually inhibited with Torin 1 and U0126, respectively. Inhibition of mTOR with Torin 1 resulted in a shift of TFEB(1-159)-nlsCARGO (but not nlsCARGO-NES) from the cytoplasm to the nucleus, as had been seen with TFEB-GFP (Figure 4.14b). Although this is presumably occurring due to elimination of S142 phosphorylation, it is possible that mTOR inhibition results in nuclear translocation of this construct by other means. In an attempt to induce dephosphorylation of S142 in another way, we used the MEK inhibitor U0126 (20 μM, 3 hours) to indirectly inhibit ERK, the other kinase already shown to phosphorylate S142 (Settembre et al., 2011). Surprisingly, this did not result

in an appreciable alteration in the localisation of TFEB(1-159)-nlsCARGO, possibly indicating either that ERK cannot phosphorylate this construct, that mTOR is the primary kinase responsible for maintaining phosphorylation of this residue, or that the S142A mutation's promotion of nuclear localisation is not via the same mechanism by which Torin 1 is promoting nuclear localisation.

Additionally, we examined the effect of inhibiting GSK3 on the ability of the TFEB N-terminus to influence localisation. Treatment of cells with the GSK3 inhibitor BIO (1.5 μM, 6 hours) did not appear to inhibit XPO1-mediated nuclear export in general, as the nlsCARGO-NES construct remained cytoplasmic. Interestingly, treatment of cells expressing TFEB(1-159)-nlsCARGO with BIO was the only condition that appeared to give an intermediate phenotype between markedly cytoplasmic and markedly nuclear (Figure 4.14b). This could indicate that GSK3 is promoting cytoplasmic localisation by a mechanism that is distinct from that affected by Torin 1, LMB and the S142A mutation. Alternatively, inhibition of GSK3 could be acting through the same mechanism but unable to fully mediate nuclear translocation in the presence of active mTOR.

Taken together, these results indicate that the TFEB N-terminus mediates nuclear export to promote cytoplasmic localisation. They are consistent with TFEB being phosphorylated on S142 by mTOR and this phosphorylation event mediating cytoplasmic localisation, possibly by promoting nuclear export. We note that it would not necessarily be phosphorylation of S142 per se that mediates changes in localisation, merely that whatever the mechanism responsible, its promotion of cytoplasmic localisation is disrupted by the S142A mutation. The S142A mutation, Torin 1 treatment and BIO treatment all interfere with the ability of the TFEB N-terminus to promote cytoplasmic localisation, but whether any or all of these are impairing TFEB-

mediated nuclear export or impairing TFEB cytoplasmic localisation by another mechanism is still unclear.

### *4.2.5 TFEB residues 129-152 harbour a functional NES*

We next attempted to narrow down the region of the TFEB N-terminus that was mediating nuclear export. We made use of an online NES prediction tool to conduct an unbiased *in silico* analysis of TFEB residues 1-159 (Fu et al., 2013). Among the hits was the hydrophobic residue-rich sequence from residues 144-149. Figure 4.15 shows that residues 144-149 fit the majority of a classical NES consensus motif for XPO1 (Φ-X-X-X-Φ-X-X-Φ-X-Φ, where X = any amino acid, and Φ = M, I, V, L, F; Güttler et al., 2010). This region of TFEB is highly conserved. Hydrophobic residues in the NES consensus positions corresponding to human TFEB residues M144, L147 and I149 are maintained in TFEB from humans to zebrafish, as well as in the other TFE family members MITF and TFE3 (Figure 4.15, highlighted in blue). We noted that this series of residues lies very close to the S142 site shown to be key for the ability of the TFEB N-terminus to mediate cytoplasmic localisation. Also interesting was that an analysis of the TFEB(1-159) fragment showed that the only region that fit the consensus motif for GSK3 (S-X-X-X-pS; Cohen & Frame, 2001) is adjacent to the putative NES, with phosphorylated S142 potentially serving as the initial priming site (Figure 4.15, priming phospho-serine in red). As we had seen GSK3 inhibition to affect the localisation of the TFEB N-terminus (see Figure 4.14b), we chose to include the conserved potential GSK3 target sites S134 and S138 in the new construct, opting to include residues 129-152 (Figure 4.15).

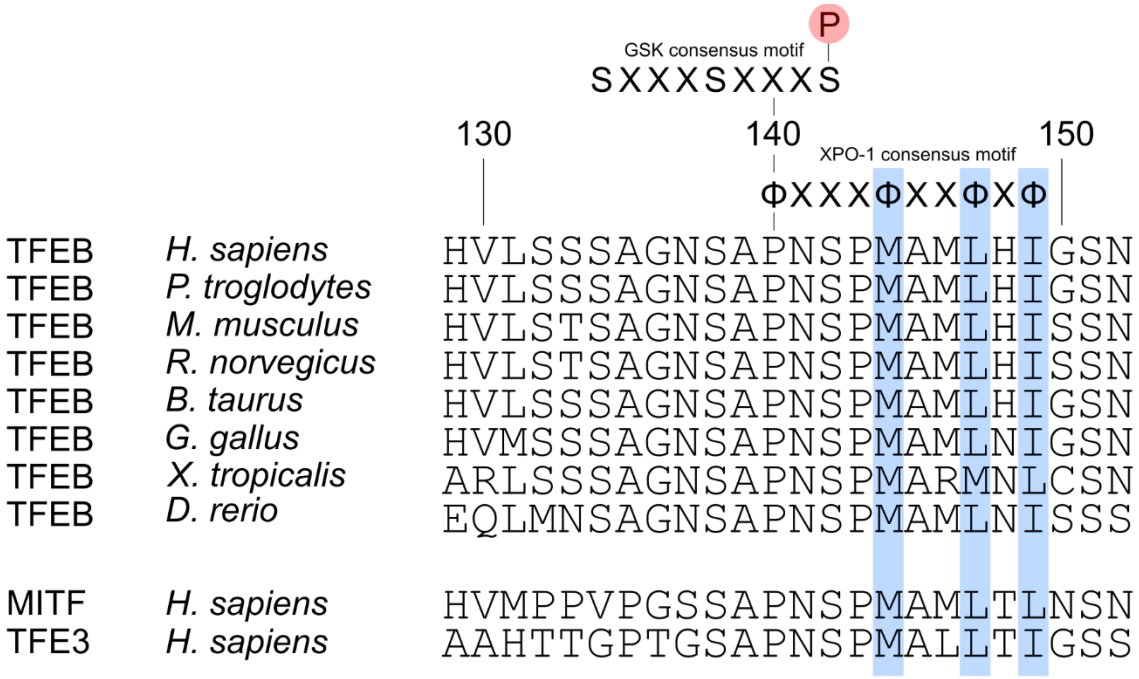



**Figure 4.15. TFEB residues 144-149 fit an NES consensus motif and are highly conserved.** Alignment of TFE family member protein sequences. Sequences corresponding to human TFEB residues 129-152 are shown for TFEB in several different species and for human MITF and TFE3. An XPO1 classical NES consensus motif is shown above, with X being any residue and Φ being a hydrophobic residue. Positions in the sequence alignment harbouring hydrophobic residues fitting the NES consensus motif are highlighted in blue. Also shown above is the GSK3 consensus motif (S-X-X-X-pS), with the required priming phosphoryation shown in red.

We first needed to check whether residues 129-152 were sufficient to mediate nuclear export. We used the nlsCARGO system to make a new fusion protein containing TFEB residues 129-152 [TFEB(129-152)-nlsCARGO]. As for previous constructs, we initially overexpressed TFEB(129-152)-nlsCARGO transiently in MCF7 cells. Although this protein was primarily nuclear in most cells, the localisation pattern was more cytoplasmic than that of nlsCARGO and responded to LMB by becoming more nuclear (Figure 4.16a). This indicates that TFEB residues 129-152 are capable of promoting XPO1-mediated nuclear export, though less efficiently that residues 1-159.

We next attempted to confirm that the hydrophobic residues identified in the *in silico* analysis indeed comprised a NES. We individually mutated each of the conserved

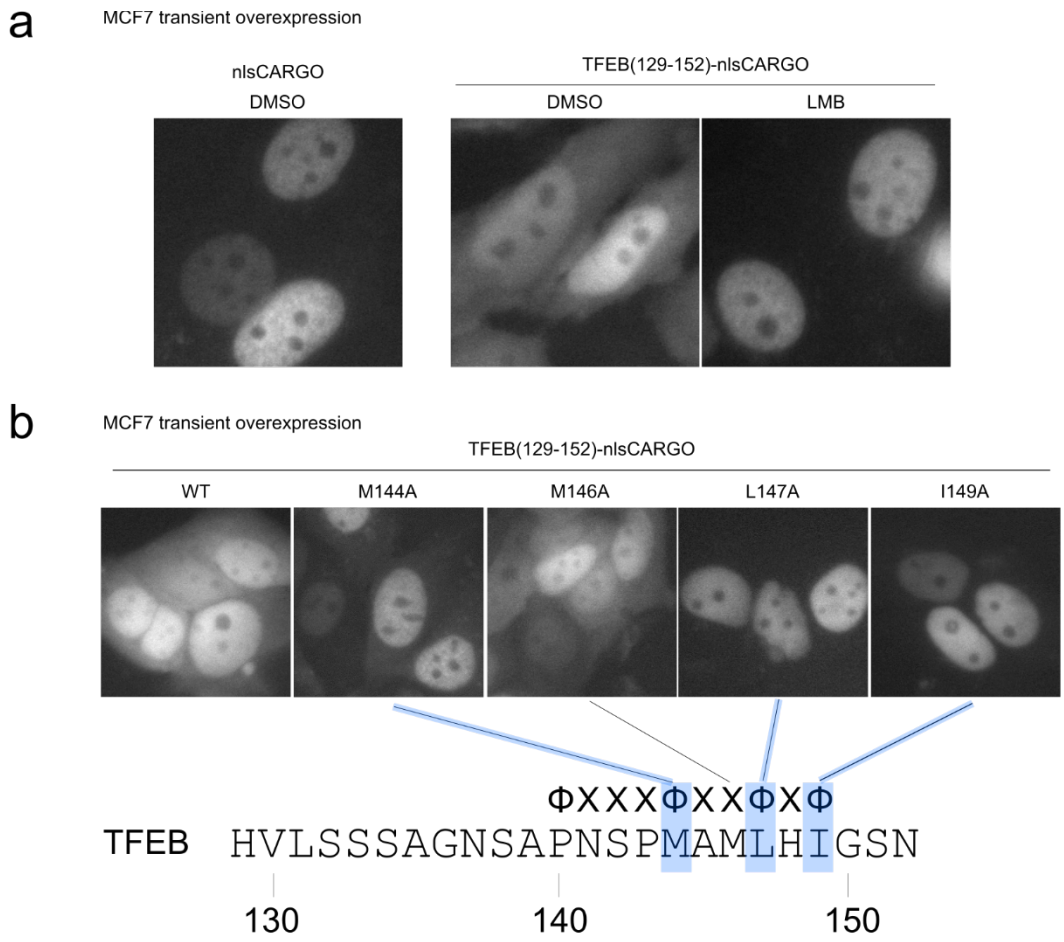



**Figure 4.16. Residues 129-152 of TFEB harbour a functional NES.** Fluorescence live cell imaging of MCF7 cells transiently overexpressing residues 129-152 of TFEB fused to a nuclear cargo protein. (a) Cells were transfected with nlsCARGO or TFEB(129-152)-nlsCARGO. After 48 hours, cells were treated with DMSO or LMB (20 nM, 2 hours) to inhibit nuclear export and imaged. (b) Cells were imaged 48 hours after being transfected with TFEB(129-152) that was either WT or harboured the indicated mutations. The sequence of human TFEB from residues 129-152 is shown, with the classical XPO-1 NES consensus motif shown above, where X is any residue and Φ is a hydrophobic residue . The location of the various mutants within the motif is indicated, with hydrophobic residues corresponding to the NES consensus motif highlighted in blue.

hydrophobic residues fitting the XPO1 NES consensus motif to alanine. We also mutated M146 to alanine to serve as a negative control – this hydrophobic residue is highly conserved and lies within the putative NES but does not correspond to one of the NES consensus motif residues (see Figure 4.15). Compared to the WT, the M144A, L147A and I149A mutations all resulted in the loss of the ability of TFEB(129-152) to mediate cytoplasmic localisation (Figure 4.16b). The M146A mutation did not result in

any change in localisation and showed a distribution similar to the WT. These data indicate that the residues 129-152 are capable of mediating nuclear export, that this export is via XPO1 and that the mutation of any of the 3 residues fitting a classical NES consensus motif results in a shift toward more nuclear localisation.

Curious as to whether the status of these residues impacted localisation of full-length TFEB-GFP, we chose the L147A and I149A mutations to stably overexpress in MCF7 cells. After separating subcellular compartments of these cells by fractionation, we assessed localisation of the TFEB-GFP mutant proteins by Western blotting. Cells expressing WT and mutant TFEB-GFP were either treated with Torin 1 (250 nM, 1 hour) or left untreated. Stably overexpressed WT TFEB-GFP appears essentially absent from the nucleus in MCF7 cells in control conditions (Figure 4.17a, lane 3). Although a small amount of TFEB(I149A)-GFP could be detected in the nucleus in the absence of Torin 1 treatment (lane 11), the same was not true of the L147A mutant. However, upon addition of Torin 1, both the L147A and I149A mutant proteins accumulate in the nucleus to a greater degree than does the WT, with the I149A again showing a stronger phenotype, although this mutant does appear to be expressed at slightly higher levels in general (Figure 4.17a, lanes 12 and 8 vs. lane 4).

This effect is also evident when comparing the amount of TFEB-GFP in the Torin 1-treated cytoplasmic and nuclear fractions for the WT and the L147A and I149A mutants. The WT shows the majority of TFEB-GFP still present in the cytoplasm, whereas the two mutants show more TFEB-GFP present in the nucleus. This is consistent with the L147A and I149A mutations preventing nuclear export when mTOR is inhibited. We also noted that although the resolution of bands is not optimal, it did not appear as though the L147A or I149A mutant proteins showed accelerated migration

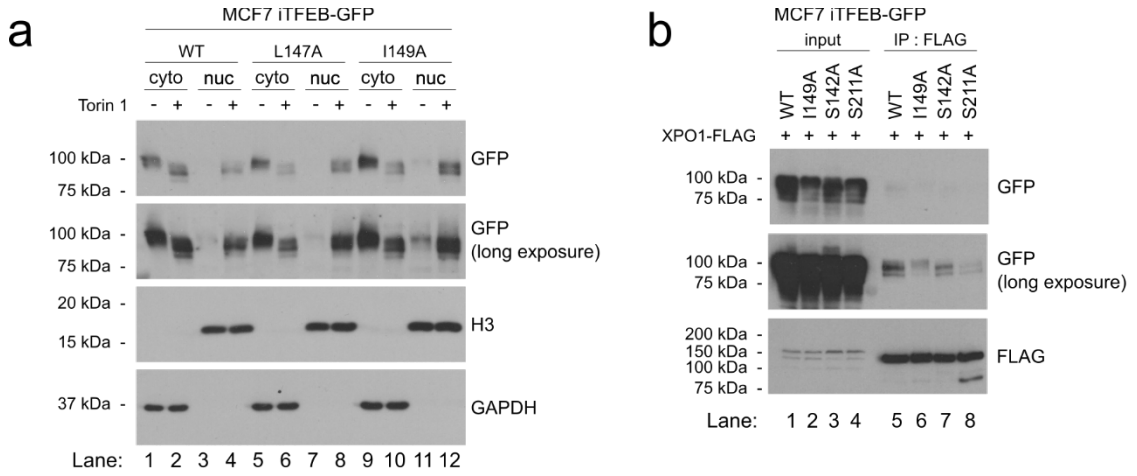



**Figure 4.17. Mutation of consensus residues within the putative NES alters the localisation of TFEB-GFP.** Localisation of stably overexpressed TFEB-GFP was examined in MCF7 cells by Western blotting of subcellular fractions. TFEB-GFP was either WT or harboured a single point mutation as indicated. (a) Cells expressing TFEB-GFP (WT, L147A or I149A) were either treated with Torin 1 (250 nM, 1 hour) or not. Cytoplasmic (cyto) and nuclear (nuc) fractions were probed with an antibody against GFP to detect TFEB-GFP. The efficacy of fractionation was assessed with antibodies against the nuclear marker histone H3 and the cytoplasmic marker GAPDH. (b) MCF7 cells expressing the indicated TFEB-GFP point mutants were transfected with XPO1-FLAG. Cells were harvested 24 hours later, with XPO1-FLAG being precipitated with an antibody against FLAG. Fractions were then blotted for GFP to detect TFEB-GFP.

compared to the WT protein in control conditions. This is consistent with neither of these point mutants interfering with phosphorylation of the neighbouring S142 residue.

We then attempted to demonstrate that the I149A point mutant interfered with binding to XPO1. Cells stably overexpressing TFEB-GFP that was either WT or harboured the I149A, S142A or S211A mutations were transiently transfected with FLAG-tagged XPO1. We then immunoprecipitated (IP) FLAG-tagged proteins and probed input and FLAG IP samples with FLAG and GFP antibodies. Although the loading of the input fractions is uneven and difficult to compare readily (this assay was done late in the course of the project and needs optimisation and repeating), this experiment is consistent with the I149A mutant showing impaired binding to XPO1 compared to the WT and S142A mutant (Figure 4.17b). Interestingly, the S211A mutant also shows impaired binding to XPO1 compared to the WT. Also, the WT,

S142A and S211A TFEB-GFP pulled down with XPO1-FLAG all show similar migration patterns, while the TFEB(I149A)-GFP in the IP fraction is primarily a slower-migrating species, possibly indicating that this mutation alters the nature of TFEB post-translational modification (Figure 4.17b).

Taken together, the data indicate that residues M144, L147 and I149 comprise a LMB-responsive NES that facilitates XPO1-mediated nuclear export of TFEB. Mutation of the hydrophobic residues partially corresponding to a classical NES consensus motif increases the nuclear localisation of TFEB-GFP, as assessed by live cell imaging and Western blotting of subcellular fractions. This is true both in the context of TFEB residues 129-152 fused to a heterologous nuclear cargo protein and when placed into full-length TFEB-GFP. Although the IP experiment lacked controls and needs repeating, it is consistent with the existence of additional NESs in TFEB. This idea is further supported by the fact that nuclear translocation with LMB appears more pronounced than that observed with the L147A and I149A mutations. This is true of both full-length TFEB-GFP and the two N-terminal fragments (1-159 and 129-152) fused to the nlsCARGO protein.

### *4.2.6 TFEB residues 129-152 mediate signalling-dependent localisation changes*

TFEB residues 129-152 appear sufficient to direct nuclear export. We noted that the S142A mutation eliminated the ability of TFEB(1-159) to promote cytoplasmic localisation and wondered if residues 129-152 were capable of directing shifts in localisation in response to mTOR, MAPK or GSK3 signalling similar to those seen with TFEB(1-159)-nlsCARGO. While we selected for TFEB(129-152)-nlsCARGO stable lines, we conducted an initial experiment using transient overexpression to compare the

localisation of nlsCARGO and TFEB(129-152)-nlsCARGO during treatment with the same panel of inhibitors used with the longer TFEB 1-159 fragment. Importantly, treatment with LMB again resulted in TFEB(129-152)-nlsCARGO adopting a nuclear localisation that was similar to nlsCARGO and noticeably more nuclear than TFEB(129-152)-nlsCARGO in control conditions (Figure 4.18a).

As this protein is present to some degree in the nucleus in control conditions during transient overexpression, it was more difficult to assess the influence of Torin 1, U0126 and BIO treatment. However, as was observed for TFEB-GFP, these drugs appeared to result in some degree of nuclear translocation of TFEB(129-152)-nlsCARGO. Whereas Torin 1 resulted in a marked shift of TFEB(1-159)-nlsCARGO to the nucleus in earlier experiments and U0126 treatment had little effect (see Figure 4.14b), the mTOR inhibitor only minimally shifted the shorter TFEB fragment, while U0126 treatment now demonstrated a higher degree of nuclear translocation (Figure 4.18a). Inhibition of GSK3 with BIO also showed a moderate shift of TFEB(129-152)-nlsCARGO to the nucleus, as had been seen with the longer 1-159 fragment. As seen with TFEB(1-159)-nlsCARGO, inclusion of the S142A mutation rendered the shorter TFEB fragment constitutively nuclear, regardless of mTOR, MAPK or GSK3 inhibition (Figure 4.18a). Western blotting of TFEB(1-159)-nlsCARGO and TFEB(129-152)-nlsCARGO showed that, when transiently transfected, these constructs both ran as multiple species, consisting of at least two bands (Figure 4.18b).

Inclusion of the S142A mutation resulted in both constructs running primarily as the lowest of these bands. This was especially evident with the 129-152 fragment and likely indicated that both of these constructs are normally present as at least two species – one that is phosphorylated on S142 and one that is not. It is tempting to conclude that the upper band corresponds to a population of TFEB that is phosphorylated on S142

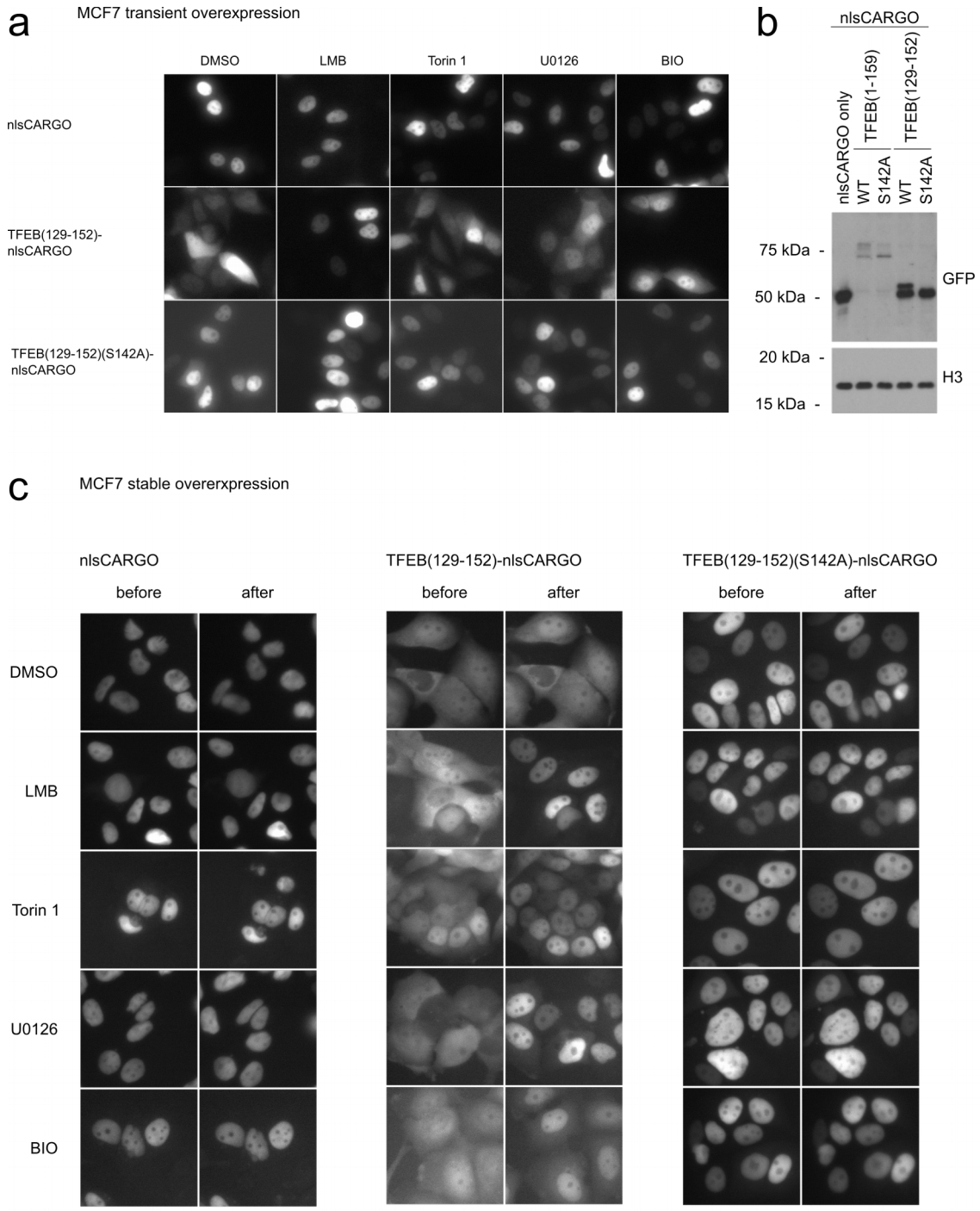



**Figure 4.18. TFEB residues 129-152 direct nuclear export and mTOR-, MAPK- and GSK3-dependent cytoplasmic localisation.** Fluorescence live cell imaging and Western blotting of MCF7 cells expressing a nuclear cargo protein (nlsCARGO), residues 129-152 of TFEB fused to nlsCARGO or the same with the addition of the S142A mutation. (a) Cells were treated with DMSO, LMB (20 nM, 2 hours), Torin 1 (250 nM, 1 hour), U0126 (20 μM, 3 hours) or BIO (1.5 μM, 6 hours) 48 hours after being transiently transfected with the indicated constructs. (b) MCF7 cells transiently overexpressing nlsCARGO, TFEB(1-159)-nlsCARGO, TFEB(129-152)-nlsCARGO or the same two TFEB constructs with the addition of the S142A mutation are lysed and examined by Western blotting using a GFP antibody to detect the various fusion proteins. Histone H3 serves as a loading control. (c) MCF7 cells stably expressing the same constructs as in (a) are incubated with various inhibitors as in (a). A given field of cells is imaged before and after treatment using time lapse fluorescence live cell imaging.

and localised to the cytoplasm and that the lower band corresponds to a population of TFEB that is not phosphorylated on S142 and is localised to the nucleus, however more studies are needed to evaluate this hypothesis.

Stable overexpression of TFEB(129-152)-nlsCARGO in MCF7 cells gave a clearer picture of the ability of this fragment to mediate changes in localisation in response to these signalling pathways. Overall, this showed the same trends as seen with transient overexpression (Figure 4.18a, c). TFEB(129-152)-nlsCARGO was again more cytoplasmic than nlsCARGO, although it did not achieve the same degree of cytoplasmic localisation as did the longer TFEB(1-159)-nlsCARGO (see Figure 4.14b). When treated with LMB, stably overexpressed TFEB(129-152)-nlsCARGO showed a marked shift from the cytoplasm to the nucleus, again confirming that, like the larger piece of the TFEB N-terminus, residues 129-152 were capable of mediating nuclear export. As we saw for the larger TFEB fragment, and with transient overexpression of TFEB(129-152)-nlsCARGO, inclusion of the S142A mutation resulted in constitutively nuclear localisation, which was unaltered by LMB (Figure 4.18c). This again implicates this residue as being important for the ability of both the larger (1-159) and smaller (129-152) fragments of the TFEB N-terminus to promote cytoplasmic localisation, possibly by affecting nuclear export.

As we had done with TFEB(1-159)-nlsCARGO, we treated cells stably expressing TFEB(129-152)-nlsCARGO with inhibitors of the mTOR, ERK and GSK3 pathways. Similar to what we saw with the longer fragment (see Figure 4.14b) and with transient overexpression of the shorter fragment (see Figure 4.18a), none of these compounds affected the constitutively nuclear localisation of the nlsCARGO protein or the TFEB(129-152)(S142A)-nlsCARGO mutant when stably overexpressed (Figure 4.18c). Inhibition of mTOR, MAPK and GSK3 signalling all increased the amount of

TFEB(129-152)-nlsCARGO in the nucleus, with GSK3 inhibition showing a more mild effect than the other inhibitors. Interestingly, this shorter TFEB fragment shows a more marked shift to the nucleus in response to U0126 treatment compared to the longer TFEB(1-159) fragment (Figure 4.18c vs. Figure 4.14b). It is possible that because TFEB(129-152) lacks the region of the N-terminus previously found to mediate tethering to the lysosome (residues 1-30; Martina & Puertollano, 2013), this construct is not able to interact with the machinery located there, including the mTOR complex. This could account for several differences seen between the 1-159 and 129-152 constructs, including the 129-152 construct being more nuclear in control conditions, being less sensitive to Torin 1 treatment and being more sensitive to U0126 (Figure 4.18c vs. Figure 4.14b).

Taken together, the data are again consistent with these 24 residues of TFEB being capable of promoting cytoplasmic localisation. Pharmacologic inhibition of nuclear export and of the mTOR, MAPK and GSK3 pathways all impair this ability, rendering TFEB(129-152)-nlsCARGO more nuclear. The S142A mutation results in this fragment being constitutively nuclear, implying that this residue is of key importance for the ability of this region to direct shifts in localisation.

### *4.2.7 S142 phosphorylation primes GSK3 to phosphorylate S138*

Inhibition of the GSK3 pathway with the inhibitor BIO promotes nuclear localisation of TFEB, both in our hands and in previous studies (Marchand et al., 2015; Perera et al., 2015). Until recently, GSK3 was thought to affect TFEB localisation by acting on C-terminal phosphorylation sites (Ploper et al., 2015). However, our data indicated that GSK3 may also act on a site between TFEB residues 129 and 152, with a

current study also supporting this hypothesis (Li et al., 2016). Narrowing down a region capable of responding to GSK3 inhibition was made easier by the fact that the first 159 residues of TFEB harboured only two residues that fit the GSK3 consensus motif, S134 and S138. TFEB(129-152)-nlsCARGO contained both of these residues and responded to GSK3 inhibition by becoming more nuclear. Accordingly, we hypothesised that GSK3 was capable of phosphorylating the TFEB N-terminus between residues 129 and 152, likely on S134, S138 or both.

To study this, we conducted an *in vitro* kinase assay. Investigating GSK3 phosphorylation is complicated by the fact that this kinase normally requires a nearby priming phosphorylation in order to phosphorylate its target residue (see Figure 4.15). To address this, SPOT technology (Winkler et al., 2009) was used to immobilise peptides corresponding to TFEB residues 129-147 onto spots on a membrane. The SPOT technique limited us to 19 residues, so we were unable to include the entirety of the TFEB(129-152) fragment shown previously to mediate GSK3-dependent cytoplasmic localisation. With the GSK3 consensus motif in mind, we centred the peptides around S134, S138 and S142.

Notably, after another kinase provides the initial priming event, GSK3 can prime for itself, as is the case with its canonical target β-catenin (Hagen et al., 2002). If a serine or threonine is available 4 residues N-terminal to the first target site, GSK3 can phosphorylate this second residue. Such a "cascade" of sites fitting the consensus motif is found in TFEB(129-152) (see Figure 4.15). Provided S142 is phosphorylated, GSK3 could theoretically phosphorylate S138. Once S138 is phosphorylated, it is possible that GSK3 could then phosphorylate S134. With these outcomes in mind, we included versions of the 129-147 peptide that would allow us to distinguish among the different single or multiple phosphorylation events.

Figure 4.19 shows the layout and results of the SPOT assay. After verifying the location of the spots corresponding to each of the peptides with UV light (Figure 4.19b, c), the membrane was incubated with purified GSK3 and [$\gamma$-$^{32}$P]-ATP and imaged with a Phosphorimager to identify incorporation of radioactive ATP (Figure 4.19d). The location and nature of the different changes made to the WT sequence in the various 12 peptides is shown. Only serine residues (Figure 4.19a, boxed residues) were altered, and these were either left as serine, modified to phospho-serine or mutated to alanine. Although the key residues of interest were S134, S138 and S142, we also included additional peptides to determine if two other serine residues that lay outside the GSK3 consensus motif (S132 and S133) could be phosphorylated (Figure 4.19a).

Throughout the different parts of Figure 4.19, red highlighting indicates peptides that were phosphorylated by GSK3. Note that spot 1 contains WT peptide and is not phosphorylated by GSK3 in this assay (Figure 4.19d), indicating that any phosphorylation of this region by GSK3 likely requires a priming event. This is an important negative control, in that GSK3 has been noted to phosphorylate substrates *in vitro* in the absence of a priming phosphorylation (Frame & Cohen, 2001).

If a priming phosphorylation was provided on S142, GSK3 was able to phosphorylate TFEB(129-147) (Figure 4.19a, d, peptide 4). Changing S138 to alanine (peptide 5) eliminated GSK3 phosphorylation, indicating that S138 was targeted by GSK3, but only when S142 was already phosphorylated. The fact that peptide 5 was not phosphorylated also argued that the other serine residues (S132, S133, S134) were either not phosphorylated or required phosphorylation of S138 to be phosphorylated. Peptide 6 shows that even when serines 132, 133 and 134 were all mutated to alanine, GSK3 could still phosphorylate the peptide, provided S142 was already phosphorylated. If the S138A mutation was introduced, the peptide is no longer phosphorylated (Figure

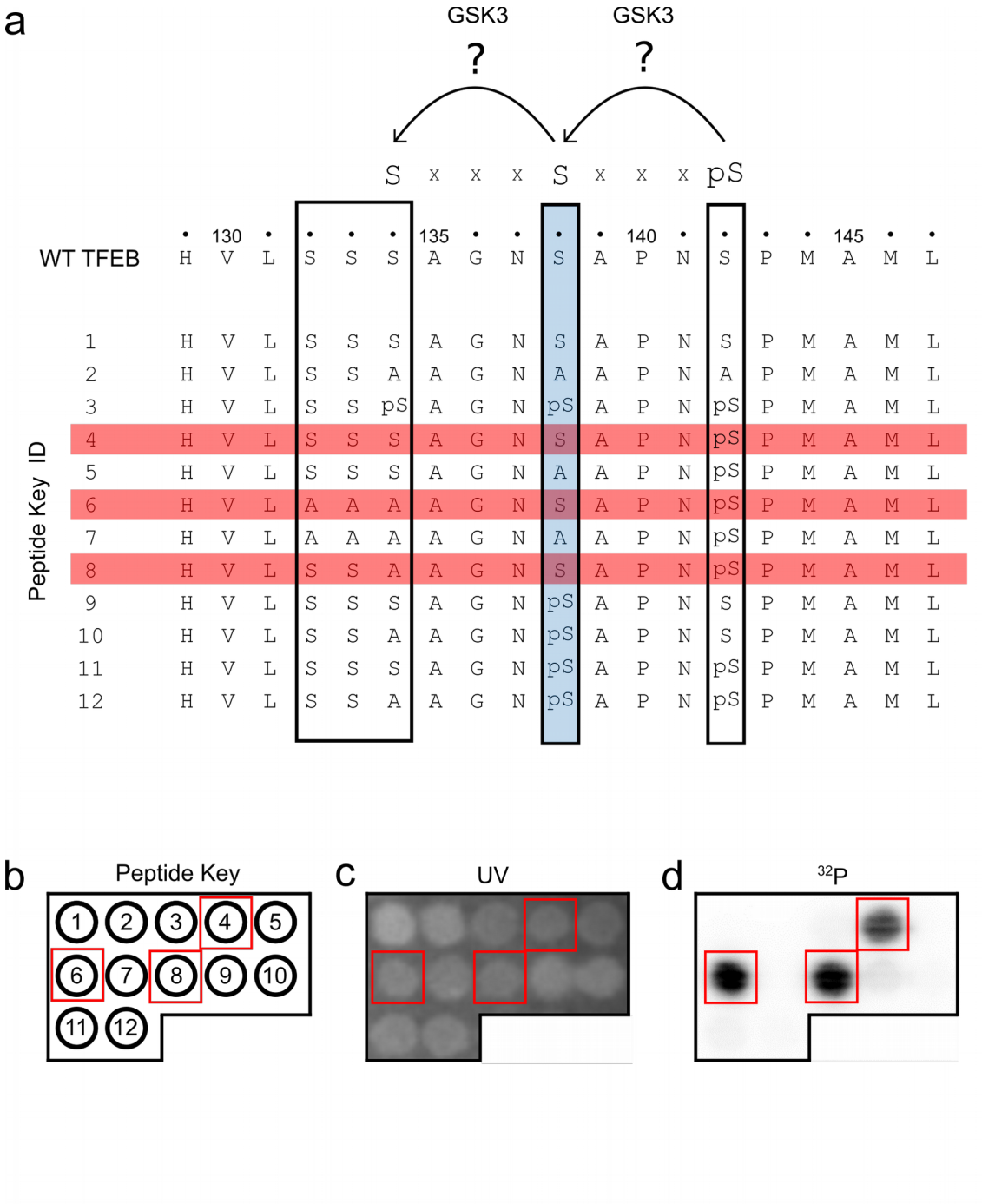



**Figure 4.19. GSK3 phosphorylates S138 in the presence of a priming phosphorylation at S142.** Peptides corresponding to TFEB residues 129-147 were immobilised on a cellulose membrane in a peptide SPOT assay. The sequence of each of the 12 peptides is shown in (a), with the WT sequence and numbering shown above. Black boxes show serine residues that could potentially be phosphorylated. These were either left as serine, mutated to alanine or altered to phosphoserine in the various different peptides. Spots on the array corresponding to the peptides shown in (a) can be found in the peptide key (b), with their positions verified with UV light in (c). After incubating the membrane with purified GSK3 and [$\gamma$-$^{32}$P]-ATP, incorporation of $^{32}$P was detected by Phosphorimager (d). Peptides that were phosphorylated are highlighted in red in (a) - (d), and S138 is highlighted in blue.

4.19d, peptide 7). The fact that peptide 6, which harbours serine-to-alanine mutations for all residues except S138, does not show decreased phosphorylation relative to peptide 4 is consistent with S138 being the only GSK3 target. This is further supported by comparing the pS142-containing peptides 8 and 4, the only difference being that peptide 8 harbours a S134A mutation. Peptide 8 shows no decrease in phosphorylation compared to peptide 4, indicating that S138 is phosphorylated while S134 is not.

We included several more peptides to more directly address whether GSK3 could phosphorylate S134. Peptide 9 contains a phosphorylated S138 but is otherwise unchanged from the WT sequence, while peptide 10 is identical but contains the S134A mutation to serve as a negative control. Neither is phosphorylated by GSK3, showing that in the presence of a priming phosphorylation at S138 (but not S142), S134 is not phosphorylated (Figure 4.19d). However, it could be that the phosphorylated S138 found in peptides 9 and 10 does not normally occur in the absence of phosphorylated S142.

To investigate whether S134 was phosphorylated by GSK3 in the presence of priming events at both S142 and S138, peptides 11 and 12 were included. These are the same as peptides 9 and 10 but include an additional priming phosphorylation at S142 (Figure 4.19a, b). Again, neither peptide is phosphorylated, indicating that S134 is not phosphorylated by GSK3 regardless of the status of S138 and S142. This also indicates that S138 is the only GSK3 target in this peptide, as no phosphorylation is observed in peptides 1 or 11 but is observed in peptide 4 (Figure 4.19d). Taken together, the data from the SPOT assay support a model in which GSK3 can phosphorylate S138 but only in the presence of a priming phosphorylation on S142. This appears to be the extent of GSK3 phosphorylation in this region – despite the fact that another serine residue fits the consensus motif for this kinase, GSK3 was unable to phosphorylate S134 in any

condition tested. It should be noted that this assay utilises short peptides immobilized onto a scaffold, so we cannot rule out that neighbouring regions of TFEB might permit GSK3 phosphorylation that was not observed or preclude GSK3 phosphorylation that was seen.

Having identified S138 as a GSK3 target site, we were curious whether altering the status of this site impacted the localisation of full-length TFEB-GFP. Each of our TFEB constructs had accumulated in the nucleus in response to GSK3 inhibition; perhaps this effect was due to loss of GSK3-mediated phosphorylation at S138. To study this, we mutated S138 to alanine to prevent GSK3-mediated phosphorylation and to aspartic acid or glutamic acid to mimic GSK3-mediated phosphorylation. We overexpressed these mutants stably in MCF7 cells, treated them with DMSO or the mTOR inhibitor Torin 1 (250 nM, 1 hour) and imaged them using fluorescence live cell imaging. WT TFEB-GFP was again cytoplasmic, with the GFP-only control being pancellular (Figure 4.20). None of the S138 point mutations appreciably altered the localisation of TFEB-GFP compared to the WT. The S142A/S211A double mutant was constitutively nuclear, as had been seen in previous experiments (Figure 4.20; also see Figure 4.13). Upon treatment with Torin 1, all TFEB-GFP constructs showed primarily nuclear localisation, with no significant difference among them. The fact that the S138A mutant and the WT are comparably cytoplasmic in control conditions could indicate that S138 is not phosphorylated in this context. It is also possible that S138 is phosphorylated but that the loss of this phosphorylation does not alter TFEB-GFP localisation. Also, as the S138D and S138E mutants are no more cytoplasmic than the WT or S138A in control or Torin 1-treated conditions, either phosphorylation of this site is not sufficient to promote cytoplasmic localisation in the presence or absence of

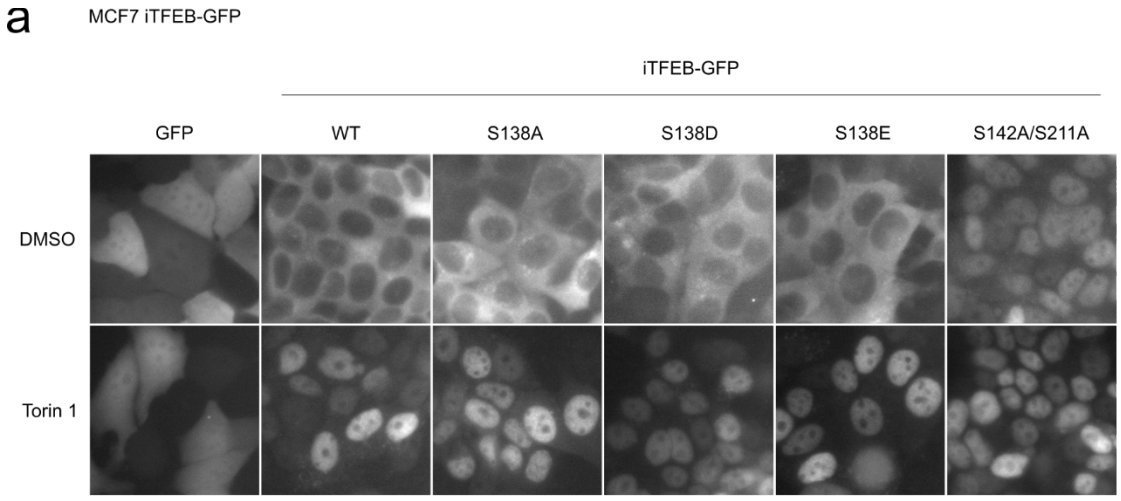



**Figure 4.20. Mutation of GSK3 target site S138 does not alter TFEB-GFP localisation in control conditions or during mTOR inhibition.** Fluorescence live cell imaging of MCF7 cells stably expressing TFEB-GFP harbouring various point mutations as indicated. Each cell line is treated either with Torin 1 (250 nM, 1 hour) or an equivalent amount of DMSO.

mTOR target site phosphorylation, or it is sufficient, and the D and E mutants do not adequately mimic phosphorylation of S138.

## 4.3 Discussion

The regulation of TFEB appears complex, with multiple signalling pathways modulating its localisation in response to multiple stimuli by impinging on its post-translational status. This complexity is evident in the literature, with conflicting evidence regarding TFEB localisation under control conditions and the role of S142 phosphorylation in regulating localisation (Peña-Llopis et al., 2011; Perera et al., 2015; Settembre et al., 2012). Additionally, there is disagreement about whether mTOR inhibits or promotes cytoplasmic localisation, under what circumstances it might do this and which residue(s) of TFEB are targeted (Martina et al., 2012; Peña-Llopis et al., 2011; Settembre et al., 2011; Settembre et al., 2012). To complicate matters further, de-

phosphorylation of TFEB residues known to influence localisation appears to be regulated, and its importance is just beginning to be investigated (Marchand et al., 2015; Medina et al., 2015).

Our data indicate that the already complicated regulation of TFEB localisation has still more variables to consider. We provide evidence that TFEB level may be a key determinant of its localisation, a finding that could help to explain some of the discrepancies in previous reports of TFEB localisation in the literature (Martina et al., 2012; Perera et al., 2015). We also confirm published findings concerning the influence of the mTOR, MAPK and GSK3 signalling pathways on TFEB nuclear translocation and show that glucose and serum starvation both result in TFEB shifting to the nuclear compartment (Marchand et al., 2015; Martina et al., 2012; Peña-Llopis et al., 2011). Next, we show that TFEB nuclear translocation in response to a diverse range of stimuli is reversible, a finding that has been confirmed in the case of amino acid starvation (Settembre et al., 2012; Stretton et al., 2015). Additionally, we present data arguing that TFEB return to the cytoplasm after nuclear translocation requires nuclear export, that this is mediated by XPO1 and that there is a functional NES between TFEB residues 144 and 149. We also show that ectopic and endogenous TFEB both exhibit what seems to be a certain level of baseline cycling through the nucleus and back to the cytoplasm, as TFEB accumulates in the nucleus in response to inhibition of nuclear export even without first inducing it to enter the nucleus by a starvation stimulus or inhibitor treatment. Lastly, we confirmed S138 as a phosphorylation target of GSK3, with this event being dependent upon a priming phosphorylation at S142.

In normal cells and virtually all neoplasms, endogenous TFEB is undetectable by immunohistochemistry (IHC), leading to the use of nuclear labelling for TFEB by IHC as a diagnostic criterion for t(6;11) renal carcinomas (Argani et al., 2005). In

contrast, TFEB is often reported to be cytoplasmic in cell culture in the absence of stimuli that promote its nuclear translocation (Marchand et al., 2015; Roczniak-Ferguson et al., 2012). But although TFEB staining is primarily nuclear in translocation RCC, it is not clear if nuclear TFEB is a causative factor in the development of the disease, nor is it clear if high levels of TFEB cause its nuclear localisation or result from its nuclear localisation. We observed that transiently overexpressed TFEB was predominantly nuclear. Using an inducible system, we then showed that low-level stable overexpression of ectopic TFEB resulted in levels 5-fold higher than endogenous TFEB and a predominantly cytoplasmic localisation pattern. Inducing TFEB expression further causes it to progressively accumulate in the nucleus, as well as resulting in an acceleration of its electrophoretic mobility. Both previous reports and our studies indicate that this accelerated migration is characteristic of loss of TFEB phosphorylation, which correlates with its nuclear localisation (Figures 4.2, 4.6, 4.12, 4.18; Martina et al., 2012; Settembre et al., 2011).

Thus, the observation that TFEB level, loss of phosphorylation and nuclear localisation all correlate is consistent with a model in which TFEB must be actively maintained in the cytoplasm via phosphorylation events, and if the mechanisms mediating this become saturated, TFEB is free to translocate to the nucleus. This could occur via inhibition of the kinases actively retaining TFEB in the cytoplasm (Roczniak-Ferguson et al., 2012), activation of the phosphatases promoting its nuclear translocation (Medina et al., 2015) or elevation of TFEB level to the point where the kinases targeting TFEB could no longer maintain its phosphorylation and cytoplasmic sequestration (Figure 4.2c). We note that a high level of TFEB could theoretically saturate cytoplasmic sequestration (e.g., 14-3-3-mediated sequestration), nuclear export or both.

We observed that TFEB nuclear translocation was reversible, whether occurring in response to a starvation stimulus or inhibition of kinases known to mediate TFEB phosphorylation. Using a photoconvertible green-to-red TFEB fusion, we demonstrated that nuclear export mediated by XPO1 was required for the redistribution of TFEB to the cytoplasm after translocation to the nucleus. Moreover, inhibition of XPO1 with LMB in the absence of any other stimulus known to promote TFEB nuclear translocation resulted in the accumulation of TFEB-GFP in the nucleus, indicating that stably overexpressed TFEB-GFP is cycling through the nucleus at steady-state in the conditions tested. This is consistent with a portion of TFEB-GFP becoming dephosphorylated in fed conditions and moving to the nucleus. There it would normally be exported to the cytoplasm by XPO1, where it would become phosphorylated and be sequestered. But in the presence of LMB, nuclear export is inhibited, and TFEB-GFP cycling through the nucleus accumulates there. We note that degradation of nuclear TFEB could still play a role in its disappearance from the nucleus, or TFEB could also be exported by mechanisms not dependent upon XPO1 (Connor et al., 2003; Holaska & Paschal, 1998).

Endogenous TFEB was also seen to show a mild accumulation in the nuclear compartment in response to LMB treatment, indicating that, like ectopic TFEB-GFP, it cycles through the nucleus to some degree at steady-state conditions in cell culture. As TFEB in nuclear fractions treated with LMB showed an accelerated migration pattern compared to control conditions, it seems that, under conditions where nuclear export is inhibited, either dephosphorylated TFEB enters the nucleus, or phosphorylated TFEB can enter the nucleus where it is then dephosphorylated.

We note that endogenous TFEB did not accumulate in the nucleus to the same extent as TFEB-GFP in response to LMB treatment, making it unclear to what extent

endogenous TFEB is subject to nuclear export in the conditions tested. This could be a quantitative effect due to the fact that TFEB-GFP is present at a higher level than endogenous TFEB (see Figure 4.4e). As TFEB is thought to be actively maintained in the cytoplasm, any increase in its level could render more of the TFEB pool dephosphorylated, resulting in more rapid cycling through the nucleus and greater accumulation in response to LMB treatment. Alternatively, the effect could be qualitative, with TFEB-GFP cycling more rapidly through the nucleus than TFEB due to the presence of the C-terminal GFP tag. For example, if this tag were to result in a degree of interference with TFEB phosphorylation at residues S142 and/or S211, TFEB-GFP could be free to cycle through the nucleus at a higher rate.

We elected to use fluorescent tags to study the localisation of TFEB, as these permitted the assessment of shifts in the localisation of ectopically expressed TFEB constructs in a given group of cells over a period of time. Although this allowed us to observe TFEB localisation in real time without the confound of examining different groups of cells for different conditions and time points, the presence of the GFP tag is not without drawbacks. For example, the location of the Dendra2 tag had profound effects on TFEB localisation, with an N-terminus tag resulting in constitutively nuclear localisation, and a C-terminal tag leading to cytoplasmic localisation. Another set of experiments made use of a tag we termed CARGO, which consisted of a GFP-GST fusion. This was then fused to one of two fragments of the TFEB coding sequence: residues 1-159 or residues 129-152. In both cases, the GFP-GST tag is significantly larger than the residues corresponding to TFEB, particularly for the TFEB(129-152) fragment. Although it is striking that this small portion of TFEB is sufficient to redirect the localisation of a tag that is comparatively massive, concerns over potential confounds arising from the use of tags in general remain. In an attempt to address this,

we are generating cell lines that stably express full-length TFEB with either an N-terminal 3xHA tag or a C-terminal 3xFLAG tag. We are also expanding our characterisation of the localisation of the endogenous protein in different conditions using a combination of immunofluorescence and subcellular fractionation. These data can then be compared with the results obtained with TFEB-GFP and the various CARGO fusions to assess whether a particular tag adversely affects TFEB localisation.After establishing that TFEB is subject to nuclear export, we attempted to ascertain whether this process was regulated by either of the two phosphorylation events already known to influence TFEB localisation. Indeed, we found that the S142A mutation, either alone or in combination with the S211A mutation, eliminated TFEB-GFP nuclear translocation in response to LMB treatment. The S211A mutant remained responsive to LMB treatment, showing pronounced nuclear translocation in response to inhibition of nuclear export. This indicated that phosphorylation of S142 may be implicated in mediating TFEB nuclear export, an interesting possibility seeing as the mechanism by which phosphorylation of S142 mediates alterations in TFEB localisation remains unknown (Settembre et al., 2011; Roczniak-Ferguson et al., 2012).

Our analysis of the S142A and S211A mutants indicated that phosphorylation of these two sites impinges on TFEB localisation by separate mechanisms, so we began to study the ability of the TFEB N-terminus (residues 1-159) to mediate shifts in the localisation of a heterologous cargo protein. We found that this region directed nuclear export and promoted nuclear translocation in response to inhibition of signalling pathways known to regulate TFEB localisation. We eventually localised this ability to residues 129-152, identifying a functional NES in the N-terminus of TFEB. This comprised a core of 3 hydrophobic residues (M144, L147, I149A) that partially matches an XPO1 consensus motif. Although these residues only match 3 of 4 positions in the

classical NES consensus motif (Φ-X-X-X-Φ-X-X-Φ-X-Φ, where X = any amino acid, and Φ = M, I, V, L, F; Güttler et al., 2010), sequences shown to bind XPO1 exhibit a high degree of heterogeneity, sometimes fitting only a portion of the above NES motif and sometimes not fitting the consensus motif at all. Experimentally validated NESs vary in the number of hydrophobic residues, the spacing of these residues and the orientation of the motif (Fung et al., 2015; Nigg, 1997), making it perhaps not surprising that the TFEB NES is only a partial match for the classical consensus motif.

The fact that mutating consensus residues in the NES located between residues 144 and 149 did not greatly affect TFEB localisation while treatment with LMB resulted in a more marked nuclear translocation could indicate that there are additional sequences in TFEB capable of mediating XPO1-dependent nuclear export. Proteins harbouring multiple NESs have been described (Ferrer et al., 2005; Xu et al., 2012), and submitting the entire TFEB coding sequence for *in silico* analysis, as was done before for the N-terminus, identified other candidate NESs, two of the most promising of which have been cloned into the nlsCARGO system for evaluation of their ability to mediate nuclear export.

One potential NES lies within the first 12 residues of TFEB. This region has already been shown to play a role in targeting TFEB to the lysosome, as mutation of several residues in this region results in TFEB nuclear translocation (Martina & Puertollano, 2013). The authors note that these mutations also eliminate TFEB binding to Rag proteins, and they conclude that the first 12 residues of TFEB are responsible for promoting TFEB cytoplasmic localisation by mediating interactions with Rag proteins resident at the lysosome (Martina & Puertollano, 2013). Interestingly, these mutations lie within the putative NES and include residue L11, which our *in silico* analysis indicates is an XPO1 NES consensus residue. Along these lines, another possible

explanation of the findings presented by Martina & Puertollano (2012) would be that these mutations interfere with XPO1-mediated nuclear export. This could then result in TFEB nuclear accumulation, preventing it from being exported to the cytoplasm and interacting with Rag proteins at the lysosomal surface.

As mTOR has been found to phosphorylate both S142 and S211, examination of the L147A and I149A mutants in combination with either the S142A or S211A mutations could further dissect the influence of the NES between residues 144-149 on TFEB localisation. Comparison of the degree of nuclear localisation seen with an I149A/S211A double mutant to an S211A single mutant treated with LMB could provide more information about the circumstances under which the newly identified NES mediates TFEB localisation and whether TFEB is likely to harbour other functional NESs.

A question that still needs answering is whether the S142A mutant can be exported. Three lines of evidence indicate that S142 phosphorylation is mediating cytoplasmic localisation by promoting nuclear export. First, inhibition of nuclear export with LMB results in the nuclear accumulation of the WT protein and the S211A mutant, but not the S142A mutant, indicating that the S142A mutant and LMB may be affecting TFEB localisation via the same pathway. Next, two different N-terminal fragments of TFEB containing both S142 and the putative NES redirect a constitutively nuclear heterologous protein to the cytoplasm, while inhibition of kinases that phosphorylate S142 diminishes this ability. Lastly, if S142 is mutated to alanine (S142A) the ability of both TFEB(1-159) and TFEB(129-152) to promote cytoplasmic localisation is abolished. These data argue that if S142 cannot be phosphorylated, the NES is no longer functional.

However, S142 status could still be mediating alterations in TFEB localisation via other means. Phosphorylation of S142 could impair nuclear import, with the S142A mutant now subject to constitutive nuclear import that outpaces nuclear export. Unfortunately, our attempts to address this possibility were complicated by the fact that the two inhibitors of nuclear import that we studied, ivermectin (Wagstaff et al., 2012) and importazole (Soderholm et al., 2011), resulted in TFEB nuclear translocation, the opposite of the result expected (data not shown). This could be due to these treatments inducing stress, as TFEB nuclear translocation has recently been implicated in the response to ER stress (Martina et al., 2016). Alternatively, impairing the nuclear import of other factors could impair TFEB cytoplasmic retention.

Another possible explanation for the constitutively nuclear localisation of the S142A mutant is that S142 could function in a manner similar to S211, mediating interaction with a cytoplasmic component and cytoplasmic sequestration. However, the fact that the S142A mutant (but not the S211A mutant) rendered TFEB insensitive to LMB would argue against this hypothesis. Lastly, the effect could be indirect, where S142 phosphorylation could promote association with the lysosome, facilitating S211 phosphorylation. Indeed, this is the proposed mechanism in a recent report for the manner by which the neighbouring S134A and S138A mutations alter TFEB localisation (Li et al., 2016). In this scenario, the S142A mutant would effectively eliminate phosphorylation on both S142 and S211; however, we observed the S142A/S211A double mutant to be significantly more nuclear than both the S211A and the S142A single mutants, indicating that S142 regulates TFEB localisation via mechanisms not dependent upon S211. Lastly, the S142A mutant could exhibit augmented binding to DNA or another component resident in the nucleus. However, this interaction would have to be sufficient to effectively eliminate nuclear export of

TFEB, as we observe the S142A mutation to virtually abolish response to LMB treatment.

GSK3 inhibition has been shown in several reports to result in TFEB nuclear translocation, but until very recently, none of these studies used site-specific methods to identify the residues phosphorylated by GSK3 (Li et al., 2016; Marchand et al., 2015; Parr et al., 2012; Perera et al., 2015). The GSK3 consensus motif indicates that this kinase requires a priming phosphorylation event 4 residues C-terminal to the target site. In the case of TFEB, our data indicate that GSK phosphorylation of S138 occurs only after phosphorylation of S142, with this site already having been documented to be phosphorylated by ERK and mTOR (Settembre et al., 2011; Roczniak-Ferguson et al., 2012). Another serine residue fitting the GSK3 consensus motif (S134) was found to not be phosphorylated, regardless of the phosphorylation status of residues S138 or S142.

It is interesting to note that a compilation of experimentally validated leucine-rich NESs shows that acidic residues are well-represented in the spaces between the hydrophobic NES consensus motif residues (Figure 4.21; la Cour et al., 2003). In particular, the positions corresponding to TFEB residues S138 and S142 most commonly harbour a glutamic acid residue, which is often used as a phosphoserine-mimicking mutation. Phosphorylation of these residues would increase the bulk of the negative charge in these areas, possibly facilitating nuclear export. Indeed, phosphorylation of two serine residues occupying similar positions in sphingosine kinase 2 (SPHK2) by protein kinase D was found to promote nuclear export of SPHK2 (Ding et al., 2007). Cyclin D1 provides another example, where T286 phosphorylation by GSK3 has been shown to mediate association with XPO1 and subsequent nuclear

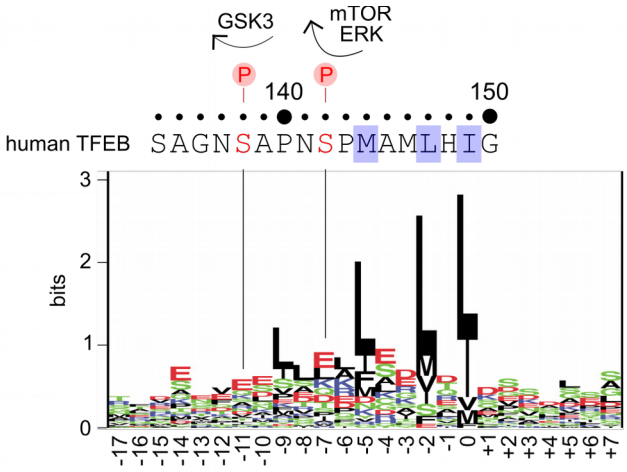



**Figure 4.21. Acidic residues predominate in NESs at the positions corresponding to TFEB S138 and S142.** A sequence logo illustrating the conservation of residues surrounding experimentally validated leucine-rich NESs that have been curated from the literature and are documented in NESbase version 1.0 (la Cour et al., 2003). Positions relative to the first residue in the NES are shown, as is an alignment with the TFEB sequence to illustrate how residues in the putative TFEB NES align with residues in the sequence logo. TFEB residues corresponding to hydrophobic NES consensus motif residues are highlighted in blue, while serine residues found to phosphorylated are shown in red. Kinases known to regulate S142 and S138 phosphorylation are indicated. Adapted from la Cour et al. (2003).

export (Alt et al., 2000). As is the case with SPHK2, this phosphosite is immediately adjacent to an NES in cyclin D1 (286-TPTDVRDVDI-295).

We note that a recent report found both S134 and S138 to be phosphorylated by GSK3 in an *in vitro* kinase assay using TFEB residues 105-300 (Li et al., 2016). Using this assay, they found that phosphorylation of TFEB(105-300) by GSK3 was decreased by the S134A and S138A mutations, with a double S134A/S138A mutant showing a further decrease in phosphorylation. Interestingly, they found that introduction of the S142A mutation did not decrease phosphorylation of TFEB(105-300) by GSK3, which is in contrast to our data indicating that S142 must be phosphorylated for TFEB(129-147) to be phosphorylated by GSK3. The authors also found that full-length TFEB-GFP harbouring the S134A and S138A mutations in isolation was slightly more nuclear than the WT protein, but the S134A/S138A double mutant showed a significant degree of nuclear translocation (Li et al., 2016). In our hands, altering the status of S138 to

prevent phosphorylation (S138A) or mimic phosphorylation (S138D and S138E) did not alter TFEB localisation (see Figure 4.20), however we did not test S134A or the S134A/S138A double mutant, as we did not find S134 to be phosphorylated by GSK3 *in vitro*.

The authors of this study also note that the S134A and S138A mutations resulted in decreased association of TFEB with lysosomes and decreased phosphorylation of S211, indicating that this might be the mechanism by which mutation of these sites mediates TFEB nuclear translocation (Li et al., 2016). We observed no alterations in the localisation of TFEB-GFP harbouring the S138A, S138D or S138E mutations, however Li et al. (2016) use HeLa cells rather than MCF-7 cells and transient expression rather than stable overexpression. Other studies have noted marked differences in TFEB localisation in different cell lines (Marchand et al., 2015), and our data indicate that TFEB localisation depends upon expression level, providing possible explanations for the discrepancies between our results and those of Li et al. (2016).

We note that our data demonstrating GSK3 phosphorylation of S138 come from a cell-free SPOT assay. This assay involves the use of short peptides immobilised on a 2-dimensional membrane, and we cannot rule out that the influence of neighbouring regions of the protein may facilitate or prohibit GSK3 recognition and phosphorylation of TFEB in various contexts. It is also possible that the presence of other co-factors or interacting partners could promote or inhibit GSK3 phosphorylation of TFEB, and the absence of these factors from our assay could have resulted in either false positives or false negatives. Attempts to confirm phosphorylation of S138 by GSK3 in cell culture are underway, with initial studies focusing on the use of the S138A mutant in conjunction with inhibitors of GSK3 activity and other point mutations. We have also introduced the S138A mutation into the TFEB(129-152)-nlsCARGO system – this

should facilitate evaluation of the effects of this mutation on TFEB localisation in the absence of the influence of other post-translational modifications, namely phosphorylation of S211.

We propose the following model for TFEB nuclear-cytoplasmic shuttling. TFEB localisation is governed by the phosphorylation status of two residues, S142 and S211, with their phosphorylation status depending on the balance of phosphorylation by mTOR, ERK and perhaps other kinases (Settembre et al., 2011; Roczniak-Ferguson et al., 2012) and dephosphorylation by calcineurin and perhaps other phosphatases (Medina et al., 2015). For both S142 and S211, phosphorylation promotes cytoplasmic localisation, with both residues normally being phosphorylated in cell culture.

When these residues are unphosphorylated, an NLS present in the TFEB basic region results in its nuclear translocation. The notion that dephosphorylation of these two residues is sufficient to drive TFEB to the nucleus is supported by two lines of evidence. First, mTOR inhibition impairs phosphorylation of both S142 and S211, resulting in a dramatic shift of TFEB from the cytoplasm to the nucleus (Settembre et al., 2012; Roczniak-Ferguson et al., 2012). Second, our data suggest that the combination of the S142A and S211A mutations renders TFEB markedly nuclear, indicating that interfering with the phosphorylation of these two sites is sufficient to counter the mechanisms maintaining TFEB in the cytoplasm.

We propose that in control conditions in cell culture, a small pool of TFEB becomes transiently dephosphorylated on S142 and/or S211 and is free to translocate to the nucleus. Provided S142 was phosphorylated by mTOR and/or ERK and remained so, TFEB is exported from the nucleus by XPO1. If S142 is dephosphorylated when it enters the nucleus or becomes dephosphorylated in the nucleus, this impairs its nuclear

export. However, phosphorylation of this residue by nuclear kinases (e.g. ERK; Zehorai et al., 2010) could subsequently facilitate its export, returning it to the cytoplasm to begin the cycle again. In conditions of kinase inhibition or stress, the balance will shift toward S142 and/or S211 becoming dephosphorylated, and TFEB nuclear translocation will be increased. This results from impaired 14-3-3-mediated sequestration in the case of S211 and impaired nuclear export in the case of S142. TFEB will remain predominantly nuclear until one or both of these two residues become(s) phosphorylated. We hypothesise that the balance of TFEB nuclear and cytoplasmic localisation in many cell lines in culture may be biased toward the cytoplasm due to rich growth conditions and mutations that activate pathways promoting TFEB cytoplasmic retention. Regulation of shuttling *in vivo* may be more finely tuned and responsive to small alterations in signalling and phosphorylation status.

The mechanisms regulating TFEB localisation are of interest, and TFEB nuclear translocation may be only half of the picture – presumably nuclear levels are the result of the balance between nuclear import and nuclear export. A more complete understanding of the driving forces governing this balance could enhance the utility of TFEB in the therapeutic setting. Indeed, TFEB overexpression is now being investigated for its potential to ameliorate symptoms in diverse conditions, ranging from paediatric glycogen storage diseases to adult-onset neurodegenerative diseases (Decressac et al., 2013; Spampanato et al., 2013). Its therapeutic value likely hinges on its nuclear presence – most studies indicate that the therapeutic benefit of TFEB lies in its ability to stimulate autophagy and induce lysosomal exocytosis (Medina et al., 2011; Spampanato et al., 2013). As such, perhaps it is enough to simply overexpress TFEB at levels that will saturate cytoplasmic retention mechanisms, resulting in nuclear localisation and the transcription of its target genes. However, high levels of nuclear

TFEB can be found naturally, and appear to be oncogenic (Kuiper et al., 2003). TFEB translocation renal cell carcinoma (RCC) involves a chromosomal translocation placing the entirety of the TFEB coding sequence under control of the highly active and constitutive *ALPHA* gene promoter. This results in an approximately 50-fold elevation of TFEB expression compared to normal renal tissue (Kuiper et al., 2003). Tissue sections of these tumours show TFEB staining to be strong and nuclear, while staining of normal adjacent tissue shows no staining for TFEB (Zhong et al., 2012). If an augmentation of TFEB levels is sufficient to result in the development of paediatric renal tumours, as is thought to be the case in t(6;11) translocation RCC, then care must be taken if overexpression of this factor is to be used therapeutically.

# Chapter 5: Discussion

### 6.1 MITF acetylation and the K206Q mutation

We demonstrated that MITF can be acetylated in two different melanoma cell lines when it is stably expressed at near endogenous levels and confirmed earlier work showing that p300-mediated acetylation takes place on residues K206 and K225. We focused on residue K206 due to its position in an MITF/DNA co-crystal structure, the recent description of a K206Q mutation in a patient with Waardenburg syndrome type 2A and the fact that our collaborators have also observed acetylation of this residue in SM-MEL-28 melanoma cells (José Rodríguez-López, personal communication). DNA binding assays using the DNA binding domain of MITF showed that an acetylation-mimicking K206Q mutation (but neither the K206R mutation nor the neighbouring K205R and K205Q mutations) greatly decreased MITF binding to a target harbouring a 5'-CATGTG-3' motif. As experimentally validated MITF targets primarily harbour one of two motifs differing only at one position in the centre of the motif (5'-CATGTG-3' or 5'-CACGTG-3'; Cheli et al., 2010), we mutated this base to change the target to the other major "class" of MITF binding motif. This facilitated K206Q binding. This alteration of motif preference was confirmed by testing the K206Q mutant protein with another target in which the endogenous sequence was 5'-CACGTG-3'. In this case, the K206Q mutant bound the WT target – however, mutation of the motif to a 5'-CATGTG-3' interfered with K206Q binding. These studies indicated that the K206Q mutation (and possibly K206 acetylation) may bias MITF DNA binding toward the 5'-CACGTG-3' motif and away from the 5'-CATGTG-3' motif.

We were unable to extend these findings to a cellular context. ChIP studies of full-length MITF-3xFLAG expressed in melanoma cell lines using the same targets examined in DNA binding assays revealed no significant difference in target binding between the WT and the K206Q mutant. Luciferase assays and assessment of

endogenous expression of a validated MITF target harbouring 5'-CATGTG-3' motifs also failed to show an impairment of the K206Q mutant relative to the WT protein. In fact, the K206Q mutant had the opposite effect, prompting an elevated level of the protein product of this gene. Although these results are contrary to those obtained with DNA binding assays, we note that the DNA binding assays were done with a carefully controlled homogenous sample of bacterially expressed protein comprising only the DNA binding domain of MITF. In the cellular context, full-length MITF-3xFLAG was used, and assessment of MITF binding in melanoma cell lines to motifs present in MITF target genes and/or the transcriptional activation of these genes is complicated by the fact that the composition of MITF dimers, the post-translational status of ectopic MITF and the post-translational status of possible endogenous binding partners are all unknown.

However, when full-length MITF harbouring the K206Q mutant (K201Q in zebrafish) was expressed in *mitfa* -/- zebrafish, melanocyte development was impaired, and this defect appeared to persist until adulthood. Thus, the two systems in which MITF(K206Q) was examined in the absence of WT MITF indicated that this mutant exhibits functional impairments – decreased binding to 5'-CATGTG-3' motifs in EMSAs and impaired melanocyte rescue *in vivo*. On the other hand, when examined in the context of a melanoma line cell harbouring endogenous MITF, the K206Q mutant shows no impairment. This might indicate that it is K206Q/K206Q MITF homodimers that exhibit functional alterations and that the K206Q mutant, unlike many other mutations observed within the MITF DNA binding domain, does not function as a dominant negative. This is consistent with the fact that skin pigmentation in humans harbouring one copy of MITF(K206Q) appears normal (Léger et al., 2012).

### 6.2 TFEB localisation and nuclear export

We identified a previously undescribed nuclear export signal (NES) in the N-terminus of TFEB. We also showed that this NES can no longer mediate nuclear export of TFEB when phosphorylation of the neighbouring mTOR and ERK phosphorylation site S142 is eliminated. Additionally, we identified a GSK3 phosphorylation site (S138), which was recently described in another study (Li et al., 2016). Interestingly, our data indicate that GSK3 phosphorylation of S138 appears to depend on the presence of a priming phosphorylation at S142. Assessment of the influence of the NES and S142 and S138 phosphorylation on full-length TFEB localisation was complicated by the existence of another mechanism regulating TFEB localisation. This mechanism is well-studied and involves the 14-3-3-mediated cytoplasmic sequestration of TFEB resulting from mTOR-dependent phosphorylation of another residue, S211. We provided genetic and pharmacologic evidence that TFEB nuclear export and the previously described S211-dependent 14-3-3 cytoplasmic sequestration mechanism function alongside each other to additively promote TFEB cytoplasmic localisation.

Using full-length TFEB-GFP harbouring mutations meant to prohibit or mimic phosphorylation of S138, we were unable to demonstrate a functional impact of S138 phosphorylation. However, we observed that both the NES mutants (L147A, I149A) and the S142A mutant showed attenuated ability to promote TFEB nuclear translocation in the context of the full-length protein, presumably due to the predominant influence of the S211-dependent sequestration mechanism. Indeed, other reports have also found this mechanism to be the dominant force driving TFEB shuttling (Settembre et al., 2012). Accordingly, we believe that the influence of GSK3 phosphorylation of S138 on TFEB localisation will be easier to assess in the context of a fragment of TFEB that omits S211 or incorporates a S211A mutation.

TFEB nuclear localisation and elevated TFEB expression have both been noted in TFEB translocation RCC tumour samples (Kuiper et al., 2004). Our studies are consistent with the finding that high levels of TFEB promote nuclear localisation and show that only by keeping expression of TFEB below a threshold did we observe TFEB adopting a predominantly cytoplasmic localisation pattern. Interestingly, we saw TFEB accumulating in the nucleus when expression was elevated to approximately 75-fold, an increase not dissimilar to that noted for the degree to which TFEB expression was elevated above endogenous expression in TFEB translocation RCC (30- to 50-fold; Kuiper et al., 2003).

Lastly, we would mention the relatively recent interest in using overexpressed TFEB therapeutically. Current interest focuses mainly on neurodegenerative conditions and paediatric glycogen storage diseases and aims to clear pathologic aggregated material. TFEB overexpression h is presumably clearing pathologic aggregates via its ability to promote autophagy and endolysosomal biogenesis at the transcriptional level (Perera et al., 2015; Settembre et al., 2011). In our systems, the effect of nuclear export on TFEB localisation appeared to be of secondary importance compared to mTOR-mediated 14-3-3 sequestration of TFEB. However, further elucidation of the mechanisms governing TFEB nuclear export and how these relate to other factors influencing its nuclear translocation could facilitate the development of ways to minimise TFEB overexpression during therapeutic applications. This could be of importance, as naturally occurring TFE*B* overexpression resulting from promoter substitution leads to its nuclear localisation and promotes the rapid formation of renal tumours in paediatric and young adult populations, possibly limiting the use of TFEB overexpression in the context of paediatric lysosomal storage disease therapy.

## 6.3 Conclusion

We have investigated the functional consequences of two different post-translational modifications of the TFE family members MITF and TFEB. Our studies provide evidence that a naturally occurring acetylation-mimicking mutation modifies MITF motif preference and alters its function *in vitro* and *in vivo*. Additionally, a novel nuclear export signal and neighboring GSK3 phosphorylation site are identified in the MITF family member TFEB. The data indicate that they are functionally linked to an adjacent mTOR/ERK phosphorylation site already known to modulate TFEB localisation via a currently unknown mechanism.

# References


Ahler, E., Sullivan, W. J., Cass, A., Braas, D., York, A. G., Bensinger, S. J., … Christofk, H. R. (2013). Doxycycline alters metabolism and proliferation of human cell lines. *PloS One*, *8*, e64561.

Aksan, I., & Goding, C. R. (1998). Targeting the microphthalmia basic helix-loop-helix-leucine zipper transcription factor to a subset of E-box elements in vitro and in vivo. *Molecular and Cellular Biology*, *18*, 6930–8.

Alt, J. R., Cleveland, J. L., Hannink, M., & Diehl, J. A. (2000). Phosphorylation-dependent regulation of cyclin D1 nuclear export and cyclin D1-dependent cellular transformation. *Genes & Development*, *14*, 3102–14.

Alt, J. R., Gladden, A. B., & Diehl, J. A. (2002). p21(Cip1) Promotes cyclin D1 nuclear accumulation via direct inhibition of nuclear export. *The Journal of Biological Chemistry*, *277*, 8517–23.

Argani, P. (2015). MiT family translocation renal cell carcinoma. *Seminars in Diagnostic Pathology*, *32*, 103–13.

Argani, P., Laé, M., Hutchinson, B., Reuter, V. E., Collins, M. H., Perentesis, J., … Ladanyi, M. (2005). Renal carcinomas with the t(6;11)(p21;q12): clinicopathologic features and demonstration of the specific alpha-TFEB gene fusion by immunohistochemistry, RT-PCR, and DNA PCR. *The American Journal of Surgical Pathology*, *29*, 230–40.

Bao, J., Zheng, L., Zhang, Q., Li, X., Zhang, X., Li, Z., … Ji, J. (2016). Deacetylation of TFEB promotes fibrillar Aβ degradation by upregulating lysosomal biogenesis in microglia. *Protein & Cell*, *7*, 417–33.

Baral, V., Chaoui, A., Watanabe, Y., Goossens, M., Attie-Bitach, T., Marlin, S., … Bondurand, N. (2012). Screening of MITF and SOX10 regulatory regions in Waardenburg syndrome type 2. *PloS One*, *7*, e41927.

Bauer, G. L., Praetorius, C., Bergsteinsdóttir, K., Hallsson, J. H., Gísladóttir, B. K., Schepsky, A., … Steingrímsson, E. (2009). The role of MITF phosphorylation sites during coat color and eye development in mice analyzed by bacterial artificial chromosome transgene rescue. *Genetics*, *183*, 581–94.

Baxter, L. L., & Pavan, W. J. (2003). Pmel17 expression is Mitf-dependent and reveals cranial melanoblast migration during murine development. *Gene Expression Patterns : GEP*, *3*, 703–7.

Beckmann, H., Su, L. K., & Kadesch, T. (1990). TFE3: A helix-loop-helix protein that activates transcription through the immunoglobulin enhancer muE3 motif. *Genes and Development*, *4*, 167–179.

Bentley, N. J., Eisen, T., & Goding, C. R. (1994). Melanocyte-specific expression of the human tyrosinase promoter: activation by the microphthalmia gene product and role of the initiator. *Molecular and Cellular Biology*, *14*, 7996–8006.

Bertolotto, C., Lesueur, F., Giuliano, S., Strub, T., de Lichy, M., Bille, K., … Bressac-de Paillerets, B. (2011). A SUMOylation-defective MITF germline mutation

predisposes to melanoma and renal carcinoma. *Nature*, *480*, 94–8.

Bertolotto, C., Abbe, P., Hemesath, T. J., Bille, K., Fisher, D. E., Ortonne, J. P., & Ballotti, R. (1998a). Microphthalmia gene product as a signal transducer in cAMP-induced differentiation of melanocytes. *The Journal of Cell Biology*, *142*, 827–35.

Bertolotto, C., Buscà, R., Abbe, P., Bille, K., Aberdam, E., Ortonne, J. P., & Ballotti, R. (1998b). Different cis-acting elements are involved in the regulation of TRP1 and TRP2 promoter activities by cyclic AMP: pivotal role of M boxes (GTCATGTGCT) and of microphthalmia. *Molecular and Cellular Biology*, *18*, 694–702.

Bertolotto, C., Bille, K., Ortonne, J. P., & Ballotti, R. (1996). Regulation of tyrosinase gene expression by cAMP in B16 melanoma cells involves two CATGTG motifs surrounding the TATA box: implication of the microphthalmia gene product. *The Journal of Cell Biology*, *134*, 747–55.

Betschinger, J., Nichols, J., Dietmann, S., Corrin, P. D., Paddison, P. J., & Smith, A. (2013). Exit from pluripotency is gated by intracellular redistribution of the bHLH transcription factor Tfe3. *Cell*, *153*, 335–47.

Bismuth, K., Skuntz, S., Hallsson, J. H., Pak, E., Dutra, A. S., Steingrímsson, E., & Arnheiter, H. (2008). An unstable targeted allele of the mouse Mitf gene with a high somatic and germline reversion rate. *Genetics*, *178*, 259–72.

Bondurand, N., Pingault, V., Goerich, D. E., Lemort, N., Sock, E., Le Caignec, C., … Goossens, M. (2000). Interaction among SOX10, PAX3 and MITF, three genes altered in Waardenburg syndrome. *Human Molecular Genetics*, *9*, 1907–17.

Boyes, J., Byfield, P., Nakatani, Y., & Ogryzko, V. (1998). Regulation of activity of the transcription factor GATA-1 by acetylation. *Nature*, *396*, 594–8.

Boyle, G. M., Woods, S. L., Bonazzi, V. F., Stark, M. S., Hacker, E., Aoude, L. G., … Hayward, N. K. (2011). Melanoma cell invasiveness is regulated by miR-211 suppression of the BRN2 transcription factor. *Pigment Cell & Melanoma Research*, *24*, 525–37.

Bronisz, A., Sharma, S. M., Hu, R., Godlewski, J., Tzivion, G., Mansky, K. C., & Ostrowski, M. C. (2006). Microphthalmia-associated transcription factor interactions with 14-3-3 modulate differentiation of committed myeloid precursors. *Molecular Biology of the Cell*, *17*, 3897–906.

Cai, X., & Liu, X. (2008). Inhibition of Thr-55 phosphorylation restores p53 nuclear localization and sensitizes cancer cells to DNA damage. *Proceedings of the National Academy of Sciences of the United States of America*, *105*, 16958–63.

Cancer Genome Atlas Network. (2015). Genomic Classification of Cutaneous Melanoma. *Cell*, *161*, 1681–96.

Carr, C. S., & Sharp, P. A. (1990). A helix-loop-helix protein related to the immunoglobulin E box-binding proteins. *Molecular and Cellular Biology*, *10*, 4384–8.

Carreira, S., Goodall, J., Denat, L., Rodriguez, M., Nuciforo, P., Hoek, K. S., … Goding, C. R. (2006). Mitf regulation of Dia1 controls melanoma proliferation and invasiveness. *Genes and Development*, *20*, 3426–3439.

Carreira, S., Goodall, J., Aksan, I., La Rocca, S. A., Galibert, M.-D., Denat, L., … Goding, C. R. (2005). Mitf cooperates with Rb1 and activates p21$^{Cip1}$ expression to regulate cell cycle progression. *Nature*, *433*, 764–769.

Carreira, S., Liu, B., & Goding, C. R. (2000). The gene encoding the T-box factor Tbx2 is a target for the microphthalmia-associated transcription factor in melanocytes. *The Journal of Biological Chemistry*, *275*, 21920–7.

Chalker, J. M., Lercher, L., Rose, N. R., Schofield, C. J., & Davis, B. G. (2012). Conversion of cysteine into dehydroalanine enables access to synthetic histones bearing diverse post-translational modifications. *Angewandte Chemie (International Ed. in English)*, *51*, 1835–9.

Cheli, Y., Giuliano, S., Fenouille, N., Allegra, M., Hofman, V., Hofman, P., … Ballotti, R. (2012). Hypoxia and MITF control metastatic behaviour in mouse and human melanoma cells. *Oncogene*, *31*, 2461–70.

Cheli, Y., Giuliano, S., Guiliano, S., Botton, T., Rocchi, S., Hofman, V., … Ballotti, R. (2011). Mitf is the key molecular switch between mouse or human melanoma initiating cells and their differentiated progeny. *Oncogene*, *30*, 2307–18.

Cheli, Y., Ohanna, M., Ballotti, R., & Bertolotto, C. (2010). Fifteen-year quest for microphthalmia-associated transcription factor target genes. *Pigment Cell & Melanoma Research*, *23*, 27–40.

Chudakov, D. M., Lukyanov, S., & Lukyanov, K. A. (2007). Using photoactivatable fluorescent protein Dendra2 to track protein movement. *BioTechniques*, *42*, 553, 555, 557 passim.

Cohen, P., & Frame, S. (2001). The renaissance of GSK3. *Nature Reviews. Molecular Cell Biology*, *2*, 769–76.

Connor, M. K., Kotchetkov, R., Cariou, S., Resch, A., Lupetti, R., Beniston, R. G., … Slingerland, J. M. (2003). CRM1/Ran-mediated nuclear export of p27(Kip1) involves a nuclear export signal and links p27 export and proteolysis. *Molecular Biology of the Cell*, *14*, 201–13.

Cronin, J. C., Wunderlich, J., Loftus, S. K., Prickett, T. D., Wei, X., Ridd, K., … Samuels, Y. (2009). Frequent mutations in the MITF pathway in melanoma. *Pigment Cell & Melanoma Research*, *22*, 435–44.

Decressac, M., Mattsson, B., Weikop, P., Lundblad, M., Jakobsson, J., & Björklund, A. (2013). TFEB-mediated autophagy rescues midbrain dopamine neurons from α-synuclein toxicity. *Proceedings of the National Academy of Sciences of the United States of America*, *110*, E1817-26.

Ding, G., Sonoda, H., Yu, H., Kajimoto, T., Goparaju, S. K., Jahangeer, S., … Nakamura, S. (2007). Protein kinase D-mediated phosphorylation and nuclear export of sphingosine kinase 2. *The Journal of Biological Chemistry*, *282*, 27493–502.

Dornan, D., Shimizu, H., Perkins, N. D., & Hupp, T. R. (2003). DNA-dependent acetylation of p53 by the transcription coactivator p300. *The Journal of Biological Chemistry*, *278*, 13431–41.

Du, J., Zhou, Y., Su, X., Yu, J. J., Khan, S., Jiang, H., … Lin, H. (2011). Sirt5 is a NAD-

dependent protein lysine demalonylase and desuccinylase. *Science (New York, N.Y.)*, *334*, 806–9.

Du, J., Widlund, H. R., Horstmann, M. A., Ramaswamy, S., Ross, K., Huber, W. E., … Fisher, D. E. (2004). Critical role of CDK2 for melanoma growth linked to its melanocyte-specific transcriptional regulation by MITF. *Cancer Cell*, *6*, 565–76.

Du, J., Miller, A. J., Widlund, H. R., Horstmann, M. A., Ramaswamy, S., & Fisher, D. E. (2003). MLANA/MART1 and SILV/PMEL17/GP100 are transcriptionally regulated by MITF in melanocytes and melanoma. *The American Journal of Pathology*, *163*, 333–43.

Dufner, A., & Thomas, G. (1999). Ribosomal S6 kinase signaling and the control of translation. *Experimental Cell Research*, *253*, 100–9.

Duquet, A., Polesskaya, A., Cuvellier, S., Ait-Si-Ali, S., Héry, P., Pritchard, L. L., … Harel-Bellan, A. (2006). Acetylation is important for MyoD function in adult mice. *EMBO Reports*, *7*, 1140–6.

Ferré-D'Amaré, A. R., Pognonec, P., Roeder, R. G., & Burley, S. K. (1994). Structure and function of the b/HLH/Z domain of USF. *The EMBO Journal*, *13*, 180–9.

Ferrer, M., Rodríguez, J. A., Spierings, E. A., de Winter, J. P., Giaccone, G., & Kruyt, F. A. E. (2005). Identification of multiple nuclear export sequences in Fanconi anemia group A protein that contribute to CRM1-dependent nuclear export. *Human Molecular Genetics*, *14*, 1271–81.

Ferron, M., Settembre, C., Shimazu, J., Lacombe, J., Kato, S., Rawlings, D. J., … Karsenty, G. (2013). A RANKL-PKC??-TFEB signaling cascade is necessary for lysosomal biogenesis in osteoclasts. *Genes and Development*, *27*, 955–969.

Fisher, D. E., Carr, C. S., Parent, L. a., & Sharp, P. a. (1991). TFEB has DNA-binding and oligomerization properties of a unique hefix-loop-helix/leucine-zipper family. *Genes and Development*, *5*, 2342–2352.

Flaherty, K. T., Infante, J. R., Daud, A., Gonzalez, R., Kefford, R. F., Sosman, J., … Weber, J. (2012). Combined BRAF and MEK inhibition in melanoma with BRAF V600 mutations. *The New England Journal of Medicine*, *367*, 1694–703.

Fong, S., Debs, R. J., & Desprez, P.-Y. (2004). Id genes and proteins as promising targets in cancer therapy. *Trends in Molecular Medicine*, *10*, 387–92.

Fornerod, M., van Baal, S., Valentine, V., Shapiro, D. N., & Grosveld, G. (1997). Chromosomal localization of genes encoding CAN/Nup214-interacting proteins--human CRM1 localizes to 2p16, whereas Nup88 localizes to 17p13 and is physically linked to SF2p32. *Genomics*, *42*, 538–40.

Frescas, D., Valenti, L., & Accili, D. (2005). Nuclear trapping of the forkhead transcription factor FoxO1 via Sirt-dependent deacetylation promotes expression of glucogenetic genes. *The Journal of Biological Chemistry*, *280*, 20589–95.

Fu, S.-C., Huang, H.-C., Horton, P., & Juan, H.-F. (2013). ValidNESs: a database of validated leucine-rich nuclear export signals. *Nucleic Acids Research*, *41*, D338-43.

Fujimoto, H., Higuchi, M., Koike, M., Ode, H., Pinak, M., Bunta, J. K., … Tsuchida, K.

(2012). A possible overestimation of the effect of acetylation on lysine residues in KQ mutant analysis. *Journal of Computational Chemistry*, *33*, 239–46.

Fung, H. Y. J., Fu, S.-C., Brautigam, C. A., & Chook, Y. M. (2015). Structural determinants of nuclear export signal orientation in binding to exportin CRM1. *eLife*, *4*. doi:10.7554/eLife.10034

Fuse, N., Yasumoto, K. ichi, Suzuki, H., Takahashi, K., & Shibahara, S. (1996). Identification of a Melanocyte-Type Promoter of the Microphthalmia-Associated Transcription Factor Gene. *Biochemical and Biophysical Research Communications*, *219*, 702–707.

Garraway, L. A., Widlund, H. R., Rubin, M. A., Getz, G., Berger, A. J., Ramaswamy, S., … Sellers, W. R. (2005). Integrative genomic analyses identify MITF as a lineage survival oncogene amplified in malignant melanoma. *Nature*, *436*, 117–122.

Giandomenico, V., Simonsson, M., Grönroos, E., & Ericsson, J. (2003). Coactivator-dependent acetylation stabilizes members of the SREBP family of transcription factors. *Molecular and Cellular Biology*, *23*, 2587–99.

Giatromanolaki, A., Kalamida, D., Sivridis, E., Karagounis, I. V, Gatter, K. C., Harris, A. L., & Koukourakis, M. I. (2015). Increased expression of transcription factor EB (TFEB) is associated with autophagy, migratory phenotype and poor prognosis in non-small cell lung cancer. *Lung Cancer (Amsterdam, Netherlands)*, *90*, 98–105.

Giuliano, S., Cheli, Y., Ohanna, M., Bonet, C., Beuret, L., Bille, K., … Bertolotto, C. (2010). Microphthalmia-associated transcription factor controls the DNA damage response and a lineage-specific senescence program in melanomas. *Cancer Research*, *70*, 3813–22.

Gnad, F., Ren, S., Choudhary, C., Cox, J., & Mann, M. (2010). Predicting post-translational lysine acetylation using support vector machines. *Bioinformatics (Oxford, England)*, *26*, 1666–8.

Goodall, J., Carreira, S., Denat, L., Kobi, D., Davidson, I., Nuciforo, P., … Goding, C. R. (2008). Brn-2 represses microphthalmia-associated transcription factor expression and marks a distinct subpopulation of microphthalmia-associated transcription factor-negative melanoma cells. *Cancer Research*, *68*, 7788–94.

Grill, C., Bergsteinsdó ttir, K., Ögmundsdó Ttir, M. H., Pogenberg, V., Schepsky, A., Wilmanns, M., … Steingrímsson, E. (2013). MITF mutations associated with pigment deficiency syndromes and melanoma have different effects on protein function. *Human Molecular Genetics*, *22*, 4357–4367.

Gu, W., & Roeder, R. G. (1997). Activation of p53 Sequence-Specific DNA Binding by Acetylation of the p53 C-Terminal Domain. *Cell*, *90*, 595–606.

Güttler, T., Madl, T., Neumann, P., Deichsel, D., Corsini, L., Monecke, T., … Görlich, D. (2010). NES consensus redefined by structures of PKI-type and Rev-type nuclear export signals bound to CRM1. *Nature Structural & Molecular Biology*, *17*, 1367–76.

Ha, C. H., Kim, J. Y., Zhao, J., Wang, W., Jhun, B. S., Wong, C., & Jin, Z. G. (2010). PKA phosphorylates histone deacetylase 5 and prevents its nuclear export, leading

to the inhibition of gene transcription and cardiomyocyte hypertrophy. *Proceedings of the National Academy of Sciences of the United States of America*, *107*, 15467–72.

Hagen, T., Di Daniel, E., Culbert, A. A., & Reith, A. D. (2002). Expression and characterization of GSK-3 mutants and their effect on beta-catenin phosphorylation in intact cells. *The Journal of Biological Chemistry*, *277*, 23330–5.

Haq, R., Shoag, J., Andreu-Perez, P., Yokoyama, S., Edelman, H., Rowe, G. C., … Widlund, H. R. (2013). Oncogenic BRAF regulates oxidative metabolism via PGC1α and MITF. *Cancer Cell*, *23*, 302–15.

Heinz, N., Hennig, K., & Loew, R. (2013). Graded or threshold response of the tet-controlled gene expression: all depends on the concentration of the transactivator. *BMC Biotechnology*, *13*, 5.

Hemesath, T. J., Price, E. R., Takemoto, C., Badalian, T., & Fisher, D. E. (1998). MAP kinase links the transcription factor Microphthalmia to c-Kit signalling in melanocytes. *Nature*, *391*, 298–301.

Hemesath, T. J., Steingrímsson, E., McGill, G., Hansen, M. J., Vaught, J., Hodgkinson, C. A., … Fisher, D. E. (1994). microphthalmia, a critical factor in melanocyte development, defines a discrete transcription factor family. *Genes & Development*, *8*, 2770–80.

Hertwig, P., 1942. Neue Mutationen und Koppelungsgruppen bei der Hausmaus. *Zeitschrift für Induktive Abstammungs- und Vererbungslehre* 80(1): 220-246.

Hodgkinson, C. A., Nakayama, A., Li, H., Swenson, L. B., Opdecamp, K., Asher, J. H., … Glaser, T. (1998). Mutation at the anophthalmic white locus in Syrian hamsters: haploinsufficiency in the Mitf gene mimics human Waardenburg syndrome type 2. *Human Molecular Genetics*, *7*, 703–8.

Hodgkinson, C. A., Moore, K. J., Nakayama, A., Steingrímsson, E., Copeland, N. G., Jenkins, N. A., & Arnheiter, H. (1993). Mutations at the mouse microphthalmia locus are associated with defects in a gene encoding a novel basic-helix-loop-helix-zipper protein. *Cell*, *74*, 395–404.

Hoek, K. S., & Goding, C. R. (2010). Cancer stem cells versus phenotype-switching in melanoma. *Pigment Cell & Melanoma Research*, *23*, 746–759.

Hoek, K. S., Eichhoff, O. M., Schlegel, N. C., Döbbeling, U., Kobert, N., Schaerer, L., … Dummer, R. (2008). In vivo switching of human melanoma cells between proliferative and invasive states. *Cancer Research*, *68*, 650–6.

Holaska, J. M., & Paschal, B. M. (1998). A cytosolic activity distinct from crm1 mediates nuclear export of protein kinase inhibitor in permeabilized cells. *Proceedings of the National Academy of Sciences of the United States of America*, *95*, 14739–44.

Hosoda, H., Miyao, T., Uchida, S., Sakai, S., & Kida, S. (2011). Development of a tightly-regulated tetracycline-dependent transcriptional activator and repressor co-expression system for the strong induction of transgene expression. *Cytotechnology*, *63*, 211–6.

Huber, W. E., Price, E. R., Widlund, H. R., Du, J., Davis, I. J., Wegner, M., & Fisher, D. E. (2003). A tissue-restricted cAMP transcriptional response: SOX10 modulates alpha-melanocyte-stimulating hormone-triggered expression of microphthalmia-associated transcription factor in melanocytes. *The Journal of Biological Chemistry*, *278*, 45224–30.

Hughes, A. E., Newton, V. E., Liu, X. Z., & Read, A. P. (1994). A gene for Waardenburg syndrome type 2 maps close to the human homologue of the microphthalmia gene at chromosome 3p12-p14.1. *Nature Genetics*, *7*, 509–12.

Hupp, T. R., Sparks, A., & Lane, D. P. (1995). Small peptides activate the latent sequence-specific DNA binding function of p53. *Cell*, *83*, 237–45.

Jacquemin, P., Lannoy, V. J., O'Sullivan, J., Read, A., Lemaigre, F. P., & Rousseau, G. G. (2001). The transcription factor onecut-2 controls the microphthalmia-associated transcription factor gene. *Biochemical and Biophysical Research Communications*, *285*, 1200–5.

Javelaud, D., Alexaki, V.-I., Pierrat, M.-J., Hoek, K. S., Dennler, S., Van Kempen, L., … Mauviel, A. (2011). GLI2 and M-MITF transcription factors control exclusive gene expression programs and inversely regulate invasion in human melanoma cells. *Pigment Cell & Melanoma Research*, *24*, 932–43.

Johnson, S. L., Nguyen, A. N., & Lister, J. A. (2011). mitfa is required at multiple stages of melanocyte differentiation but not to establish the melanocyte stem cell. *Developmental Biology*, *350*, 405–13.

Kaffman, A., Rank, N. M., O'Neill, E. M., Huang, L. S., & O'Shea, E. K. (1998). The receptor Msn5 exports the phosphorylated transcription factor Pho4 out of the nucleus. *Nature*, *396*, 482–6.

Kalderon, D., Roberts, B. L., Richardson, W. D., & Smith, A. E. (1984). A short amino acid sequence able to specify nuclear location. *Cell*, *39*, 499–509.

Kamieniarz, K., & Schneider, R. (2009). Tools to tackle protein acetylation. *Chemistry & Biology*, *16*, 1027–9.

Kawakami, K., Shima, A., & Kawakami, N. (2000). Identification of a functional transposase of the Tol2 element, an Ac-like element from the Japanese medaka fish, and its transposition in the zebrafish germ lineage. *Proceedings of the National Academy of Sciences of the United States of America*, *97*, 11403–8.

Kido, K., Sumimoto, H., Asada, S., Okada, S. M., Yaguchi, T., Kawamura, N., … Kawakami, Y. (2009). Simultaneous suppression of MITF and BRAF V600E enhanced inhibition of melanoma cell proliferation. *Cancer Science*, *100*, 1863–9.

Klein, K., Werner, K., Teske, C., Schenk, M., Giese, T., Weitz, J., & Welsch, T. (2016). Role of TFEB-driven autophagy regulation in pancreatic cancer treatment. *International Journal of Oncology*, *49*, 164–72.

Kuiper, R. P., Schepens, M., Thijssen, J., Schoenmakers, E. F. P. M., & van Kessel, A. G. (2004). Regulation of the MiTF/TFE bHLH-LZ transcription factors through restricted spatial expression and alternative splicing of functional domains. *Nucleic Acids Research*, *32*, 2315–22.

Kuiper, R. P., Schepens, M., Thijssen, J., van Asseldonk, M., van den Berg, E., Bridge,

J., … van Kessel, A. G. (2003). Upregulation of the transcription factor TFEB in t(6;11)(p21;q13)-positive renal cell carcinomas due to promoter substitution. *Human Molecular Genetics*, *12*, 1661–9.

la Cour, T., Gupta, R., Rapacki, K., Skriver, K., Poulsen, F. M., & Brunak, S. (2003). NESbase version 1.0: a database of nuclear export signals. *Nucleic Acids Research*, *31*, 393–6.

Lamonica, J. M., Vakoc, C. R., & Blobel, G. A. (2006). Acetylation of GATA-1 is required for chromatin occupancy. *Blood*, *108*, 3736–8.

Landschulz, W. H., Johnson, P. F., & McKnight, S. L. (1988). The leucine zipper: a hypothetical structure common to a new class of DNA binding proteins. *Science (New York, N.Y.)*, *240*, 1759–64.

Larribere, L., Hilmi, C., Khaled, M., Gaggioli, C., Bille, K., Auberger, P., … Bertolotto, C. (2005). The cleavage of microphthalmia-associated transcription factor, MITF, by caspases plays an essential role in melanocyte and melanoma cell apoptosis. *Genes & Development*, *19*, 1980–5.

Lauss, M., Haq, R., Cirenajwis, H., Phung, B., Harbst, K., Staaf, J., … Jönsson, G. (2015). Genome-Wide DNA Methylation Analysis in Melanoma Reveals the Importance of CpG Methylation in MITF Regulation. *The Journal of Investigative Dermatology*, *135*, 1820–8.

Lee, M., Goodall, J., Verastegui, C., Ballotti, R., & Goding, C. R. (2000). Direct regulation of the Microphthalmia promoter by Sox10 links Waardenburg-Shah syndrome (WS4)-associated hypopigmentation and deafness to WS2. *The Journal of Biological Chemistry*, *275*, 37978–83.

Léger, S., Balguerie, X., Goldenberg, A., Drouin-Garraud, V., Cabot, A., Amstutz-Montadert, I., … Pingault, V. (2012). Novel and recurrent non-truncating mutations of the MITF basic domain: genotypic and phenotypic variations in Waardenburg and Tietz syndromes. *European Journal of Human Genetics : EJHG*, *20*, 584–7.

Levy, C., Khaled, M., Iliopoulos, D., Janas, M. M., Schubert, S., Pinner, S., … Novina, C. D. (2010). Intronic miR-211 assumes the tumor suppressive function of its host gene in melanoma. *Molecular Cell*, *40*, 841–9.

Levy, C., Khaled, M., & Fisher, D. E. (2006). MITF: master regulator of melanocyte development and melanoma oncogene. *Trends in Molecular Medicine*, *12*, 406–14.

Levy, C., Sonnenblick, A., & Razin, E. (2003). Role played by microphthalmia transcription factor phosphorylation and its Zip domain in its transcriptional inhibition by PIAS3. *Molecular and Cellular Biology*, *23*, 9073–80.

Li, Y., Xu, M., Ding, X., Yan, C., Song, Z., Chen, L., … Yang, C. (2016). Protein kinase C controls lysosome biogenesis independently of mTORC1. *Nature Cell Biology*, *18*, 1065–1077.

Lichty, J. J., Malecki, J. L., Agnew, H. D., Michelson-Horowitz, D. J., & Tan, S. (2005). Comparison of affinity tags for protein purification. *Protein Expression and Purification*, *41*, 98–105.

Lister, J. A., Capper, A., Zeng, Z., Mathers, M. E., Richardson, J., Paranthaman, K., …

Patton, E. E. (2014). A conditional zebrafish MITF mutation reveals MITF levels are critical for melanoma promotion vs. regression in vivo. *The Journal of Investigative Dermatology*, *134*, 133–40.

Lister, J. A., Close, J., & Raible, D. W. (2001). Duplicate mitf Genes in Zebrafish: Complementary Expression and Conservation of Melanogenic Potential. *Developmental Biology*, *237*, 333–344.

Lister, J. A., Robertson, C. P., Lepage, T., Johnson, S. L., & Raible, D. W. (1999). nacre encodes a zebrafish microphthalmia-related protein that regulates neural-crest-derived pigment cell fate. *Development (Cambridge, England)*, *126*, 3757–67.

Loercher, A. E., Tank, E. M. H., Delston, R. B., & Harbour, J. W. (2005). MITF links differentiation with cell cycle arrest in melanocytes by transcriptional activation of INK4A. *The Journal of Cell Biology*, *168*, 35–40.

Lopez-Girona, A., Furnari, B., Mondesert, O., & Russell, P. (1999). Nuclear localization of Cdc25 is regulated by DNA damage and a 14-3-3 protein. *Nature*, *397*, 172–5.

Loughery, J., Cox, M., Smith, L. M., & Meek, D. W. (2014). Critical role for p53-serine 15 phosphorylation in stimulating transactivation at p53-responsive promoters. *Nucleic Acids Research*, *42*, 7666–80.

Lowings, P., Yavuzer, U., & Goding, C. R. (1992). Positive and negative elements regulate a melanocyte-specific promoter. *Molecular and Cellular Biology*, *12*, 3653–62.

Ma, P. C., Rould, M. A., Weintraub, H., & Pabo, C. O. (1994). Crystal structure of MyoD bHLH domain-DNA complex: perspectives on DNA recognition and implications for transcriptional activation. *Cell*, *77*, 451–9.

Magers, M. J., Udager, A. M., & Mehra, R. (2015). MiT Family Translocation-Associated Renal Cell Carcinoma: A Contemporary Update With Emphasis on Morphologic, Immunophenotypic, and Molecular Mimics. *Archives of Pathology & Laboratory Medicine*, *139*, 1224–33.

Mansky, K. C., Sankar, U., Han, J., & Ostrowski, M. C. (2002). Microphthalmia transcription factor is a target of the p38 MAPK pathway in response to receptor activator of NF-kappa B ligand signaling. *The Journal of Biological Chemistry*, *277*, 11077–83.

Marchand, B., Arsenault, D., Raymond-Fleury, A., Boisvert, F.-M., & Boucher, M.-J. (2015). Glycogen Synthase Kinase-3 (GSK3) Inhibition Induces Prosurvival Autophagic Signals in Human Pancreatic Cancer Cells. *Journal of Biological Chemistry*, *290*, 5592–5605.

Marin Zapata, P. A., Beese, C. J., Jünger, A., Dalmasso, G., Brady, N. R., & Hamacher-Brady, A. (2016). Time course decomposition of cell heterogeneity in TFEB signaling states reveals homeostatic mechanisms restricting the magnitude and duration of TFEB responses to mTOR activity modulation. *BMC Cancer*, *16*, 355.

Martina, J. A., Diab, H. I., Brady, O. A., & Puertollano, R. (2016). TFEB and TFE3 are novel components of the integrated stress response. *The EMBO Journal*, *35*, 479–95.

Martina, J. A., Diab, H. I., Lishu, L., Jeong-a, L., Patange, S., Martina, J. A., …

Puertollano, R. (2014). The Nutrient-Responsive Transcription Factor TFE3 Promotes Autophagy , Lysosomal Biogenesis , and Clearance of Cellular Debris. *Science Signaling*, *7*, 1–16.

Martina, J. A., & Puertollano, R. (2013). Rag GTPases mediate amino acid-dependent recruitment of TFEB and MITF to lysosomes. *The Journal of Cell Biology*, *200*, 475–491.

Martina, J. A., Chen, Y., Gucek, M., & Puertollano, R. (2012). MTORC1 functions as a transcriptional regulator of autophagy by preventing nuclear transport of TFEB. *Autophagy*, *8*, 903–14.

Matsuyama, A., Shimazu, T., Sumida, Y., Saito, A., Yoshimatsu, Y., Seigneurin-Berny, D., … Yoshida, M. (2002). In vivo destabilization of dynamic microtubules by HDAC6-mediated deacetylation. *The EMBO Journal*, *21*, 6820–31.

Matsuzaki, H., Daitoku, H., Hatta, M., Aoyama, H., Yoshimochi, K., & Fukamizu, A. (2005). Acetylation of Foxo1 alters its DNA-binding ability and sensitivity to phosphorylation. *Proceedings of the National Academy of Sciences of the United States of America*, *102*, 11278–83.

McGill, G. G., Haq, R., Nishimura, E. K., & Fisher, D. E. (2006). c-Met expression is regulated by Mitf in the melanocyte lineage. *The Journal of Biological Chemistry*, *281*, 10365–73.

McGill, G. G., Horstmann, M., Widlund, H. R., Du, J., Motyckova, G., Nishimura, E. K., … Fisher, D. E. (2002). Bcl2 regulation by the melanocyte master regulator Mitf modulates lineage survival and melanoma cell viability. *Cell*, *109*, 707–18.

Medina, D. L., Di Paola, S., Peluso, I., Armani, A., De Stefani, D., Venditti, R., … Ballabio, A. (2015). Lysosomal calcium signalling regulates autophagy through calcineurin and TFEB. *Nature Cell Biology*, *17*, 288–99.

Medina, D. L., Fraldi, A., Bouche, V., Annunziata, F., Mansueto, G., Spampanato, C., … Ballabio, A. (2011). Transcriptional activation of lysosomal exocytosis promotes cellular clearance. *Developmental Cell*, *21*, 421–430.

Merrell, K., Wells, S., Henderson, a, Gorman, J., Alt, F., Stall, a, & Calame, K. (1997). The absence of the transcription activator TFE3 impairs activation of B cells in vivo. *Molecular and Cellular Biology*, *17*, 3335–44.

Miller, A. J., Levy, C., Davis, I. J., Razin, E., & Fisher, D. E. (2005). Sumoylation of MITF and Its Related Family Members TFE3 and TFEB. *Journal of Biological Chemistry*, *280*, 146–155.

Murakami, H., & Arnheiter, H. (2005). Sumoylation modulates transcriptional activity of MITF in a promoter-specific manner. *Pigment Cell Research / Sponsored by the European Society for Pigment Cell Research and the International Pigment Cell Society*, *18*, 265–77.

Murre, C., McCaw, P. S., & Baltimore, D. (1989). A new DNA binding and dimerization motif in immunoglobulin enhancer binding, daughterless, MyoD, and myc proteins. *Cell*, *56*, 777–83.

Nair, S. K., & Burley, S. K. (2003). X-ray structures of Myc-Max and Mad-Max recognizing DNA. Molecular bases of regulation by proto-oncogenic transcription

factors. *Cell*, *112*, 193–205.

Neumann, H., Hancock, S. M., Buning, R., Routh, A., Chapman, L., Somers, J., … Chin, J. W. (2009). A method for genetically installing site-specific acetylation in recombinant histones defines the effects of H3 K56 acetylation. *Molecular Cell*, *36*, 153–63.

Nigg, E. A. (1997). Nucleocytoplasmic transport: signals, mechanisms and regulation. *Nature*, *386*, 779–87.

Nobukuni, Y., Watanabe, A., Takeda, K., Skarka, H., & Tachibana, M. (1996). Analyses of loss-of-function mutations of the MITF gene suggest that haploinsufficiency is a cause of Waardenburg syndrome type 2A. *American Journal of Human Genetics*, *59*, 76–83.

Okamura, H., Aramburu, J., García-Rodríguez, C., Viola, J. P., Raghavan, A., Tahiliani, M., … Rao, A. (2000). Concerted dephosphorylation of the transcription factor NFAT1 induces a conformational switch that regulates transcriptional activity. *Molecular Cell*, *6*, 539–50.

Opdecamp, K., Vanvooren, P., Rivière, M., Arnheiter, H., Motta, R., Szpirer, J., & Szpirer, C. (1998). The rat microphthalmia-associated transcription factor gene (Mitf) maps at 4q34-q41 and is mutated in the mib rats. *Mammalian Genome : Official Journal of the International Mammalian Genome Society*, *9*, 617–21.

Opdecamp, K., Nakayama, A., Nguyen, M. T., Hodgkinson, C. A., Pavan, W. J., & Arnheiter, H. (1997). Melanocyte development in vivo and in neural crest cell cultures: crucial dependence on the Mitf basic-helix-loop-helix-zipper transcription factor. *Development (Cambridge, England)*, *124*, 2377–86.

Ota, T., Suzuki, Y., Nishikawa, T., Otsuki, T., Sugiyama, T., Irie, R., … Sugano, S. (2004). Complete sequencing and characterization of 21,243 full-length human cDNAs. *Nature Genetics*, *36*, 40–5.

Pagliuca, A., Bartoli, P. C., Saccone, S., Della Valle, G., & Lania, L. (1995). Molecular cloning of ID4, a novel dominant negative helix-loop-helix human gene on chromosome 6p21.3-p22. *Genomics*, *27*, 200–3.

Palmieri, M., Impey, S., Kang, H., di Ronza, A., Pelz, C., Sardiello, M., & Ballabio, A. (2011). Characterization of the CLEAR network reveals an integrated control of cellular clearance pathways. *Human Molecular Genetics*, *20*, 3852–66.

Parr, C., Carzaniga, R., Gentleman, S. M., Van Leuven, F., Walter, J., & Sastre, M. (2012). Glycogen synthase kinase 3 inhibition promotes lysosomal biogenesis and autophagic degradation of the amyloid-β precursor protein. *Molecular and Cellular Biology*, *32*, 4410–8.

Pastore, N., Brady, O. A., Diab, H. I., Martina, J. A., Sun, L., Huynh, T., … Puertollano, R. (2016). TFEB and TFE3 cooperate in the regulation of the innate immune response in activated macrophages. *Autophagy*, *12*, 1240–58.

Pastore, N., Blomenkamp, K., Annunziata, F., Piccolo, P., Mithbaokar, P., Maria Sepe, R., … Brunetti-Pierri, N. (2013). Gene transfer of master autophagy regulator TFEB results in clearance of toxic protein and correction of hepatic disease in alpha-1-anti-trypsin deficiency. *EMBO Molecular Medicine*, *5*, 397–412.

Peña-Llopis, S., Vega-Rubin-de-Celis, S., Schwartz, J. C., Wolff, N. C., Tran, T. A. T., Zou, L., … Brugarolas, J. (2011). Regulation of TFEB and V-ATPases by mTORC1. *The EMBO Journal*, *30*, 3242–58.

Peng, C., Lu, Z., Xie, Z., Cheng, Z., Chen, Y., Tan, M., … Zhao, Y. (2011). The first identification of lysine malonylation substrates and its regulatory enzyme. *Molecular & Cellular Proteomics : MCP*, *10*, M111.012658.

Perera, R. M., Stoykova, S., Nicolay, B. N., Ross, K. N., Fitamant, J., Boukhali, M., … Bardeesy, N. (2015). Transcriptional control of autophagy-lysosome function drives pancreatic cancer metabolism. *Nature*, *524*, 361–5.

Perk, J., Iavarone, A., & Benezra, R. (2005). Id family of helix-loop-helix proteins in cancer. *Nature Reviews. Cancer*, *5*, 603–14.

Pingault, V., Ente, D., Dastot-Le Moal, F., Goossens, M., Marlin, S., & Bondurand, N. (2010). Review and update of mutations causing Waardenburg syndrome. *Human Mutation*, *31*, 391–406.

Ploper, D., Taelman, V. F., Robert, L., Perez, B. S., Titz, B., Chen, H.-W., … De Robertis, E. M. (2015). MITF drives endolysosomal biogenesis and potentiates Wnt signaling in melanoma cells. *Proceedings of the National Academy of Sciences of the United States of America*, *112*, E420-9.

Pogenberg, V., Ögmundsdóttir, M. H., Bergsteinsdóttir, K., Schepsky, A., Phung, B., Deineko, V., … Wilmanns, M. (2012). Restricted leucine zipper dimerization and specificity of DNA recognition of the melanocyte master regulator MITF. *Genes and Development*, *26*, 2647–2658.

Polesskaya, A., Duquet, A., Naguibneva, I., Weise, C., Vervisch, A., Bengal, E., … Harel-Bellan, A. (2000). CREB-binding protein/p300 activates MyoD by acetylation. *The Journal of Biological Chemistry*, *275*, 34359–64.

Potterf, S. B., Furumura, M., Dunn, K. J., Arnheiter, H., & Pavan, W. J. (2000). Transcription factor hierarchy in Waardenburg syndrome: regulation of MITF expression by SOX10 and PAX3. *Human Genetics*, *107*, 1–6.

Prendergast, G. C., & Ziff, E. B. (1991). Methylation-sensitive sequence-specific DNA binding by the c-Myc basic region. *Science (New York, N.Y.)*, *251*, 186–189.

Primot, A., Mogha, A., Corre, S., Roberts, K., Debbache, J., Adamski, H., … Galibert, M.-D. (2010). ERK-regulated differential expression of the Mitf 6a/b splicing isoforms in melanoma. *Pigment Cell & Melanoma Research*, *23*, 93–102.

Prince, S., Carreira, S., Vance, K. W., Abrahams, A., & Goding, C. R. (2004). Tbx2 directly represses the expression of the p21(WAF1) cyclin-dependent kinase inhibitor. *Cancer Research*, *64*, 1669–74.

Qiu, Y., Guo, M., Huang, S., & Stein, R. (2004). Acetylation of the BETA2 transcription factor by p300-associated factor is important in insulin gene expression. *The Journal of Biological Chemistry*, *279*, 9796–802.

Read, A. P., & Newton, V. E. (1997). Waardenburg syndrome. *Journal of Medical Genetics*, *34*, 656–65.

Richon, V. M., Emiliani, S., Verdin, E., Webb, Y., Breslow, R., Rifkind, R. A., & Marks,

P. A. (1998). A class of hybrid polar inducers of transformed cell differentiation inhibits histone deacetylases. *Proceedings of the National Academy of Sciences of the United States of America*, *95*, 3003–7.

Roczniak-Ferguson, A., Petit, C. S., Froehlich, F., Qian, S., Ky, J., Angarola, B., … Ferguson, S. M. (2012). The Transcription Factor TFEB Links mTORC1 Signaling to Transcriptional Control of Lysosome Homeostasis. *Science Signaling*, *5*(228), ra42.

Sáez-Ayala, M., Montenegro, M. F., Sánchez-Del-Campo, L., Fernández-Pérez, M. P., Chazarra, S., Freter, R., … Rodríguez-López, J. N. (2013). Directed phenotype switching as an effective antimelanoma strategy. *Cancer Cell*, *24*, 105–19.

Saito, H., Yasumoto, K.-I., Takeda, K., Takahashi, K., Fukuzaki, A., Orikasa, S., & Shibahara, S. (2002). Melanocyte-specific microphthalmia-associated transcription factor isoform activates its own gene promoter through physical interaction with lymphoid-enhancing factor 1. *The Journal of Biological Chemistry*, *277*, 28787–94.

Sardiello, M., Palmieri, M., di Ronza, A., Medina, D. L., Valenza, M., Gennarino, V. A., … Ballabio, A. (2009). A gene network regulating lysosomal biogenesis and function. *Science (New York, N.Y.)*, *325*, 473–477.

Sartorelli, V., Puri, P. L., Hamamori, Y., Ogryzko, V., Chung, G., Nakatani, Y., … Kedes, L. (1999). Acetylation of MyoD directed by PCAF is necessary for the execution of the muscle program. *Molecular Cell*, *4*, 725–34.

Saxe, J. P., Tomilin, A., Schöler, H. R., Plath, K., & Huang, J. (2009). Post-translational regulation of Oct4 transcriptional activity. *PloS One*, *4*, e4467.

Schepsky, A., Bruser, K., Gunnarsson, G. J., Goodall, J., Hallsson, J. H., Goding, C. R., … Hecht, A. (2006). The Microphthalmia-Associated Transcription Factor Mitf Interacts with -Catenin To Determine Target Gene Expression. *Molecular and Cellular Biology*, *26*, 8914–8927.

Selzer, E., Wacheck, V., Lucas, T., Heere-Ress, E., Wu, M., Weilbaecher, K. N., … Jansen, B. (2002). The melanocyte-specific isoform of the microphthalmia transcription factor affects the phenotype of human melanoma. *Cancer Research*, *62*, 2098–103.

Settembre, C., De Cegli, R., Mansueto, G., Saha, P. K., Vetrini, F., Visvikis, O., … Ballabio, A. (2013). TFEB controls cellular lipid metabolism through a starvation-induced autoregulatory loop. *Nature Cell Biology*, *15*, 647–658.

Settembre, C., Zoncu, R., Medina, D. L., Vetrini, F., Erdin, S., Erdin, S., … Ballabio, A. (2012). A lysosome-to-nucleus signalling mechanism senses and regulates the lysosome via mTOR and TFEB. *The EMBO Journal*, *31*, 1095–108.

Settembre, C., Di Malta, C., Polito, V. A., Arencibia, M. G., Vetrini, F., Erdin, S., … Ballabio, A. (2011). TFEB Links Autophagy to Lysosomal Biogenesis. *Science*, *332*, 1429–1433.

Shao, W., & Espenshade, P. J. (2012). Expanding roles for SREBP in metabolism. *Cell Metabolism*, *16*, 414–9.

Shen, T., Zong, C., Hamelberg, D., McCammon, J. A., & Wolynes, P. G. (2005). The

folding energy landscape and phosphorylation: modeling the conformational switch of the NFAT regulatory domain. *FASEB Journal : Official Publication of the Federation of American Societies for Experimental Biology*, *19*, 1389–95.

Shimano, H. (2009). SREBPs: physiology and pathophysiology of the SREBP family. *The FEBS Journal*, *276*, 616–21.

Shin, I., Rotty, J., Wu, F. Y., & Arteaga, C. L. (2005). Phosphorylation of p27Kip1 at Thr-157 interferes with its association with importin alpha during G1 and prevents nuclear re-entry. *The Journal of Biological Chemistry*, *280*, 6055–63.

Shoag, J., Haq, R., Zhang, M., Liu, L., Rowe, G. C., Jiang, A., … Arany, Z. (2013). PGC-1 coactivators regulate MITF and the tanning response. *Molecular Cell*, *49*, 145–57.

Smith, S. D., Kelley, P. M., Kenyon, J. B., & Hoover, D. (2000). Tietz syndrome (hypopigmentation/deafness) caused by mutation of MITF. *Journal of Medical Genetics*, *37*, 446–8.

Soderholm, J. F., Bird, S. L., Kalab, P., Sampathkumar, Y., Hasegawa, K., Uehara-Bingen, M., … Heald, R. (2011). Importazole, a small molecule inhibitor of the transport receptor importin-β. *ACS Chemical Biology*, *6*, 700–8.

Song, W., Wang, F., Savini, M., Ake, A., di Ronza, A., Sardiello, M., & Segatori, L. (2013). TFEB regulates lysosomal proteostasis. *Human Molecular Genetics*, *22*, 1994–2009.

Spampanato, C., Feeney, E., Li, L., Cardone, M., Lim, J.-A., Annunziata, F., … Raben, N. (2013). Transcription factor EB (TFEB) is a new therapeutic target for Pompe disease. *EMBO Molecular Medicine*, *5*, 691–706.

Steingrímsson, E., Copeland, N. G., & Jenkins, N. a. (2004). Melanocytes and the microphthalmia transcription factor network. *Annual Review of Genetics*, *38*, 365–411.

Steingrimsson, E., Tessarollo, L., Pathak, B., Hou, L., Arnheiter, H., Copeland, N. G., & Jenkins, N. a. (2002). Mitf and Tfe3, two members of the Mitf-Tfe family of bHLH-Zip transcription factors, have important but functionally redundant roles in osteoclast development. *Proceedings of the National Academy of Sciences of the United States of America*, *99*, 4477–82.

Steingrímsson, E., Tessarollo, L., Reid, S. W., Jenkins, N. a, & Copeland, N. G. (1998). The bHLH-Zip transcription factor Tfeb is essential for placental vascularization. *Development (Cambridge, England)*, *125*, 4607–4616.

Stretton, C., Hoffmann, T. M., Munson, M. J., Prescott, A., Taylor, P. M., Ganley, I. G., & Hundal, H. S. (2015). GSK3-mediated raptor phosphorylation supports amino-acid-dependent mTORC1-directed signalling. *The Biochemical Journal*, *470*, 207–21.

Strub, T., Giuliano, S., Ye, T., Bonet, C., Keime, C., Kobi, D., … Davidson, I. (2011). Essential role of microphthalmia transcription factor for DNA replication, mitosis and genomic stability in melanoma. *Oncogene*, *30*, 2319–32.

Sundqvist, A., & Ericsson, J. (2003). Transcription-dependent degradation controls the stability of the SREBP family of transcription factors. *Proceedings of the National*

*Academy of Sciences of the United States of America*, *100*, 13833–8.

Sykes, S. M., Mellert, H. S., Holbert, M. A., Li, K., Marmorstein, R., Lane, W. S., & McMahon, S. B. (2006). Acetylation of the p53 DNA-binding domain regulates apoptosis induction. *Molecular Cell*, *24*, 841–51.

Szymczak-Workman, A. L., Vignali, K. M., & Vignali, D. A. A. (2012). Design and construction of 2A peptide-linked multicistronic vectors. *Cold Spring Harbor Protocols*, *2012*, 199–204.

Tachibana, M. (1997). Evidence to suggest that expression of MITF induces melanocyte differentiation and haploinsufficiency of MITF causes Waardenburg syndrome type 2A. *Pigment Cell Research / Sponsored by the European Society for Pigment Cell Research and the International Pigment Cell Society*, *10*, 25–33.

Takeda, K., Takemoto, C., Kobayashi, I., Watanabe, A., Nobukuni, Y., Fisher, D. E., & Tachibana, M. (2000). Ser298 of MITF, a mutation site in Waardenburg syndrome type 2, is a phosphorylation site with functional significance. *Human Molecular Genetics*, *9*, 125–32.

Tassabehji, M., Newton, V. E., Liu, X. Z., Brady, A., Donnai, D., Krajewska-Walasek, M., … Reardon, W. (1995). The mutational spectrum in Waardenburg syndrome. *Human Molecular Genetics*, *4*, 2131–7.

Thurber, A. E., Douglas, G., Sturm, E. C., Zabierowski, S. E., Smit, D. J., Ramakrishnan, S. N., … Sturm, R. A. (2011). Inverse expression states of the BRN2 and MITF transcription factors in melanoma spheres and tumour xenografts regulate the NOTCH pathway. *Oncogene*, *30*, 3036–48.

Tietz, W. (1963). A syndrome of deaf-mutism associated with albinism showing dominant autosomal inheritance. *American Journal of Human Genetics*, *15*, 259–64.

Tsunemi, T., Ashe, T. D., Morrison, B. E., Soriano, K. R., Au, J., Roque, R. A. V., … La Spada, A. R. (2012). PGC-1α rescues Huntington's disease proteotoxicity by preventing oxidative stress and promoting TFEB function. *Science Translational Medicine*, *4*, 142, ra97.

Urlinger, S., Baron, U., Thellmann, M., Hasan, M. T., Bujard, H., & Hillen, W. (2000). Exploring the sequence space for tetracycline-dependent transcriptional activators: novel mutations yield expanded range and sensitivity. *Proceedings of the National Academy of Sciences of the United States of America*, *97*, 7963–8.

Vance, K. W., Carreira, S., Brosch, G., & Goding, C. R. (2005). Tbx2 is overexpressed and plays an important role in maintaining proliferation and suppression of senescence in melanomas. *Cancer Research*, *65*, 2260–8.

Vazquez, F., Lim, J.-H., Chim, H., Bhalla, K., Girnun, G., Pierce, K., … Puigserver, P. (2013). PGC1α expression defines a subset of human melanoma tumors with increased mitochondrial capacity and resistance to oxidative stress. *Cancer Cell*, *23*, 287–301.

Vega, R. B., Harrison, B. C., Meadows, E., Roberts, C. R., Papst, P. J., Olson, E. N., & McKinsey, T. A. (2004). Protein kinases C and D mediate agonist-dependent cardiac hypertrophy through nuclear export of histone deacetylase 5. *Molecular*

*and Cellular Biology*, *24*, 8374–85.

Verastegui, C., Bertolotto, C., Bille, K., Abbe, P., Ortonne, J. P., & Ballotti, R. (2000). TFE3, a Transcription Factor Homologous to Microphthalmia, Is a Potential Transcriptional Activator of Tyrosinase and TyrpI Genes. *Molecular Endocrinology*, *14*, 449–456.

Vetrini, F., Auricchio, A., Du, J., Angeletti, B., Fisher, D. E., Ballabio, A., & Marigo, V. (2004). The microphthalmia transcription factor (Mitf) controls expression of the ocular albinism type 1 gene: link between melanin synthesis and melanosome biogenesis. *Molecular and Cellular Biology*, *24*, 6550–9.

Voronova, A., & Baltimore, D. (1990). Mutations that disrupt DNA binding and dimer formation in the E47 helix-loop-helix protein map to distinct domains. *Proceedings of the National Academy of Sciences of the United States of America*, *87*, 4722–6.

Waardenburg, P. J. (1951). A new syndrome combining developmental anomalies of the eyelids, eyebrows and nose root with pigmentary defects of the iris and head hair and with congenital deafness. *American Journal of Human Genetics*, *3*, 195–253.

Wade, D. R., & Burkart, M. E. (1978). The role of adenosine 3',5'-cyclic monophosphate in the density-dependent regulation of growth and tyrosinase activity of B-16 melanoma cells. *Journal of Cellular Physiology*, *94*, 265–73.

Wagstaff, K. M., Sivakumaran, H., Heaton, S. M., Harrich, D., & Jans, D. A. (2012). Ivermectin is a specific inhibitor of importin α/β-mediated nuclear import able to inhibit replication of HIV-1 and dengue virus. *The Biochemical Journal*, *443*, 851–6.

Wang, Z., Wu, Y., Li, L., & Su, X.-D. (2013). Intermolecular recognition revealed by the complex structure of human CLOCK-BMAL1 basic helix-loop-helix domains with E-box DNA. *Cell Research*, *23*, 213–24.

Wang, R., Cherukuri, P., & Luo, J. (2005). Activation of Stat3 sequence-specific DNA binding and transcription by p300/CREB-binding protein-mediated acetylation. *The Journal of Biological Chemistry*, *280*, 11528–34.

Weilbaecher, K. N., Hershey, C. L., Takemoto, C. M., Horstmann, M. A., Hemesath, T. J., Tashjian, A. H., & Fisher, D. E. (1998). Age-resolving osteopetrosis: a rat model implicating microphthalmia and the related transcription factor TFE3. *The Journal of Experimental Medicine*, *187*, 775–85.

Weis, K. (2003). Regulating access to the genome: nucleocytoplasmic transport throughout the cell cycle. *Cell*, *112*, 441–51.

Wellbrock, C., & Arozarena, I. (2015). Microphthalmia-associated transcription factor in melanoma development and MAP-kinase pathway targeted therapy. *Pigment Cell & Melanoma Research*, *28*, 390–406.

Wellbrock, C., Rana, S., Paterson, H., Pickersgill, H., Brummelkamp, T., & Marais, R. (2008). Oncogenic BRAF regulates melanoma proliferation through the lineage specific factor MITF. *PloS One*, *3*, e2734.

Wellbrock, C., & Marais, R. (2005). Elevated expression of MITF counteracts B-RAF-stimulated melanocyte and melanoma cell proliferation. *The Journal of Cell*

*Biology*, *170*, 703–8.

Wen, W., Meinkoth, J. L., Tsien, R. Y., & Taylor, S. S. (1995). Identification of a signal for rapid export of proteins from the nucleus. *Cell*, *82*, 463–73.

Widlund, H. R., Horstmann, M. A., Price, E. R., Cui, J., Lessnick, S. L., Wu, M., … Fisher, D. E. (2002). Beta-catenin-induced melanoma growth requires the downstream target Microphthalmia-associated transcription factor. *The Journal of Cell Biology*, *158*, 1079–87.

Winkler, D. F. H., Hilpert, K., Brandt, O., & Hancock, R. E. W. (2009). Synthesis of peptide arrays using SPOT-technology and the CelluSpots-method. *Methods in Molecular Biology (Clifton, N.J.)*, *570*, 157–74.

Wu, M., Hemesath, T. J., Takemoto, C. M., Horstmann, M. A., Wells, A. G., Price, E. R., … Fisher, D. E. (2000). c-Kit triggers dual phosphorylations, which couple activation and degradation of the essential melanocyte factor Mi. *Genes & Development*, *14*, 301–12.

Wu, Y., Lin, J. C., Piluso, L. G., Dhahbi, J. M., Bobadilla, S., Spindler, S. R., & Liu, X. (2014). Phosphorylation of p53 by TAF1 inactivates p53-dependent transcription in the DNA damage response. *Molecular Cell*, *53*, 63–74.

Xiao, Q., Yan, P., Ma, X., Liu, H., Perez, R., Zhu, A., … Lee, J.-M. (2015). Neuronal-Targeted TFEB Accelerates Lysosomal Degradation of APP, Reducing Aβ Generation and Amyloid Plaque Pathogenesis. *The Journal of Neuroscience : The Official Journal of the Society for Neuroscience*, *35*, 12137–51.

Xiao, Q., Yan, P., Ma, X., Liu, H., Perez, R., Zhu, A., … Lee, J.-M. (2014). Enhancing astrocytic lysosome biogenesis facilitates Aβ clearance and attenuates amyloid plaque pathogenesis. *The Journal of Neuroscience : The Official Journal of the Society for Neuroscience*, *34*, 9607–20.

Xu, D., Farmer, A., Collett, G., Grishin, N. V., & Chook, Y. M. (2012). Sequence and structural analyses of nuclear export signals in the NESdb database. *Molecular Biology of the Cell*, *23*, 3677–3693.

Xu, W. S., Parmigiani, R. B., & Marks, P. A. (2007). Histone deacetylase inhibitors: molecular mechanisms of action. *Oncogene*, *26*, 5541–52.

Xu, W., Gong, L., Haddad, M. M., Bischof, O., Campisi, J., Yeh, E. T., & Medrano, E. E. (2000). Regulation of microphthalmia-associated transcription factor MITF protein levels by association with the ubiquitin-conjugating enzyme hUBC9. *Experimental Cell Research*, *255*, 135–43.

Yang, J., Bardes, E. S., Moore, J. D., Brennan, J., Powers, M. A., & Kornbluth, S. (1998). Control of cyclin B1 localization through regulated binding of the nuclear export factor CRM1. *Genes & Development*, *12*, 2131–43.

Yasumoto, K., Yokoyama, K., Shibata, K., Tomita, Y., & Shibahara, S. (1994). Microphthalmia-associated transcription factor as a regulator for melanocyte-specific transcription of the human tyrosinase gene. *Molecular and Cellular Biology*, *14*, 8058–70.

Yavuzer, U., Keenan, E., Lowings, P., Vachtenheim, J., Currie, G., & Goding, C. R. (1995). The Microphthalmia gene product interacts with the retinoblastoma protein

in vitro and is a target for deregulation of melanocyte-specific transcription. *Oncogene*, *10*, 123–34.

Yokoyama, S., Woods, S. L., Boyle, G. M., Aoude, L. G., MacGregor, S., Zismann, V., … Brown, K. M. (2011). A novel recurrent mutation in MITF predisposes to familial and sporadic melanoma. *Nature*, *480*, 99–103.

Yokoyama, S., Feige, E., Poling, L. L., Levy, C., Widlund, H. R., Khaled, M., … Fisher, D. E. (2008). Pharmacologic suppression of MITF expression via HDAC inhibitors in the melanocyte lineage. *Pigment Cell & Melanoma Research*, *21*, 457–63.

Zehorai, E., Yao, Z., Plotnikov, A., & Seger, R. (2010). The subcellular localization of MEK and ERK--a novel nuclear translocation signal (NTS) paves a way to the nucleus. *Molecular and Cellular Endocrinology*, *314*, 213–20.

Zhang, T., Zhou, Q., Ogmundsdottir, M. H., Möller, K., Siddaway, R., Larue, L., … Pignoni, F. (2015). Mitf is a master regulator of the v-ATPase, forming a control module for cellular homeostasis with v-ATPase and TORC1. *Journal of Cell Science*, *128*, 2938–50.

Zhang, Y., & Zhao, J. (2015). TFEB Participates in the Aβ-Induced Pathogenesis of Alzheimer's Disease by Regulating the Autophagy-Lysosome Pathway. *DNA and Cell Biology*, *34*, 661–8.

Zhao, X., Gan, L., Pan, H., Kan, D., Majeski, M., Adam, S. A., & Unterman, T. G. (2004). Multiple elements regulate nuclear/cytoplasmic shuttling of FOXO1: characterization of phosphorylation- and 14-3-3-dependent and -independent mechanisms. *The Biochemical Journal*, *378*, 839–49.

Zhong, M., De Angelo, P., Osborne, L., Paniz-Mondolfi, A. E., Geller, M., Yang, Y., … Cai, D. (2012). Translocation renal cell carcinomas in adults: a single-institution experience. *The American Journal of Surgical Pathology*, *36*, 654–62.